A STUDY OF NMDA RECEPTOR/PSD-95 MEMBRANE ASSOCIATED GUANYLATE KINASE INTERACTIONS

Sarah Louise Cousins

A Thesis Submitted for the Degree of Doctor of Philosophy of the University of London

Department of Biological and Pharmaceutical Chemistry
The School of Pharmacy
University of London
29-39 Brunswick Square
London
WC1N 1AX

This thesis describes research conducted in the School of Pharmacy, University of London between October 2003 and June 2007 under the supervision of Prof. F. A. Stephenson. I certify that the research described is original and that any parts of the work that have been conducted in collaboration are clearly indicated. I also certify that I have written all the text herein and have clearly indicated by suitable citation any part of this dissertation that has already appeared in publication.

Signature [signature] Date 17/08/07

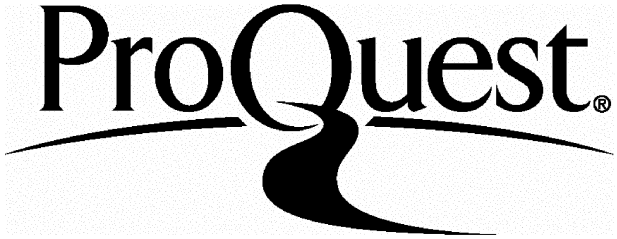

Abstract

N-Methyl-D-aspartate (NMDA) receptors are a subclass of excitatory ionotropic glutamate neurotransmitter receptors. There are four major subclasses of NMDA receptors formed by the co-assembly of different NMDA receptor subunits, i.e. NR1/NR2A, NR1/NR2B, NR1/NR2C and NR1/NR2D. These subclasses have distinct physiological properties and distinct temporal and spatial patterns of distribution in neurones. NMDA receptors are trafficked to dendritic spines in neurons where they are thought to be anchored in the post-synaptic membrane by their association with the postsynaptic density-95 (PSD-95) membrane associated guanylate kinase (MAGUK) family of scaffolding proteins. PSD-95 is the prototypic member of this family which also includes channel associated protein of synapse–110 (Chapsyn-110), synapse associated protein97 (SAP97) and SAP102. The association between PSD-95 and the NR1/NR2A and NR1/NR2B receptor subtypes has been well characterized and shown to be important for the regulation of receptor cell surface expression. However there is a paucity of knowledge with regard to the association between NR1/NR2C and NR1/NR2D subtypes and PSD-95 and also all four major NMDA receptor subclasses and the other members of the PSD-95 MAGUK family. The aim of this thesis therefore was to investigate the association between the PSD-95 MAGUK proteins and the four major NMDA receptor subclasses and the effects of this association on NMDA receptor expression and cell surface trafficking. Each major NMDA receptor subclass was co-expressed with PSD-95 MAGUK family members in human embryonic kidney (HEK) 293 cells and the expressed proteins analysed by immunoprecipitation assays, quantitative immunoblotting and cell surface ELISA assays. In addition, the association between NR1/NR2A NMDA receptors and PSD-95 was studied in more detail which included the mapping of a new PSD-95 binding motif in the NR2A C-terminal domain and a study of the role of protein kinase A phosphorylation in receptor/scaffold association and cell surface trafficking. Finally, a yeast two-hybrid screen was conducted to identify novel NR1/NR2D NMDA receptor associated proteins. Differential association with the PSD-95 MAGUK family and NMDA receptors was discovered. This may be important for the regulation of cell surface receptor number, the stabilisation, clustering, turnover and compartmentalisation of NMDA receptor subtypes in neurons during development and in the mature brain.

Contents

Chapter 3: Results I Discussion I

Chapter 5: Results III Discussion III

Appendices

List of Figures

List of Tables

List of Abbreviations

Ade	Adenine
AKAP	A-kinase-anchoring protein
AMPA	α-amino-3-hydroxy-5-methylisoxazole-4-propionic acid
AP	Adaptor protein
AP5	DL-2-amino-5-phophonopentanoic acid
BSA	Bovine serum albumin
CaCMKII	Calcium calmodulin kinase II
cAMP	Cyclic adenosine monophosphate
cDNA	Complementary deoxyribonucleic acid
cfu	Colony forming units
chapsyn-110	Channel-associated protein of synapses-110
CREB	cAMP response element binding protein
DAG	Diacylglycerol
DMEM/F-12	Dulbecco's modified Eagles medium nutrient mixture F-12 HAM
DMSO	Dimethyl sulfoxide
DNA	Deoxyribonucleic acid
dNTP	Deoxynucleoside-5'-triphosphate
DTT	Dithiothreitol
EDTA	Ethylenedinitrilotetracetatic acid
ELISA	Enzyme-linked immunoadsorbent assay
ER	Endoplasmic reticulum
ERAD	Endoplasmic reticulum associated degradation
FBS	Fetal bovine serum
FCS	Fetal calf serum
FRET	Fluorescence resonance energy transfer
G/C	Guanine/cytosine
GFP	Green fluorescent protein
GK	Guanylate kinase
GKAP	Guanylate kinase domain-associated protein
Hela	Henrietta Lack
HBS	HEPES buffered saline
HBSS	Hanks buffered salt solution
HEK 293	Human embryonic kidney cells
HEPES	N-(2-Hydroxyethyl)piperazine-N'-(2-ethanesulfonic acid)
His	Histidine
HRP	Horseradish peroxidase
Ig	Immunoglobulin
IP_3	Inositol triphosphates
IPTG	Isopropylthio-β-D-galactosidase
KIF	Kinesin superfamily
LAOBP	Leucine/arginine/ornithine-binding proteins
LB	Lennox B broth
LDH	Lactate dehydrogenase
Leu	Leucine
LIVBP	Leucine/isoleucine/valine binding protein
LTD	Long-term depression
LTP	Long-term potentiation
MAGUK	Membrane associated guanylate kinase

mGlu	Metabotropic glutamate
MOPS	3-N-[morpholino]propane-sulphonic acid
mPins	Mammalian homologue of Drosophila melanogaster partner of inscuteable
mRNA	Messenger ribonucleic acid
NF-L	Neurofilament subunit L
NMDA	N-methyl-D-aspartate
NMR	Nuclear magnetic resonance
nNOS	Neuronal nitric oxide synthase
NR1	NMDA receptor type 1 subunit
NR2	NMDA receptor type 2 subunit
NR3	NMDA receptor type 3 subunit
NZ amine	Casein hydrolysate
OD	Optical denisty
ori	Bacterial origin of replication
P	Postnatal day
PBS	Phosphate buffered saline
PCR	Polymerase chain reaction
PDZ	PSD-95, Dlg and ZO-1
PEG	Polyethylene glycol
PKA	Protein kinase A
PKC	Protein kinase C
PMSF	Phenylmethylsulphonyl fluoride
PSD	Postsynaptic density
PSD-95	Post-synaptic density-95
PTK	Protein tyrosine kinase
SAP	Synapse associated protein
SAP	Shrimp alkaline phosphatase
SAP-90	Synapse-associated protein 90
SD	Standard deviation
SDS	Sodium dodecyl sulphate
SDS-PAGE	Sodium dodecyl sulphate polyacrylamide gel electrophoresis
SH3	Src homology 3
SPAR	Spine-associated Rap-guanosine-triphosphatase activatin protein
Tac	Interleukin 2 receptor
TBE	Tris-Borate-EDTA buffer
TE	Tris-EDTA
TEMEED	N,N,N',N' - tetramethylethylene diamine
TM	Transmembrane
Tris	Tris(hydroxymethyl)aminomethane
Triton® X-100	4-(1,1,3,3-Tetramethylbutyl)phenyl-polyethylene glycol
Trp	Tryptophan
Tween®-20	Polyethylene glycol sorbitan monolaurate
X-gal	5-bromo-4-chloro-3-indoyl-β-D-galactosidase
YPAD	Yeast extract peptone dextrose with adenine
ZO-1	Zonula occludens-1

Acknowledgements

I firstly wish to thank Prof. F. A. Stephenson for her help and guidance over the last four years. If this PhD were to be thought of as a journey, then I couldn't think of a better guide than Prof. F. A. Stephenson. Her teachings of scientific thought will be an invaluable asset to me in the future.

I also wish to thank Dr. Kieran Brickley for his help and advice during my PhD studies. In addition, I wish to thank him for the immunisations and the antibody purifications at the start of my project.

Many thanks to Dr. Karine Pozo. We started out on the PhD journey within the same year and became good friends.

Thank you to Dr. Michalis Papadakis and Dr. Miriam Smith for their help in teaching me the mammalian cell transfections and the yeast two-hybrid system.

I would like to thank Dr. Anna Kenny for her moral support during the writing of this thesis.

I would also like to thank Dr. Blaise Mathias-Costa, Dr. Gurmail Ojla and all of the project students that I worked together with in Anne's laboratory.

Lastly, I thank my family and friends for their support during my PhD and forgiving me the many weekends that I dedicated to my work.

CHAPTER 1

INTRODUCTION

1.1 Glutamatergic synapses

Neurones are highly specialised cells found in the central nervous system which send and receive information. A neurone comprises of a cell body, one extended, thin process termed the axon which meets other neuronal cells on small processes called dendrites. Dendrites have small protrusions called dendritic spines which form the majority of synapses. A synapse is formed between the terminus of the axon and the post-synaptic membrane of dendritic spines to transfer information between neurones. The two major types of synapses found are electrical and chemical synapses. Chemical synapses pass their information between neurones via neurotransmitters. Neurotransmitters are small molecule transmitters which are synthesised in neurones and packaged into vesicles found in pre-synaptic sites. Depending on the neurotransmitter released, synapses are divided into two major groups; inhibitory and excitatory synapses. The major neurotransmitters found for inhibitory synapses are γ-aminobutyric (GABA) and glycine. L-Glutamate is the major neurotransmitter found for excitatory synapses. Following both electrical activity and the associated calcium influx, the vesicles containing the neurotransmitter fuse to the presynaptic membrane. This causes the release of neurotransmitter which diffuses across the synaptic cleft and binds to the respective receptors in the post-synaptic membrane. The binding of the neurotransmitter results in the activation of these receptors and the propagation of the signal.

Glutamatergic synapses contain two major types of receptors in the post-synaptic membrane; ionotropic and metabotropic receptors. Metabotropic glutamate (mGlu) receptors are guanine nucleotide-binding (G) protein coupled receptors. To date eight genes have been cloned for mGlu receptors, mGluR1-mGluR8 (for review see Pin and Duvoisin, 1995; Conn and Pin, 1997). These have been divided into three main groups according to their amino acid sequence similarities, pharmacological properties and downstream coupled signalling pathways (for review see Pin and Duvoisin, 1995). Within each group the amino acid similarity is ~ 70 % however when comparing between groups there is ~ 40 % amino acid similarity. Group I comprises mGluR1 and mGluR5, which are coupled to the activation of phospholipase C via the G_q class of G protein (PLC, for review

see Conn and Pin, 1997). PLC hydrolyses phosphatidylinositol (PIP_2) to synthesise two messengers, inositol triphosphates (IP_3) and diacylglycerol (DAG). IP_3 causes the release of the secondary messenger, calcium ions, from intracellular stores. The production of DAG results in the activation of protein kinase C (PKC), a major signalling enzyme which has many protein phosphorylation targets. Group II comprises mGluR2 and mGluR3 whilst Group III comprises mGluR4, mGluR6, mGluR7 and mGluR8. Both Groups II and III of the mGluR inhibit the enzyme adenylyl cyclase via coupling to the G_i class of G proteins (for review see Conn and Pin, 1997). Adenylyl cyclase catalyses the hydrolysis of adenosine 5'-triphosphate (ATP) to generate another secondary messenger, cyclic adenosine monophosphate (cAMP) and pyrophosphate. cAMP activates protein kinase A (PKA) which is another major regulatory kinase. The glutamate ionotropic receptors are a family of ligand-gated ion channels and are the focus of this thesis. They are described in more detail in Section 1.2.

In general, glutamate receptors are located at pre-synaptic, synaptic, peri-synaptic or extra-synaptic sites. It is thought that mGluRs are predominantly present at extra-synaptic sites but are also found at pre-synaptic sites. The ionotropic receptors are present at synaptic, peri-synaptic or extra-synaptic sites (for review see Takumi *et al.*, 1999). Underneath the postsynaptic membranes of glutamatergic synapses is a highly organised, electron dense region which is referred to as the post-synaptic density (PSD). The PSD contains a high concentration of proteins required to propagate the stimulus, for example cell-adhesion, cytoskeleton, scaffolding, adaptor proteins and signalling molecules such as kinases and phosphatases (for review see Boeckers, 2006). Many studies, therefore have focused on the association and regulation of glutamate receptors with these accessory proteins. Figure 1.1 summarises the structure of an excitatory, glutamatergic synapse.

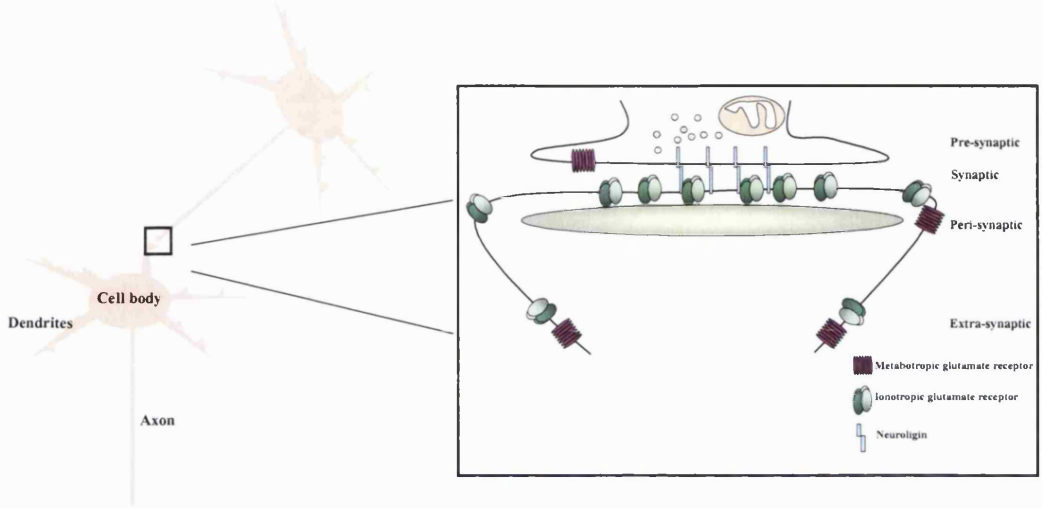

Figure 1.1 Diagram summarising a glutamatergic synapse

The above diagram summarises the major features of a glutamatergic synapse. Vesicles containing the neurotransmitter glutamate are found at pre-synaptic sites. Following both electrical activity and the associated calcium influx the vesicles containing the neurotransmitter fuse to the pre-synaptic membrane and release the neurotransmitter. Synaptic ionotropic glutamate receptors are clustered opposite the glutamate release sites. Some receptors are located in peri-synaptic positions. The postsynaptic density (PSD) is an electron dense region which contains a high concentration of proteins such as cell-adhesion, cytoskeleton, scaffolding and adaptor proteins and signalling molecules such as kinases and phosphatases which are required to propagate the signal. The metabotropic receptors and certain subclasses of ionotropic glutamate receptors are located in extra-synaptic sites. Lastly, metabotropic receptors are also found at pre-synaptic sites.

1.2 The ionotropic glutamate receptors

The ionotropic glutamate receptors are a family of ligand-gated cation channels which mediate the majority of the excitatory neurotransmission in the central nervous system. They are divided into 3 major families depending on their differential selectivity for glutamate analogues, i.e. α-amino-3-hydroxy-5-methylisoxazole-4-propionic acid (AMPA), *N*-methyl-D-aspartate (NMDA) and kainate receptors (for review see Dingledine *et al.*, 1999). AMPA and kainate receptors are closely related when compared to NMDA receptors which are functionally distinct. Both AMPA and kainate receptors mediate the short and fast excitatory postsynaptic currents (EPSCs). They are voltage-independent sodium, potassium and some are calcium permeable ion channels. In their resting state neurones have a resting potential of ~ - 60 mV, a relatively high intracellular concentration

of potassium ions and a relatively high extracellular concentration of sodium ions. The activation of AMPA and kainate receptors results in an influx of sodium ions down their electrochemical gradient causing depolarisation of the postsynaptic membrane. This membrane depolarisation is vital for the activation of NMDA receptors. For their activation, NMDA receptors require the binding of glutamate, the co-agonist, glycine and the removal of a voltage-dependent magnesium ion block (for review see McBain and Mayer, 1994; Sucher *et al.*, 1996; Dingledine *et al.*, 1999). Thus NMDA receptors are considered to be coincidence receptors of synaptic input as they require the binding of the co-agonists, glutamate and glycine, and membrane depolarisation (for review see Bliss and Collingridge, 1993). NMDA receptors mediate comparatively slow and long lasting EPSCs. They are voltage-dependent, calcium permeable ion channels.

Ionotropic glutamate receptors are transmembrane proteins which are formed by the co-assembly of a number of different subunits encoded by separate genes. The AMPA receptor GluR1 subunit was the first ionotropic glutamate receptor subunit to be cloned by Hollmann *et al.* (1989). This was subsequently followed by the identification of the remaining subunits of the ionotropic glutamate receptor family. A summary of the ionotropic glutamate receptor family of subunits is shown in Figure 1.2. The AMPA receptor subunit family comprises GluR1-GluR4 subunits (Hollmann *et al.*, 1989; Keinanen *et al.*, 1990). Kainate receptors are formed by the co-assembly of GluR5-GluR7, KA1 and KA2 subunits (Bettler *et al.*, 1990; 1992; Egebjerg *et al.*, 1991; Werner *et al.*, 1991; Herb *et al.*, 1992). NMDA receptor subunits comprise NR1, NR2A-NR2D, NR3A and NR3B subunits (Moriyoshi *et al.*, 1991; Meguro *et al.*, 1992; Kutuwada *et al.*, 1992; Ikeda *et al.*, 1992; Ciabarra *et al.*, 1995; Nishi *et al.*, 2001; Matsuda *et al.*, 2002). Lastly, glutamate orphan receptor subunits, δ1 and δ2, have been identified, although their exact function is unknown (Yamazaki *et al.*, 1992; Araki *et al.*, 1993). Ionotropic glutamate receptors are only assembled from subunits within their individual family. AMPA and kainate receptors are known to assemble as either homomers or heteromers and are tetrameric in structure (Mayer, 2005; 2006). The combination of subunits which co-assemble influences the receptor properties, in terms of their conductance, ionic permeability and trafficking.

Subunit	Alternative nomenclature	
mGluR1		Metabotropic glutamate receptor subunits
mGluR2		
mGluR3		
mGluR4		
mGluR5		
mGluR6		
mGluR7		
mGluR8		
GluR1	GluRA	AMPA receptor subunits
GluR2	GluRB	
GluR3	GluRC	
GluR4	GluRD	
GluR5		Kainate receptor subunits
GluR6		
GluR7		
KA1		
KA2		
NR1	ζ1	NMDA receptor subunits
NR2A	ε1	
NR2B	ε2	
NR2C	ε3	
NR2D	ε4	
NR3A	χ1	
NR3B	χ2	
δ1		Orphan receptors
δ2		

Figure 1.2 Summary of the metabotropic and ionotropic glutamate receptor subunits

Indeed, AMPA receptors forming homomeric receptors of GluR1, GluR3 or GluR4 subunits were found to be calcium permeable. The presence of GluR2 subunits resulted in the receptors being calcium impermeable. Further analysis revealed the presence of R764 which is glutamine in the same position for GluR1, GluR3 and GluR4 subunits. GluR2 subunits were found to be ribonucleic acid (RNA)-edited at amino acid position 764 from a glutamine to an arginine (for review see Dingledine *et al.*, 1999). NMDA receptors are the

focus of this thesis. A more detailed description of NMDA receptor subunits and their properties are discussed in Section 1.3.

1.3 NMDA receptors: general properties

As mentioned previously, NMDA receptors are calcium permeable ion channels which are activated following membrane depolarisation and the binding of the co-agonists glycine and glutamate. The activation of NMDA receptor coupled calcium ion signalling pathways is important for many neural functions such as development, learning and memory and in neurological diseases.

NMDA receptors are involved in long-term potentiation (LTP) and long-term depression (LTD) which are both forms of synaptic plasticity that are thought to underlie synaptic memory and learning. LTP is characterised by a persistent increase in the size of the synaptic component which can be invoked by induction. Many induction methods can be used to induce LTP in hippocampal neurones, for example, one method used is a train of 50-100 stimuli at 100 Hz or more (for review see Bliss and Collingridge, 1993). The pharmacological blockage of NMDA receptor function resulted in LTP being unable to be induced. This implied that NMDA receptor activation was the first stage of LTP (for review see Bliss and Collingridge, 1993). The activation of NMDA receptors causes an elevation in calcium ions which results in the activation of enzymes that strengthen the synapse. An example of an enzyme implicated in LTP is calcium calmodulin kinase II (CaMKII). Indeed, CaMKII knock-out mice demonstrated impaired hippocampal LTP (Silva *et al.*, 1992a, b). Once activated by calcium ions, CaMKII is able to autoactivate itself thus it becomes calcium-independent. The active form of CaMKII phosphorylates AMPA receptors which maintains their cell surface expression and also promotes the trafficking of more AMPA receptors to the synapse. However, synapses have been identified which only have cell surface expressed NMDA receptors but not AMPA receptors, even though intracellular AMPA receptors were present (Richmond *et al.*, 1996; Gomperts *et al.*, 1998; Carroll *et al.*, 1999; Liao *et al.*, 1999; Noel *et al.*, 1999; Pickard *et al.*, 2001). This population of synapses were termed silent synapses (for review see Malenka and Nicoll, 1997; Isaac, 2003). In addition to AMPA receptors, CaMKII also

phosphorylates the cyclic AMP control response element-binding protein (CREB) which is a transcription factor that may activate a number of genes required to maintain LTP.

LTD is characterised by a sustained reduction in the strength of synapses. In hippocampal neurones, LTD can be induced by stimulation at 1-5 Hz for several minutes (for review see Lisman, 2001a). The dephosphorylation of CaMKII by a phosphatase cascade inactivates this enzyme and results in a lower calcium input into the neurone. This is thought to be the mechanism which underlies the induction of LTD (for review see Bliss and Collingridge, 1993; Lisman *et al.*, 2001b).

Although the NMDA receptor-mediated calcium ion influx is essential for activation of signalling pathways, an excess can lead to excitotoxicity. Excitotoxicity is thought to be the mechanism for central nervous system damage during ischaemia, trauma and other neurological disorders. Excess calcium ions in the neurone may activate calcium ion-dependent pathways that are normally dormant or operate at low levels (for review see Sattler and Tymianski, 2000). In addition, NMDA receptors are thought to play a role in many neurological diseases for example Huntington's disease, Alzheimer's disease and schizophrenia. Thus NMDA receptors are considered targets for therapeutic intervention. Both NMDA receptor agonists and antagonists are required for the treatment of neurological diseases, for example in schizophrenia there is a down regulation of NMDA receptor function and the need for agonists to increase receptor activity. Conversely, in neurological diseases linked to excitotoxic cell death, such as cerebral stroke, there is a requirement for antagonists which would decrease NMDA receptor activity. The study of certain NMDA receptor subtypes allows specific drug targets to be identified (for review see Paoletti and Neyton, 2007).

1.4 Structure of NMDA receptors

1.4.1 NMDA receptor genes

As mentioned previously, there are seven separate NMDA receptor genes encoding the subunits NR1, NR2A-NR2D, NR3A and NR3B (Moriyoshi *et al.*, 1991; Meguro *et al.*,

1992; Kutuwada *et al.*, 1992; Ikeda *et al.*, 1992; Ciabarra *et al.*, 1995; Nishi *et al.*, 2001; Matsuda *et al.*, 2002). A summary of the NMDA receptor subunits is shown in Figure 1.2. The first NMDA receptor subunit cDNA to be cloned encoded the NR1 subunit. This was identified by expression cloning using *Xenopus* oocytes (Moriyoshi *et al.,* 1991). The subunit was originally named NMDAR1, an alternative nomenclature used is ζ1, however the commonly used name is now NR1. The NR1 subunit is present in all NMDA receptors and termed the obligatory subunit. NR1 subunits contain the co-agonist glycine binding domain, which is described in further detail in Section 1.4.3. The immature NR1 subunit was found to be 938 amino acids in length with a predicted molecular mass of 105 kDa. Further analysis of the NR1 subunit amino acid sequence showed that it shared ~ 22 - 26 % amino acid identity with GluR1-GluR4 AMPA receptor subunits and GluR5 and GluR6 kainate receptor subunits. The NR1 gene is alternatively spliced at three positions which results in eight splice variants. The exons which are alternatively spliced are exon 5, exon 21 and exon 22. Exons are termed 'N' or 'C' depending on whether the exon is present in the N-terminal or C-terminal domain. Exon 5 forms the N1 cassette, exon 21 corresponds to the C1 cassette and exon 22 forms the C2 cassette. The NR1 subunit splice variants are named NR1-1a, b - NR1-4a, b. NR1 subunits containing the N1 cassette are termed 'b' i.e. NR1-1b, NR1-2b, NR1-3b and NR1-4b. NR1 subunits which contain the C1 cassette are NR1-1a, b and NR1-3a, b. NR1 subunits containing the C2 cassette are NR1-1a, b and NR1-2a, b. The absence of the C2 cassette causes an introduction of a STOP codon which results in a shorter C-terminal domain. This truncated C-terminal is referred to as the C2' cassette (for review see Zukin and Bennett, 1995). A summary of the NR1 subunit splice variants is shown in Figure 1.3.

The NR2 subunits are considered the modulatory subunits of NMDA receptors. Each NR2 subunit contains the glutamate binding domain, which is described in more detail in Section 1.4.3. The first cDNA to be cloned was the NR2A subunit, which was followed by the isolation of NR2B, NR2C and NR2D cDNAs (Meguro *et al.*, 1992; Kutsuwada *et al.*, 1992; Ikeda *et al.,* 1992). The co-expression of NR1/NR2 cDNA in *Xenopus* oocytes resulted in a higher response to glutamate and glycine than the expression of NR1 subunits alone and the responses were more characteristic of those observed *in vivo* (Meguro *et al.*, 1992;

Kutsuwada *et al.*, 1992; Ikeda *et al.,* 1992). The subunits were originally named ϵ1- ϵ4, however the commonly used names are now NR2A-NR2D. The immature NR2A, NR2B, NR2C and NR2D subunits are composed of 1464, 1482, 1239 and 1323 amino acids, respectively and have predicted molecular weights of 163, 162, 133 and 140 kDa, respectively. The NR2 subunits share 38 - 52 % amino acid identities within thier own family, 29 % amino acid identity with the NR1 subunit and 11 - 18 % amino acid identity with GluR1-GluR4, GluR5, GluR6, KA1, KA2 subunits.

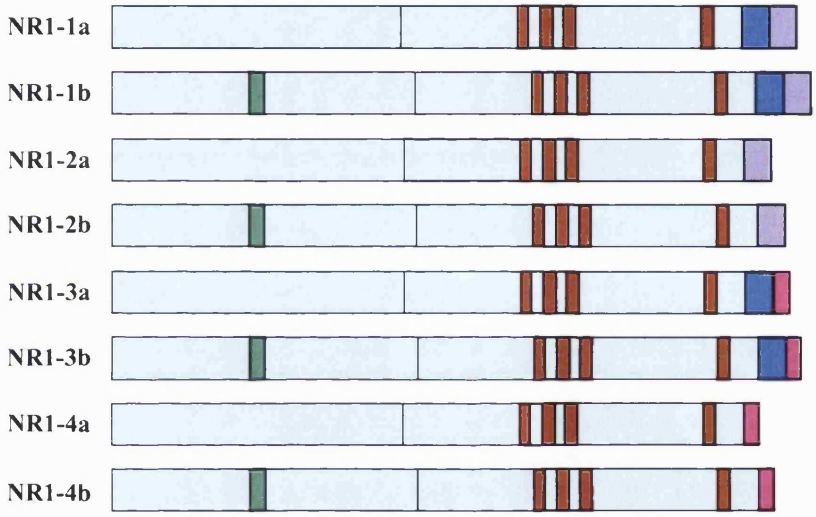

Figure 1.3 Diagram to summarise the NR1 subunit isoforms

The diagram summarises the NR1 splice variants. There are 3 splice sites which give rise to 8 splice variants. The transmembrane domains are shown as . The cassettes are depicted as; N1 cassettes the C1 cassette the C2 cassette and the C2' cassette.

A third NMDA receptor subunit class was identified, this was the NR3 subfamily. The NR3A cDNA was first identified followed by the cDNA for NR3B subunits (Ciabarra *et al.*, 1995; Nishi *et al.*, 2001; Matsuda *et al.*, 2002). The NR3A and NR3B subunits share 55 % amino acid identity with each other and have ~ 28 % amino acid identity with the NR1 and NR2 subunits. The subunits were originally called χ1 and χ2, however the commonly used name is now NR3A and NR3B.

1.4.2 NMDA receptor subunit topology

All NMDA receptor subunits share the same common predicted membrane topology. When the NR1 and NR2 subunits were originally identified, hydrophobicity analysis predicted that all of the NMDA receptor subunits consisted of 4 transmembrane domains, M1-M4, with an extracellular N-termini and C-termini (Moriyoshi *et al.*, 1991; Meguro *et al.*, 1992; Ikeda *et al.*, 1992). However, the identification of *N*-glycosylation sites, phosphorylation sites and the glutamate and glycine binding sites led to a revision of the predicted NMDA receptor subunit predicted topology (Hollmann *et al.*, 1989). Membrane proteins are *N*-glycosylated only on their extracellular domains. Mutations which affected the predicted *N*-glycosylation sites in the M3-M4 region, which in the 4 transmembrane model would be intracellular, demonstrated that the M3-M4 region is in fact extracellular (Wood *et al.*, 1995). Since the M2 region of the NR1 subunit shared a high degree of homology with the M2 region of the potassium ion channel, it was predicted that, like the potassium ion channel, the M2 region of NR1 subunits also formed a hairpin loop (Wood *et al.*, 1995). The introduction of the FLAG epitope on the N-terminal domain and within the M3-M4 region revealed that both of these were localized extracellularly (Hirai *et al.*, 1996). Polyclonal antibodies raised against a region in the predicted C-terminal domain of NR1 subunits did not show any immunoreactivity when used for the detection of cell surface expressed NR1/NR2A NMDA receptors in human embryonic kidney (HEK) 293 cells, thus suggesting an intracellular localization of this domain (Chazot *et al.*, 1995). In addition, epitope FLAG tagging of the C-terminal domain confirmed the intracellular localization of this domain (Hirai *et al.*, 1996). Phosphorylation sites were identified in exon 21 of the C-terminal domain of NR1 subunits (Tingley *et al.*, 1993). In addition, the C-terminal domain of NR2B subunits was found to be essential for the PKC modulation of NMDA receptor function (Mori *et al.*, 1993). Phosphorylation is thought to occur only in intracellular compartments due to the availability of the necessary kinases and phosphatases. Thus the identification of phosphorylation sites on the NR1 C-terminal domain provided further evidence of an intracellular C-terminal domain. Lastly, the identification of the amino acids essential for the glycine and glutamate binding sites resulted in the prediction of extracellular location (for review see Lynch and Guttmann,

2001). Thus, NMDA receptor subunits were predicted to have 3 transmembrane domains (TM1, TM3 and TM4) with a re-entrant loop (M2) following TM1. A schematic diagram depicting the predicted NMDA receptor subunit topology is shown in Figure 1.4.

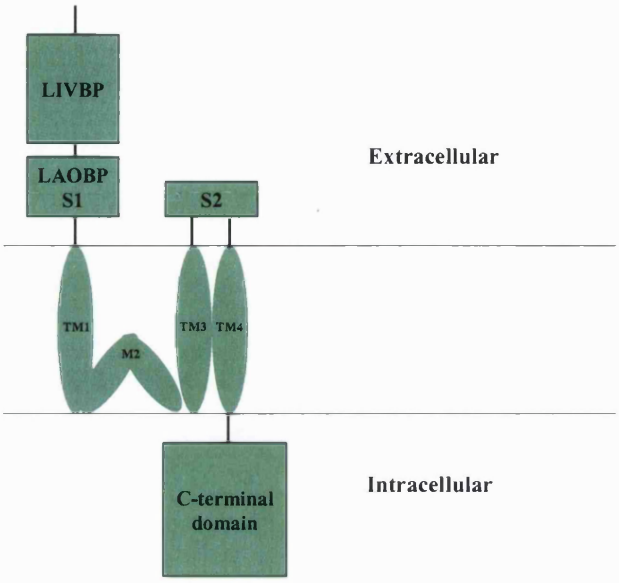

Figure 1.4 Schematic diagram of the topology of NMDA receptor subunits
NMDA receptor subunits have three predicted transmembrane domains (TM1, TM3 and TM4) and a re-entrant loop (M2). The N-terminus is extracellular and divided into two separate domains owing to their homology with either the bacterial leucine isoleucine valine binding protein (LIVBP) and the bacterial leucine alanine orthinine binding protein (LAOBP). The LAOBP domain forms half of the ligand binding domain along with S2 domain. NMDA receptors have an intracellular C-terminal domain.

The N-terminal domain is extracellular, which is further subdivided into two separate domains based on the homology with bacterial amino acid binding proteins. The first 400 amino acids are homologous with the bacterial leucine isoleucine valine binding protein (LIVBP), thus called the LIVBP domain. The remaining portion of the N-terminal domain is homologous with the bacterial leucine alanine orthinine binding protein (LAOBP) and forms the LAOBP or S1 domain. The N-terminus is followed by TM1, the re-entrant loop (M2) which forms the channel pore and then TM3. After TM3 the polypeptide is then predicted to form an extracellular loop creating the S2 domain. The S1 and S2 domains together form the ligand binding domain for the subunit. The crystal structure for the NR1 subunit glycine and NR2 subunit glutamate ligand binding domains have both been reported and are described further in Section 1.4.3. Lastly, the S2 domain is followed by TM4 and an intracellular C-terminal domain.

1.4.3 Ligand binding domains of NMDA receptor subunits

As mentioned above, the activation of NMDA receptors requires the binding of the co-agonists glycine and glutamate. The glycine binding site for NMDA receptors was found to reside in the NR1 subunit and the glutamate binding site were found to be in the NR2 subunit. The location of the binding sites were shown by the expression of NR1 or NR2 subunits alone in either *Xenopus* oocytes or mammalian expression systems and analysed by radioligand binding assays with either glutamate or glycine antagonists to demonstrate, for example, that only NR1 subunits bind glycine antagonists (Grimwood *et al.*, 1995; Kendrick *et al.*, 1996; Chazot *et al.*, 1998). The amino acids vital for glycine and glutamate binding for NMDA receptor subunits were characterised by mutational analysis followed by structural, electrophysiological or radioligand binding characterisation. Amino acids present in both the S1 and the S2 domain were found to be essential for the high affinity binding for glycine or glutamate. The binding of glycine to NR1 subunits was found to be dependent on amino acids in the S1 domain, E388, R390, Y392, Y466, D481, K483, T500, N502 and R505 and in the S2 domain amino acids A696, A714, V717 and D732 (Kuryatov *et al.*, 1994; Wafford *et al.*, 1995; Hirai *et al.*, 1996; Williams *et al.*, 1996; Wood *et al.*, 1997; Armstrong *et al.*, 1998; Sandhu *et al.*, 1999; Foucaud *et al.*, 2003; for review see Lynch and Guttmann, 2001). The binding of glutamate to NR2A subunits was found to be dependent on K456 and H466 of the S1 domain and V666 and T671 in the S2 domain (Laube *et al.*, 1997; Anson *et al.*, 1998). Thus both the S1 and S2 domains form the glycine and glutamate binding domains. The S1 domain is homologous with the bacterial LAOBP which had the X-ray crystallographic structure determined by Oh *et al.* (1993). It was shown that the LAOBP X-ray crystal structure is comprised of 2 globular domains joined together with a short peptide, which forms a 'clamshell' like structure. This 'clamshell' structure was found to exist in an equilibrium between open and closed states (Oh *et al.*, 1993). The binding of the ligand, lysine, stabilized the closed state of the 'clamshell' structure (Oh *et al.*, 1993). The determination of the X-ray crystal structure for the GluR2 AMPA receptor subunit ligand binding domain revealed a similar 'clamshell' structure (Armstrong *et al.*, 1998; Armstrong and Gouaux, 2000; for review see Dingledine *et al.*, 1999). The X-ray crystal structure of the NR1 glycine binding S1S2 domain was

resolved Furukawa and Gouaux (2003) and was shown to have a similar bilobed 'clamshell' structure as found for the GluR2 ligand binding domain. In the presence of the glycine site antagonist, 5,7-dichlorokynurenic acid (DCKA), the 'clamshell' structure was fixed open. Conversely, in the presence of either glycine, D-serine (DS) or D-cycloserine (DCS (DS = an agonist and DCS = a partial agonist)), the structure was stabilized in the closed state (Furukawa and Gouaux, 2003). The X-ray crystal structure of the S1S2 domain for the NR2A subunit with glutamate was resolved by Furukawa *et al.* (2005). The S1S2 domains of NR1 and NR2A subunits are thought to form a NR1-NR2A heterodimer. Disulphide crosslinking at the NR1-NR2A heterodimer interface followed by electrophysiological analysis confirmed the X-ray crystal structure of a NR1-NR2A heterodimer is present in full length receptors (Furukawa *et al.*, 2005).

1.4.4 Quaternary structure of NMDA receptors

Functional NMDA receptors are formed by the co-assembly of NR1 subunits with NR2 and/or NR3 subunits. The molecular sizes of both native and recombinant NMDA receptor complexes have been analysed by a variety of methods. For example, synaptic proteins were isolated, chemically cross-linked, analysed by SDS-PAGE followed by immunoblotting and NMDA receptor complexes with a molecular weight of 603 - 750 kDa were identified (Brose *et al.*, 1993; Blahos and Wenthold, 1996). In addition, recombinant NR1/NR2A/NR2C NMDA receptors were analysed by native PAGE followed by immunoblotting revealing NMDA receptor complexes with a molecular weight of 780 - 850 kDa (Chazot *et al.*, 1994). Further, recombinant NR1/NR2A NMDA receptors were analyzed by blue native PAGE followed by immunoblotting and NMDA receptor complexes with a molecular weight of ~ 860 kDa were identified (Meddows *et al.*, 2001).

Kinetic analysis in the presence of both glutamate and glycine antagonists demonstrated that there are two binding sites per receptor for glutamate and glycine (Benveniste and Mayer, 1991; Clements and Westbrook, 1991). Thus, as NR1 subunits contain the glycine binding site and NR2 subunits contain the glutamate binding site it was thought that NMDA receptors have at least two copies of NR1 subunits and two copies of NR2 subunits to provide two binding sites for glycine and glutamate, respectively. This observation was

supported by the work of Behe *et al.* (1995). A point mutation of N598R in the M2 region of NR1 subunits resulted in characteristic conductance properties. When both wild-type and N598R mutated NR1 subunits were co-expressed with NR2A subunits in *Xenopus* oocytes, conductance properties characteristic of either wild-type receptors, mutant receptors or a population of receptors which gave a median response were observed. It was deduced from this observation that two NR1 subunits were present in NMDA oliogomers (Behe *et al.*, 1995). Therefore the above studies suggested that NMDA receptors assemble as tetramers. Further evidence demonstrating that NMDA receptors are tetrameric was shown by a variety of approaches. The high-affinity binding of glycine and glutamate was shown to be dependent on NR1 E387 and NR2B K387, whilst the mutation of NR1 R505 and NR2B R493 abolished the channel function. The above mutations were used to calculate the number of subunits present per receptor using dose-response relationships, it was calculated that there are two NR1 subunits and two NR2 subunits present in a functional NMDA receptor (Laube *et al.*, 1998). Additional evidence was provided by the crystal structure of the ligand binding core of the NR1-NR2A heterodimer (Furukawa *et al.*, 2005). The NR1-NR2A heterodimer was suggested to be the functional unit in tetrameric NMDA receptors (Furukawa *et al.*, 2005). Lastly, tandem constructs of NR1 and NR2 subunits were generated with one subunit lacking both the C-terminal domain and TM4 allowing the extracellular S2 domain which follows TM3 to be genetically fused to the N-terminal domain of the second subunit. From these studies an NMDA receptor was shown to assemble as a tetramer (Schorge and Colquhoun, 2003). However, some studies have proposed that NMDA receptors exist as pentamers. For example, Hawkins *et al.* (1999) demonstrated by immunoprecipitation experiments, the existence of recombinant NR1/NR2A/NR2B^{FLAG}/NR2B$^{c\text{-}Myc}$ NMDA receptors. A population of NMDA receptors were identified in the adult forebrain which contained NR1 subunits and three NR2 subunits has also been reported (Hawkins *et al.*, 1999). In addition, when N598Q was mutated in both NR1 and NR2B subunits simultaneously this resulted in an intermediate current when expressing a combination of wild-type and mutant subunits in *Xenopus* oocytes. From these results it was concluded that there are three NR1 subunits and two NR2 subunits present per NMDA receptor (Premkumar and Auerbach, 1997).

From the above studies it was shown that two NR1 subunits and two NR2 subunits are present in NMDA receptors (Benveniste and Mayer, 1991; Clements and Westbrook, 1991; Behe *et al.*, 1995). Therefore the predicted molecular size of a NMDA receptor tetramer would be ~ 600 kDa and a pentamer would be ~715 – 780 kDa (assuming that the molecular weight of NR1 and NR2 subunits are 115 and 180 kDa, respectively). Thus, the above molecular size studies suggest that NMDA receptors could assemble as either a tetramer or pentamer. The molecular weight of experimental evidence suggests that NMDA receptors are tetrameric. AMPA receptors have been demonstrated to assemble as tetramers (Mayer, 2006). Since AMPA receptors are also ionotropic glutamate receptors which share some homology with NMDA receptors, this is more supportive data suggesting that NMDA receptors assemble as tetramers.

1.5 NMDA receptor subtypes

As mentioned previously, the obligatory NR1 subunits co-assemble with the modulatory NR2 subunits to form NMDA receptors. The subtypes of NMDA receptors were determined by both immunoprecipitation and electrophysiology studies. As mentioned above in Section 1.4.4, the expression of NMDA receptor subunits in heterologous cells resulted in the co-assembly of NR1/NR2 receptors. Immunoprecipitation studies demonstrated that NR1/NR2 NMDA receptor complexes exist in the brain. For example, NR1/NR2A receptor complexes were identified both in the forebrain and cerebellum of adult mice, NR1/NR2B receptors were found preferentially in the forebrain, NR1/NR2C receptors were found in the cerebellum and NR1/NR2D receptors were present in the forebrain and thalamus (Sheng *et al.*, 1994; Blahos and Wenthold, 1996; Chazot and Stephenson, 1997a; Luo *et al.*, 1997; Dunah *et al.*, 1998; for review see Stephenson, 2001). Lastly, NR1/NR3A and NR1/NR3B receptors were also identified in the brain (Chatterton *et al.*, 2002). In addition to NR1/NR2A, NR1/NR2B, NR1/NR2C, NR1/NR2D and NR1/NR3 NMDA receptors, immunoprecipitation studies have also identified populations of receptors which contain different combinations of subunits. For example, NMDA receptor complexes isolated from rat brains were found to contain two different NR1 isoforms, i.e. C2 (either NR1-1 or NR1-2) and C2' (either NR1-3 or NR1-4) cassettes (Blahos and Wenthold, 1996; Chazot and Stephenson, 1997). Additionally, different

combinations of NR2 subunits have been found present in the same NMDA receptor. NR1/NR2A/NR2B, NR1/NR2A/NR2D and NR1/NR2B/NR2D NMDA receptors were identified in the brain (Sheng *et al.*, 1994; Blahos and Wenthold, 1996; Chazot and Stephenson, 1997a; Luo *et al.*, 1997; Dunah *et al.*, 1998). NR1/NR2A/NR2C NMDA receptors were found to assemble following their co-expression in HEK 293 cells (Chazot *et al.*, 1994). Lastly, NR1/NR2B/NR3A NMDA receptor complexes were identified in cerebrocortical extracts (Das *et al.*, 1998).

Each recombinant NR1/NR2 receptor was found to have unique channel properties which led to their subsequent identification in brain slices. NMDA receptor subtypes are divided into two main classes, 'high conductance' and 'low conductance' (Momiyama *et al.,* 1996). Both recombinant and native NR1/NR2A and NR1/NR2B receptors are considered to have a 'high conductance' whilst NR1/NR2C and NR1/NR2D receptors have a 'low conductance' (Stern *et al.*, 1992; Farrant *et al.*, 1994; Williams, 1995; Takahashi *et al.*, 1996; Buller and Monaghan, 1997; Brimecombe *et al.*, 1997). Further, the NMDA receptor subtypes differ in their single-channel characteristics (Stern *et al.*, 1992), fractional calcium currents (Burnashev *et al.*, 1992), voltage-dependent magnesium blockage (Kutsuwada *et al.*, 1992; Monyer *et al.*, 1992; 1994; Ishii *et al.*, 1993; Momiyama *et al.*, 1996) and their macroscopic kinetic properties (Monyer *et al.*, 1992; 1994). In addition, NR1/NR3A/NR3B receptors were found to be unaffected by the application of glutamate and NMDA when co-expressed in *Xenopus* oocytes (Chatteron *et al.*, 2002). As mentioned previously, NR1 subunits contain the glycine binding site for NMDA receptors, further investigation revealed that NR3 subunits also have a glycine binding site (Madry *et al.*, 2007; Awobuluyi *et al.*, 2007). The application of glycine to NR1/NR3 receptors resulted in their activation when co-expressed in *Xenopus* oocytes (Madry *et al.*, 2007; Awobuluyi *et al.*, 2007). Thus, each receptor subtype was found to have distinct properties that correlates with the *in vivo* receptor characterisation by immunoprecipitation studies, i.e. NR1/NR2A, NR1/NR2B, NR1/NR2C and NR1/NR2D NMDA receptors form the major subtypes found in the brain. However, as found in immunoprecipitation studies, the existence of NMDA receptors containing two different NR2 subunits have been identified *in vivo* by electrophysiology. For example, NR1/NR2A/NR2B NMDA receptors were

observed in the brain by electrophysiological studies (Tovar and Westbrook, 1999; Thomas *et al.*, 2006). Additionally, NR1/NR2A/NR2C, NR1/NR2A/NR2D and NR1/NR2B/NR2D NMDA receptors were shown to assemble following their co-expression in *Xenopus* oocytes (Wafford *et al.*, 1993; Buller and Monaghan, 1997; Cheffings and Colquhoun, 2000). The expression of NR1/NR2A/NR3A NMDA receptors in *Xenopus* oocytes were found to have a smaller unitary conductance, a shorter open time and lower calcium permeability (Das *et al.*, 1998). Thus again demonstrating that the combination of subunits present in functional NMDA receptors influences their properties. Table 1.1 summarises the different properties of each major NMDA receptor subtype.

NMDA receptor subtype	**Magnesium sensitivity**	**Conductance**	**Distribution**
NR1/NR2A	High	High	Forebrain and cerebellum
NR1/NR2B	High	High	Forebrain
NR1/NR2C	Low	Low	Cerebellum
NR1/NR2D	Low	Low	Forebrain and thalamus.
NR1/NR2A/NR2B	Combination of two NR2 properties	Combination of two NR2 properties	Not determined
NR1/NR2A/NR2C	Combination of two NR2 properties	Combination of two NR2 properties	Not determined
NR1/NR2A/NR2D	Combination of two NR2 properties	Combination of two NR2 properties	Not determined
NR1/NR2B/NR2D	Combination of two NR2 properties	Combination of two NR2 properties	Not determined
NR1/NR3A	Low	Low	Amygdala, brainstem, hippocampus, hypothalamus, spinal cord and thalamus
NR1/NR3B	Low	Low	Cortex and thalamus

Table 1.1 Table summarising the major properties and locations of the major NMDA receptor subtypes

The functional significances of NMDA receptor subunits were demonstrated by the generation of knock-out mice. $NR1^{-/-}$ and $NR2B^{-/-}$ knock-out mice died shortly after birth (Forrest *et al.*, 1994; Li *et al.*, 1994; Kutsuwada *et al.*, 1996). However, $NR2A^{-/-}$, $NR2C^{-/-}$ and $NR2D^{-/-}$ knock-out mice survived and developed normally. Further analysis revealed that $NR2A^{-/-}$ knock-out mice had a reduced hippocampal LTP and an impaired spatial and

contextual learning (Sakimura *et al.*, 1995; Kiyama *et al.*, 1998). A difference in the conductance properties was observed in cerebellar granule cells of $NR2C^{-/-}$ knock-out mice (Ebralidze *et al.*, 1996). A double knock-out of both NR2A and NR2C genes resulted in motor discoordination which was not observed for the respective single knock-out mice (Kadotani *et al.*, 1996). $NR2D^{-/-}$ knock-out mice displayed a reduced spontaneous activity (Ikeda *et al.*, 1995). Therefore, although the NR1 and NR2B subunits are vital for development, the other NR2 subunits are required for specific functions. The NR2 subunits all have extended C-terminal domains which are thought to link NMDA receptors to their respective downstream signalling pathways, which are described in more detail below. The functional significance of the NR2 C-terminal domains was investigated by the generation of $NR2^{\Delta C/\Delta C}$ mice which expressed the NR2 subunit minus the C-terminal domains. $NR2A^{\Delta C/\Delta C}$ mice displayed impaired synaptic plasticity and contextual memory, $NR2B^{\Delta C/\Delta C}$ mice died perinatally and $NR2C^{\Delta C/\Delta C}$ mice had defects with their motor coordination (Sprengel *et al.*, 1998). These observed phenotypes are similar to the knock-out mice of the complete subunit. Thus, this demonstrates the importance of the NR2 C-terminal domains which link NMDA receptors to their downstream signalling pathways. However, NMDA receptors were still trafficked to the cell surface in the absence of their NR2 C-terminal domains. For example, hippocampal Schaffer collateral-CA1 pyramidal cell synapses prepared from $NR2A^{\Delta C/\Delta C}$ mice had a decrease in the cluster frequencies of synaptic NR2A-containing NMDA receptors whilst the total receptor numbers remained unchanged in extrasynaptic sites (Steigerwald *et al.*, 2000). Both embryonic neocortical and cerebral neurones prepared from $NR2B^{\Delta C/\Delta C}$ mice, when hand reared, also showed a decrease in the number of synaptic receptors but the resulting conductance was similar to that observed from wild-type mice (Mori *et al.,* 1998; Mohrmann *et al.*, 2002).

As well as differences in functional properties, the major NMDA receptor subtypes have different pharmacological properties, different cellular and sub-cellular localisations and developmental patterns of expression. With regard to the pharmacological characterisation of NMDA receptor subtypes, a selective antagonist, ifenprodil was identified for NR1-1a/NR2B NMDA receptors (Williams, 1993). Ifenprodil was found to have a 400-fold lower affinity for recombinant NR1-1a/NR2A receptors when compared to recombinant

NR1-1a/NR2B receptors (Williams, 1993). It is a voltage-independent, non-competitive antagonist that binds to the N-terminal domain of NR2B subunits (Gallagher *et al.*, 1996; Perin-Dureau *et al.*, 2002). The binding site for ifenprodil was localised in the cleft formed of the 'clamshell' structure of the LIVBP domain of NR2B subunits. Further, the amino acids found to be essential for the binding of ifenprodil were identified as being NR2B V42, D101, T103, D104, E106, I150, F176, F182, T223, K234, E236, L261, G264 and R337 which are all present in the two lobes of the LIVBP domain which are in the centre of the cleft (Gallagher *et al.*, 1996; Perin-Dureau *et al.*, 2002). The identification of NVP-AAM077, from Novartis, was thought to be a selective NR1/NR2A antagonist (Liu *et al.*, 2004). However, further study revealed that there was only a 10-fold difference in the affinity of NVP-AAM077 to NR2A- and NR2B-containing receptors (Neyton and Paoletti, 2006). It was also shown to be a strong antagonist for NR2C- and NR2D-containing receptors (Feng *et al.*, 2004). NR1/NR2A NMDA receptors were found to be inhibited by nanomolar concentrations of zinc ions (Paoletti *et al.*, 1997; Choi and Lipton, 1999). The voltage-dependent inhibition from zinc ions was similar when comparing recombinant NR1-1a/NR2A and NR1-1a/NR2B receptors. However, the voltage-independent inhibition was found to occur at lower zinc ion concentrations for NR1-1a/NR2A receptors (Paoletti *et al.*, 1997). The zinc ions bind to the N-terminal domain of NR2A subunits in a similar fashion as the binding of ifenprodil to NR2B subunits.

The NMDA receptor subunits also show a distinct pattern of expression. Messenger ribonucleic acid (mRNA) encoding the NR1 subunit is present throughout the mature rat brain (Moriyoshi *et al.*, 1991; Monyer *et al.*, 1992; Brose *et al.*, 1993). The highest expression of NR1 mRNA and protein was found in the cerebellum, cerebral cortex, hippocampus, hypothalamus and olfactory bulb (Moriyoshi *et al.*, 1991). In contrast to the ubiquitous expression of NR1 subunits in the brain, the different NR2 subunits show a more selective distribution of expression. The distribution of NR2 subunits in the brain have been addressed by both *in situ* hybridization and immunocytochemistry. NR2A subunits were found to be expressed in the cerebral cortex, forebrain and hippocampus (Monyer *et al.*, 1992; Wang *et al.*, 1995; Wenzel *et al.*, 1995; Portera-Cailliau *et al.*, 1996; Laurie *et al.*, 1997). NR2A subunits are undetected at postnatal day 2 (P2) and their

expression levels increase from P12 into the mature brain (Wang *et al.*, 1995; Portera-Cailliau *et al.*, 1996). NR2B subunits are also mainly expressed in the cerebral cortex, forebrain and hippocampus (Monyer *et al.*, 1992; Wang *et al.*, 1995; Wenzel *et al.*, 1995; Portera-Cailliau *et al.*, 1996; Laurie *et al.*, 1997; Thompson *et al.*, 2000). However, the expression levels of NR2B are down-regulated in the mature brain. NR2B subunits show their highest level of expression neonatally and in the early postnatal brain after which their expression declines at P22 (Wang *et al.*, 1995; Portera-Cailliau *et al.*, 1996). Therefore a developmental switch is observed between the expression of NR2A and NR2B subunits. In addition, NR2D subunits are developmentally expressed. NR2D subunits are highly expressed during the embryonic stages of development and rise to their highest levels at P7 after which a decline is observed (Dunah *et al.*, 1996; Monyer *et al.*, 1994). NR2D subunits are expressed highly in the brainstem, hippocampus, midbrain structures and thalamus (Dunah *et al.*, 1998; Thompson *et al.*, 2002; Laurie *et al.*, 1997). Lastly, NR2C subunits are highly concentrated in the cerebellum but also found in the olfactory bulb and thalamus (Monyer *et al.*, 1992; Farrant et al., 1994; Wenzel *et al.*, 1995; Laurie *et al.*, 1997). Similar to NR2A subunit expression, the NR2C subunit is only expressed in the mature brain where expression is detected from P9 onwards (Monyer *et al.*, 1994).

The major subtypes of NMDA receptors are preferentially located in different sub-cellular locations, i.e. synaptic or extra-synaptic sites. For example, NR1/NR2D NMDA receptors are thought to be located at extra-synaptic sites (Misra *et al.*, 2000; Brickley *et al.*, 2003). As described above, there is a developmental switch between the expression of NR2A and NR2B subunits. NR2B-containing NMDA receptors form a major population of synaptic receptors in the immature brain (Kew *et al.*, 1998; Li *et al.*, 1998; Tovar and Westbrook, 1999). In the mature brain the number of NR2A-containing receptors increases to become the major population of synaptic NMDA receptors whilst NR2B-containing receptors are thought to be located in extra-synaptic sites (Flint *et al.*, 1997; Li *et al.*, 1998; Stocca and Vicini, 1998; Tovar and Westbrook, 1999; Mohrmann *et al.*, 2000; Townsend *et al.*, 2003). However, the evidence does not provide such a clear cut division between NR2A-containing receptors always being present in synaptic sites and NR2B-containing receptors always present in extra-synaptic locations (Stocca and Vincini, 1998; Townsend *et al.*,

2003). Indeed, Thomas *et al.* (2006) demonstrated that NR2B-containing NMDA receptors can be present in synaptic sites and NR2A-containing NMDA receptors are also located in extra-synaptic sites in hippocampal neurons. It was thought that the different use of either NMDA receptor specific subtype antagonists or the blockage of synaptic receptors using the NMDA receptor open channel blocker, MK-801, resulted in the discrepancy between the results (Thomas *et al.*, 2006). Indeed it was recently demonstrated that NR2A- and NR2B-containing NMDA receptors move between synaptic and extra-synaptic sites in neurones (Groc *et al.*, 2006). This demonstrates that NMDA receptors are mobile at the cell surface and are not statically expressed within one site.

The localisation of NMDA receptors has been found to influence their downstream signalling pathways. For example, it was demonstrated by a pharmacological approach that extra-synaptic NMDA receptors inhibited the CREB pathway leading to neurotoxicity. In contrast, synaptic NMDA receptors activated the CREB pathway, which were found to be anti-apoptotic (Hardingham *et al.*, 2002). In addition to the CREB pathway, the Ras/ERK pathway is differentially regulated by synaptic and extra-synaptic NMDA receptors. Ivanov *et al.* (2006) found that extra-synaptic NMDA receptors inhibited the ERK pathway whilst synaptic NMDA receptors activated the ERK pathway. The ERK pathway drives GluR1-containing AMPA receptors into the synapse and thus is a form of LTP. Conversely, a decrease in the cell surface expression of GluR1-containing AMPA receptors is a form of LTD. This was found to be NMDA receptor subtype specific as either incubation with ifenprodil, over-expression of NR2B subunits or RNAi against NR2A subunits in hippocampal neurones all resulted in a decrease of ~ 40 % of GluR1-containing AMPA receptor cell surface expression (Kim *et al.*, 2005), thus demonstrating that NR2B-containing NMDA receptors reduced the cell surface expression of GluR1-containing AMPA receptors. Further, the stimulation of synaptic NMDA receptors resulted in an increase in the GluR1-containing AMPA receptor cell surface expression (Kim *et al.*, 2005).

1.6 Assembly and trafficking of NMDA receptors

Membrane proteins are translated, assembled and folded in the endoplasmic reticulum (ER). During each stage of assembly the membrane proteins must pass quality control check points to ensure they are correctly folded and assembled before being forward trafficked to the cell surface. Once translated in the ER, membrane proteins are often associated with ER-resident chaperone and folding proteins. Chaperone and folding proteins associate with newly synthesised proteins to ensure that they fold into the correct conformation. For example, the chaperone proteins calnexin and calreticulin bind to immature glycoproteins and assist with their folding. This stage of quality control is considered the 'primary quality control' stage. The 'secondary quality control' is specific to individual proteins. For example, the protein may have ER retention signals such as the H/KDEL motif for soluble proteins and di-lysine (e.g. KKXX) or di-arginine (e.g. RXR) motifs for membrane proteins. ER retention signals may be exposed once the membrane protein folds into the correct conformation. These signals are often then subsequently sterically masked either by the binding of another subunit or another protein such as a scaffolding protein enabling forward trafficking. The membrane protein is then packaged into COPII-containing vesicles and forward trafficked to the Golgi apparatus. The newly made membrane proteins bear oligosaccharide chains made from a series of mannose repeats. These oligosaccharide chains are modified by enzymes present in the Golgi apparatus which remove the mannose groups from the proteins and complex mannose chains are generated by the addition of galactose and N-acetylneuraminic acid residues. In addition, the proteins may be phosphorylated and further checks are carried out to ensure that the mature protein has the correct conformation in the Golgi apparatus. The correctly folded mature proteins are then forward trafficked from the Golgi apparatus to the cell surface membrane via kinesin- or exocyst-dependent vesicles. Misfolded proteins are packaged into COPI-containing vesicles and are trafficked back to the ER and subsequently degraded via the ER-associated degradation (ERAD) process (for review see Teasdale and Jackson, 1996; Ellgaard and Helenius, 2003; Fleck, 2006).

The cell surface expression of membrane proteins can be regulated by motifs found in their intracellular domains. For example, YXXΦ (where X is any amino acid and Φ is a

hydrophobic amino acid) and dileucine motifs. These motifs serve as interaction sites for adaptor proteins. This YXXΦ motif is recognised by adaptor protein (AP) complexes. Each AP complex is composed of four separate proteins which are indicated in brackets; AP-1 (γ-ß1-μ1-σ1), AP-2 (α-ß2-μ2-σ2), AP-3 (δ-ß3-μ3-σ3) or AP-4 (ϵ-ß4-μ4-σ4). Each AP complex has its own specificity in recognising their protein interactors (for review see Bonifacino and Dell'Angelica, 1999). Proteins containing the dileucine motif are internalised via a different family of adaptor proteins known as the Golgi-localized, γear-containing ARF-binding (GGA) proteins. In addition to the above interaction motifs, cell surface membrane proteins can also be ubiquitinated on intracellular lysine residues which provides a signal for their internalisation (for review see Bonifacino and Traub, 2003). Once internalised, membrane proteins face one of two fates; they are either recycled back to the cell membrane or they are degraded (for review see Robinson *et al.*, 1996). A summary of the synthesis, trafficking and endocytosis of transmembrane receptors is shown in Figure 1.5.

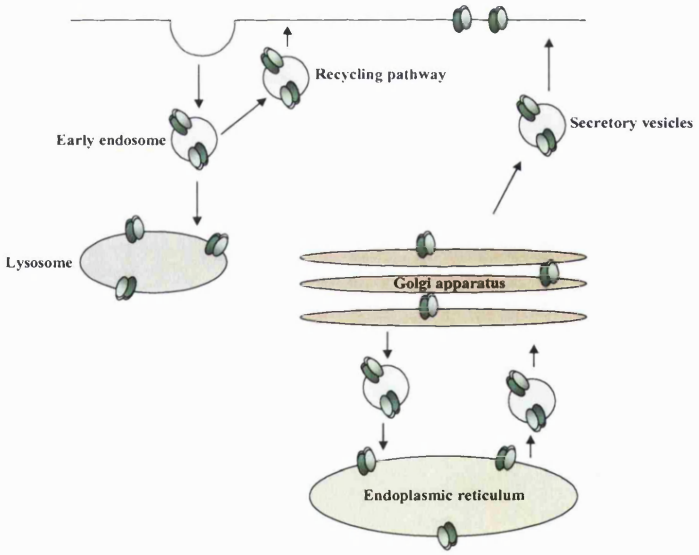

Figure 1.5 Schematic diagram summarising the synthesis, trafficking and endocytosis of transmembrane receptors

Transmembrane proteins are synthesised and assembled in the endoplasmic reticulum (ER). They are then packaged into vesicles and forward transported to the Golgi apparatus where they are further processed. If the proteins are miss-folded at this stage they are retrograde transported back to the ER for degradation. Mature proteins are transported in secretory vesicles to the cell surface. Internalised proteins face one of two fates; they are either degraded or recycled back to the cell membrane.

1.6.1 Assembly of NMDA receptors

As previously mentioned, the formation of functional NMDA receptors requires the co-assembly of both NR1 and NR2 subunits. The first step in the assembly of NMDA receptors is thought to be the formation of dimers which are then assembled as a dimer of dimers. As described in Section 1.4.4, tandem constructs of NR1 and NR2 subunits were generated with one subunit lacking the C-terminal domain and TM4 allowing the extracellular S2 domain which follows TM3 to be genetically fused to the N-terminal domain of the second subunit. From these constructs it was deduced that NMDA receptors probably assemble as a dimer of dimers (Schorge and Colquhoun, 2003). The specific determinants required for the assembly of NMDA receptors from NR1 and NR2 subunits has been investigated by the generation of point mutations, deletions and chimeras following their expression in heterologous cell lines. As mentioned in Section 1.4.2, the N-terminal domain of NMDA receptors can be divided into two separate domains, the LIVBP domain and the S1 domain, see Figure 1.4. Meddows *et al.* (2001) created a series of deletions in the NR1 N-terminal domain and found that the deletion of amino acids 1-380, i.e. the whole LIVBP domain, resulted in no cell surface expression of NR1/NR2A NMDA receptors when expressed in HEK 293 cells. This demonstrated that the N-terminal domain of NR1 subunits is vital for the cell surface expression of NMDA receptors. In another report, NR1-2a$^{c\text{-}Myc}$ epitope-tagged subunits where the c-Myc tag was inserted after amino acid 81 in the LIVBP domain, resulted in no cell surface expression of NR1-2a$^{c\text{-}Myc}$/NR2A NMDA receptors following their co-expression in HEK 293 cells (Papadakis *et al.*, 2004). Although no cell surface expression was observed, both immunoprecipitation and radioligand binding studies revealed that NR1-2a$^{c\text{-}Myc}$ subunits associated with NR2A subunits but these receptor complexes were retained the in ER (Papadakis *et al.*, 2004). A high molecular weight immunoreactive band for NR1-2a subunits of ~ 226 kDa which corresponded to the size of a NR1-NR1 dimer was observed in immunoblots from recombinant NR1-2a/NR2A receptors (Papadakis *et al.*, 2004). However this ~ 226 kDa immunoreactive band was absent from recombinant NR1-2a$^{c\text{-}Myc}$/NR2A NMDA receptors (Papadakis *et al.*, 2004). The insertion of the c-Myc tag at amino acid 81 was close to a cysteine residue at position 79 resulting in the hypothesis that cysteine residues may be involved in disulphide bridges between NR1 subunits. Of the three cysteine residues found

in the NR1-2a LIVBP domain, point mutations of C79A and C308A resulted in an impaired cell surface expression of NR1-2a^{C79A}/NR2A and NR1-2a^{C308A}/NR2A NMDA receptors. Further, C79 of NR1 subunits was found to be responsible for the formation of NR1-NR1 inter-subunit disulphide bridges, i.e. NR1-NR1 dimers (Papadakis *et al.*, 2004). As shown in Papadakis *et al.* (2004), NR1-NR1 dimer formation was also shown by using fluorescently tagged NR1 subunits and fluorescence resonance energy transfer (FRET) measurements (Qiu *et al.*, 2005). Using a similar FRET approach, fluorescently tagged NR2A and NR2B subunits also resulted in the formation of NR2A-NR2A, NR2B-NR2B and NR2A-NR2B dimers (Qiu *et al.*, 2005). The formation of NR2B-NR2B dimers was found to be independent of the NR2B C-terminal domain (Yang *et al.*, 2007). This was demonstrated by the deletion of the C-terminal domain from expressed NR2B subunits and the subsequent observation of NR2B^{TRUNC}-NR2B^{TRUNC} dimer formation (Yang *et al.*, 2007). Conversely, the X-ray crystal structure of the S1S2 domains of NR1 and NR2A subunits have been shown to form a NR1-NR2A heterodimer. Disulphide crosslinking at the NR1-NR2A heterodimer interface followed by electrophysiological analysis confirmed the X-ray crystal structure of a NR1-NR2A heterodimer present in full length receptors (Furukawa *et al.*, 2005).

In agreement with NMDA receptors co-assembling as dimer of dimers, AMPA receptors are also thought to assemble in a similar fashion. The initial formation of dimers for AMPA receptor subunits was found to be mediated by their N-terminal LIVBP domain (Ayalon and Stern-Bach, 2001). The specific regulation of assembly was investigated using chimeras of GluR3 AMPA receptor subunits and GluR6 kainate receptor subunits. The N-terminal LIVBP domains of both subunits were divided into four regions, N1-N4 and chimeras containing different combinations were generated. It was deduced that exchanging the N1 and N3 regions was required for the heteromerization of subunits but protein-protein interactions were still observed. Whilst exchanging the N2 and N4 regions resulted in a decreased homomeric activity but heteromerization of subunits still remained. The N1 region was found to be required for the formation of dimers (Ayalon *et al.*, 2005). The finding that the N1 region of AMPA receptor subunits are required for the formation of

dimers is in agreement with that by Papadakis *et al.* (2004), who demonstrated that C79 of NR1-2a subunits was vital for dimer formation.

As mentioned above, NMDA receptors are thought to assemble as a dimer of dimers. This co-assembly of NR1 and NR2A subunits was found to occur in the ER by use of Brefeldin-A, a drug which inhibits the trafficking of proteins out of the ER (McIlhinney *et al.,* 1998). As described more in Section 1.6.2, the successful expression of NMDA receptors requires the co-expression of NR1 and NR2 subunits. NR2A subunits are retained in the ER in heterologous cell lines, unless they are co-expressed with NR1 subunits to form heteromeric complexes (McIlhinney *et al.,* 1998). NR2 subunits were also found to be retained in the ER in CA1 pyramidal hippocampal neurones prepared from $NR1^{-/-}$ knock-out mice which again demonstrated that NR1/NR2 NMDA receptors must be co-assembled before their release from the ER (Fukaya *et al.*, 2003). *In vivo,* neurones contain a pool of unassembled NR1 subunits (Chazot and Stephenson, 1997b; Huh and Wenthold, 1999; Vazhappilly and Sucher, 2002). This pool of unassembled NR1 subunits were found to be rapidly turned over with a half-life of 2 h compared to a 34 h half-life for NR1 subunits when assembled as NR1/NR2 NMDA receptors (Huh and Wenthold, 1998). Thus due to the presence of this unassembled pool of NR1 subunits in the ER, it was hypothesised that the rate limiting factor in the assembly of NMDA receptors was the translation of NR2 subunits (Prybylowski *et al.*, 2002).

1.6.2 Trafficking of NMDA Receptors

NMDA receptors have specific 'secondary quality control' signals that have been identified in both NR1 and NR2 C-terminal domains. The NR1 isoforms were found to be differentially trafficked to the cell surface. NR1-1a,b subunits were not expressed on the cell surface unless co-expressed with either NR1-4b or NR2B subunits (Okabe *et al.*, 1999). However, NR1-2a,b, NR1-3a,b and NR1-4a,b subunits were all expressed on the cell surface in fibroblasts in the absence of NR2 subunits (Okabe *et al.*, 1999). The different C-terminal domains of the NR1 isoforms were genetically fused onto the human interleukin-2 receptor α subunit (Tac) receptor to generate Tac chimeras. Tac receptors are normally constitutively expressed on the cell surface of neurones and heterologous cell lines (Roche

et al., 2001). Therefore any differences observed in the Tac chimera cell surface expression is a result of regulation by the NR1 C-terminal domain. Tac chimeras not containing the NR1 C1 cassette were trafficked to the cell surface more efficiently than the Tac-C1 and Tac-C0-C1-C2 chimeras (Scott *et al.*, 2001). Further investigation using the above Tac NR1 chimeras revealed that an RRR (amino acids 893-895) motif present in the NR1 C1 cassette acted as an ER retention motif (Standley *et al.*, 2000; Scott *et al.*, 2001; Xia *et al.*, 2001). This ER retention motif was found to be regulated by phosphorylation of serine residues found adjacent to the RRR motif. Phosphomimetic mutations of S896E and S897E overcame the ER retention caused by the NR1 C1 cassette (Scott *et al.*, 2001; Xia *et al.*, 2001). Although NR1-1a,b and NR1-3a,b subunits both contain the NR1 C1 cassette, NR1-3a,b subunits were expressed on the cell surface whilst NR1-1a,b subunits were not. NR1-1a,b subunits contain the NR1 C2 cassette whilst NR1-3a,b subunits contain the NR1 C2' cassette, see Figure 1.3. The ER retention caused by the NR1 C1 cassette was found to be overcome if the NR1 C2' cassette was present in the same C-terminal domain (Scott *et al.*, 2001; Xia *et al.*, 2001). The last five amino acids present on the C2' cassette, VSTVV, were found to be vital to promote the release of the ER retention (Scott *et al.*, 2001; Xia *et al.*, 2001). It was hypothesised that the association of NR1 isoforms containing the NR1 C2' cassette with a post-synaptic density-95 (PSD-95), drosophila discs-large (dlg) and zonal occludence 1 (ZO-1) (PDZ) domain-containing protein masked the ER retention signal found on the NR1 C1 cassette, (Standley *et al.*, 2000). (PSD-95 and PDZ-containing proteins are described in more detail in Sections 1.8 and 1.9). All of the above studies were carried out on the single NR1 subunits and NR1 Tac chimeras and the function of this identified RRR motif has not been investigated for assembled NMDA receptors. Thus the association of NR2 subunits with NR1 subunits to form NMDA receptors may mask this RRR motif. For example, the cell surface expression of $GABA_B$ receptors requires the co-assembly of GB1 and GB2 subunits. The GB1 subunit contains the RRR motif which acts as an ER retention motif that is masked when co-assembled with GB2 subunits (Margeta-Mitrovic *et al.*, 2000).

The ER retention of NR2B subunits was also investigated by the Tac chimera approach. It was found that Tac-NR2B chimeras containing amino acids 1315-1482 of the NR2B C-terminal domain were trafficked to the cell surface which indicated that the ER retention

motifs were not located within this region (Hawkins *et al.*, 2004). Further truncations of the NR2B C-terminal domain at Y1040 and Y985 resulted in an increased cell surface expression of Tac-NR2B chimeras (Hawkins *et al.*, 2004). Putative ER retention motifs were identified within this deleted region of the NR2B C-terminal domain as KRRK, KKR and RRR (amino acids 1079-1082, 1090-1092 and 1100-1102, respectively) however mutation of these motifs resulted in no change in the Tac-NR2B chimera cell surface expression (Hawkins *et al.*, 2004). However, the NR2B C-terminal domain was found to have an ER export motif, HLFY, amino acids 840-843 (Hawkins *et al.*, 2004). Further analysis revealed that this HLFY motif was vital for the export of assembled NR1/NR2B NMDA receptors following their expression in HEK 293 cells (Hawkins *et al.*, 2004). This motif was recently further refined by Yang *et al.* (2007), who found that a EHL motif (amino acids 839-841 for NR2B subunits and amino acids 838-840 for NR2A subunits) was responsible for the delivery of functional NMDA receptors to the cell surface in HEK 293 cells. Thus the overlapping EHL/HLFY motif present at the beginning of the predicted C-terminal domains of NR2A and NR2B subunits appears to play a role in the export of assembled receptors from the ER.

1.6.3 Trafficking of NMDA receptors to the cell surface membrane

Once NMDA receptors have been co-assembled they are trafficked to the cell membrane via three different mechanisms, a kinesin superfamily 17 (KIF17) complex, the exocyst complex and a mammalian homologue of Drosophila melanogaster partner of inscuteable (mPins) complex. The first mechanism of NMDA receptor trafficking to be identified was via a motor dependent vesicle transport complex, the KIF17 complex. NR2B-containing NMDA receptor/mLin-7/mLin-2/mLin-10/KIF17 complexes were found to be present in the brain, where KIF17 is a motor protein and the mLin proteins act as adaptor proteins (Setou *et al.*, 2000). The KIF17 complex was demonstrated not to enter post-synaptic sites, rather it transported NR2B-containing NMDA receptors to extra-synaptic regions (Guillaud *et al.*, 2003). The over-expression of KIF17 in transgenic mice resulted in an increase in the NR2B-containing NMDA receptor expression and conversely, knock-down of KIF17 expression resulted in a decrease of NR2B subunit expression thus substantiating the role of the KIF17 complex in the trafficking of NR2B-containing NMDA receptors to

the cell membrane (Wong *et al.*, 2002; Guillaud *et al.*, 2003). In addition to the KIF17 complex, an exocyst complex was also found to traffic NMDA receptors to the cell surface. NR2B-containing NMDA receptor/synapse associated protein102 (SAP102)/Sec8 complexes were found in the brain, where Sec8 is a component of the exocyst complex (Sans *et al.*, 2003; for review see Lipschutz and Mostov, 2002). Lastly, both NR2B-containing NMDA receptor/SAP102/mPins and NR2B-containing NMDA receptors/PSD-95/mPins complexes were found in the brain (Sans *et al.*, 2005). It was demonstrated that in *Drosophila,* Pins interacts with a PSD-95 homolog, Discs large and this complex is involved in the Frizzled signalling pathway which regulates cell polarity and asymmetric cell division (Bellaiche *et al.*, 2001). It is notable that in each of these trafficking mechanisms a PSD-95 membrane associated guanylate kinase (MAGUK) family member is involved. In addition, both the exocyst complex and the mPins complex were found to be formed in the ER demonstrating that the PSD-95 MAGUK family can associate with NMDA receptors early during the secretory pathway (Sans *et al.*, 2003; 2005). All of the studies to date have focused on NR2B-containing NMDA receptors.

1.6.4 Regulation of the cell surface expression of NMDA receptors

Once NMDA receptors are expressed at the cell surface, a number of regulatory mechanisms have been identified which control their stability. This cell surface regulation of NMDA receptors has been investigated by the use of Tac chimeras and yeast two-hybrid interaction studies. The major focus of these studies has been on the NR2A and NR2B C-terminal domains. The determinants of the cell surface expression of NR2B-containing NMDA receptors was investigated by using Tac-NR2B chimeras which had amino acids 1315-1482 of the NR2B C-terminal domain genetically fused to the Tac receptor. Like all NR2 subunits, the last for amino acids of the NR2B C-terminal domain are the ESDV PDZ domain interaction motif, which is described in more detail in Section 1.9. The deletion of the last 7 amino acids on the Tac-NR2B chimera resulted in an increased internalisation rate. However, deletion of the last 11 amino acids from the NR2B C-terminal domain resulted in a reduced internalisation rate (Roche *et al.*, 2001). Closer inspection of the amino acid sequence revealed an internalisation consensus motif, YEKL was present within the last 11 amino acids of the NR2B C-terminal domain. Indeed, a point mutation of

Y1472A, i.e. YEKL → AEKL, resulted in a decrease in the observed internalisation rate when Tac-NR2B^{Y1472A} chimeras were expressed in both Henrietta Lack (HeLa) cells and in hippocampal neurones (Lavezzari *et al.*, 2003). These motifs were also found to regulate the sub-cellular localisation of NR2B-containing NMDA receptors in hippocampal neurones. Single Y1472A or double point mutations of Y1472A and S1480A (a mutation in the PDZ domain binding motif, i.e. ESDV → EADV) resulted in NR2B-containing receptors localising in synaptic sites in hippocampal neurones at a higher density compared to wild-type receptors (Prybylowski *et al.*, 2005). The internalisation of NR2B-containing NMDA receptors was found to be regulated by the phosphorylation of Y1472 present in the YEKL motif. This phosphorylation of Y1472 disrupted the interaction between NR2B-containing NMDA receptors and the scaffolding protein PSD-95, thus promoting the internalization of the receptor (Nakazawa *et al.*, 2001). This tyrosine residue is also conserved in the NR2A C-terminal domain, where a putative internalisation motif, YKKM, is present. However, Tac-NR2A chimeras (containing amino acids 1304-1482 of the NR2A C-terminal domain) with a deletion of the last 11 amino acids did not show any change in their internalisation rates (Lavezzari *et al.*, 2004). Rather than a tyrosine based internalisation motif, the NR2A C-terminal domain was found to have a dileucine internalisation motif. The point mutation of L1320A resulted in a decrease in the internalisation of Tac-NR2A^{L1320A} chimeras (Lavezzari *et al.*, 2004). As mentioned above, the YXXΦ motifs are known to bind adaptor protein complexes. It was found that the NR2B C-terminal domain interacts with the adaptor protein, μ2. This interaction was abolished by the point mutation of Y1472A (Lavezzari *et al.*, 2003). Additionally, a strong interaction was observed between the NR2A and NR2B C-terminal domains and the μ1 and μ4 adaptor proteins, whilst the NR2A C-terminal domain only weakly associated with μ2 (Lavezzari *et al.*, 2004). This suggests there is a differential interaction and regulation of NR2A- and NR2B-containing NMDA receptors.

NMDA receptors have also been found to be ubiquitinated which controls their cell surface expression. Strangely, it was found that the N-terminal domain of NR1 subunits interacted with the F-box protein Fbx2, which is known to link protein substrates to the ubiquitin E3 ligase, a member of the ubiquitin conjugation complex (Kato *et al.*, 2005). Lastly, glycine

was shown to prime the clathrin-dependent internalisation of NMDA receptors (Nong *et al.*, 2003).

Once internalised, NMDA receptor subtypes are thought to undergo either the recycling or the degradation pathway. When NR1/NR2B NMDA receptors are expressed in hippocampal neurones robust recycling is observed. However, removal of the whole NR2B C-terminal domain resulted in only 20 % of the receptor being recycled (Scott *et al.*, 2004). Tac chimeras demonstrated that the first 20 amino acids present on the C-terminal domain of either NR1, NR2A or NR2B subunits promoted the internalisation of the receptor and they showed a preference for the degradation pathway (Scott *et al.*, 2004). It was hypothesised that both NR1 and NR2 subunits contain primary endocytosis signals which are additive and these motifs form an endocytic ring near the intracellular mouth of the NMDA receptor (Scott *et al.*, 2004). Interestingly, Lavezzari *et al.* (2004) demonstrated that ~ 50 % Tac-NR2B chimeras co-localised with the recycling endosome marker, Rab11, compared to ~ 25 % of Tac-NR2A chimeras. The Tac-NR2A chimeras showed higher co-localisation with the late endosome marker, Rab9 (Lavezzari *et al.*, 2004). This suggests that NR2A-containing NMDA receptors favour degradation whilst NR2B-containing NMDA receptors favour recycling.

1.7 The membrane associated guanylate kinase (MAGUK) family of proteins

The PSD-95 family of proteins are a sub-family of a larger group of proteins known as the MAGUK family. The MAGUK family of scaffolding proteins are multi-domain containing proteins which link proteins together forming intracellular signalling pathways. The family contains a diverse range of proteins with the distinguishing feature that links them together being a guanylate kinase-like (GK) domain present in each protein. Although the GK-like domain shares ~ 40% sequence identity with the yeast guanylate kinase it does not have any catalytic activity (Olsen and Bredt, 2003). In addition to the GK-like domain, all family members also contain one or more copies of a PDZ domain, which was named after the first proteins this protein-protein interaction domain was identified in; PSD-95, drosophila discs-large (dlg) and the tight junction protein zonal occludence 1 (ZO-1). The GK-like and PDZ domains are described in more detail in Section 1.9. The MAGUK

family of proteins are divided into 5 major sub-families according to their amino acid identities (Montogomery *et al.*, 2004). The first sub-family of MAGUKs are the p55 proteins, which also includes VAM1 and DLG2. These proteins are characterised by containing a single PDZ domain, a Src homology 3 (SH3) domain and GK-like domain. The second sub-family contains two PDZ domains, a single GK-like domain and an SH3 domain, and has members including PALS1 and CARD11. Thirdly, a sub-family which includes the ZO proteins contains three N-terminal PDZ domains, a SH3 domain and a GK-like domain. The fourth sub-family contains proteins such as MAGI and S-SCAM contains two WW domains, an N-terminal GK-like domain followed by 5 PDZ domains. Lastly, and the focus in this thesis is the PSD-95 family, which have three N-terminal PDZ domains, an SH3 domain and a GK-like domain. The PSD-95 MAGUK family comprises of PSD-95 (alternative nomenclature SAP90, Cho *et al.*, 1992; Kistner *et al.*, 1993), channel-associated protein of synapses-110 (chapsyn-110, PSD-93, Kim *et al.*, 1995; 1996a; Brenman *et al.*, 1996a), SAP97 (hDlg, Muller *et al.*, 1995) and SAP102 (NE-dlg, Muller *et al.*, 1996). A schematic diagram of the PSD-95 MAGUKs is shown in Figure 1.6.

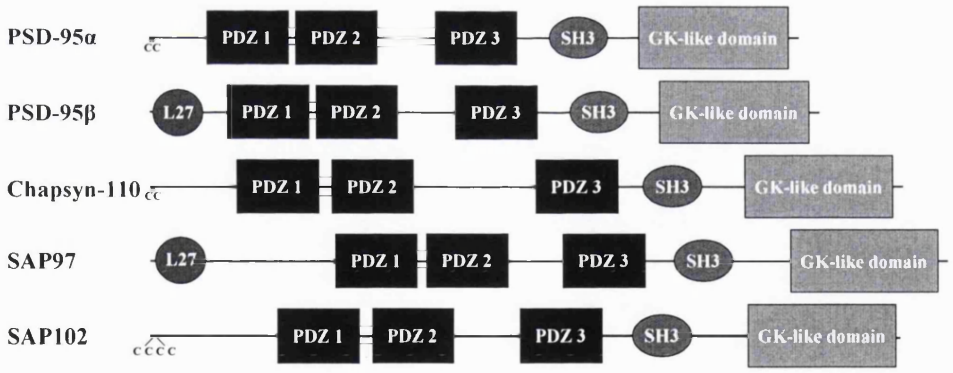

Figure 1.6 Schematic diagram to compare the PSD-95 MAGUK family

The PSD-95 MAGUK family comprises of PSD-95, chapsyn-110, SAP97 and SAP102. PSD-95α and PSD-95β are the two most common splice variants of PSD-95. The above diagram shows the length of the PSD-95 MAGUK proteins. Each PSD-95 MAGUK has an N-terminal region and then the conserved three PDZ domains, a SH3 domain and a C-terminal guanylate kinase (GK) like domain. An additional protein interaction domain is found at the N-terminus of both SAP97 and PSD-95β.

1.8 PSD-95 MAGUK family structure

The PSD-95 MAGUK family exist as splice variants, where they are predominantly alternatively spliced at their N-termini. For example, the most abundantly expressed PSD-95 isoform is PSD-95α which has two cysteines at amino acid present at positions 3 and 5. These residues have been implicated in both the formation of disulphide bridges or being palmitoylated (Topinka and Bredt, 1998; Hsueh *et al.*, 1997; Hsueh and Sheng, 1999; El-Husseini *et al.*, 2000). As found for PSD-95, the N-terminus of PSD-93 is also alternatively spliced. Both PSD-93α and PSD-93β isoforms have cysteine residues on their N-terminal domains which are located at different positions, i.e. PSD-93α has cysteine residues at amino acid positions 5, 7 and 12 on the N-terminal domain whilst PSD-93β has cysteine residues present at 3 and 5, which is similar to PSD-95α (Brenman *et al.*, 1996). Chapsyn-110 is the equivalent to PSD-93α and will be referred to as chapsyn-110 throughout this thesis. In contrast, although SAP102 has four cysteines and three histidines present at the N-terminus, these are thought to be involved in heavy metal binding (El-Husseini *et al.*, 2000). Another PSD-95 isoform is PSD-95β which forms 10 % of the total PSD-95 population and differs at the N-terminus. It contains an additional protein interaction domain, the L27 domain which replaces the cassette which contains C3 and C5 (Chetkovich *et al.*, 2002; Bence *et al.*, 2005). Although SAP97α contains cysteine residues at the N-terminus, the predominant isoform is SAP97β, similar to PSD-95β, which has an N-terminal L27 domain present (Schluter *et al.*, 2006). All further references to SAP97 in this thesis will refer to the SAP97β isoform. This L27 domain is thought to be an organisation centre for protein complexes required for cell polarity. In addition to the above PSD-95 isoforms, 3 additional splice variants have been identified. The remaining 3 splice variants are; PSD-95γ, which has a 60 amino acid truncation at the start of the N-terminus removing C3 and C5, PSD-95α-2b which has a 33 amino acid insertion between PDZI and PDZII domains and PSD-95α-Δ18 which is truncated in the GK-like domain (Bence *et al.*, 2005).

Following the N-terminus are three PDZ domains found on all of the PSD-95 MAGUK family members. The association between PSD-95 and NMDA receptors was first demonstrated by Kornau *et al.* (1995). It was shown that both NR2A and NR2B C-terminal

domains interacted with PSD-95 (Kornau *et al.*, 1995). This association was found to be mediated via either the PDZI and PDZII domains of PSD-95 with the E(T/S)XV motif present at the distal C-terminus of both NR2A and NR2B subunits (Kornau *et al.*, 1995; Niethammer *et al.*, 1996). The PDZII domain was found to have the highest affinity for the NR2A and NR2B C-terminal domains (Niethammer *et al.*, 1996). Similarly, the PDZII domain of SAP102 was demonstrated by ELISA assays to bind a peptide corresponding to the last 9 amino acids of the NR2B C-terminal domain with the highest affinity, with an EC_{50} = 6 nM (Muller *et al.*, 1996). The other PDZ domains bound with a lower affinity when compared to the PDZII domain, EC_{50} = 30 nM for PDZI domains and EC_{50} = 1μM for PDZIII domains (Muller *et al.*, 1996). PDZ domains are approximately ~ 90 amino acids in length and characterised by the presence of a GLGF motif (for review see Garner *et al.*, 2000; Hung and Sheng, 2002; Sheng and Sala, 2001). This GLGF motif forms a carboxylate-binding loop which binds distal C-terminal sequences (for review see Garner *et al.*, 2000; Hung and Sheng 2002; Sheng and Sala, 2001). The X-ray crystallographic structure of the PDZIII domain of PSD-95 was found to contain six β strands and two α helices (Doyle *et al.*, 1996). The distal C-terminus of the ligand, KETSV, was shown to bind via the carboxylate-binding loop, β strand B and α helix B (Doyle *et al.*, 1996). Figure 1.7 shows a ribbon diagram of the PDZIII of PSD-95.

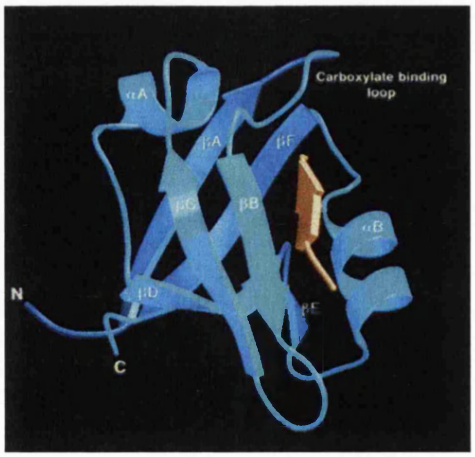

Figure 1.7 A ribbon diagram showing the three-dimensional fold of the PDZIII domain of PSD-95

The X-ray crystallographic structure of the PDZIII domain was found to contain six β strands and two α helices. The GLGF motif forms a carboxylate-binding loop which in conjunction with βB and αB binds the ligand. The above diagram is from Doyle *et al.* (1996).

The amino acid consensus sequence for the binding of the PSD-95 family of PDZ domains was determined by use of solid-phase colorimetric and in-solution fluorescence polarimetric peptide binding assays which measures the affinities for solubilised peptide libraries. The optimal sequence for the ligand to bind to the PDZ domains from mDlg was determined as being a hydrophobic amino acid present at the distal C-terminus and at a serine, threonine or a tyrosine present at the -2 position (Songyang *et al.*, 1997). From these studies it was deduced that the optimal PDZ domain consensus sequence was E(S/T)X(V/I), where X represents any amino acid (Songyang *et al.*, 1997). The specificity of the amino acids needed for optimal binding of the PDZ domains of PSD-95 was further characterised by Lim *et al.* (2002). It was found that P^0, i.e. the distal amino acid on the C-terminus, valine gave the highest affinity in comparison to other hydrophobic residues such as leucine, isoleucine and phenylalanine (Lim *et al.*, 2002). Position P^1 had a greater flexibility of the amino acid present with the exception of lysine which abolished the binding to the PDZ domains. The replacement of serine with threonine at position P^2 resulted in an increase in the PDZ domain binding. Position P^3 requires glutamate for the high affinity binding, as substitution with aspartate resulted in a decreased affinity. Lastly, the P^4 position requires the presence of a hydrophobic or a positively charged amino acid (Lim *et al.*, 2002). Interestingly, amino acids at positions further down the peptide sequence of the ligand made limited contributions to the binding of the PDZ domains (Lim *et al.*, 2002). Thus the consensus binding sequence for PDZ domains is a distal C-terminal (E/Q)(S/T)(D/E/Q/N)V motif (Lim *et al.*, 2002). Thus this is in agreement with the distal C-terminal motifs present on NR2A and NR2B subunits that were shown to interact via the ESDV motif. However, although this association was shown to be mediated by the distal C-terminal ES(D/E)V motif, Bassand *et al.*, (1999) demonstrated that the removal of the ESDV motif of NR2A C-terminal domain did not stop the association with PSD-95. In addition, Rutter (2000) and Papadakis (2004) found that recombinant NR1-1a/NR2A^{TRUNC} NMDA receptors, where the ESDV motif was deleted from NR2A subunits, still co-immunoprecipitated with PSD-95. In contrast, Prybylowski *et al.* (2005) found that recombinant NR1/NR2B^{S1480A} NMDA receptors no longer co-immunoprecipitated with PSD-95, where S1480A is a point mutation in the PSD-95 binding motif, i.e. ESDV → EADV.

Following the PDZ domains is an SH3 domain, which is a common protein-protein interaction domain found in many scaffolding and cell signalling protein molecules. SH3 domains are approximately ~ 60 amino acids in length (for review see Mayer, 2001; Shawn, 2005). The SH3 domain was found to interact with the GK-like domain creating an intramolecular interaction which is important in regulating the ion-clustering activity of PSD-95 (Shin *et al.*, 2000; Tavares *et al.*, 2001). In addition to binding the GK-like domain within the same protein, the SH3 domain is also able to associate with other GK-like domains from different members of the PSD-95 MAGUK family (Shin *et al.*, 2000). Thus demonstrating that the intermolecular interactions between the PSD-95 MAGUK family could aid the formation of larger scaffolding complexes (Shin *et al.*, 2000).

1.9 The function of the PSD-95 MAGUK family

The functional significance of the PSD-95 MAGUK family was investigated by the generation of knock-out mice. For example, PSD-95 mutant mice were created by truncating the protein after the PDZII domain (Migaud *et al.*, 1998). PSD-95 mutant mice had an enhanced LTP and impaired learning with no other obvious phenotype. It was hypothesised that due to the high amino acid identity between the PSD-95 MAGUK family members a functional redundancy existed. Indeed, SAP102 was shown to be up-regulated in double PSD-93$^{-/-}$ and PSD-95$^{-/-}$ knock-out mice and was able to compensate for the trafficking of AMPA receptors (Elias *et al.*, 2006). In addition NMDA receptor mediated EPSCs at hippocampal CA1 synapses of PSD-93$^{-/-}$ and PSD-95$^{-/-}$ knock-out mice, which also had the expression of SAP102 knocked down, were found not to be greatly reduced (Elias *et al.*, 2006). In contrast, PSD-93 mutant mice, where the protein was deleted in the PDZII domain, showed a decrease in the cell surface expression of NMDA receptors in spinal dorsal horn neurones prepared from PSD-93 mutant mice was observed (Tao *et al.*, 2003). PSD-93 mutant mice also were found to have blunted NMDA receptor related pain (Tao *et al.*, 2003). SAP102$^{-/-}$ knock-out mice, generated by the introduction of a frame shift in the N-terminus of the SAP102 gene, were found to have an altered LTP and spike-time-dependent plasticity in a restricted range of stimulation conditions (Cuthbert *et al.*, 2007). Further analysis revealed that in these conditions SAP102 couples NMDA receptors to the ERK pathway (Cuthbert *et al.*, 2007). Lastly, disruption of the SAP97 gene resulted in

death perinatally (Caruana and Bernstein, 2001). These above studies demonstrate the importance that each PSD-95 MAGUK plays in both development and their scaffolding properties they elicit on specific signalling pathways.

The PSD-95 MAGUK family are differentially distributed in the brain. The expression of the PSD-95 family was investigated by both *in situ* hybridisation and immunoblotting. PSD-95 was shown to be present in both the cerebellum and forebrain (Cho *et al.*, 1992). Chapsyn-110 is expressed in the cerebellum, cerebral cortex, hippocampus, sub-cortical regions and in non-neuronal tissues such as the adrenal, thymus and submandibular glands (Kim *et al.*, 1995; 1996; Brenman *et al.*, 1996a). SAP97 is widely expressed in the brain such as the cerebral cortex, hippocampus, olfactory bulb and the spinal cord (Muller *et al.*, 1995). Lastly, SAP102 was found predominantly in cerebellum, cerebral cortex, hippocampus and olfactory bulb (Muller *et al.*, 1996). When examining the protein expression at a sub-cellular level PSD-95 and PSD-93 are both expressed in post-synaptic sites (El-Husseini *et al.*, 2000). However, SAP97 and SAP102 are both thought to be localised in presynaptic and postsynaptic sites (Muller *et al.*, 1995; El-Husseini *et al.*, 2000). The PSD-95 MAGUK family also have a distinct but overlapping developmental expression profile. SAP102 expression peaks in the neonatal brain which declines after day P10 but is still expressed in the mature brain (Sans *et al.*, 2000). PSD-95 and PSD-93 are the major PSD-95 MAGUK members expressed in the mature brain (Sans *et al.*, 2000). There are two alternatively spliced SAP97 isoforms, with mRNAs of 4.9 and 4.4 kb. The 4.9 kb mRNA for SAP97 is present in the first postnatal week and remains constant, in contrast the 4.4 kb appears at day P15 and declines in the mature brain (Muller *et al.*, 1995).

It has been found that the N-terminal domains of the PSD-95 family members play a role in their trafficking and targeting properties. The palmitoylation signal on PSD-95 was found to be essential for its synaptic localisation in hippocampal neurones (Craven *et al.*, 1999; Firestein *et al.*, 2000). In addition to the palmitoylation motif, the clustering and localisation of PSD-95 was also found to be dependent on PDZI and PDZII domains and a C-terminal sequence (residues 13-25 of the distal C-terminal domain, Hsueh *et al.*, 1997;

Craven *et al.*, 1999). Conversely, although PSD-93 was demonstrated to be palmitoylated at its N-terminus, this signal is not required for its synaptic localisation (Firestein *et al.*, 2000). In contrast to the synaptic distribution observed for both PSD-95 and PSD-93, SAP102 was found to have a diffuse distribution in the dendritic cytoplasm with only a modest enrichment in synapses (El-Husseini *et al.*, 2000; Firestein *et al.*, 2000). Lastly, SAP97 was found to have a diffuse distribution in hippocampal neurones (Craven *et al.*, 1999). The properties the different N-terminal domains elicits onto the targeting of each PSD-95 family member were further investigated by the generation of chimeras. The first 30 or 64 amino acids of PSD-93α were genetically fused onto PSD-95α and both these chimeras were found to be located in the synaptic sites, even though they did not contain the palmitoylation signal (Firestein *et al.*, 2000). In addition, when replacing the N-terminal domain of PSD-95 with that of SAP102, this was found to result in a distribution more characteristic of SAP102 (El-Husseini *et al.*, 2000). Thus, the N-terminal domains of the PSD-95 family all contain specific information which facilitates their sub-cellular localisation.

As mentioned above, the cysteine residues 3 and 5 of PSD-95 are also thought to also be involved in disulphide bridges (Hsueh *et al.*, 1997; Hsueh and Sheng, 1999). PSD-95 was found to form disulphide multimers due to the presence of immunoreactive bands with molecular weights corresponding to ~ 300 – 350 kDa in non-reduced protein samples (Hsueh *et al.*, 1997; Hsueh and Sheng, 1999). Point mutations of C3 and C5, PSD-$95^{C3S,C5S}$, abolished the formation of ternary complexes of PSD-$95^{C3S,C5S}$/K_v 1.4/FascicinII, a potassium channel subunit and a cell adhesion molecule respectively (Hsueh and Sheng, 1999). Thus it was thought that two molecules of PSD-95 associate and this multimer then interacts with different binding partners to form a complex (Hsueh and Sheng, 1999).

1.10 The association of NMDA receptors and the PSD-95 MAGUK family of proteins

PSD-95 was first identified as a NMDA receptor interacting protein following a yeast two-hybrid screen using the NR2A C-terminal domain as bait (Kornau *et al.*, 1995). Further, chapsyn-110 and SAP102 cDNA were both first identified and cloned on the basis of their

association with NMDA receptors (Kim *et al.*, 1995; 1996a; Brenman *et al.*, 1996a). Lastly, SAP97 was also found to interact with NMDA receptors (Gardoni *et al.*, 2003). A table summarising the known interactions between the NR2 subunits and the PSD-95 family is shown in Table 1.2.

	PSD-95	**PSD-93/chapsyn-110**	**SAP97**	**SAP102**
NR2A	- Kornau *et al.* (1995) Association determined by yeast two-hybrid interactions.	- Sans *et al.* (2000) Association demonstrated by immunoprecipitation from hippocampal tissue.	- Gardoni *et al.* (2003) Association demonstrated by immunoprecipitation from rat brain homogenates and synaptosomes.	- Sans *et al.* (2000) Association demonstrated by immunoprecipitation from hippocampal tissue. - Muller *et al.* (1996) Association demonstrated by immunoprecipitation from rat brain.
NR2B	- Kornau *et al.* (1995) Association determined by yeast two-hybrid interactions.	- Sans *et al.* (2000) Association demonstrated by immunoprecipitation from hippocampal tissue.	Wang *et al.* (2005) C-terminal of NR2B with SAP97 Using high resolution NMR.	- Sans *et al.* (2000) Association demonstrated by immunoprecipitation from hippocampal tissue. - Muller *et al.* (1996) Association demonstrated by immunoprecipitation from rat brain.
NR2C	-Chen *et al.* (2006) Association determined by yeast two-hybrid interactions.	Not determined.	Not determined.	-Chen *et al.* (2006) Association determined by yeast two-hybrid interactions.
NR2D	- Kornau *et al.* (1995) Association determined by yeast two-hybrid interactions. - Mi *et al.* (2004) Association demonstrated by immunoprecipitation from in hippocampal tissue.	Not determined.	Not determined.	Not determined.

Table 1.2 Table summarising the interactions between the NR2 subunits and the PSD-95 MAGUK

Although the association between PSD-95 and the NR2 subunits have been identified, there are conflicting reports with regards to the interaction between PSD-95 and the NR1 subunits. The NR1 subunits containing the NR1 C2' cassette, i.e. NR1-3a,b and NR1-4a,b have the putative PDZ binding motif, STVV, present at their C-termini. Kornau *et al.* (1995) demonstrated an association between the NR1-3 and NR1-4 C-terminal domains and PSD-95. However, this association of NR1-4 subunits with PSD-95 was not reproduced by Mattar *et al.* (2005).

1.10.1 Regulation of NMDA receptors by the PSD-95 MAGUK family

The association between NMDA receptors and the PSD-95 MAGUK family have been found to influence the receptors properties. For example, the association between PSD-95 and NMDA receptors was found to alter both their cell surface expression and channel properties *in vitro*. The co-expression of PSD-95 resulted in the clustering of recombinant NR1/NR2A and NR1/NR2B NMDA receptors (Kim *et al.*, 1996). Further, a decrease in Tac-NR2B chimera internalisation was observed in the presence of PSD-95 (Roche *et al.*, 2001). A selective ESDV-dependent enhancement of total NR2A and NR2B subunit expression was found when NR1-1a/NR2A and NR1-1a/NR2B NMDA receptors where co-expressed with PSD-95α (Rutter and Stephenson, 2000). This PSD-95 mediated enhancement of NR2A and NR2B subunit expression was demonstrated to be translated into an enhanced cell surface expression of NR1/NR2A and NR1/NR2B NMDA receptors (Yamada *et al.*, 1999; Rutter *et al.*, 2002; Lin *et al.*, 2004). Thus, PSD-95 stabilises the cell surface expression of NMDA receptors in heterologous cell lines. In addition, PSD-95 is thought to modulate the gating of NR1/NR2A NMDA receptors (Yamada *et al.*, 1999; 2002; Rutter *et al.*, 2002; Lin *et al.*, 2004). For example, PSD-95 was found to decrease the sensitivity of the channels to glutamate and zinc ions (Yamada *et al.*, 1999; 2002; Rutter *et al.*, 2002).

The cell surface expression of NMDA receptors is thought to be regulated by the cleavage of their C-terminal domains. The NR2A-NR2C C-terminal domains have all been demonstrated to be selectively cleaved *in vitro* by calpain, a calcium-dependent protease (Bi *et al.*, 1998; Guttmann *et al.*, 2001). This cleavage of the NR2A C-terminal domain

was found to decrease the number of functional receptors present on the cell surface in HEK 293 cells (Guttmann *et al.,* 2002). In addition, the NR2B C-terminal domain was found to be selectively cleaved by calpain in hippocampal neurones (Simpkins *et al.*, 2003). It is thought that this selective cleavage by calpain on the NR2A-NR2C C-terminal domains is a mechanism which controls the receptor number present at the synapse. This calpain-meditated cleavage was found to be blocked by PSD-95 when co-expressed with recombinant NR1/NR2A and NR1/NR2B NMDA receptors (Dong *et al.*, 2004).

NMDA receptors are also regulated by phosphorylation which is carried out by both kinases and phosphatases. For example, it was found that phosphorylation by PKC resulted in an enhancement of NR1-1a/NR2A and NR1-1a/NR2B NMDA receptor mediated currents (Grant *et al.*, 1998). However, co-expression with PSD-95 was shown to inhibit this PKC mediated potentiation of NR1/NR2A and NR1/NR2B NMDA receptors (Yamada *et al.*, 1999; 2002; Lin *et al.*, 2006). NMDA receptors were also found to be regulated by both protein tyrosine kinases (PTK) and protein tyrosine phosphatases (PTP; Wang and Salter, 1994). This phosphorylation by the PTKs was found to regulate the NMDA receptor function (Wang and Salter, 1994). The inhibition of PTKs resulted in a decrease in the observed NMDA receptor whole cell current, in contrast NMDA receptors were potentiated in the presence of either a constitutively active PTK, Src, or inhibitors of PTPs (Wang and Salter, 1994). PTKs and PTPs are brought into close proximity to NMDA receptors via PSD-95 which associates with PTKs such as Src, Fyn and Pyk2 tyrosine kinases and PTPξ tyrosine phosphatase (Natazawa *et al.*, 2001; Kalia and Salter, 2003; Seabold *et al.*, 2003). For example, Fyn was found to phosphorylate Y1472 of NR2B subunits *in vivo* (Natazawa *et al.*, 2001). As mentioned previously, Y1472 of NR2B subunits was identified as part of an internalisation motif and the phosphorylation on this tyrosine residue regulated the cell surface expression of NR2B-containing NMDA receptors described in Section 1.7.2 (Lavezzari *et al.*, 2003). Indeed, the phosphorylation of Y1472 of NR2B subunits was enhanced when LTP was induced in the CA1 region of the hippocampus, suggesting the importance of Y1472 in synaptic plasticity (Natazawa *et al.*, 2001). In addition, PSD-95 is also associated indirectly with kinases and phosphatases via another scaffolding protein, A-kinase anchoring protein 79/150 (AKAP 79/150). Ternary

complexes of NR2B/PSD-95/AKAP79/150 were identified *in vitro* (Colledge *et al.*, 2000). AKAP79/150 associates with PKA, PKC and PP2B (Coghlan *et al.*, 1995; Klauck *et al.*, 1996; Colledge *et al.*, 2000). Thus the PSD-95/AKAP79/150 complex brings kinases and phosphatases into close proximity to NMDA receptors providing a mechanism to control their phosphorylation state. Figure 1.8 summarises the trafficking and downstream signalling pathways that the PSD-95 MAGUK family elicits on to NMDA receptors.

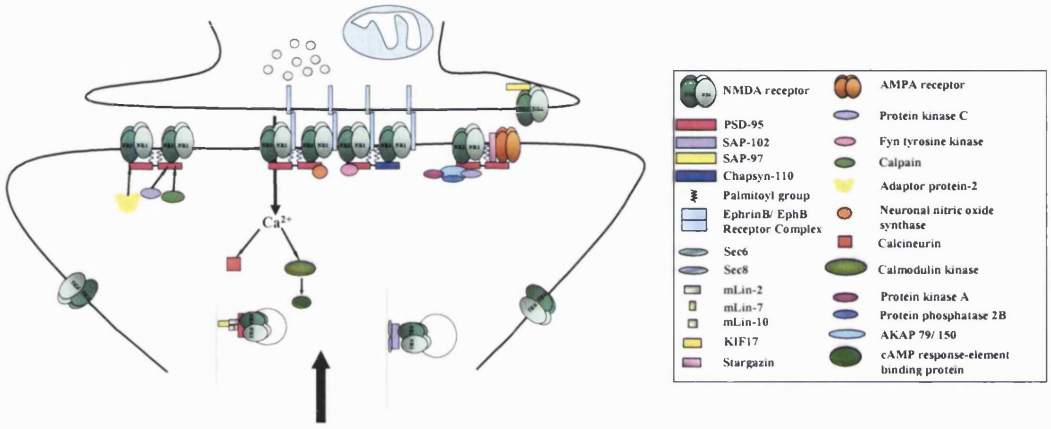

Figure 1.8 Schematic diagram of trafficking and downstream signalling pathways that the PSD-95 MAGUK family elicits on NMDA receptors

Phosphorylation was found to regulate the interactions between NMDA receptors and the PSD-95 family. For example, Chung *et al.* (2004) demonstrated that S1480 is phosphorylated by casein kinase II (CK2), i.e. the serine present in the ESDV PDZ binding motif, and this was phosphorylation was found to disrupt the association with PSD-95 and SAP102. As mentioned previously, PSD-95 causes the potentiation of recombinant NR1/NR2A NMDA receptor currents (Yamada *et al.*, 1999). However, a phosphomimetic point mutation in the ESDV motif, S1462E of NR2A subunits, abolished this potentiation of recombinant NR1/NR2A^{S1462E} NMDA receptors (Lin *et al.*, 2006). In contrast, S1244 of NR2C subunits, which is close to the ESEV PDZ binding motif, was shown to be phosphorylated by both PKC and PKA (Chen *et al.*, 2006). A phosphomimetic mutation of S1244E of the NR2C C-terminal did not disrupt the association with PSD-95 or SAP102 (Chen *et al.*, 2006). Interestingly, NR1/NR2C^{S1244E} NMDA receptors were found to have an acceleration in the channel activation and decay kinetics of the response thus demonstrating that the phosphorylation at S1244 affected ion channel gating (Chen *et al.*,

2006). In addition to NMDA receptors, phosphorylation of other PSD-95 binding ligands have been found to disrupt their interactions. For example, the inward rectifier K^+ channel, Kir 2.3 contains the C-terminal PDZ binding motif ESAI. This serine residue is phosphorylated by protein kinase A (PKA) and its phosphorylation disrupts the association between PSD-95 and Kir 2.3 subunits (Cohen *et al.*, 1996). Additionally another inward rectifier K^+ channel subunit, Kir 2.2 was found to interact with SAP97 via the PDZ binding domain motif, SEI (Leonoudakis *et al.*, 2001). This serine is a putative PKA phosphorylation site, in the presence of forskolin (an adenylate cyclase activator) resulted in a decrease in the association between SAP97 and the Kir 2.2 C-terminal domain (Leonoudakis *et al.*, 2001). PSD-95 interacts with an AMPA receptor interacting protein called stargazin via the C-terminal PDZ motif TPV (Chen *et al.*, 2000). The phosphorylation of this threonine residue disrupted the association with PSD-95 (Choi *et al.*, 2002). Thus, together these studies demonstrate that phosphorylation inhibits the association between PSD-95 and its binding partners.

The PSD-95 family themselves are phosphorylated and this was found to influence their sub-cellular localisation. For example, the phosphorylation of SAP97 on S39, by CaCMKII, was shown to be the driving force to move NR2A/SAP97 complexes from the ER (Mauceri *et al.*, 2004; 2007). The phosphorylation of SAP97 on S232 disrupted the interaction with NR2A subunits thereby assisting the localisation of NR2A containing NMDA receptors into the postsynaptic membrane (Gardoni *et al.*, 2003; Mauceri *et al.*, 2007). When PSD-95 is phosphorylated on S73 this disrupts the association with NR2A subunits but not NR2B subunits (Gardoni *et al.*, 2006). Therefore, phosphorylation provides a dynamic method of regulation for these protein interactions in synapses.

1.11 NMDA receptors as a component of a macromolecular complex

As mentioned previously, NMDA receptors are associated with many proteins which assist with their trafficking and regulation at the cell surface. Proteins have been found to associate with NMDA receptors predominantly via yeast two-hybrid screening methodology. Table 1.3 summarises the major NMDA receptor interacting proteins. NMDA receptors are known to be associated with a large complex of proteins in the PSD,

which have been identified by a mass spectrometry proteomic approach (Husi and Grant, 2001a,b; Collins *et al.*, 2005). This group of proteins was termed the NMDA receptor complex (Husi and Grant, 2001a,b; Collins *et al.*, 2005).

Name of protein	Reference
Apolipoprotein E receptor 2 (ApoEr2)	Hoe *et al.* (2006)
Calmodulin	Ehlers *et al.* (1996)
Calmodulin kinase II	Strack and Colbran (1998)
D1 dopamine receptors	Lee *et al.* (2002) ; Fiorentini *et al.* (2003); Pei *et al.* (2004)
EphB receptors	Dalva *et al.* (2000)
NADH dehydrogenase subunit 2 (ND2)	Gingrich *et al.* (2004)
Neuronal intermediate filaments	Ehlers *et al.* (1998)
PSD-95 MAGUK family; PSD-95, PSD-93, SAP102, SAP97	See Table 1.2
Synaptic adhesion-like moelcules (SALM1-SALM4)	Wang *et al.* (2006)
Yotiao	Lin *et al.* (1998)
α-actinin -2	Wyszynski *et al.* (1997)

Table 1.3 Table to summarise the major NMDA receptor interacting proteins

The major proteins which interact with NMDA receptors can be divided into either other receptors or scaffolding proteins. For example, many receptors are thought to be associated with NMDA receptors, such as D1 dopamine receptors, EphB receptors and the apolipoprotein E receptor 2 (Dalva *et al.*, 2000; Lee *et al.*, 2002; Hoe *et al.*, 2006;). This association between the different receptors has been found to regulate the properties of each receptors. For example, the association between NMDA receptors and D1 dopamine receptor has been found to regulate the cell surface expression of both receptors. The D1 receptor C-terminal domain was found to associate with NMDA receptors via two distinct interaction sites, one present on NR1-1a subunits and the second present on NR2A subunits (Lee *et al.*, 2002). This association was found to decrease the NMDA receptor-mediated currents and excitotoxicity in hippocampal neurones was found (Lee *et al.*, 2002). These effects are thought to be due to a decrease in NMDA receptor cell surface expression (Lee

et al., 2002). Conversely, it was shown that there was an increase in the cell surface expression of D1 dopamine receptors following the activation of NMDA receptors (Scott *et al.*, 2002; 2006; Fiorentini *et al.*, 2003; Pei *et al.*, 2004). In addition, scaffolding proteins have been found to associate with NMDA receptors, such as α-actinin-2, calmodulin, neuronal intermediate filaments, Yotiao and the PSD-95 MAGUK family (Ehlers *et al.*, 1996; Wyszynski *et al.*, 1997; Ehlers *et al.*, 1998; Lin *et al.*, 1998). The PSD-95 MAGUK family of proteins are scaffolding proteins which are thought to serve as a 'hub' linking NMDA receptors to other signalling and regulatory proteins. Table 1.4 summarises the known PSD-95 interactors and their preferred interaction domain. The proteins that associate with PSD-95 can be grouped into main four classes; receptor subunits, scaffolding proteins, regulatory proteins and proteins involved in trafficking. Thus, the PSD-95 MAGUK family have been demonstrated to be involved in the localisation and targeting, scaffolding for signalling complexes, anchoring to cytoskeleton and the clustering/aggregation of their binding partners (for review see Sheng and Pak, 2000).

1.12 Aims of this Thesis

As had been addressed in this introduction, the PSD-95 MAGUK family of proteins play an important role in the trafficking and stabilisation of NMDA receptors. Therefore, the aims of this thesis were:

- To investigate the association between each of the PSD-95 MAGUK proteins and the four major NMDA receptor subtypes and the effects this association had on the total subunit expression and the NMDA receptor cell surface expression.

- To address the role of a putative PKA phosphorylation site present at the distal C-terminal domains of NR2A subunits and its possible role in regulating the association with PSD-95.

- To investigate the determinants in the NR2A and NR2B C-terminal domains which facilitate their association with PSD-95.

- Lastly, NR2D-containing NMDA receptors form a distinct subtype of receptors which are thought to be located predominantly in the extrasynaptic sites; therefore a yeast two-hybrid screen was carried out to identify proteins interacting with the NR2D C-terminal domain.

Name of protein	PSD-95 domain of interaction	Reference
5-HT2C receptors	PDZI, PDZII, PDZIII	Bécamel *et al.* (2004)
AKAP79/150	SH3/GK-like	Colledge *et al.* (2000)
Apolipoprotein E receptor 2 (ApoEr2)	PDZI	Hoe *et al.* (2006)
BEGAIN	GK-like	Deguchi *et al.* (1998)
Citron	PDZIII	Furuyashiki *et al.* (1999); Zhang *et al.* (1999)
CRIPT	PDZIII	Passafaro *et al.* (1999)
Cypin	Not determined	Akum *et al.* (2004)
D1 dopamine receptor	N-terminal	Zhang *et al.* (2007)
ErbB4 (receptor tyrosine kinase)	PDZI, PDZII, PDZIII	Garcia *et al.* (2000); Huang *et al.* (2000)
FasciclinII	PDZII	Hsueh and Sheng, 1999
Fyn, Src, Lyn, Yes	PDZIII	Kaila and Salter (2003); Tezuka et al. (1999)
GKAP/SAPAP	GK-like	Kim *et al.* (1997); Takeuchi *et al.* (1997); Naisbitt *et al.* (1997)
GluR6	PDZI	Garcia *et al.* (1998)
K channels, Kv1	PDZI, PDZII	Kim *et al.* (1995)
Kainate receptor subunit KA2	SH3	Garcia *et al.* (1998)
Kalirin-7 (GDP/GTP exchange factor (GEF) for Rac1)	Not determined	Penzes *et al.* (2001)
KIFBα	PDZI, PDZII, PDZIII	Mok *et al.* (2002)
Kir2, Kir3, Kir4 and Kir5	PDZI, PDZII	Nehring *et al.* (2000)
MAGUIN	PDZII, PDZIII	Yao *et al.* (1999)
mPins	SH3, GK-like	Sans *et al.* (2005)
Neuroligin	PDZIII	Irie *et al.* (1997)
nNOS	PDZII	Brenman *et al.* (1996)
NMDA receptor subunits NR2A and NR2B	PDZI, PDZII, PDZIII	See Table 1.2
PRR7	PDZIII	Murata *et al.* (2005)
SALM1	Not determined	Wang et al. (2006)
Semaphorin Sema4C	PDZI, PDZII	Inagaki *et al.* (2001)
SPAL, a Rap-specific GTPase activating protein	GK-like	Roy *et al.* (2002)
SPAR, a Rap-specific GTPase activating protein	GK-like	Pak *et al.* (2001)
Src	N-terminal	Kalia *et al.* (2006)
Stargazin family of proteins	PDZI, PDZII, PDZIII	Chen *et al.* (2000)
synGAP	PDZI, PDZII, PDZIII	Chen *et al.* (1998)
Tyrosine kinase Pyk2	SH3	Seabold *et al.* (2003)
β1-adrenergic receptor	PDZIII	Lim *et al.* (2002)

Table 1.4 Table summarising the major proteins known to associate with PSD-95

CHAPTER 2

MATERIALS AND METHODS

2.1 MATERIALS

2.1.1 Molecular biology reagents

BD Bioscience Falcon polypropylene round bottom tubes, selective dropout supplements, Difco ™ yeast nitrogen base without amino acids, cDNA mouse brain library (pACT2), and the Matchmaker™ 3 yeast two-hybrid system were purchased from Clontech, a Takara Bio company (Saint-Germain-en-Laye, France). The restriction enzymes with their buffers and DNA molecular weight markers were purchased from Fermentas (Yorkshire, U.K). Lennox B broth and SELECT agar powder were from Invitrogen (Paisley, U.K.). Isopropyl-ß-D-thio-galactopyranoside (IPTG), peptone, yeast extract and x-α-gal (5-bromo-4-chloro-3-indolyl-α-D-galactopyranoside) were purchased from Melford Laboratories (Suffolk, U.K.). The Phusion™ high-fidelity DNA polymerase was purchased from New England Biolabs (Hertfordshire, U.K.). Shrimp alkaline phosphatase (SAP) and the dNTPs (dATP, dCTP, dGTP and dTTP) were from Promega (Southampton, U.K.). Ampicillin, DNA sodium salt from salmon testes, ethidium bromide, GenElute™ HP maxiprep kit, kanamycin, phenol:chloroform:isoamyl alcohol (25:24:1) and polyethylene glycol (molecular weights 3500 and 8000) were purchased from Sigma-Aldrich (Poole, U.K.). QuikChange® II XL site-directed mutagenesis kits were from Stratagene (Amsterdam, Netherlands). QIAfilter plasmid giga kits and QIAquick PCR purification kits were from Qiagen (West Sussex, U.K.). Agarose 'Electran' molecular biology grade and D-glucose were purchased from VWR International Ltd (Dorset, U.K).

2.1.2 Mammalian cell reagents

Penicillin and streptomycin (10,000 units/ml) and SeeBlue® pre-stained standard molecular weight markers were from Invitrogen (Paisley, U.K.). K-Blue substrate was from Neogen (Scotland, U.K.). CytoTox 96® non-radioactive cytotoxicity assay was from Promega (Southampton, U.K.). Sodium bicarbonate solution (7.5 % w/v), bacitracin, benzamidine, Dulbecco's modified Eagles medium nutrient mixture F-12 HAM (DMEM/F-12), powdered and liquid (without L-glutamine) media, foetal bovine serum (FBS), forskolin, phosphatase inhibitor cocktail 1, Hanks balanced salt solution, ketamine-HCl, phenylmethanesulphonyl fluoride (PMSF), poly-D-lysine hydrobromide, protein A Sepharose, Triton X-100®, trypsin inhibitor-chicken egg white, trypsin inhibitor-II-S and

trypsin-EDTA were purchased from Sigma-Aldrich (Poole, U.K.). HEK 293 cells were purchased from the European collection of cell cultures (Wiltshire, U.K.).

2.1.3 All other chemical reagents

Coomassie brilliant blue G-250 dye and poly-prep chromatography columns were purchased from BioRad (Hemel Hampstead, U.K.). Dithiothreitol (DTT) was purchased from Melford Laboratories (Suffolk, U.K.). Protogel (30% [w/v] acrylamide: 0.8% [w/v] bis-acrylamide (37.5:1), ammonium persulphate and *N,N,N',N'*-tetramethylethylenediamine (TEMED) were purchased from National Diagnostics (Yorkshire, U.K.). 4-(2-Hydroxyethyl)piperazine-1-ethanesulphonic acid (HEPES), 5-amino-2,3-dihydro-1,4-phthalazinedione (luminol), boric acid, calcium chloride, bovine serum albumin (BSA), dimethyl sulphoxide (DMSO), D-sorbitol, ethylene glycol-bis(2-aminoethylether)-N,N,N',N'-tetraacetic acid (EGTA), lithium acetate, sodium acetate anhydrous, sodium dodecyl sulphate (SDS), thiopropyl-Sepharose 6B, trans-4-hydroxycinnamic acid (p-coumaric acid) and Tween-20® were purchased from Sigma-Aldrich (Poole, U.K.). Ammonium acetate, citric acid, di-sodium hydrogen orthophosphate, glycerol, glycine, potassium chloride, sodium chloride, sodium hydroxide pellets and Tris (hydroxymethyl) aminomethane (Tris) were purchased from VWR International Ltd (Dorset, U.K). Protran® nitrocellulose membranes were purchased from Whatman (Kent, U.K.). Where appropriate, chemicals purchased were of Analar standard. All other chemicals were bought from commercial sources.

2.1.4 DNA constructs

2.1.4.1 Mammalian expression plasmids

The pCIS vector was a gift from Dr.C. Gorman (Genentech, San Francisco, U.S.A.). The NMDA receptor cDNA clones were a gift from Professors S. Nakanishi (Kyoto, Japan) and M. Mishina (Nigata, Japan). The pCISNR1-1a, pCISNR2A and pCISNR2B clones were constructed as in Cik *et al.* (1993), Chazot *et al.* (1994), pCISNR2C and pcDNANR2D clones were constructed as in Chopra *et al.* (2000). The pCISNR2A^{TRUNC} and pCISNR2B^{TRUNC} clones were generated as in Rutter and Stephenson (2000). The pGW1-PSD-95α$^{c\text{-}Myc}$ (the c-Myc tag, EQKLISEEDL, was cloned at amino acid 12 of PSD-95α),

pGW1-Chapsyn-110$^{c\text{-}Myc}$ (the c-Myc tag was positioned prior to the N-terminus), pCMVneoSAP-102$^{c\text{-}Myc}$ (the c-Myc tag was positioned prior to the N-terminus) and pGW1-SAP-97 clones were kind gifts from Dr M. Sheng (Boston, U.S.A). The pGW1-PSD-95β clone was a kind gift from Dr. D. Bredt (San Francisco, California, USA). The vector maps are shown in Appendix 2.1-2.3. The accession numbers for each of the clones used are shown in Table 2.1.

Protein name	Species	Nucleotide accession number	Protein accession number
NMDA receptor subunits			
NR1-1a	Rat	U08261	AAB50926
NR1-1b	Rat	U08263	AAB50928
NR1-2a	Rat	U08262	AAB50927
NR1-2b	Rat	U08264	AAB50929
NR1-3a	Rat	U08265	AAB50930
NR1-3b	Rat	U08266	AAB50931
NR1-4a	Rat	U08267	AAB50932
NR1-4b	Rat	U08268	AAB50933
NR2A	Mouse	D10217	P35436
NR2B	Mouse	D10651	Q01097
NR2C	Mouse	D10694	Q01098
NR2D	Mouse	D12822	Q03391
PSD-95 MAGUK proteins			
PSD-95	Rat	M96853	P31016
Chapsyn-110	Rat	U49049	Q63622
SAP97	Rat	U14950	Q62696
SAP102	Rat	U50147	Q62936

Table 2.1 Accession numbers for the NMDA receptor subunits and the PSD-95 MAGUK family of proteins

2.1.4.2 Yeast two-hybrid expression vectors

Vector Name	Nutritional Selection Marker	Antibiotic marker
pGBKT7	Trp	Kanamycin (50 μg/ml)
pGAD10	Leu	Ampicillin (50 μg/ml)
pACT2	Leu	Ampicillin (50 μg/ml)

The vector maps are shown in Appendix 2.4.

Table 2.2 Summary of the major cloning vectors used in the yeast two-hybrid system

2.1.5 Bacterial strains

DH5α E. coli - Genotype: *F⁻, ϕ80lacZΔM15, Δ(lacZYA-argF)U169, deoR, recA1, endA1, hsdR17(r_k^-, m_k^+), phoA, supE44, thi-1, gyrA96, relA1, λ⁻*. DH5α *E.coli* was used for all molecular cloning and amplification of plasmid DNA. This strain was purchased from Invitrogen (Paisley, U.K).

XL10-Gold E. coli – Genotype *Tet^rΔ (mcrA)183 Δ(mcrCB-hsdSMR-mrr)173 endA1 supE44 thi-1 recA1 gyrA96 relA1 lαv Hte [F' proAB $lacI^q$ZΔM15 Tn10 (Tet^r)Tn5 (Kan^r) Amy.* XL10-Gold *E.coli* was used for the QuikChange® II XL Site-Directed Mutagenesis reactions. The kit was purchased from Stratagene (Amsterdam, Netherlands).

BNN132 E.coli – Genotype: *(Cre^+ strain) endA1 gyr96 thi hsdR17 supE44 relA1 Δ (lac-proAB) (F' traD36 $proAB^+$ $lacI^q$ Z Δ M15) (λ kan-Cre).* BNN132 *E.coli* was the bacterial strain which contained the cDNA mouse brain library and was purchased from Clontech, a Takara Bio company (Saint-Germain-en-Laye, France).

2.1.6 Yeast strains

AH109 *S. cerevisiae* - Genotype: *MATa, trp1-901, leu2-3, 112, ura3-52, his3-200, gal4Δ, gal80Δ, LYS2:: $GAL1_{UAS}$-$GAL1_{TATA}$-HIS3, $GAL2_{UAS}$-$GAL2_{TATA}$-ADE2, URA : : $MEL1_{UAS}$-$MEL1_{TATA}$-lacZ.* The AH109 yeast strain was used for all yeast two-hybrid experimental work and was purchased from Clontech, a Takara Bio company (Saint-Germain-en-Laye, France).

Y187 *S. cerevisiae* - Genotype: *MATα, ura3-52, his3-200, ade2-101, trp1-901, leu2-3, 112, met⁻, gal4D, gal80D, URA3::$GAL1_{UAS}$-$GAL1_{TATA}$-lacZ.* The Y187 yeast strain was used for yeast mating assays and was purchased from Clontech, a Takara Bio company (Saint-Germain-en-Laye, France).

2.1.7 Antibodies

Affinity-purified anti-NMDA receptor antibodies were developed in-house. Anti-NR1 17-35 (anti-NR1 pan), anti-NR1 911–920 (anti-NR1 C2), anti-NR2A/2B 1435–1445 (using the NR2A amino acid residues 1454-1464) and anti-NR2B 46–60 Cys polyclonal antibodies were prepared and characterized as previously described (Chazot *et al.* 1994; Chazot and Stephenson 1997a, b). Anti-NR2C 1227-1237 and anti-NR2D 1307-1323 antibodies were prepared and characterised as in Chazot *et al.* (1994) and Thompson *et al.* (2000) respectively. A summary of the peptide sequences used for all in-house antibodies are shown in Table 2.3. Anti-SAP97 (115-133) and anti-SAP102 (83-100) antibodies were purchased from AbCam (Cambridge, U.K.). Anti-Rab5 antibodies and anti-calnexin antibodies were purchased from EMD Bioscience (Nottingham, U.K.). The anti-FLAG antibodies were purchased from Sigma-Aldrich (Poole, U.K.). Anti-Myc tag, clone 4A6, antibodies were purchased from Upstate, Cell-signalling Solutions. (Milton Keynes, U.K). Horseradish peroxidase (HRP)-linked anti-rabbit immunoglobins (Ig) antibodies and HRP-linked anti-mouse Ig antibodies were purchased from Amersham Pharmacia (Chalfont St.Giles, U.K.).

Table 2.3 Peptide sequences used for the production of anti-NMDA receptor antibodies

NMDA receptor subunit accession number	Antibody	Antigen sequence	Mode of covalent coupling to carrier protein
NR1-1a – AAB50926, NR1-1b – AAB50928, NR1-2a - AAB50927, NR1-2b – AAB50929, NR1-3a - AAB50930, NR1-3b – AAB50931, NR1-4a – AAB50932 NR1-4b – AAB50932, Rat sequences.	NR1 pan	NR1 17-35 + C * TRKHEQMFREAVNQANKRHC	The peptide was linked via the C-terminal cysteine
NR1-1a – AAB50926, NR1-1b – AAB50928, NR1-2a - AAB50927, NR1-2b – AAB50929, Rat sequences.	NR1 C2	NR1 911-920* LQLCSRHRES	The peptide sequence is linked via the N-terminal leucine using the glutaraldehyde coupling.
NR2A – P35436, Mouse sequence.	NR2A	*NR2A 1381-1394 + K at N-terminal** KRCPSDPYKHSLPSQ	An N-terminal lysine has been added for coupling
NR2A – P35436, Mouse sequence.	NR2A	*NR2A 44-58 + C at C-terminal** *HDVTERELRNLWGPEC*	The peptide was coupled using the C-terminal cysteine.
NR2A/B - Q01097, Mouse sequences.	NR2A/B	anti-NR2A/2B (using the NR2A amino acid residues 1454-1464)* *YKKMPSTESDV*	The peptide was coupled via the N-terminal using the glutaraldehyde method.
NR2B – Q01097, Mouse sequence.	NR2B	NR2B 46-60 + C at C-terminal* *DEVAIKDAHEKDDKHC*	The peptide was coupled using the C-terminal cysteine.
NR2C – Q01098, Mouse sequence.	NR2C	NR2C 1227-1237* WRRVSSLESEV	The peptide was coupled via the N-terminal using the glutaraldehyde method.
NR2D – Q03391, Mouse sequence.	NR2D	NR2D 1307-1323* LGTRRGSAHFSSLESEV	The peptide was coupled via the N-terminal using the glutaraldehyde method.

* Numbering of sequences from immature peptide, i. e. all sequences include the signal peptide

2.1.8 Oligonucleotide primers used for either polymerase chain reaction, mutagenesis or nucleotide sequencing

Polymerase chain reaction (PCR) and sequencing oligonucleotide primers were purchased from Sigma-Proligo (Paris, France). All mutagenesis primers were purchased from MWG-Biotech (Ebersberg, Germany) and were HPLC purified by the manufacturer.

Mutagenesis oligonucleotide primer name	**Mutagenesis oligonucleotide primer sequence**
pCISNR2A^{S1459A} forward primer	5'GTGTGTACAAGAAAATGCCT**GC**TATTGAATCTGATG 3'
pCISNR2A^{S1459A} reverse primer	5 ' CATCAGATTCAATA**GC**AGGCATTTTCTTGTACACAC 3 '
pCISNR2A$^{T1441-STOP}$ forward primer	5' AATAACATGTACTCT**TAG**CCCAGGGTTTTAAATTCCTGCAGC 3'
pCISNR2A$^{T1441-STOP}$ reverse primer	5' GCTGCAGGAATTTAAAACCCTGGG**CTA**AGAGTACATGTTATT 3'
pCISNR2A$^{N1157-STOP}$ forward primer	5' TACCAAGATCACAATGAG**TAG**TTCCGCAAGGGGGACTCCACA 3'
pCISNR2A$^{N1157-STOP}$ reverse primer	5' TGTGGAGTCCCCCTTGCGGAA**CTA**CTCATTGTGATCTTGGTA 3'
pCISNR2B$^{FLAG/TRUNC}$ forward primer	5' GAGAAACTTTCTAGTATT**T**AGTCTGATGTCTGAGTGAGGG 3'
pCISNR2B$^{FLAG/TRUNC}$ reverse primer	5' CCCTCACTCAGACATCAGACT**A**AATACTAGAAAGTTTCTC 3'
pGBKT7NR2D^{TRUNC} forward primer	5' GCTCTGCGCACTTCTCC**T**GACTGGAGTCCGAGG 3'
pGBKT7NR2D^{TRUNC} reverse primer	5' CCTCGGACTCCAG**T**CAGGAGAAGTGCGCAGAGC 3'

Table 2.4 Summary of oligonucleotide primer sequences used for site-directed mutagenesis

The nucleotides which were mutated to generate the point mutation are shown in bold within each oligonucleotide primer sequence.

PCR oligonucleotide primer name	PCR oligonucleotide primer sequence
NR2D C-termini forward primer	**AAAAGAATTC**GAACACCTTGTGTACTGG
NR2D C-termini forward primer2	**AAAAGAATTC**CACCTTGTGTACTGGCGA
NR2D C-termini reverse primer	**AAAAGGATCC**TCATACCTCGGACTCCAG
NR2D C-termini reverse primer2	**AAAAGGATCC**TCGGGTGTTCTTGAGGCT
NR2D C-termini reverse primer3	**AAAAGGATCC**TCCTCTAGATCATACCTC

Table 2.5 Summary of oligonucleotide primers used for PCR reactions

Forward primers contained the *EcoRI* restriction endonuclease site (5' GAATTC 3') and the reverse primers contained the *BamHI* restriction endonuclease site (5' GGATCC 3'). The restriction endonuclease sites are shown in bold. Each oligonucleotide primer contains additional bases at the 5' end to aid the binding of the restriction endonuclease.

Sequencing oligonucleotide primer name	Sequencing oligonucleotide primer sequence
pCISNR2A^{S1459A}	5' GACAGTCGGGGCCAC 3'
pCISNR2A$^{T1441\text{-}STOP}$	5, TGCCATCACAGGCAGTAA 3'
pCISNR2A$^{N1157\text{-}STOP}$	5' GCCTCTAAATACCCCAAG 3'
pCISNR2B$^{FLAG/TRUNC}$	5' GGGGCTGTGCCAGGTCGTTTCC 3'
pGBKT7 forward primer	5' TCATCGGAAGAGACTAGT 3'

Table 2.6 Summary of oligonucleotide primers used for nucleotide sequencing

Plasmid DNAs were sent to MWG-Biotech for nucleotide sequencing (Ebersberg, Germany).

2.2 METHODS

2.2.1 Molecular biology methods

All solutions were sterilised either by filtration through a 0.22 μm pore size or by autoclaving at 121°C for 20 min.

2.2.1.1 Bacterial methods

2.2.1.1.1 Preparation of *DH5α E.coli* chemically competent cells

DH5α E.coli cells were streaked from glycerol stocks onto a Lennox B Broth (LB) 1.7 % (w/v) agar plate using a sterile loop. The plate was inverted and incubated for 12 - 16 h at 37°C. A 5 ml LB media pre-culture was inoculated with a single colony of *DH5α E.coli* cells and incubated at 37°C for 12 - 16 h at 200 rpm. The culture, 0.5 ml was used to inoculate a total volume 50 ml LB media containing 0.5 ml 20% (w/v) glucose and 0.5 ml 1 M $MgSO_4$ (solution A). The culture was incubated at 37°C at 250 rpm until an optical density $(OD)_{\lambda = 600\ nm} = 0.6 - 0.7$ was obtained. The culture was rapidly transferred into a pre-chilled 50 ml sterile centrifuge tube and chilled on ice for 10 min. The cells were pelleted by centrifugation at 2,500 × g for 10 min at 4°C using a Megafuge 1.0 R, Heraeus centrifuge (DJB, Buckinghamshire, U.K). The supernatant was decanted and the pellet resuspended in 0.5 ml LB media. Once resuspended, 2.5 ml storage solution (36% (v/v) glycerol, 12 % (w/v) polyethylene glycol (PEG, MW 7500), 12 mM $MgSO_4.7H_2O$, made in LB, pH 7) was added and thoroughly mixed by gentle pipetting. The competent cells were immediately aliquoted as 100 μl fractions and stored at -80°C until use. The competent cells were used within 3 months.

2.2.1.1.2 Preparation of *DH5α E.coli* electroporation competent cells

DH5α E.coli cells were streaked from glycerol stocks onto a Lennox L Broth (LB) 1.7 % (w/v) agar plate using a sterile loop. The plate was inverted and incubated for 12 - 16 h at 37°C. A 50 ml LB media pre-culture was inoculated using a single colony of *DH5α E.coli*

cells. The culture was incubated at 37°C for 12 - 16 h at 200 rpm. The culture was divided into 2 × 25 ml aliquots and used to inoculate 2 × 500 ml LB media in 1.5 L flasks. The cells were incubated at 37°C at 250 rpm until an $OD_{\lambda = 600nm} = 0.35$ was obtained. The cultures were cooled on ice for 15 min. Each subsequent step was performed on ice or at 4°C. The cultures were divided into 4 × 250 ml centrifuge tubes and pelleted by centrifugation at 1000 × g for 20 min at 4°C in a JLA 16.250 rotor using a Beckman centrifuge (Beckman Coulter Ltd, Buckinghamshire, U.K.). The pellets were washed in 500 ml ice-cold sterile distilled deionised water (ddH_2O) and centrifuged as above. The pellets were resuspended in 250 ml ice-cold 10 % (v/v) glycerol and centrifuged as above. The pellets were combined in 10 ml ice-cold 10 % (v/v) glycerol and centrifuged as above. Lastly, the pellet was resuspended in 1 ml GYT medium (10 % glycerol (v/v), 0.125 % (w/v) yeast extract, 0.25 % (w/v) peptone) and diluted to 2×10^{10} - 3×10^{10} cells/ml. The cells were rapidly divided into 40 µl aliquots, snap frozen and stored at -80°C until use. The competent cells were used within 6 months.

2.2.1.1.3 Chemical transformation of *DH5α E.coli* competent cells

For all routine plasmid DNA amplification and molecular cloning *DH5α E.coli* chemically competent cells were used, Section 2.2.1.1.1. Aliquots of *DH5α E.coli* chemically competent cells were taken from storage at -80°C and immediately put onto ice. The cells were defrosted for 5 min on ice. The plasmid to be transformed (~ 1 µg) was added to the cells and incubated for 30 min on ice followed by a heat shock for 1 min at 42 °C. The cells were incubated on ice for a further 10 min. They were diluted 1/10 by the addition of 900 µl SOC solution (LB media supplemented with 1 ml 20% (w/v) glucose and 5 ml 10 × salt solution (250 mM KCl, 100 mM $MgCl_2.H_2O$, 100 mM $MgSO_4.H_2O$) in a 1.5 ml sterile centrifuge tube. The cells were incubated at 37°C for 1 h at 250 rpm. The cells were pelleted by centrifugation for 2 min at 6,000 × g and the cell pellet gently resuspended in 100 µl SOC solution. The cell suspension was plated onto selective plates, either 50 µg/ml ampicillin LB 1.7 % (w/v) agar or 50 µg/ml kanamycin LB 1.7 (w/v) agar plates depending upon the resistance conferred by the plasmid. The plates were inverted and incubated for 16 h at 37°C. Once colonies appeared, they were selected for further study or the plates were wrapped in Parafilm and stored at 4°C for a maximum of 1 week.

2.2.1.1.4 Transformation of XL10-Gold *E.coli* ultracompetent cells

Plasmid DNA created by site-directed mutagenesis was always transformed into XL10-Gold *E.coli* ultracompetent cells, Section 2.2.1.2.10. An aliquot of XL10-Gold *E.coli* ultracompetent cells was defrosted on ice. The cells were rapidly divided as 45 µl aliquots into pre-chilled 14 ml BD Bioscience Falcon polypropylene round bottom tubes. To each aliquot of cells, 2 µl β-mercaptoethanol was added. The tubes were agitated every 2 min for a total of 10 min while on ice. To each aliquot of cells, 4 µl of either the control or mutagenesis Dpn I-treated plasmid DNA was added and gently swirled. The cells were incubated on ice for 30 min. The cells were heat shocked for 30 sec at 42°C then returned to ice for 2 min. To each aliquot of cells, 0.5 ml, pre-heated to 42°C, NZY+ broth (1 % (w/v) NZ amine (casein hydrolysate), 0.5 % (w/v) yeast extract, 0.5 % (w/v) NaCl, pH 7.5, supplemented with 12.5 mM $MgCl_2$, 0.4 % (w/v) glucose) was added. The cultures were incubated at 37°C for 1 h at 250 rpm. The culture was divided into 2 × 250 µl aliquots and plated on 2 × LB 1.7 % (w/v) agar plates containing either ampicillin (50 µg/ml) or kanamycin (50 µg/ml), as appropriate. The plates were inverted and incubated at 37°C for 16 h. Once colonies appeared, they were selected for further study or the plates were wrapped in Parafilm and stored at 4°C for a maximum of 1 week.

2.2.1.1.5 Transformation by electroporation of *DH5α E.coli* competent cells

Electroporation of plasmid DNA to *DH5α E.coli* competent cells provided a means of high transformation efficiency of the bacteria. This was necessary for the transformation of plasmid DNA isolated from yeast since this is often contaminated by genomic DNA which greatly decreases the overall transformation efficiency. A 40 µl aliquot of electro-competent cells was defrosted at room temperature and added into a pre-chilled 1.5 ml 0.1 cm spaced electroporation cuvette, Section 2.2.1.1.2. Plasmid DNA isolated from yeast, 4 µl was added to the cell suspension, Section 2.2.1.3.8. The cells were electroporated using a Flowgen Easyject Plus electroporator. Cells were shocked at 2500 V for 5 msec with the electroporator set at 25 µF capacitance and 201 Ohms shunt resistance. The cell suspension was immediately added to 1 ml SOC solution and incubated at 37°C for 1 h at 250 rpm. The cells were pelleted by centrifugation for 2 min at 6,000 × g and the cell pellet

resuspended in 100 µl SOC solution. The cell suspension was plated onto 50 µg/ml ampicillin LB 1.7 % (w/v) agar selective plates. The plates were inverted and incubated for 16 h at 37°C. Once colonies appeared, they were selected for further study or the plates were wrapped in Parafilm and stored at 4°C for a maximum of 1 week.

2.2.1.1.6 Glycerol stocks of transformed *DH5α E.coli* cells

A single 1 - 5 day old colony of pre-transformed *DH5α E.coli* cells was picked from a selective agar plate and used to inoculate 5 ml LB media containing the correct selective antibiotic, either 50 µg/ml ampicillin or 50µg/ml kanamycin, as appropriate. The culture was grown at 37°C for 12 - 16 h at 250 rpm. The glycerol stock was prepared by the addition of 500 µl 50% (v/v) glycerol to 1 ml 12 – 16 h culture. This was thoroughly mixed by inversion and stored at -80°C until use. Glycerol stocks were kept for a maximum of 1 year.

2.2.1.1.7 Mini preparation of plasmid DNA

A single colony of pre-transformed *DH5α E.coli* cells from a selective plate was picked and used to inoculate either 2 ml LB media (6 h culture) or 5 ml LB media (12 - 16 h culture) containing the correct selective antibiotic, either 50 µg/ml ampicillin or 50µg/ml kanamycin, as appropriate. The culture was grown at 37 °C at 250 rpm. The culture, 1.5 ml was transferred into a sterile 1.5 ml centrifuge tube and centrifuged at 6,000 × g for 2 min at room temperature. The supernatant was aspirated and the pellet resuspended by gentle pipetting in 200 µl resuspension buffer (50 mM Tris(hydroxymethyl)aminomethane-HCl (Tris-HCl), pH 8.0, containing 10 mM ethylenediaminetetraacetic acid (EDTA) and 100 µg/ml RNase A). Lysis buffer, 200 µl (200 mM NaOH, 1% (w/v) sodium dodecyl sulphate (SDS)) was added. This was mixed by inversion a total of 6 times. Neutralisation buffer (3.0 M potassium acetate), 200 µl was added. The mixture was gently inverted 6 times until a white precipitate formed. The tubes were incubated at -20°C for 10 min. The precipitate was removed by centrifugation at 12,000 × g for 10 min at room temperature. The supernatant was carefully transferred into a new sterile 1.5 ml centrifuge tube. Isopropanol, 400 µl was added to the supernatant and mixed by inversion. The tubes were centrifuged at

12,000 × g for 10 min at room temperature. The supernatant was discarded and 200 µl ice-cold 70 % (v/v) ethanol was added to the pellet. The DNA pellet was washed by vortexing for ~ 5 sec and centrifuged at 12,000 × g for 4 min at room temperature. The supernatant was removed and the plasmid DNA pellet was air-dried for ~ 15 min. The plasmid DNA was resuspended in TE buffer (10 mM Tris-HCl, pH 8.0 and 1 mM EDTA) and stored at -20°C until use.

2.2.1.1.8 Maxi preparation of plasmid DNA

The GenElute™ HP plasmid maxiprep kit was used for all large scale plasmid DNA extractions. A single colony of pre-transformed *DH5α E.coli* cells was picked from a selective plate and grown in 400 ml LB media containing the correct selective antibiotic, 50 µg/ml ampicillin or 50 µg/ml kanamycin, as appropriate. The culture was incubated at 37°C for 12 - 16 h at 250 rpm. The cell volume required was calculated to give a total cell mass of 750, where the total cell mass equalled:

- Total Cell Mass = $OD_{\lambda= 600}$ × ml of culture

The corresponding volume of 12 - 16 h culture which gave a cell density of 750 was pelleted by centrifugation at 5,000 × g for 10 min at 4°C, using a JLA 16.250 rotor in a Beckman centrifuge. The pellet was resuspended in 12 ml resuspension buffer by gentle pipetting. Lysis buffer, 12 ml, was added, mixed by inversion a total of 6 times and incubated for 4 min. The lysis was terminated by the addition of 12 ml ice-cold neutralisation buffer. This was thoroughly mixed by inversion a total of 6 times until a white precipitate formed. Binding buffer, 9 ml, was added and the lysed cell solution was poured into a GenElute™ HP maxiprep filter syringe. Plasmid DNA was filtered from the cell debris by passing the lysed cell solution through the GenElute™ HP maxiprep filter syringe.

The GenElute™ HP maxiprep binding column was equilibrated by the addition of 12 ml column preparation buffer. This solution was passed through the binding column by centrifugation at 3,000 × g for 2 min at 20°C using a Megafuge 1.0 R centrifuge. The filtrate from the lysed cells containing the plasmid DNA was added to the equilibrated binding column and centrifuged at 3,000 × g for 2 min at 20°C. This step was repeated

until all the filtrate had passed through the GenElute™ HP maxiprep binding column. Wash buffer 1, 12 ml, was added to the GenElute™ HP maxiprep binding column and the binding column was centrifuged at 3,000 × g for 2 min at 20°C. Wash buffer 2, 12 ml was added and the binding column was centrifuged at 3,000 × g for 5 min at 20°C. The plasmid DNA was eluted into 2 ml TE buffer (10 mM Tris-HCl, pH 8.0 and 1 mM EDTA) by centrifugation at 3,000 × g for 5 min at 20°C. The plasmid DNA-containing filtrate was passed through the GenElute™ HP maxiprep binding column an additional two times, as above. Plasmid DNA was characterised as below and stored as aliquots of 100 µl at -20°C until use.

The plasmid DNA concentration was measured by reading the $OD_{\lambda = 260\ nm}$. An $OD_{\lambda = 260\ nm}$ of 1.0 meant a DNA concentration of 50 µg/ml. The plasmid DNA purity was measured by the ratio $OD_{\lambda = 260\ nm}/OD_{\lambda = 280\ nm}$. An $OD_{\lambda = 260\ nm}/OD_{\lambda = 280\ nm}$ ratio of 1.8 - 2.0 is indicative of a pure DNA extraction. The plasmid DNA preparation was checked by enzyme restriction digestion to ensure that the correct plasmid had been amplified, Section 2.2.1.2.1.

The amplification of pcDNANR2D did not give high yields of plasmid DNA following the above method, therefore the starting culture was doubled to 800 ml LB media containing 50 µg/ml ampicillin. Consequently the total cell mass was increased to 1500. The above method was followed but each of the reagents was increased to twice the volume. In order to pass all the lysed cell suspension through the one GenElute™ HP maxiprep filter syringe, an additional centrifugation step was included. After the addition of 18 ml binding buffer, the white precipitate was removed by centrifugation at 14,000 × g for 30 min at 4°C. The resulting supernatant was passed through the GenElute™ HP maxiprep filter syringe and the above method was followed.

2.2.1.1.9 Giga preparation of plasmid DNA

The QIAfilter plasmid Giga kit was used according to the manufacturer's instructions. This kit can purify up to 10 mg plasmid DNA which is required when extracting the mouse brain cDNA library plasmid DNA. The pACT2 mouse brain cDNA library had been previously

amplified, Section 2.2.1.3.5.1. A wet weight of 7.5 g *E.coli* cells containing the pACT2 mouse brain cDNA library was used for each Giga preparation of plasmid DNA. The 7.5 g wet weight *E.coli* cells was resuspended in 125 ml P1 buffer (50 mM Tris-HCl, pH 8.0, 10 mM EDTA, 100 µg/ml RNase A). Lysis was started by the addition of 125 ml P2 buffer (200 mM NaOH, 1 % (w/v) SDS) and mixed by gentle inversion a total of 6 times. The lysis reaction was allowed to proceed for 4 min. The lysis was terminated by addition of 125 ml P3 buffer (3.0 M potassium acetate, pH 5.5) and mixed by inversion 6 times. The lysed cells were poured into a QIAfilter Giga cartridge and incubated for 10 min. The lysate was filtered into a sterile 1 L bottle under vacuum. FWB2 buffer (1 M potassium, acetate, pH 5.0) 50 ml, was added to the precipitate and gently mixed using a sterile spatula. Any remaining liquid was drawn through the QIAfilter Giga cartridge under vacuum and added to the original lysate. To begin to purify the plasmid DNA, a QIAGEN-tip 10000 was equilibrated with 75 ml QBT buffer (750 mM NaCl, 50 mM 4-morpholinepropanesulphonic acid (MOPS), pH 7.0, 15 % (v/v) isopropanol and 0.15 % (v/v) Triton X-100®), this was filtered under gravity. All the plasmid DNA was added to the equilibrated filter and passed through under gravity. The column was washed under gravity with 600 ml QC buffer (1.0 M NaCl, 50 mM MOPS, pH 7.0 and 15 % (v/v) isopropanol). The plasmid DNA was eluted under gravity in 100 ml QF buffer (1.25 M NaCl, 50 mM Tris-HCl, pH 8.5 and 15 % (v/v) isopropanol). Plasmid DNA was precipitated by the addition of 70 ml isopropanol, mixed by inversion and centrifuged at 15,000 × g for 30 min at 4°C using a JA-14 rotor in a Beckman centrifuge. The supernatant was carefully decanted and the pellet was washed with 10 ml ice-cold 70 % (v/v) ethanol. The plasmid DNA was pelleted by centrifugation at 15,000 × g for 10 min at 4°C, as above. The supernatant was carefully removed and the pellet was allowed to air-dry for ~ 20 min. The plasmid DNA was resuspended in 2 ml TE buffer (10 mM Tris-HCl, pH 8.0 and 1 mM EDTA). The plasmid DNA concentration was measured by reading the $OD_{\lambda = 260\ nm}$. An $OD_{\lambda = 260\ nm}$ of 1.0 meant a DNA concentration of 50 µg/ml. The plasmid DNA purity was measured by the ratio $OD_{\lambda = 260\ nm}/OD_{\lambda = 280\ nm}$. An $OD_{\lambda = 260\ nm}/OD_{\lambda = 280\ nm}$ ratio of 1.8 - 2.0 is indicative of a pure DNA extraction. Lastly the plasmid DNA was aliquoted and stored at -20 °C until use.

2.2.1.2 Molecular cloning methods

2.2.1.2.1 Restriction endonuclease digestion

Restriction endonuclease digestions were performed for both diagnostic purposes and for the cloning of PCR products. When digesting plasmid DNA for diagnostic purposes, restriction endonuclease digestions were conducted in sterile 0.5 ml centrifuge tubes containing 0.5 μg (~ 0.5 μl) plasmid DNA, 1 - 3 units of each restriction endonuclease, 1 μl or 2 μl (1 × or 2 × concentrated) Tango™ restriction endonuclease buffer (33 mM Tris-acetate, pH 7.9, 10 mM magnesium acetate, 66 mM potassium acetate, 0.1 mg/ml bovine serum albumin (BSA)) made to a total volume of 10 μl with ddH_2O. This was incubated for 1 h at 37°C. The reaction was terminated by the addition of 2 μl 6 × DNA loading buffer (50 % (v/v) glycerol, 20 % (w/v) EDTA, 100 mM Tris–HCl, pH 8.0, 0.1% (w/v) bromophenol blue, 0.1 % (w/v) xylene cyanol). The digested DNA was analysed by 1 % (w/v) flat bed agarose gel electrophoresis, Section 2.2.1.2.2

When digesting PCR products, the above method was followed using ~ 500 ng PCR product and the restriction endonuclease digestion was incubated for 2 h before being terminated by PCR purification, Section 2.2.1.2.7. The digested PCR product was then ready for ligation into the cloning vector, Section 2.2.1.2.9.

2.2.1.2.2 Flat bed agarose gel electrophoresis for DNA analysis

Plasmid DNA or PCR products were analysed by 1 % (w/v) flat bed agarose gel electrophoresis. Electrophoresis was carried out using a Flowgen MH 1070 minigel apparatus. A 1 % (w/v) agarose solution was made in 1 × Tris-borate-EDTA buffer (TBE, 90 mM Tris-HCl, pH 8.0, 90 mM boric acid, 4 mM EDTA). The agarose was dissolved by boiling for ~ 90 sec in a microwave oven. Once the agarose had cooled to ~ 40°C, 2 μl ethidium bromide was added to the agarose solution and mixed. The agarose solution was poured between two metal bars and a comb was placed 2 cm from the top of the gel. The agarose solution was allowed to solidify for 20 min. The metal bars and comb were removed and the agarose gel was covered in 50 ml 1 × TBE buffer. Each DNA sample was

prepared by the addition of ~ 0.5 µg DNA, 2 µl 6 × DNA loading buffer and ddH_20 (5 - 9.5 µl) to give a 12 µl total volume. The DNA samples were loaded and electrophoresis was carried out at 54 V for 1 h. Gels were imaged using a Flowgen transilluminator UV light source λ = 312 nm in conjunction with a Kodak DC120 206 M digital camera.

2.2.1.2.3 Ethanol precipitation of plasmid DNA

Ethanol precipitation of plasmid DNA was used to either concentrate or purify plasmid DNA. To 1 volume plasmid DNA, 0.12 volumes 3 M sodium acetate and 2.5 volumes ice-cold ethanol were added into a 1.5 ml sterile centrifuge tube. The mixture was incubated for 2 h at -80°C. Plasmid DNA was pelleted by centrifugation at 12,000 × g for 30 min at 4°C. The supernatant was carefully discarded and 200 µl ice-cold 70 % (v/v) ethanol was added to wash the plasmid DNA pellet. The plasmid DNA was pelleted by centrifugation at 12,000 × g for 3 min at 4°C. The supernatant was removed and the plasmid DNA pellet was allowed to air dry for ~ 15 min. The plasmid DNA pellet was either resuspended in the appropriate volume of TE buffer (10 mM Tris-HCl, pH 8.0 and 1 mM EDTA) and stored at -20°C until use or sent as a dry plasmid DNA precipitate (~ 1.5 µg) to MWG-Biotech for nucleotide sequencing.

2.2.1.2.4 Design of PCR oligonucleotide primers

The following criteria were followed when designing oligonucleotide primers for PCR amplification of DNA sequences:

- The primer must be at least 18 bases in length.
- The melting temperatures of oligonucleotide primers were calculated using the Wallace *et al.* (1979) rule:

  Melting Temperature = (4[G + C] + 2[A + T])

  where: [G + C] = number of guanine + cytosine bases and [A + T] = number of adenine + thymine bases. The optimal melting temperature of an oligonucleotide primer was in the range of 52 °C - 60 °C.
- The melting temperature for a pair of primers must be within 10°C of each other.
- The guanine/cytosine (G/C) content should be between 40 - 60 %.

- Repeats of the same base were avoided and care was taken to ensure that the primers did not have any complementary sequences (palindromes) either within itself or with the other primer in the pair.
- To facilitate the cloning of PCR products into cloning vectors restriction endonuclease sites were added to the 5' end of each primer. To assist with the binding of the restriction endonuclease to the PCR product additional bases were included at the 5' end of each primer.

2.2.1.2.5 Design of oligonucleotide primers for nucleotide sequencing

The following criteria were used in the design of oligonucleotide primers for plasmid DNA nucleotide sequencing of plasmid DNA constructs:

- The length of the oligonucleotide primer should be 18 - 30 nucleotides in length.
- The melting temperature should be between 55°C - 75°C, using the Wallace *et al.* (1979) rule, see Section 2.2.1.2.4.
- The G/C content should be between 40 - 60 %.
- The oligonucleotide primer should anneal ~ 80 - 150 nucleotides from the region from which the nucleotide sequence is to be determined.

2.2.1.2.6 PCR cycles used for amplification of DNA

For the PCR amplification of DNA sequences, the following reaction was mixed in a 0.5 ml sterile PCR tube; 33 µl sterile ddH_2O, 10 µl 5 × Phusion™ GC buffer or 10 µl 5 × Phusion™ HF buffer, 1 µl 10 mM deoxynucleoside-5'-triphosphates (dNTP), 1.5 µl 10 µM forward primer, 1.5 µl 10 µM reverse primer, 100 ng template DNA, 1 µl dimethyl sulphoxide (DMSO) and 0.5 µl Phusion™ DNA polymerase (2 U/µl).

Each PCR reaction had two control reactions carried out in parallel. The above reaction was prepared in the absence of either the template plasmid DNA or the Phusion™ DNA polymerase. This ensured the resulting PCR product was a specific amplification of the desired sequence and not a contaminant.

The test and control reactions were cycled using a PTC-100®, Peltier Thermal cycler, (MJ Research, Minnesota, USA) using the below parameters:

Segment	Cycles	Temperature	Time
1	1	98°C	30 sec
2	30	98 °C	10 sec
		55 °C	20 sec
		72°C	15 sec/ kb of DNA
3	1	72 °C	5 min

The resulting PCR products were analysed using flat bed agarose gel electrophoresis, Section 2.2.1.2.2.

2.2.1.2.7 Purification of PCR products

The Qiagen QIAquick PCR purification kit was used to purify PCR products from molecular cloning enzymes and to change the PCR product into a desired buffer. To the PCR reaction mixture, 5 volumes PB buffer was added. The solution was transferred to a QIAquick column and centrifuged at 15,000 × g for 1 min at room temperature. The flow-through was discarded. The QIAquick column was washed with 750 µl PE buffer and centrifuged for 1 min at 15,000 × g at room temperature. The flow-through was removed and the QIAquick column was centrifuged as above to remove all traces of buffer. The QIAquick column was put into a sterile 1.5 ml centrifuge tube and 30 µl 10 mM Tris-HCl, pH 8.0 was added to elute the PCR product. The column was centrifuged at 15,000 × g for 1 min at room temperature. The purified PCR product was used immediately for all subsequent reactions.

2.2.1.2.8 5' Dephosphorylation of cloning vectors using shrimp alkaline phosphatase

Vectors were dephosphorylated to minimise the background caused by their recircularization. The following reaction was carried out in a 0.5 ml sterile centrifuge tube; 1 x shrimp alkaline phosphatase (SAP) buffer (20 mM Tris-HCl, pH 8.0, 10 mM $MgCl_2$), 1 - 5 µg restriction endonuclease digested vector and 1 unit SAP enzyme. The reaction was incubated at 37°C for 1 h. The SAP reaction was terminated by heat inactivation at 65°C for 20 min. Dephosphorylated vectors were used for all subsequent cloning of PCR products.

2.2.1.2.9 Ligation reactions

Restriction endonuclease digested PCR products were ligated into the restriction endonuclease digested and dephosphorylated vectors by the addition of T4 DNA ligase and thermocycling. A ligation reaction was made containing; 1 x ligation buffer (66 mM Tris-HCl, pH 7.5, 5 mM $MgCl_2$, 1 mM dithiothreitol (DTT), 1 mM ATP), 1.5 units T4 DNA ligase together with restriction endonuclease digested + dephosphorylated vector and restriction endonuclease digested PCR product, in a ratio of approximately 1:1. The ratios of the vector DNA and PCR product were determined by qualitative analysis from gel images gained from 1 % (w/v) flat bed agarose gel electrophoresis analysis, Section 2.2.1.2.2. The reaction was incubated for 16 h cycling between 10°C for 1 min and 30°C for 1 min (Lund *et al.*, 1996). Ligation samples were then transformed into chemically competent *DH5α E.coli* cells, Section 2.2.1.1.3.

2.2.1.2.10 *In vitro* site-directed mutagenesis

The QuikChange® II XL site-directed mutagenesis kit was used to create the following point mutations, $pCISNR2A^{S1459A}$, $pCISNR2A^{T1441\text{-}STOP}$, $pCISNR2A^{N1157\text{-}STOP}$, $pCISNR2B^{FLAG/TRUNC}$ and $pGBKT7NR2D^{TRUNC}$, using pCISNR2A (9.8 kb), $pCISNR2B_{FLAG}$ (9.8 kb) and pGBKT7NR2D (8.8 kb) as the template DNA, as appropriate. A summary of the strategy employed for *in vitro* site-directed mutagenesis is illustrated in Figure 2.1.

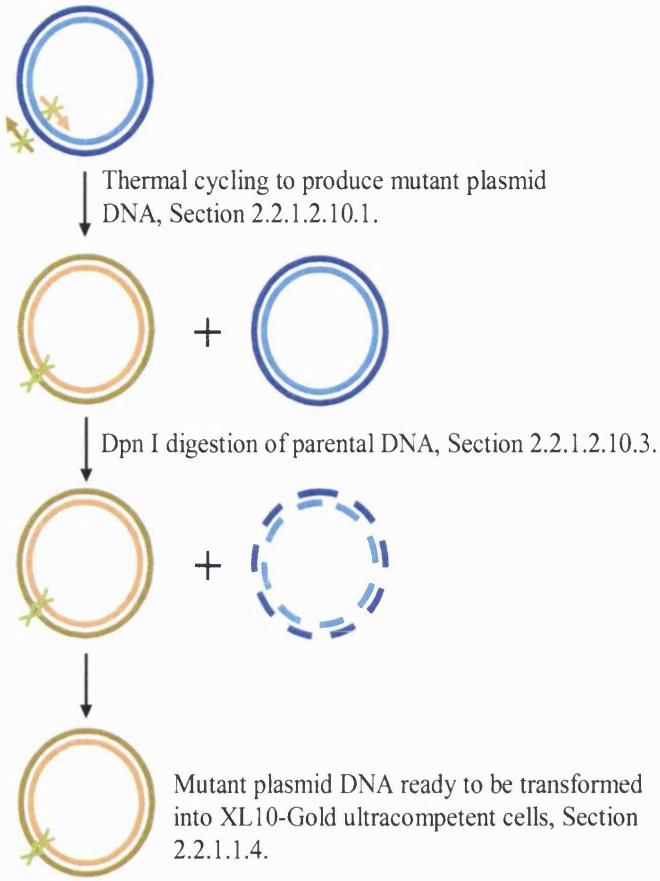

Figure 2.1 Summary of the site-directed mutagenesis strategy

Oligonucleotide primers were designed with the desired mutation (indicated with a cross) which hybridised to the parental plasmid DNA. Thermal cycling generated mutations within the amplified plasmid DNA. The parental DNA was digested with *Dpn I* and the mutant plasmid DNA was transformed into XL10-Gold ultracompetent cells. The figure was adapted from Stratagene's "QuikChange® II XL Site-Directed Mutagenesis Kit" Manual.

2.2.1.2.10.1 Design of mutagenesis primers

The following criteria were followed when designing mutagenesis primers:

- Both primers must contain the mutation and anneal to opposite sides of the plasmid.
- The primers should be 25-45 nucleotides in length.
- The melting temperature of the primers should be ≥78 °C.

- The mutation should be in the centre of the primer and have ~ 10-15 nucleotides flanking each side of the mutation.
- The primers should have a minimum of 40 % GC content and the primers must start and end with one or more G or C bases.
- Primers must be purified by reverse phase chromatography.

A summary of the primers used are shown in Figures 2.2.

Figure 2.2 A summary of the oligonucleotide mutagenesis primers used to generate pCISNR2A^{S1459A}, pCISNR2A$^{T1441\text{-}STOP}$, pCISNR2A$^{N1157\text{-}STOP}$, pCISNR2B$^{FLAG/TRUNC}$ and pGBKT7NR2D^{TRUNC}

Oligonucleotide mutagenesis primers used for the generation of pCISNR2A^{S1459A}

Peptide sequence:

Arg|Val|Tyr|Lys|Lys|Met|Arg|**Ser**|Ile|Glu|Ser|Asp|Val

Plus Strand

Template DNA:

5'GT|GTG|TAC|AAG|AAA|ATG|CCT|**AG**T|ATT|GAA|TCT|GAT|G 3'

Mutagenesis primers:

5'GT|GTG|TAC|AAG|AAA|ATG|CCT|**GC**T|ATT|GAA|TCT|GAT|G 3'

Minus Strand

Template DNA:

3'CA|CAC|ATG|TTC|TTT|TAC|GGA|**TC**A|TAA|CTT|AGA|CTA|C 5'

Mutagenesis primers:

3'CA|CAC|ATG|TTC|TTT|TAC|GGA|**CG**A|TAA|CTT|AGA|CTA|C 5'

Mutated Peptide Sequence:

Arg|Val|Tyr|Lys|Lys|Met|Arg|**Ala**|Iso|Glu|Ser|Asp|Val

Serine 1459 had the codon AGT mutated into the STOP codon GCT. Shown above are the primers used to generate the pCISNR2A^{S1459A} mutant using pCISNR2A as the parental plasmid DNA. The primers were 36 nucleotides in length, had a G/C content of 39 % and a melting temperature of 73°C. The melting temperature for these mutagenesis primers are below the recommended minimum, however due to the nature of the nucleotide sequence at the C-terminal of NR2A being AT rich this was the only option.

Oligonucleotide mutagenesis primers for the generation of pCISNR2A$^{T1441\text{-}STOP}$

Peptide Sequence:

Asn|Asn|Met|Tyr|Ser|**Thr**|Arg|Arg|Val|Leu|Asn|Ser|Cys|Ser

Plus Strand

Template DNA:

5' AAT|AAC|ATG|TAC|TCT|**ACC**|CCC|AGG|GTT|TTA|AAT|TCC|TGC|AGC 3'

Mutagenesis primers:

5' AAT|AAC|ATG|TAC|TCT|**TAG**|CCC|AGG|GTT|TTA|AAT|TCC|TGC|AGC 3'

Minus Strand

Template DNA :

3'TTA|TTG|TAC|ATG|AGA|**TGG**|GGG|TCC|CAA|AAT|TTA|AGG|ACG|TCG 5'

Mutagenesis primers:

3'TTA|TTG|TAC|ATG|AGA|**ATC**|GGG|TCC|CAA|AAT|TTA|AGG|ACG|TCG 5'

Mutated peptide sequence:

Asn|Asn|Met|Tyr|Ser|**STOP**

Theonine 1441 had the codon ACC mutated into the STOP codon TAG. Above are the primers which were used to generate the pCISNR2A$^{T1441\text{-}STOP}$ mutant, using pCISNR2A as the parental plasmid DNA. The mutagenesis primers were 42 nucleotides in length, had a G/C content of 40 % and a melting temperature of 78°C.

Oligonucleotide mutagenesis primers for the generation of pCISNR2A$^{N1157\text{-}STOP}$

Peptide Sequence:

Tyr|Gln|Asp|His|Asn|Glu|**Asn**|Phe|Arg|Lys|Gly|Asp|Ser|Thr

Plus Strand

Template DNA:

5'TAC|CAA|GAT|CAC|AAT|GAG|**ATT**|TTC|CGC|AAG|GGG|GAC|TCC|ACA 3'

Mutagenesis primers:

5'TAC|CAA|GAT|CAC|AAT|GAG|**TAG**|TTC|CGC|AAG|GGG|GAC|TCC|ACA 3'

Minus Strand

Template DNA:

3'ATG|GTT|CTA|GTG|TTA|CTC|**TAA**|AAG|GCG|TTC|CCC|CTG|AGG|TGT 5'

Mutagenesis primers:

3'ATG|GTT|CTA|GTG|TTA|CTC|**ATC**|AAG|GCG|TTC|CCC|CTG|AGG|TGT 5'

Mutated peptide Sequence:

Tyr|Gln|Asp|His|Asn|Glu|**STOP**

Asparagine 1157 had the codon ATT mutated into the STOP codon TAG. Above are the mutagenesis primers used to generate the pCISNR2A$^{N1157\text{-}STOP}$ mutant, using pCISNR2A as the parental plasmid DNA. The mutagenesis primers were 42 nucleotides in length, had a G/C content of 50 % and a melting temperature of 83°C.

Oligonucleotide mutagenesis primers for the generation of pCISNR2B$^{TRUNC/FLAG}$

Peptide Sequence:

Glu|Lys|Leu|Ser|Ser|Ile|**Glu**|Ser|Asp|Val|STOP

Plus Strand

Template DNA:

5'GAG|AAA|CTT|TCT|AGT|ATT|**G**AG|TCT|GAT|GTC|TGA|GTG|AGG|G 3'

Mutagenesis primers:

5'GAG|AAA|CTT|TCT|AGT|ATT|**T**AG|TCT|GAT|GTC|TGA|GTG|AGG|G 3'

Minus Strand

Template DNA:

3'CTC|TTT|GAA|AGA|TCA|TAA|**C**TC|AGA|CTA|CAG|ACT|CAC|TCC|C 5'

Mutagenesis primers:

3'CTC|TTT|GAA|AGA|TCA|TAA|**A**TC|AGA|CTA|CAG|ACT|CAC|TCC|C 5'

Mutated peptide sequence:

Glu|Lys|Leu|Ser|Ser|Ile|**STOP**

Glutamate 1479 had the codon GAG, this was mutated to TAG. Above are the mutagenesis primers used to generate the pCISNR2B$^{TRUNC/FLAG}$ mutant, using pCISNR2B^{FLAG} as the parental plasmid DNA. The mutagenesis primers were 40 residues in length, with a G/C content of 40 % and a melting temperature of 79°C.

Oligonucleotide mutagenesis primers for the generation of pGBKT7NR2D^{TRUNC}

Peptide Sequence:

Gly|Ser|Ala|His|Phe|Ser|**Ser**|Leu|Glu|Ser|Glu|Val

Plus Strand

Template DNA:

5' GC|TCT|GCG|CAC|TTC|TCC|**A**G**C**||CTG|GAG|TCC|GAG|G 3'

Mutagenesis primers:

5' GC|TCT|GCG|CAC|TTC|TCC|**T**G**A**||CTG|GAG|TCC|GAG|G 3'

Minus Strand

Template DNA:

3' CG|AGA|CGC|GTG|AAG|AGG|**T**C**G**|GAC|CTC|AGG|CTC|C 5'

Mutagenesis primers:

3' CG|AGA|CGC|GTG|AAG|AGG|**A**C**T**|GAC|CTC|AGG|CTC|C 5'

Mutated peptide sequence:

Gly|Ser|Ala|His|Phe|Ser|**STOP**

Serine 1318 had the codon AGC mutated into the STOP codon TGA. Above are the mutagenesis primers used to generate the pGBKT7NR2D^{TRUNC}, using pGBKT7NR2D as the parental plasmid DNA. The mutagenesis primers were 33 residues in length, had a G/C content of 64 % and a melting temperature of 81°C.

When the oligonucleotide primer hybridises to the plasmid DNA, the resulting amplified plasmid DNA contains the mutation. The kit contained the DNA polymerase, *PfuUltra* which has a high fidelity rate (4.3×10^{-7} mutations per base per duplication). This was particularly important when amplifying the above constructs which had a size of ~ 10 kB. Parental plasmid DNA was previously amplified in *E.coli* cells and therefore is methylated or hemi-methylated. This allows the newly synthesised mutant plasmid DNA created by PCR to be distinguished from the template parental plasmid DNA. The restriction endonuclease, *Dpn I* specifically digests plasmid DNA which is methylated or hemi-methylated, thus leaving only newly synthesised mutant plasmid DNA. The newly synthesised mutant plasmid DNA was transformed into XL10-Gold *E.coli* ultracompentent cells, Section 2.2.1.1.7. The XL10-Gold *E.coli* strain has the advantage of the Hte phenotype which helps to facilitate the transformation of larger plasmids. The resulting colonies were amplified and a mini-preparation of plasmid DNA was carried out, Section 2.2.1.1.7. Lastly, the plasmid DNA was nucleotide sequenced to verify the correct mutation had been generated.

In parallel with the above mutagenesis reactions, a control reaction was carried out, Section 2.2.1.2.10.2 – 2.2.1.2.10.3. The QuikChange® II XL site-directed mutagenesis kit contained the control plasmid pWhitescript™. The pWhitescript™ contains the gene for the β-galactosidase enzyme. Expression of β-galactosidase results in the enzyme breaking down 5-bromo-4-chloro-3-indoyl-β-D-galactosidase (X-gal) to form a blue product. However, a C → T mutation creates a TAA STOP codon instead of a CAA glutamine codon is present in the pWhitescript™. Therefore the mutagenesis oligonucleotide primers mutate this TAA STOP codon into the CAA glutamine codon to give the full length protein. The successfully mutated pWhitescript™ is easily visualised by a blue colony phenotype on LB ampicillin (50 μg/ml) 1.7 % (w/v) agar plates in the presence 80 μl/ml X-gal and 20 mM isopropylthio-β-D-galactosidase (IPTG).

2.2.1.2.10.2 Thermal cycling to produce mutant plasmid DNA

For each mutagenesis reaction the following mixture was made in a 0.5 ml PCR tube; 5 μl 10 × reaction buffer, 10 ng dsDNA template, 125 ng forward oligonucleotide, 125 ng

reverse oligonucleotide, 1 µl dNTP mix, 3 µl QuikSolution and ddH_2O to a final volume 50 µl. This was pulsed for ~ 5 sec in a benchtop centrifuge to ensure all components were mixed and removed from the sides of the tubes. To the reaction, 1 µl (2.5 U/µl) *PfuUltra* DNA polymerase was added. The reactions were cycled using a PTC-100®, Peltier Thermal cycle using the below parameters:

Segment	Cycles	Temperature	Time
1	1	95°C	1 min
2	18	95 °C	50 sec
		60 °C	50 sec
		68 °C	2 min/ kb of plasmid length
3	1	68 °C	7 min

2.2.1.2.10.3 Digestion of Parental DNA

Once the mutagenesis reactions were complete, 1 µl *Dpn I* (10 U/µl) was added and samples incubated for 1 h at 37°C. The newly synthesised mutant plasmid DNA was then transformed into XL10-Gold *E.coli* ultracompetent cells, Section 2.2.1.1.4.

2.2.1.3 Yeast two-hybrid methods

All yeast work was carried out in a dedicated laminar flow hood. Each item was lightly sprayed before use with 70 % (v/v) ethanol to ensure sterility. All solutions were sterilised either by filtration through a 0.22 µm pore size or by autoclaving at 121°C for 20 min.

2.2.1.3.1 Revival of yeast strains

AH109 and Y187 *S. cerevisiae* yeast strains were used for all yeast work. Using a sterile loop, a small fraction of yeast cells were scraped from frozen glycerol stocks and streaked onto yeast extract peptone dextrose with adenine (YPAD) 2 % (w/v) agar plates (2% (w/v) peptone, 1% (w/v) yeast extract, 2% (w/v) glucose, 0.003% (w/v) adenine hemisulphate,

pH 5.8). The plates were inverted and incubated at 30°C for 2 - 3 days until colonies grew. The yeast colonies were used for all subsequent yeast work. The plates were stored at 4°C wrapped with Parafilm for a maximum of 3 weeks. The transformation efficiency decreased as the yeast cells aged therefore yeast cells no older than 3 weeks were used.

2.2.1.3.2 Preparation of glycerol stocks of AH109 or Y189 *S. cerevisiae* cells

A single colony of AH109 or Y189 *S. cerevisiae* cells was picked and used to inoculate 5 ml YPAD media (2% (w/v) peptone, 1% (w/v) yeast extract, 2% (w/v) glucose, 0.003% (w/v) adenine hemisulphate, pH 5.8). The culture was grown at 30°C for 16 h at 250 rpm. A glycerol stock was prepared by taking 850 µl 16 h culture and adding 150 µl 100 % glycerol to give a 15 % (v/v) glycerol stock solution. The glycerol stock was stored at -80°C until use. Glycerol stocks were kept for up to one year.

2.2.1.3.3 Preparation of competent AH109 or Y187 *S. cerevisiae* cells

Competent yeast cells were prepared according to the method of Schiestl and Gietz (1989). A 16 - 18 h culture was prepared by inoculating 5 ml YPAD media with a single colony of AH109 or Y189 *S. cerevisiae* cells. The culture was grown at 30°C for 16 - 18 h at 250 rpm. A starting $OD_{\lambda= 600nm}$ of 0.15 was prepared in 50 ml YPAD media. This was prepared by measuring the $OD_{\lambda= 600nm}$ from a 1/10 dilution of the 16 - 18 h culture and dividing the $OD_{\lambda= 600nm}$ value by 0.15 to give the dilution factor. The starting volume of the culture, 50 ml was then divided by the above dilution factor to give the volume of 16 - 18 h culture to add to the 50 ml YPAD media. The culture was incubated at 30°C at 250 rpm for ~ 4 h until an $OD_{\lambda= 600nm}$ of 0.4 - 0.5 was obtained. The cells were pelleted by centrifugation in a 50 ml sterile tube at 2,500 × g at room temperature using a Megafuge 1.0 R centrifuge. The supernatant was discarded, the pellet was resuspended in 25 ml ddH_2O and the cells were pelleted by centrifugation as above. The supernatant was discarded and the cells were resuspended in 12.5 ml lithium sorbitol solution (100 mM lithium acetate, 10 mM Tris-HCl, pH 8.0, 1 mM EDTA, pH 8.0 and 1 M sorbitol) and pelleted by centrifugation as above. The supernatant was discarded and the cells resuspended in 300 µl lithium sorbitol solution, 80 µl salmon sperm DNA (2 µg/ml, freshly boiled for 5 min then rapidly cooled in ice for 5 min) and 1 ml lithium PEG solution (100 mM lithium acetate, 10 mM Tris-HCl,

pH 8.0, 1 mM EDTA, pH 8.0 and 40% (w/v) PEG (molecular weight 3500)). This was thoroughly mixed and the cell suspension was divided into aliquots of 100 µl. Aliquots of competent cells were either transformed straight away or stored at -80°C for a maximum of 3 months, Section 2.2.1.3.4.

2.2.1.3.4 Small scale transformation of AH109 or Y189 *S. cerevisiae* cells using the lithium acetate method

Positive and negative controls were always carried out in parallel to the test co-transformations. The positive control was the co-transformation of the SV40 large T-antigen (amino acids 84-708, cloned in pACT2, termed pTD1-1) with the murine p53 protein (amino acids 72-390, cloned in pGBT9, termed pVA3-1). The negative controls included the co-transformation of every construct with the corresponding empty vector, i.e. pTD1-1 contains the activation domain therefore would be co-transformed with pGBKT7 which has the DNA-binding domain. The principle behind the yeast two-hybrid is described in Section 6.1.2.

Competent AH109 or Y189 *S. cerevisiae* cells were transformed either immediately after preparation or after being defrosted at room temperature for 5 min, Section 2.2.1.3.3. The desired plasmid DNA (500 ng) was added to each tube of competent yeast cells. Samples of yeast cells were mixed by gently vortexing for ~ 2 sec and incubated for 20 min at room temperature. To each sample of yeast cells, 12 µl DMSO was added and mixed by gentle vortexing for ~ 2 sec. The yeast cells were heat shocked for 10 min at 42°C. Yeast cells were pelleted by centrifugation at 12,000 × g for 30 sec at room temperature. The supernatant was removed and the transformed yeast cells were resuspended in 200 µl ddH_2O. The transformed yeast cells were divided into 2 × 100 µl aliquots and plated onto selective dropout media plates. One aliquot was plated onto a -leucine/-tryptophan (-Leu/-Trp) dropout medium, 2 % (w/v) agar plate and the other aliquot of transformed yeast cells was plated onto one -leucine/-tryptophan/-histidine/-adenine (-Leu/-Trp/-His/-Ade) dropout medium, 2 % (w/v) agar. The plates were inverted and incubated at 30°C for 3 - 5 days until colonies appeared. The colony numbers were recorded at this point. The plates were wrapped in Parafilm and stored at 4°C for a maximum of 3 weeks.

Yeast cell growth on -Leu/-Trp selective dropout plates indicated successful co-transformation of both the DNA-binding domain containing and activation domain containing plasmids. The determination of protein interactions required yeast cell growth present on the -Leu/-Trp/-His/-Ade selective dropout plates. Yeast cell growth on the -Leu/-Trp/-His/-Ade selective dropout plates demonstrates the activation of reporter genes, summarised in Section 6.1.2.

2.2.1.3.5 Yeast-two hybrid library screening to identify positive interactors for the NR2D subunit C-terminal domain

An overview of the screening methods carried out are shown in Figure 2.3.

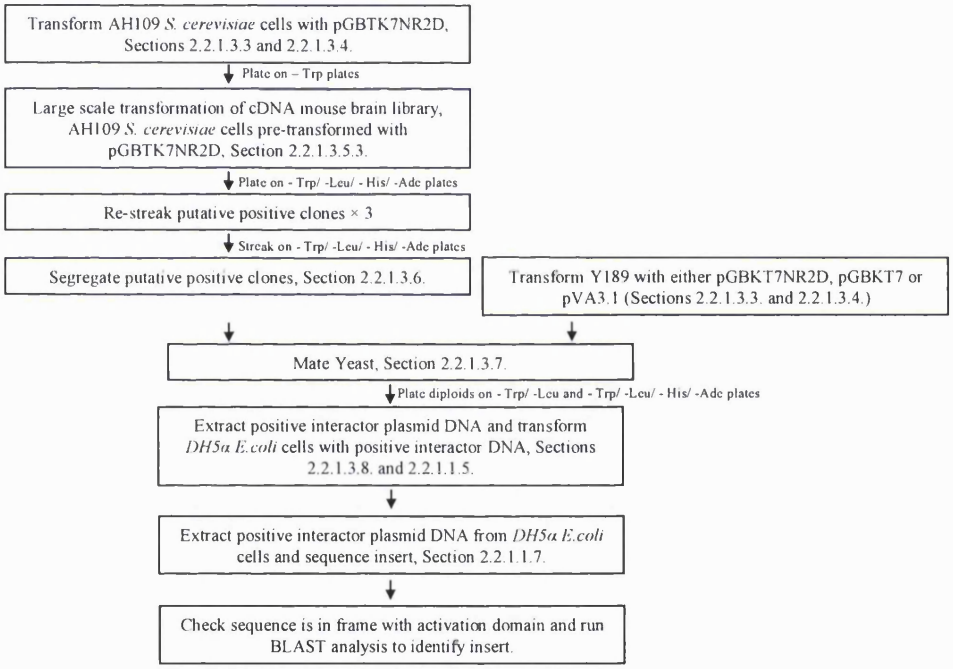

Figure 2.3 Identification of positive interactions of the NR2D C-terminal domain by mouse brain cDNA library screening using the yeast two-hybrid system

The above flow diagram shows the methods used to identify positive interactions in the yeast two-hybrid following cDNA mouse brain library screening using pGBKT7NR2D clones as bait..

2.2.1.3.5.1 Amplification of mouse brain cDNA library cloned into pACT2

The mouse brain cDNA library was sourced from 200 BALB/c males, aged 9 – 12 weeks, normal whole brains. The number of independent clones present was 3.5×10^6 which had an average insert size of 2.0 kb and a range of 0.4 – 4.0 kb. The library was amplified as

instructed by the manufacturer. Briefly, a 1 ml aliquot of the cDNA mouse brain library was defrosted on ice. The library, 1 µl, was added to 1 ml LB media creating dilution A. From dilution A, 1 µl was added to 1 ml LB media creating dilution B. The cell suspensions were plated onto LB 1.7 % (w/v) agar 50 µg/ml ampicillin, as follows: plate 1 = 1 µl dilution A in 50 µl LB, plate 2 = 50 µl dilution B and plate 3 = 100 µl dilution B. The plates were inverted and incubated at 30°C for 36 h. The cDNA mouse brain library was derived from a phage system therefore by growing the cells at 30°C this ensured that any residual phage present would not lyse the cultures. The colony forming units (cfu) / ml were calculated by:

- cfu/ ml for dilution A = number of colonies × 10^3× 10^3

  Therefore the cfu /ml = 4×10^8

The library was amplified so that each independent clone was represented at least 3 times thereby ensuring that rare clones were present. Since the library contained 3.5×10^6 independent clones to ensure 3 × coverage it was necessary to amplify:

- $3.5 \times 10^6 \times 3 = 10.5 \times 10^6$ clones

The manufacturer guidelines estimated that each 10 mm Petri dish holds 20,000 colonies:

- 10.5×10^6 / 20,000 = 525 LB 1.7 % (w/v) agar/ 50 µg/ml ampicillin plates.

The titration of the library revealed there were 4×10^8 cfu/ml. A comprehensive coverage of the library required 10.5×10^6 clones to be amplified. Therefore the volume of the master stock of the cDNA mouse brain library taken was:

- Volume of master stock of library containing 10.5×10^6 clones = number of clones to be screened/ cfu/ml

  $= 10.5 \times 10^6 / 4 \times 10^8 = 26.26$ µl.

This volume of master stock of library needed to be diluted in LB media to ensure each plate was evenly covered. The manufacturer recommended plating a volume of 150 µl LB media per 10 mm LB 1.7 % (w/v) agar / 50 µg/ml ampicillin plate, therefore:

= 150 µl per plate × number of plates required

= 150 × 525 = 78.75 ml.

The master cDNA mouse brain library stock, 26.26 µl was added to 78.75 ml LB media and 150 µl aliquots were plated onto 525 LB 1.7 % (w/v) agar / 50 µg/ml ampicillin plates. The plates were inverted and incubated for 36 h at 30°C. The resulting colonies were scraped

into 3.8 ml LB/ 25 % (v/v) glycerol per plate thus giving a total volume of 2 L. This was divided into 50 ml fractions and stored at -80°C until use. The mouse brain cDNA library plasmid DNA was extracted by conducting a Giga preparation of plasmid DNA, Section 2.2.1.1.9.

2.2.1.3.5.2 Small scale transformation of competent AH109 *S. cerevisiae* cells using the lithium acetate method to test the titre of cDNA mouse brain library

The mouse brain cDNA library was titred in order to calculate the amount of plasmid DNA necessary to give adequate coverage of the library. AH109 *S. cerevisiae* cells were transformed with pGBKT7NR2D and the transformed yeast cells were plated on -Trp single dropout 2 % (w/v) agar plates, as pGBKT7 confers the tryptophan nutritional marker, Section 2.2.1.3.4. A single colony was used to inoculate 5 ml -Trp single drop-out media and this was incubated at 30°C for 16 - 18 h at 250 rpm. The 16 - 18 h culture was used to inoculate 50 ml YPAD with a starting $OD_{\lambda= 600nm}$ of 0.15, Section 2.2.1.3.3. The culture was grown until an $OD_{\lambda= 600nm}$ of 0.4 - 0.5 was obtained. The cells were prepared as in Section 2.2.1.3.3. The competent cells were transformed with 1 µg pACT2 cDNA mouse brain library plasmid DNA, Section 2.2.1.3.5.1. The transformed yeast cells were plated onto -Leu/-Trp selective dropout plates. The plates were inverted and incubated at 30°C for 3 - 4 days until colonies appeared. The manufacturer recommended the number of independent clones in the library was 3.5×10^6. To screen 3.5×10^6 independent clones would require ~ 70000 clones/plate when using 50 × 240 mm plates. The small scale transformation using 1 µg of library resulted in ~ 20000 clones on one 240 mm plate. Therefore 3.5 × this amount of cDNA mouse brain library was required to give 1 × library coverage, i.e. 175 µg cDNA mouse brain library DNA per screen. A large scale library screen required 3 × this amount to ensure rare clones are represented, i.e. 525 µg cDNA mouse brain library plasmid DNA per screen.

2.2.1.3.5.3 Large scale transformation of AH109 *S. cerevisiae* cells using the lithium acetate method

The library screen using the NR2D C-terminal domain with the cDNA mouse brain library was carried out using the method described by Agatep *et al.* (1998). A single colony of

AH109 *S. cerevisiae* cells pre-transformed with pGBKT7NR2D was used to inoculate 50 ml -Trp single drop-out media. The culture was grown at 30°C for 20 h at 250 rpm. The culture, 37.5 ml was pelleted by centrifugation in a 50 ml sterile tube at 2,500 × g for 10 min at room temperature using a Megafuge 1.0 R centrifuge. The supernatant was discarded and the pellet was resuspended in 150 ml YPAD media. The culture was incubated at 30°C for ~ 4 h at 250 rpm until an $OD_{\lambda = 600\ nm}$ of 0.2 was obtained. The culture was divided into 3 × 50 ml sterile centrifuge tubes and the cells were pelleted by centrifugation as above. The supernatants were discarded and each pellet was resuspended in 25 ml sterile ddH_2O. The cells were centrifuged as above and the supernatants discarded. The cell pellets were combined in 3 ml 100 mM lithium acetate in a 50 ml sterile centrifuge tube, incubated at 30°C for 15 min and pelleted as above. A transformation mix was made containing the following: 7.2 ml 50 % (w/v) PEG (MW 3500), 1.08 ml 1 M lithium acetate, 1.5 ml salmon sperm DNA (2 µg/ml) and 1.1 ml cDNA mouse brain library plasmid DNA (made up to 1.1 ml with ddH_2O) to give a final volume of the whole transformation mix of 10.88 ml. The entire transformation mix was used to resuspend the cell pellet and the resulting cell suspension was incubated for 30 min at 30°C. The cells were heat shocked for 45 min at 42°C with the tube being agitated every 5 min. Lastly, the cells were pelleted as above and resuspended in 20 ml ddH_2O and plated onto 50 × 150 mm -Leu/-Trp/-His/-Ade selective dropout 2 % (w/v) agar plates. The plates were inverted and incubated at 30°C for 5 - 7 days, until colonies appeared.

The resulting colonies were streaked onto fresh -Leu/-Trp/-His/-Ade selective dropout 2 % (w/v) agar 150 mm plates and re-streaked every 4 days on fresh -Leu/-Trp/-His/-Ade selective dropout 2 % (w/v) agar 150 mm plates for a total of 3 times. Yeast cells are able to host multiple copies of plasmids which are lost over time. Therefore, by regularly culturing the yeast cells on fresh selective dropout medium only the interacting cDNA library clones should be present. Glycerol stocks of each colony were made at this point and stored at -80°C while the analysis of each putative positive was conducted, Section 2.2.1.3.5.4.

2.2.1.3.5.4 Identification of positive interactors

In order to process a large number of putative positive interactors a yeast mating strategy was carried out. Yeast mating provided a convenient method to screen putative positive interactors by avoiding extracting the putative positive plasmid DNA and the subsequent re-transformation of competent yeast cells. Yeast mating occurs when two different yeast strains containing complementary genotypes, i.e. an 'a' and 'α', are mixed in a rich medium such as YPAD media. The yeast strain AH109 has the 'a' genotype and the Y189 yeast strain has the 'α' genotype. Thus mixing of an AH109 yeast colony with a Y187 yeast colony results in the transfer of plasmid DNA between the different yeast strains to form diploid yeast cells.

For each putative positive, the clone was segregated from pGBKT7NR2D, Section 2.2.1.3.6. The clone was present in AH109 *S. cerevisiae* cells as this was the yeast strain used to perform the library screen.

The segregated clone was then used to mate with the Y187 yeast strain pre-transformed with the following baits:

- The bait to demonstrate a reproducible interaction, i.e. pGBKT7NR2D or pGBKT7NR2D^{TRUNC},
- An empty bait vector to test for auto-activation of reporter genes,
- An unrelated construct to establish if the positive binds indiscriminately to an unrelated protein. The positive control, murine $p53_{72\text{-}390}$ (pVA3-1) was used.

At this stage the positive interactors were divided into two groups, strong interactors and weak interactors depending on the number of colonies observed from the yeast mating.

Once a true interactor had been identified, the plasmid DNA was extracted from yeast, Section 2.2.1.3.9. The clone was transformed by electroporation into DH5α *E.coli* cells, Section 2.2.1.1.5. The library clones were present in pACT2 which contained an ampicillin marker and the bait had a kanamycin marker thus allowing for selection between the prey and bait plasmids. Lastly, the clone was amplified by a mini-preparation of plasmid DNA,

Section 2.2.1.1.7. Three mini preparations of plasmid DNA were carried out for each positive clone identified. Restriction endonuclease digestions were completed and the inserts were sorted according to their size, Section 2.2.1.2.1. Each positive interactor was analysed in triplicate because, unlike bacteria, yeast cells are able to replicate more than one plasmid. By analysing three separate clones it was possible to ensure the correct clone was selected. Plasmid DNA with a minimum insert size of 1000 bases was sent for nucleotide sequencing. The clone was analysed to ensure the sequence was in frame with the activation domain using software from ExPASy (www.expasy.org/tools). A BLAST search was conducted using the NCBI database (www.ncbi.nlm.nih.gov/BLAST) to identity the clone.

2.2.1.3.6 Segregation of yeast plasmids

Yeast cells were segregated to obtain a yeast colony which theoretically only contained the cDNA mouse brain library clone and thus could be mated to test the specificity of the interaction. The method by Gietz *et al.* (1997) was employed. For each putative positive interactor a single colony of AH109 *S. cerevisiae* cells from the library screen was used to inoculate 2 ml YPAD media. The cultures were grown at 30°C for 22 h at 250 rpm. The cDNA mouse brain library was cloned into pACT2 which had a leucine nutritional marker. Therefore 10 µl of the 20 h culture was used to inoculate 2 ml -Leu drop-out media. This was incubated at 30°C for 48 h at 250 rpm. A 1/5 dilution of the 48 h culture was prepared and 5 µl of the above dilution was added to 90 µl sterile ddH_2O and plated onto a -Leu medium single dropout, 2 % (w/v) agar plate. The plates were inverted and incubated at 30°C for 2 days. Once colonies appeared, each plate of yeast cells were replica plated onto a -Trp medium single dropout 2 % (w/v) agar plate using a square of sterile cotton velvet. The -Trp plates were inverted and incubated at 30°C for 2 days until colonies appeared. Colonies which did not grow on the -Trp plate but were present on the -Leu plate were picked using a sterile loop and re-plated onto fresh -Leu single dropout 2 % (w/v) agar plates as 1 cm^2 squares. The plates containing the segregated colonies were inverted and incubated for 2 days at 30°C, until colonies appeared. The yeast cells were now a homogenous population of cells containing theoretically only the cDNA mouse brain library clone and they were therefore ready to be mated, Section 2.2.1.3.7.

2.2.1.3.7 Yeast mating

The segregated cDNA library clones were present in AH109 *S. cerevisiae* cells, Section 2.2.1.3.6. The Y189 *S. cerevisiae* cells were pre-transformed with either pGBKT7NR2D (and/or pGBKT7NR2D^{TRUNC}), pGBKT7 or pVA3-1, Sections 2.2.1.3.3 and 2.2.1.3.4. The method from 'Yeast Methods Handbook' by Clontech was followed.

Single colonies were picked of AH109 *S. cerevisiae* cells were picked containing the putative positive cDNA library clone and Y189 *S. cerevisiae* cells containing the above pre-transformed controls were added into separate aliquots of 200 µl YPAD media in a 1.5 ml sterile centrifuge tube. Yeast cells were dispersed by vortexing for ~ 10 sec. To each well of a sterile 24 well tissue culture plate, 200 µl YPAD media was added. Then 45 µl of the above AH109 *S. cerevisiae* cell suspension was added to four separate wells. To each of the wells, 45 µl Y189 *S. cerevisiae* cell suspension pre-transformed with either pGBKT7NR2D, pGBKT7NR2D^{TRUNC}, pGBKT7 or pVA3-1, i. e. each well would contain AH109 *S. cerevisiae* cells containing the putative positive and Y189 *S. cerevisiae* cells containing either pGBKT7NR2D, pGBKT7NR2D^{TRUNC}, pGBKT7 or pVA3-1. As a positive control, yeast mating was carried out with AH109 *S. cerevisiae* cells pre-transformed with the pTD1-1 and Y187 *S. cerevisiae* cells pre-transformed with pVA3-1. As a negative control AH109 *S. cerevisiae* cells pre-transformed with pACT2 were mated with Y187 *S. cerevisiae* cells pre-transformed with pGBKT7. The 24 well tissue culture plate was incubated at 30°C for 18 h at 250 rpm. Aliquots of the diploid cells, 100 µl were plated onto both -Leu/-Trp selective dropout 2 % (w/v) agar plates and -Leu/-Trp/-His/-Ade selective dropout 2 % (w/v) agar plates. The plates were inverted and incubated for 3 - 5 days at 30°C until colonies appeared. The colonies were counted after this period of time.

The -Leu/-Trp selective dropout plates should show growth demonstrating the formation of diploid yeast cells. A true positive interaction with the NR2D C-terminal domain would show growth on the -Leu/-Trp/-His/-Ade selective dropout plates for NR2D and/or NR2D^{TRUNC} but show no growth with pVA3-1 and pGBKT7.

2.2.1.3.8 Extraction of putative positive plasmid DNA from yeast cells

Plasmid DNA for the cDNA mouse brain library clones found to specifically interact with NR2D and/or $NR2D^{TRUNC}$ C-terminal domains was extracted from the yeast cells ready to by amplified in *DH5α E.coli* cells with the purpose to identify the cDNA fragment. A well isolated single colony of AH109 *S. cerevisiae* cells which contained the positive cDNA clone was streaked onto a -Leu selective dropout 2 % (w/v) plate into a ~ 3 cm^2 square. The plate was inverted and incubated for 3 days at 30°C. A 10 mm^2 patch of cells was scraped from the -Leu selective dropout plate and added to 50 µl sterile ddH_2O in a 1.5 ml sterile centrifuge tube and resuspended by vortexing for ~ 10 sec. The yeast cell walls were digested by the addition of 10 µl lyticase (5 U/µl) and incubated at 37°C for 1 h at 1,000 rpm in an Eppendorf ThermoMixer (Cambridge, U.K.). The yeast cell walls were further disrupted by the addition of 10 µl 20 % (w/v) SDS. This was mixed thoroughly for 1 min at 1,400 rpm. The samples were put through a freeze–thaw cycle by freezing for 1 h at -20°C, defrosting at room temperature and finally the samples were thoroughly vortexed for ~ 20 sec. The volume was adjusted to 200 µl by addition of 130 µl sterile ddH_2O. To isolate plasmid DNA, 200µl phenol:chloroform:isoamyl alcohol (25:24:1) was added and mixed vigorously for 5 min by vortexing at room temperature. The samples were centrifuged at 12,000 × g for 10 min at room temperature. The top layer was carefully transferred to a new 1.5 ml sterile centrifuge tube. The DNA was precipitated by addition of 8 µl 10 M ammonium acetate and 500 µl ethanol. This was incubated for 1 h at -80°C. The DNA was pelleted by centrifugation at 12,000 × g for 10 min at room temperature. The supernatant was discarded and the tubes re-centrifuged at 12,000 × g for 1 min at room temperature. The supernatant was carefully aspirated. The pellet was air-dried for ~ 15 min and resuspended in 20 µl 10 mM Tris-HCl, pH 8.0. The DNA was stored at -20°C until use. The concentration of plasmid DNA extracted was very low and possibly contaminated by genomic DNA, thus the method of transforming *DH5α E.coli* cells was by electroporation, Section 2.2.1.1.5.

2.2.1.3.9 Extraction of protein from yeast cells

To test for the successful expression of constructs in yeast cells following transformation of the yeast, a yeast cell lysate was prepared and analysed by SDS-PAGE followed by

immunoblotting, Section 2.2.2.10. The method from Stratagene CytoTrap® Vector Kit instruction manual was employed. A single colony of yeast cells pre-transformed with the desired construct, pGBKT7 and untransformed yeast cells was used to inoculate separate 5 ml of the correct selective media; e. g. pGBKT7NR2D contains the Trp nutritional marker therefore was grown in -Trp single drop-out media. The cultures were grown at 30°C for 48 h at 250 rpm. The cells were collected by centrifugation in a 15 ml tube at 1,000 × g for 5 min at 4°C. The supernatant was discarded and the cell pellet resuspended in 200 µl cell lysis buffer (140 mM NaCl, 2.7 mM KCl, 10 mM Na_2HPO_4, 1.8 mM KH_2PO_4, 1 % (v/v) Triton X-100®, 1 mM PMSF, 10 µg/ml aprotinin, 1 µM pepstatin A, 100 µM leupeptin and 1 µg/ml chymostatin). An equal volume of acid-washed glass beads was added to each sample and they were vortexed at maximum speed for 5 min at 4°C. The samples were centrifuged at 12,000 × g for 5 min at 4°C. The supernatant was transferred into a fresh 1.5 ml centrifuge tube. An additional 100 µl cell lysis buffer was added to the glass beads and vortexed for 5 min at full speed at 4°C. The samples were centrifuged at 12,000 × g for 5 min at 4°C. The resulting supernatants were combined. The proteins were snap frozen and stored at -20°C until use.

2.2.2 Expression in mammalian cells

2.2.2.1 Culturing of human embryonic kidney (HEK) 293 cells

For all cell culture equipment sterile techniques were employed throughout. In addition, when removing or placing an item in either the laminar flow hood dedicated to tissue culture work or the mammalian cell incubator, each item was lightly sprayed with 70 % (v/v) ethanol to maintain sterility. All solutions were sterilised either by filtration through a 0.22 µm pore size or by autoclaving at 121°C for 20 min.

2.2.2.2 Preparation of cell culture media

For routine sub-culturing of HEK 293 cells, modified Eagles medium nutrient mixture F-12 HAM (DMEM/F-12) containing L-glutamine was used. The media was prepared by the addition of 15.6 g powdered Dulbecco's modified Eagles medium nutrient mixture F-12 HAM (DMEM/F-12) to ~ 500 ml sterile water, 100 ml foetal bovine serum (FBS), 20 ml

penicillin/streptomycin (10,000 units/ml) and 40 ml 7.5 % (w/v) $NaHCO_3$. The volume was made up to 1 L and the pH adjusted to pH 7.6 using 10 M NaOH. The media was filter sterilised through a 0.22 μm Nalgene filter.

The above described cell culture media was replaced 3 h before transfection with DMEM/F-12 L-glutamine free media. This was made by adding 100 ml FBS, 20 ml penicillin/streptomycin (10,000 units/ml) and 24 ml 7.5 % (w/v) $NaHCO_3$ to liquid DMEM/F-12 without L-glutamine to a total volume 1 L and the pH was adjusted to pH 7.6 using 10 M NaOH. The media was sterilised by filter sterilisation through a 0.22 μm Nalgene filter.

2.2.2.3 Storage of HEK 293 cells in liquid nitrogen

HEK 293 cells that had reached 70 % confluence were used to make liquid nitrogen stocks. HEK 293 cells were harvested using the method described in Section 2.2.2.5. The 12 ml HEK 293 cell suspension was centrifuged at 1,000 × g for 10 min at room temperature in a sterile 15 ml centrifuge tube. The supernatant was discarded and the pellet was resuspended in 600 μl DMSO, 600 μl FBS and 4.8 ml DMEM/F-12 media containing L-glutamine. The cell suspension was divided as 1 ml aliquots in 1.8 ml cryotubes and frozen for 24 h at -80°C. The following day the tubes were placed in liquid nitrogen, -150°C, until use.

2.2.2.4 Reviving HEK 293 cell stocks from liquid nitrogen storage

An aliquot of HEK 293 cells was taken from storage in liquid nitrogen and rapidly defrosted in a water bath at 37°C, Section 2.2.2.3. The HEK 293 cell suspension was poured into 50 ml, pre-warmed to 37°C, DMEM/F-12 media containing L-glutamine. The cells were pelleted by centrifugation at 1,000 × g for 10 min at room temperature. The supernatant was decanted and the pellet resuspended in 10 ml, pre-warmed to 37°C, DMEM/F-12 media containing L-glutamine. The cell suspension was added to a 250 ml Cellstar sterile cell culture flask and incubated at 37°C in the presence of 5 % CO_2. The following day the media was aspirated and replaced with 10 ml, pre-warmed to 37°C,

DMEM/F-12 media containing L-glutamine. Once the HEK 293 cells had reached ~ 90 % confluence they were sub-cultured, Section 2.2.2.5.

2.2.2.5 Sub-culturing of HEK 293 cells

Once ~ 90 % confluent the HEK 293 cells required sub-culturing. This was approximately every 3 - 5 days. Media was aspirated from a flask of confluent HEK 293 cells and the cells were washed by gently passing 10 ml, pre-warmed to 37°C, Hanks buffered salt solution (HBSS) gently over the cells. The HBSS was removed and 2 ml trypsin-EDTA (0.5 mg/ml porcine trypsin in HBSS) was added onto the cells. This was incubated for 50 sec at room temperature. The flask was gently tapped to dislodge the cells and 10 ml DMEM/F-12 containing L-glutamine media, pre-warmed to 37°C, was added. The cells were mixed thoroughly by pipetting up and down. The 12 ml cell suspension was divided equally between 4 flasks. An additional 9 ml DMEM/F-12 containing L-glutamine media, pre-warmed to 37°C, was added to each flask. The flasks were incubated at 37°C and cultured in the presence of 5 % CO_2 for 24 h prior to transfection or until ~ 90 % confluent when the HEK 293 cells were sub-cultured again, as above.

For the measurement of cell surface NMDA receptor expression, it was necessary to culture HEK 293 cells in tissue culture grade 24 well plates. The tissue culture grade 24 well plates were prepared by the addition of 1 ml 1 µg/ml poly-D-lysine in ddH_2O to each well. This was incubated for 3 h at room temperature. The poly-D-lysine solution was aspirated and the wells were washed with 3 × 1 ml ddH_2O. The plate was air-dried for 20 min at room temperature. A flask of HEK 293 cells was sub-cultured as above, the 12 ml cell suspension was diluted 1/6 and 685 µl from the diluted cell suspension was added to each well to give ~ 40 % cell confluence on the day of transfection. The plates were incubated at 37°C supplemented with 5 % CO_2 for 24 h prior to transfection.

The HEK 293 cells were routinely used for ~ 20 passages (2 months) before reviving a new aliquot of HEK 293 cells for subsequent use, Section 2.2.2.4. This was necessary since an increase in passage number resulted in decreased transfection efficiency and particularly gave irreproducible NMDA receptor cell surface expression.

2.2.2.6 Transient transfection of HEK 293 cells by the calcium phosphate method

HEK 293 cells were sub-cultured to be ~ 40 % confluence on the day of transfection, Section 2.2.3.4. Three h prior to transfection the cell culture media was aspirated and replaced with 10 ml, pre-warmed to 37°C, DMEM/F-12 L-glutamine free media. Each flask was incubated for 3 h at 37°C in the presence of 7.5 % CO_2. A master mix of plasmid DNAs to be used for the transfection were prepared. For the expression of NR1/NR2 NMDA receptors, 10 µg DNA was used per flask at a ratio of 1:3, i.e. 2.5 µg NR1: 7.5 µg NR2. This ratio was used for all NMDA receptor transfections. For the expression of NR1/NR2 NMDA receptors + PSD-95 MAGUK proteins, the amount of DNA was increased to 20 µg per flask with a 1:1 ratio of NR1/NR2: PSD-95 MAGUK, i. e. 2.5 µg NR1: 7.5 µg NR2: 10 µg PSD-95 MAGUK protein. Control samples contained the empty pCIS vector, i.e. 2.5 µg NR1: 7.5 µg NR2: 10 µg pCIS.

The following combinations of clones were used:

pCISNR1-1a/pCISNR2A/pCIS	pCISNR1-1a/pCISNR2A/pGW1PSD-95α$^{c\text{-}Myc}$
pCISNR1-1a/pCISNR2A/pGW1PSD-95β	pCISNR1-1a/pCISNR2A/pGW1PSD-95α ^{C3,5S}
pCISNR1-1a/pCISNR2A/pGW1chapsyn-110$^{c\text{-}Myc}$	pCISNR1-1a/pCISNR2A/pGW1SAP-97
pCISNR1-1a/pCISNR2A/pCMVneoSAP-102$^{c\text{-}Myc}$	pCISNR1-1a/pCISNR2A^{TRUNC}/pCIS
pCISNR1-1a/pCISNR2A^{TRUNC}/pGW1PSD-95α$^{c\text{-}Myc}$	pCISNR1-1a/pCISNR2A$^{T1441\text{-}STOP}$/pCIS
pCISNR1-1a/ pCISNR2A$^{T1441\text{-}STOP}$/pGW1PSD-95α$^{c\text{-}Myc}$	pCISNR1-1a/pCISNR2A$^{N1157\text{-}STOP}$/pCIS
pCISNR1-1a/ pCISNR2A$^{N1157\text{-}STOP}$/pGW1PSD-95α$^{c\text{-}Myc}$	pCISNR1-1a/pCISNR2A^{S1459A}/pCIS
pCISNR1-1a/pCISNR2A^{S1459A} /pGW1PSD-95α$^{c\text{-}Myc}$	pCISNR1-1a/pCISNR2B/pCIS
pCISNR1-1a/pCISNR2B/pGW1PSD-95α$^{c\text{-}Myc}$	pCISNR1-1a/pCISNR2B/pGW1chapsyn-110$^{c\text{-}Myc}$
pCISNR1-1a/pCISNR2B/pGW1SAP-97	pCISNR1-1a/pCISNR2B/pCMVneoSAP-102$^{c\text{-}Myc}$
pCISNR1-1a/pCISNR2B^{FLAG}/pCIS	pCISNR1-1a/pCISNR2B^{FLAG} /pGW1PSD-95α$^{c\text{-}Myc}$
pCISNR1-1a/pCISNR2B$^{FLAG/TRUNC}$/pCIS	pCISNR1-1a/pCISNR2B$^{FLAG/TRUNC}$ /pGW1PSD-95α$^{c\text{-}Myc}$
pCISNR1-1a/pCISNR2C/pCIS	pCISNR1-1a/pCISNR2C/pGW1PSD-95α$^{c\text{-}Myc}$
pCISNR1-1a/pCISNR2C/pGW1chapsyn-110$^{c\text{-}Myc}$	pCISNR1-1a/pCISNR2C/pGW1SAP-97
pCISNR1-1a/pCISNR2C/pCMVneoSAP-102$^{c\text{-}Myc}$	pCISNR1-1a/pcDNANR2D/pCIS
pCISNR1-1a/pcDNANR2D/pGW1PSD-95α$^{c\text{-}Myc}$	pCISNR1-a/pcDNANR2D/pGW1chapsyn-110$^{c\text{-}Myc}$
pCISNR1-1a/pcDNANR2D/pGW1SAP-97	pCISNR1-a/pcDNANR2D/pCMVneoSAP-102$^{c\text{-}Myc}$

For each flask to be transfected, two sterile 1.5 ml centrifuge tubes were prepared. One tube contained 500 µl 2 × HEPES buffer saline (2 × HBS, 50 mM N-(2-hydroxyethyl) piperazine-N'-(2-ethanesulphonic acid) (HEPES), pH 7.12, 280 mM NaCl, 1.1 mM Na_2HPO_4). The second tube contained 450 µl of the required plasmid DNA + 1/10 (v/v) TE buffer (10 mM Tris-HCl, pH 8.0 and 10 mM EDTA, diluted 1/10 (v/v) with ddH_2O). The transfection solution was started by the addition of 50 µl, preheated to 37°C, 2.5 M $CaCl_2$ to the tube containing the plasmid DNA + 1/10 (v/v) TE buffer. The tube was shaken vigorously for 15 sec. The DNA mixture was added drop-wise to the 2 × HBS at a rate of one-drop every ~ 4 sec. This solution was mixed by gentle pipetting up and down with a 1 ml pipette tip a total of three times.

The transfection solution was added to the HEK 293 cells by slowly pipetting the solution into a corner of the flask under the surface of the media. The flask was rotated slowly 3 × to ensure the DNA precipitate was evenly distributed over the cells. To prevent the NMDA receptor mediated cell death when NR1/NR2A or NR1/NR2B combinations were co-transfected, cells were cultured post-transfection in the presence of a NMDA receptor antagonist, ketamine (Cik *et al.,* 1993). Therefore, all experiments expressing either NR1/NR2A or NR1/NR2B NMDA receptors were cultured in the presence of 1 mM ketamine. NR1/NR2C and NR1/NR2D NMDA receptors do not result in cytotoxicity when expressed in HEK 293 cells so it was not necessary to add ketamine to the cell culture media (Chazot *et al.*, 1994; Chopra *et al.*, 2000). The cells were then returned to the incubator at 37°C in the presence of 5 % CO_2. Transfected HEK 293 cells were cultured for 20 - 24 h post-transfection and the cell homogenates were collected and analysed by either quantitative immunoblotting or immunoprecipitations.

For the cell surface NMDA receptor expression studies the cells were sub-cultured to be ~ 40 % confluent on the day of transfection, Section 2.2.2.5. Three h prior to the transfection the cell culture media was replaced with 1.2 ml, pre-warmed to 37°C, DMEM/F-12 L-glutamine free media per well. The cells were incubated at 37°C in the presence of 7.5 % CO_2. The transfection mixture was prepared as described above. From the 1 ml final transfection solution, 97 µl was added drop-wise to each well. For each combination being

tested 3 × wells of cells were transfected to obtain triplicate measurements. For each plate one row of cells were sham-transfected with pCIS alone to allow for background recordings. HEK 293 cells were cultured in the presence of 1 mM ketamine post-transfection to stop NMDA receptor mediated cell death. The cells were then returned to the incubator at 37°C in the presence of 5 % CO_2. The transfected HEK 293 cells were cultured for 24 h post-transfection before the measurement of cell surface NMDA receptor expression by ELISA assay was carried out, Section 2.2.2.13.

2.2.2.7 Cell cytotoxicity assays

The expression of NR1/NR2A or NR1/NR2B NMDA receptor subunit combinations in mammalian cells results in cell death. This is explained by the activation of NMDA receptors by glutamate and glycine present in the cell culture media followed by an influx of calcium ions leading to cell death (Cik *et al.*, 1993). This cell death is prevented by culturing the cells in the presence of a NMDA receptor antagonist such as ketamine. Thus the measurement of cytotoxicity post-transfection is a useful parameter of the cell surface, functional NMDA receptor expression and also the transfection efficiency. For the determination of cytotoxicity post-transfection the Cytotox96^{TM} non-radioactive assay was employed, as described in Chazot *et al.* (1996). This assay measures the enzyme, lactate dehydrogenase (LDH) activity which is present in the media of lysed cells.

Flasks of either transfected or sham transfected HEK 293 cells were cultured in the presence and absence of 1 mM ketamine post-transfection. Sham transfected flasks were included as a control to remove background cell death which occurs through the natural cell cycle, any LDH present in the FBS used for the media and the phenol red contribution which was present in both the media and the HBSS. One ml samples of cell culture media were taken 20 h after transfection and centrifuged at 12,000 × g for 5 min at room temperature to remove the cell debris. The supernatants were transferred to new 1.5 ml centrifuge tubes and placed on ice. The samples were diluted 1/3 and 1/10 with HBSS.

To gain the total quantity of LDH present in the flask of sham-transfected HEK 293 cells, the sham transfected flask was put through a freeze-thaw cycle (30 min at -80°C and 15 min

at 37°C) to lyse the cells. A 1 ml aliquot of cell culture media was taken and centrifuged at 12,000 × g for 5 min at room temperature. The resulting supernatant was diluted 1/10 and 1/20 with HBSS. Background values were determined by using HBSS alone.

A 50 µl aliquot of each sample was added in triplicate to a 96 well ELISA plate. The substrate mix, 50 µl, was added and the reaction was incubated for 30 min at room temperature in the dark. The reaction was terminated by the addition of 50 µl stop solution (1 M acetic acid). The $OD_{\lambda = 490\ nm}$ was recorded using a Dynatech minireader.

The $OD_{\lambda = 490\ nm}$ values were corrected according to both their dilution factor and the sham transfected samples. The percentage of LDH activity was calculated as below:

$$\frac{\text{LDH activity in NR1/NR2A or NR1/NR2B transfected culture (- ketamine) - Background}}{\text{Total LDH activity in sham transfected (after freeze thaw cycle) - Background}} \times 100$$

As mentioned previously, the percentage cytotoxicity can be a measure of transfection efficiency. Routinely co-expression of either NR1/NR2A or NR1/NR2B NMDA receptors resulted in a transfection efficiency ranging between 10 - 30 %.

2.2.2.8 Preparation of transfected HEK 293 cell homogenates

HEK 293 cells were harvested 22-24 h post-transfection. The media was aspirated and the cells were scraped using a sterile cell scraper into 10 ml ice-cold phosphate buffered saline (1 × PBS, 137 mM NaCl, 27 mM KCl, 10 mM $Na_2HPO_4.12H_2O$, 1.8 mM KH_2PO_4, pH 7.6). The cell suspension was collected and put into a 35 ml JA20 Beckman centrifuge tube. The cells were pelleted at 1,000 × g for 10 min at 4 °C using a Beckman JA - 21 rotor in a Beckman centrifuge. The supernatant was discarded and the pellet homogenised in 5 ml homogenisation buffer (50 mM Tris-citrate, pH 7.4, 5 mM EDTA, 5 mM EGTA) for ~ 20 strokes using a tight 7 ml Wheaton Dounce glass-glass homogeniser. An additional 30 ml homogenisation buffer was added. The samples were centrifuged at 27,000 × g for 30 min at 4 °C. The resulting pellet was homogenised in homogenisation buffer for ~ 40 strokes to a final concentration of 0.5 mg protein/ml. Typically a 250 ml flask of transfected cells would yield ~ 1 mg protein. The homogenised protein samples were either

used for detergent solubilisation for use in immunoprecipitations or aliquoted and snap frozen in liquid nitrogen then stored at -20 °C until analysis by immunoblotting, Section 2.2.2.11.

2.2.2.9 Methanol/chloroform precipitation of proteins

Proteins from HEK 293 cell homogenates or yeast cell extracts were precipitated either immediately after harvesting or after being defrosted on ice. To precipitate the proteins, aliquots of 100 µl (~ 50 µg protein) were mixed with 4 volumes of methanol in a 1.5 ml centrifuge tube. The tubes were briefly vortexed and centrifuged at 10,000 × g for ~ 5 sec at room temperature. One volume of chloroform was added, the samples were vortexed and centrifuged as above. Three volumes of water were added to the samples, vortexed and centrifuged at 12,000 × g for 1 min at room temperature. The upper aqueous phase was removed and the proteins were precipitated by addition of one volume of methanol. The samples were centrifuged at 12,000 × g for 4 min at room temperature. The supernatant was decanted and the centrifuge tube gently tapped on tissue to remove residual liquid. The samples were dried under vacuum for 15 min. They were either stored at -20°C prior to use or analysed by immunoblotting, Section 2.2.2.11.

2.2.2.10 SDS-PAGE

SDS-PAGE was conducted under reducing conditions using mini gels. Routinely 7 % polyacrylamide gels were run for analysis. For each gel, one glass plate (8 cm × 10 cm), one aluminium plate (8 cm × 10 cm), and two 0.75 mm spacers were rinsed with 70% (v/v) ethanol. The two spacers were put on either side of the aluminium plate with the glass plate on top. These were assembled into a Mighty Small™ dual gel caster (Hoefer, San Francisco, CA, USA).

2.2.2.10.1 Preparation of separating gel

All polyacrylamide gels contained 7 % (w/v) acrylamide. The separating gel solution was made with; 6.2 ml ddH_2O, 3 ml separating gel buffer (1.5 M Tris-HCl, pH 8.8, 8 mM EDTA, 0.4 % (w/v) SDS), 2.8 ml ProtoGel® (37.5:1 acrylamide to bisacrylamide stabilized solution) and 6 µl N,N,N',N' - tetramethylethylene diamine (TEMED) was prepared and

degased under vacuum for 30 min. The polymerisation was initiated by the addition of 10% (w/v) ammonium persulphate, 60 µl. The solution was poured gently between the glass plate and aluminium plate to reach ~ 3 cm below the top of the glass plate. To ensure an even surface on the top of the gel, ~ 300 µl 50 % (v/v) butan-1-ol was added. Gels were polymerised for 1 h. The butan-1-ol was removed by washing 3 × with ~ 5 ml ddH_2O.

2.2.2.10.2 Preparation of stacking gel

The polyacrylamide gels were transferred from the Mighty Small™ gel caster onto the Mighty Small™ electrophoresis unit. The stacking gel solution was made with; 2.3 ml ddH_2O, 1 ml stacking buffer (0.5 M Tris-HCl, pH 6.8, 8 mM EDTA, and 0.4% (w/v) SDS), 650 µl ProtoGel® and 6 µl TEMED. The stacking solution was degased under vacuum for 30 min. The polymerisation reaction was initiated by the addition of 10 % ammonium persulphate, 80 µl. The acrylamide solution was added directly to the separating gel and a comb immediately positioned. The stacking gels were polymerised for 30 min. Once the stacking gels had polymerised, the buffer reservoirs were filled with electrode buffer (50 mM Tris-HCl, pH 8.8, 384 mM glycine, 1.8 mM EDTA, 1.8 % (w/v) SDS) and the comb was gently removed. Any residual polyacrylamide was removed by pipetting electrophoresis buffer into the wells.

2.2.2.10.3 Preparation of protein samples

Samples previously precipitated by the methanol/chloroform method were prepared as follows, Section 2.2.2.9. To each sample; 8.5 µl ddH_2O, 5 µl 3 × SDS-PAGE sample buffer (30 mM NaH_2PO_4, pH 7, 30 % (v/v) glycerol, 0.05 % (w/v) bromophenol blue, 7.5 % (w/v) SDS) and 1.5 µl 1 M DTT were added. The samples were vortexed for ~ 5 sec and centrifuged at 12,000 × g for 1 min at room temperature. The samples were heated to 75°C for 8 min whilst shaking at 1,400 rpm in an Eppendorf ThermoMixer. The protein samples were collected in the bottom of the tubes by another cycle of vortexing and centrifugation, as above.

2.2.2.10.4 Electrophoresis of samples

The protein samples were loaded into the gel lanes using a Hamilton syringe. Empty lanes were loaded with 15 µl 1 × sample buffer. One lane per gel had 4 µl of SeeBlue® pre-stained standard protein molecular weight markers loaded. The SeeBlue® pre-stained standard protein molecular weight markers contained the following proteins (kDa): myosin, 250; BSA, 98; glutamate dehydrogenase, 64; alcohol dehydrogenase, 50; carbonic anhydrase, 36; myoglobin, 30; lysozyme, 16; aprotinin, 6; insulin B chain, 4. Each gel was run at 8 mAmp constant current through the stacking gel then 10 mAmp constant current through the separating gel. Once the bromophenol blue dyefront had run to the bottom of the gel the proteins were transferred onto nitrocellulose membranes, Section 2.2.2.11.1.

2.2.2.11 Immunoblotting

2.2.2.11.1 Transfer of proteins from polyacrylamide gel to nitrocellulose membranes

Once SDS-PAGE was completed the proteins were transferred onto nitrocellulose membranes using a wet transfer process, Section 2.2.2.10. To transfer the proteins a sandwich was made of two pieces of blotting paper, soaked in transfer buffer (25 mM Tris, 172 mM glycine, 20% (v/v) methanol, ~ pH 8.5) and a piece of nitrocellulose membrane (soaked in transfer buffer). The polyacrylamide gel was placed on the nitrocellulose membrane and two additional pieces of blotting paper were placed on top (also soaked in transfer buffer). A 2 ml burette was rolled across the sandwich to remove any air bubbles. The sandwich was put between two pieces of sponge and into a transfer cassette. The cassette was put into a Mighty Small™ transfer tank containing transfer buffer to fully cover the cassette with the polyacrylamide gel facing the cathode. The transfer was conducted either for 16 h at 14 V or for 2.5 h at 50 V, with water circulation to cool the apparatus. When removing the nitrocellulose membrane from the tank, the size of the nitrocellulose was trimmed to exactly the same size as the gel. Nitrocellulose membranes were stored in 1 × PBS at 4°C until immunoblotting was conducted, Section 2.2.2.14.2.

2.2.2.11.2 Immunoblotting

Proteins were visualised by immunoblotting using the appropriate antibodies. The nitrocellulose membrane was blocked for 1 h in 5 % powdered milk (Marvel, low fat powdered milk powder) and 0.05% polyethylene glycol sorbitan monolaurate (Tween-20®) in 1 × PBS at 37°C with gentle rotation. The primary antibody was incubated in concentrations ranging from 0.5 - 2 µg/ml for either 1 h at 37°C or 16 h at 4°C. The antibody concentrations used are shown in Table 2.7.

The membranes were washed 4 × 10 min in 2.5 % powdered milk and 0.05 % Tween-20® in 1 × PBS at 37°C with gentle rotation. The secondary antibody, either horseradish peroxidase (HRP)-linked anti-rabbit IgG antibodies or HRP-linked anti-mouse IgG antibodies were prepared as a 1/2000 dilution in 2.5 % powdered milk and were incubated for 1 h at 37°C with gentle rotation. The membranes were washed 4 × 10 min in 2.5 % powdered milk and 0.05 % Tween®-20 at 37°C with gentle rotation.

Antibody Specificity	Concentration of antibody used for Western blots
Anti-NR1 (pan) (17-35)	1 µg/ml
Anti-NR1-C2 (911-920)	1 µg/ml
Anti-NR2A-Extracellular (44-58)	5 µg/ml
Anti-NR2A-Intracellular (1381-1394)	1 µg/ml
Anti-NR2A/B (1435–1445 (using the NR2A amino acid residues 1454-1464))	1 µg/ml
Anti-NR2C (1227 – 1237)	1 µg/ml
Anti-NR2D (1307 – 1323)	2 µg/ml
Anti-c-Myc	1/1000 dilution
Anti-FLAG	1/1000 dilution
Anti–calnexin	1/7500 dilution
Anti-Rab5	1/500 dilution

Table 2.7 Summary of the concentrations the antibodies were used

The membranes were briefly washed in 1 × PBS. A 10 ml aliquot of 0.8 M luminol (100 mM Tris-HCl, pH 8.5 and 0.8 M luminol) and a 100 µl aliquot of 11 mg/ml hydroxycinnamic acid (p-coumaric acid) were defrosted. The 100 µl p-coumaric acid was added to the 10 ml luminol solution and mixed. The membrane was put face up into an

empty tray. The exposure was initiated by the addition of 7 µl hydrogen peroxide to the luminol mixture, vortexed and poured over the membrane. This was incubated for 1 min and the membrane was tapped on tissue to remove the excess liquid. The membrane was then put into a plastic sleeve. Tracker tape was used to mark the positions of the molecular weight markers. The immunoblots were imaged using GeneGnome Chemiluminescence Capture and Analysis System (Syngene, Cambridge, U.K.).

When quantitative immunoblotting was carried out the immunoreactive bands were quantified using GeneGnome Tools software. The background was deducted from the resulting pixel values for each immunoblot. Means were calculated for the triplicate samples and further analysis was carried out when the variance between values was no more that 10 %. All results shown are the mean ± standard error of the mean (SEM), unless specified otherwise.

2.2.2.12 Detergent solubilisation of HEK 293 cell homogenates and immunoprecipitation of transfected HEK 293 cell homogenates

Immunoprecipitation assays were carried out to see if proteins were able to co-immunoprecipitate with each other following their co-expression in HEK 293 cells. For immunoprecipitations using transfected HEK 293 cells the method of Chazot *et al.* (1994) was followed.

Three flasks of HEK 293 cells were harvested 24 h post-transfection and were pooled together, Section 2.2.2.8. The resulting cell homogenate was resuspended in 2 ml solubilisation buffer (50 mM Tris-citrate, pH 7.4, 240 mM NaCl, 5 mM EDTA, 5 mM EGTA, 1 mM PMSF, bacitracin (5 µg/ml), soyabean trypsin inhibitors (5 µg/ml), benzamidine HCl (5 µg/ml), ovomucoid trypsin inhibitor (5 µg/ml) and 1% (v/v) Triton X-100®) to a final concentration of 1.5 mg protein/ml. The cell homogenate was thoroughly homogenised with ~ 40 strokes using a tight 7 ml Wheaton Dounce glass-glass homogeniser followed by incubation for 1 h with gentle rotation at 4°C. Samples were diluted to 1 mg protein/ml with the above solubilisation buffer and soluble fractions collected by centrifugation at 100,000 × g for 40 min at 4°C using a MLA 80 rotor in a

Beckman Optima™ MAX-E ultracentrifuge. Each detergent-solubilised sample was divided into 2 × 800 µl fractions ready for immediate use to start immunoprecipitation assays. The remaining 200 µl of each sample was snap frozen and stored at -20°C until future analysis by immunoblotting.

The immunoprecipitation assay was started by the addition of 5 µg of the appropriate primary affinity-purified anti-NMDA receptor antibodies to one aliquot and 5 µg non-immune antibodies to the second aliquot. The final volumes of each assay were adjusted with 1 × PBS to ensure they were both the same final volume. The antibodies were incubated for 16 h with gentle rotation at 4°C. Antibody complexes were precipitated by the addition of 5 mg protein A Sepharose and samples were incubated for 2 h with gentle rotation at 4 °C. The samples were centrifuged at 600 × g for 15 sec. The supernatants were removed and the antibody-protein A Sepharose complex was gently washed with 1 ml solubilisation buffer (50 mM Tris-citrate, pH 7.4, 240 mM NaCl, 5 mM EDTA, 5 mM EGTA, 1 mM PMSF, bacitracin (5 µg/ml), soyabean trypsin inhibitors (5 µg/ml), benzamidine HCl (5 µg/ml), ovomucoid trypsin inhibitor (5 µg/ml) and 1% (v/v) Triton X-100®) followed by centrifugation at 600 × g for 15 sec at room temperature. This wash step was repeated a total of three times. On the final wash the supernatant was completely removed using a Hamilton syringe. To the pellet, 20 µl 3 × SDS-PAGE sample buffer and 5 µl 1 M DTT was added. The samples were heated to 75°C for 8 min. The proteins were collected by centrifugation at 600 × g for 15 sec at room temperature and the supernatant transferred into a fresh 1.5 ml centrifuge tube using a Hamilton syringe. The supernatants were then made up to the required volume with 1 × SDS-PAGE sample buffer and analysed by immunoblotting, Section 2.2.2.11. The supernatant collected from protein A Sepharose using anti-NMDA receptor antibodies shall be referred to as the immune pellet and the supernatant from the non-immune antibodies as the non-immune pellet.

For experiments investigating the association of proteins when phosphorylated, HEK 293 cells were incubated with 20 µM forskolin or 0.1 % (v/v) DMSO solvent control for 30 min

prior to harvesting. When harvesting the cells all solutions contained a 1/100 dilution of the phosphatase inhibitor cocktail 1.

2.2.2.13 Cell surface ELISA assays

Cell surface NMDA receptor expression was analysed by ELISA assays. NMDA receptor expression at the cell surface requires the co-assembly of both NR1 and NR2 subunits (McIlhinney *et al.*, 1998). All cell surface assays employed affinity-purified antibodies which were directed at the N-terminus of either NR2A or NR2B subunits. The method developed by Rutter *et al.* (2000) was followed. Sham transfected HEK 293 cells were always processed alongside NMDA receptor transfected HEK 293 cells. This allowed the non-specific binding of the antibodies to be deducted from the NMDA receptor transfected absorbance thus giving specific absorbance values. Means were calculated for the triplicate values for both sham transfected and NMDA receptor transfected HEK 293 cells. Analysis was only carried out when the variance of triplicate samples was no more than 10 %. The specific absorbance was calculated by deducting the sham transfected mean absorbance from the NMDA receptor mean absorbance. All results shown are the mean ± standard error of the mean (SEM), unless specified otherwise.

HEK 293 cells were transfected and ELISA assays were performed 24 h post-transfection, Section 2.2.2.6. The cell culture media was aspirated and the cells were washed with 500 µl 1 × PBS. For cell surface measurements, HEK 293 cells were fixed for 5 min with 500 µl 4 % (w/v) paraformaldehyde at room temperature. This was removed by aspiration followed by washing with 500 µl 1 × PBS. Non-specific sites were blocked using 4 % (w/v) Marvel, low fat powdered milk powder in 1 × PBS for either 30 min or until the end of blocking the total protein measurement, as described below.

To gain the total protein measurements, HEK 293 cells were permeabilised. The cell culture media was aspirated and HEK 293 cells were washed with 500 µl 1 × PBS and fixed for 30 min with 500 µl 4 % (w/v) paraformaldehyde. Cells were washed with 500 µl 1 × PBS and permeabilised by the addition of 500 µl 0.25 % (v/v) Triton X-100® in 1 ×

PBS for 5 min. The cells were washed with 500 µl 1 × PBS and the non-specific sites were blocked with 4 % (w/v) fat free milk solution in 1 × PBS 500 µl for 30 min.

If both cell surface and total protein measurements were being conducted at the same time the tissue culture plate was treated the same from this step onwards. After the blocking step, the primary affinity-purified antibodies, 250 µl per well were incubated for 1 h. The primary affinity-purified antibodies were used at the following concentrations; anti-NR2A (44-58) antibodies = 0.125 µg/ml and anti-NR2B (46-60) antibodies = 0.5 µg/ml diluted in the above blocking solution. Each well was washed with 250 µl blocking solution for a total of 4 × 10 min. The secondary antibodies were incubated for 1 h, 250 µl HRP-linked anti-rabbit immunoglobins (Ig) antibodies diluted 1/2000 in the above blocking solution. Each well was washed with 250 µl blocking solution a total of 3 × 10 min. Lastly, 250 µl 1 × PBS was added to each well. The plates were developed by the addition of 900 µl K-Blue substrate which was incubated for a total of 25 min at room temperature in the dark and the $OD_{\lambda = 650\ nm}$ was measured.

For experiments investigating the association of proteins when phosphorylated, HEK 293 cells were incubated with 20 µM forskolin or 0.1 % (v/v) DMSO solvent control for 30 min prior to the start of the ELISA assay.

2.2.2.14 Protein quantification using the Bio-Rad assay

BSA was diluted to a final concentration of 1 mg/ml using ddH_2O. A series of dilutions of this stock solution were made in triplicate to give; 10 µg, 8 µg, 6 µg, 4 µg, 2 µg and 0 µg BSA each in a total volume of 800 µl. The test samples were diluted 1/10 and 1/100 with ddH_2O. Coomassie brilliant blue G-250 dye Bio-Rad protein assay, 200 µl was added to each. The samples were incubated at room temperature for 30 min. The $OD_{\lambda = 595\ nm}$ were measured. A calibration curve was constructed for the protein standards and the protein concentrations of the test samples determined.

2.2.2.15 Generation of anti-NMDA receptor amino acid sequence directed antibodies

Co-expression of PSD-95α with NR1/NR2B NMDA receptors resulted in an enhanced cell surface expression in HEK 293 cells (Rutter *et al.*, 2002). Recently it was demonstrated that NR1/NR2A NMDA receptors also showed an enhancement of cell surface expression in the presence of PSD-95 (Lin *et al.*, 2004). Thus to further investigate the properties of NR1/NR2A NMDA receptor cell surface expression in the presence of the PSD-95 MAGUK family and the newly generated above mutations, antibodies directed against NR2A extracellular determinants were generated. These were required as the currently available C-terminally directed antibodies would not have access to their epitope for cell surface studies. Anti-peptide antibodies have been successfully designed and used in the laboratory. An advantage of anti-peptide antibodies is an increase of the specificity. The peptide requires coupling to the carrier protein thyroglobulin, for antibody production. The antibody affinity column must have the peptide coupled using the same method as used when coupling the carrier protein.

When designing anti-peptide antibodies a number of considerations were taken:

- The amino acid sequence must be specific to the target protein.
- The conformation of the peptide must mimic the native protein, for example if the C-terminus of a protein was chosen then this would be coupled via the N-terminus of the peptide.
- The peptide should be 10 - 19 amino acids in length and > 85 % pure by HPLC analysis.
- The method of coupling the peptide to both the carrier protein and affinity resin is important. An additional cysteine residue was added to the C-terminus thereby creating a unique coupling site. Cysteine residues are coupled via thiol linkage.

The peptide sequence chosen was amino acids 44-58 Cys of the immature NR2A sequence (peptide designed by Prof. F. A. Stephenson, School of Pharmacy, U.K.). The peptide sequence was:

HDVTERELRNLWGPE<u>C</u>

An additional cysteine residue was added at the C-terminus of the peptide to provide a unique site of coupling. BLAST searches (http://www.ncbi.nlm.nih.gov/BLAST) of the whole and fragments of the peptide were completed to ensure the peptide was a unique sequence found in the NR2A subunit. The epitope is present near the N-terminus of the mature NR2A subunit which gave a higher probability of successful antibody binding. Further, previous experience in the laboratory has shown that anti-NR2B (46-60) antibodies, which are directed to a similar location, work well in ELISA assays.

All immunisations for anti-NMDA receptor antibodies were conducted by Dr Kieran Brickley. Affinity purification of all anti-NMDA receptor antibodies were completed by both Dr Kieran Brickley and myself.

2.2.2.15.1 Coupling of the NR2A (44-58) Cys peptide to carrier protein

The NR2A (44-58) peptide was coupled to the carrier protein thyroglobulin. This was required as immunisation of the peptide alone would not create an antigenic response from the rabbit. Therefore coupling the peptide to thyroglobulin would result in the generation of polyclonal antibodies directed against both the peptide and thyroglobulin.

The thyroglobulin was dissolved as 20 mg/ml in 10 mM potassium phosphate, pH 7.2. This was dialysed with gentle agitation for 16 h at 4°C. The thyroglobulin was adjusted to a final concentration of 16 mg/ml. Thyroglobulin, 250 µl, was slowly added to 85 µl *m*-maleimidobenzoyl-*N*-hydroxysuccinimide ester (MBS) to a final concentration of 3 mg/ml in dimethylformamide. This was incubated for 30 min with gentle agitation at room temperature. The activated thyroglobulin was desalted by passing through a 20 ml Bio-gel

P30 column which had been equilibrated with 50 mM potassium phosphate pH 6.0. The eluted fractions were collected as 1 ml aliquots and monitored by recording the $OD_{\lambda = 280\ nm}$.

The peptide was reduced by dissolving the peptide 10 mg/ml in 10 mM potassium phosphate, pH 7.2. DTT was added to a final concentration of 200 mM and incubated for 1 h at room temperature. The peptide was desalted by passing through 20 ml Bio-gel P2 using 10 mM potassium phosphate, pH 7.2. The peptide concentration was adjusted to 5 mg/ml.

The peptide was conjugated to the activated thyroglobulin by adding 1 ml of the reduced peptide (5 mg/ml) to 3 ml activated thyroglobulin. These were incubated with gentle agitation for 3 h at room temperature. NaCl was added to a final concentration of 0.9 % (w/v). The conjugated peptide, 1 mg/ml was then extensively dialysed against 2 L 1 × PBS for 16 h at 4°C. The dialysis was repeated a total of 3 times. The coupled peptide was stored at -20°C as 200 µl aliquots, until use.

2.2.2.15.2 Production of antibody affinity columns for the purification of anti-NR2A (44 - 58) antibodies

The anti-NR2A (44-58) peptide was coupled via the cysteine residue present at the C-terminus to create an affinity resin. Thiolpropyl-Sepharose 6B (350 mg) was swollen in 10 ml ddH_2O for 5 min and pelleted by centrifugation at 800 × g for 1 min at room temperature. The thiolpropyl-Sepharose 6B was washed with 15 ml 0.1 M Tris-HCl, pH 8.0, 0.3 M NaCl, 1 mM EDTA. The thiolpropyl-Sepharose 6B was allowed to sediment by gravity for ~ 5 min and the supernatant was discarded. To the thiolpropyl-Sepharose 6B pellet, NR2A 44-58 Cys (5 mg/ml diluted in 0.1 M Tris-HCl, pH 8.0, 0.3 M NaCl, 1 mM EDTA) was added. This was gently mixed by inversion and incubated for 2 h at room temperature with gentle rotation. The peptide affinity Sepharose was centrifuged at 400 × g for 30 sec at room temperature. The supernatant was discarded; 1 ml 0.1 M Tris-HCl, pH 8.0, 0.3 M NaCl, 1 mM EDTA was added and gently mixed. This was pelleted by centrifugation at 400 × g for 30 sec at room temperature. The peptide affinity Sepharose was washed with 10 ml 0.1 M Tris-HCl, pH 8.0, 0.3 M NaCl, 1 mM EDTA, followed by

centrifugation at 400 × g for 30 sec at room temperature. The supernatant was discarded and the wash step repeated once with 0.1 M Tris-HCl, pH 8.0, 0.3 M NaCl, 1 mM EDTA and then 2 × 100 mM citric acid, pH 4.5, washes were completed. Excess reactive thiol groups were blocked by the addition of 10 ml 0.1 M Tris-HCl, pH 8.0, 0.3 M NaCl, 1 mM EDTA and 1 mM β-mercaptoethanol and incubated for 45 min with gentle rotation at room temperature. The peptide affinity Sepharose was poured into a Bio-Rad poly-prep chromatography column and 25 ml of 100 mM citric acid, pH 4.5, was allowed to pass through by gravity. Lastly the column was washed with 10 ml 1 × PBS by gravity. The column was stored at 4°C containing ~ 4 ml 1 × PBS with 0.05% (w/v) sodium azide, until use. This shall now be referred to as the peptide affinity column.

2.2.2.15.3 Affinity purification of anti-NMDA receptor antibodies

The peptide affinity column was washed with 10 ml 1 × PBS to remove the sodium azide present. Once the level of 1 × PBS reached 0.5 cm from the top of the resin, 3 - 4 ml of serum was added. The serum was re-circulated though the column for 3 h at a rate of 4 ml/h at room temperature. The serum was removed and the column washed with 100 ml 1 × PBS at a rate of 40 ml/h. The antibodies were eluted by the addition of 10 ml 50 mM glycine, pH 2.4, at a rate of 4 ml/h. The eluted antibodies were collected as ~ 500 µl fractions and immediately neutralised by the addition of ~ 40 µl 1 M Tris-HCl, pH 8.0. The antibody concentration was monitored by reading the $OD_{\lambda = 280\ nm}$. Elution was continued until all antibodies were eluted from the column. The column was neutralised with ~ 50 ml 1 × PBS until the pH of the column was neutral. The column was then stored at 4°C containing ~ 4 ml 1 × PBS containing 0.05% (w/v) sodium azide, until use.

The antibody fractions giving an $OD_{\lambda = 280\ nm} = 0.15$ or above were dialysed against 2 L 1 × PBS for 16 h at 4°C with gentle stirring. The concentration of the antibodies was measured by reading the $OD_{\lambda = 280\ nm}$. An $OD_{\lambda = 280\ nm} = 1.36$ was equivalent to 1 mg/ml protein. The antibodies were then stored in cryotubes containing 0.05% (w/v) sodium azide at 4°C until use.

2.2.2.16 Preparation of P2 membranes from mouse brain

Brains from adult mice were quickly removed and treated on ice. The wet weight of each was recorded. The tissue was homogenised in 10 ml homogenisation buffer (50 mM Tris-citrate, pH 7.4, 5 mM EDTA, 5 mM EGTA, 0.32 M sucrose, 1 mM PMSF, bacitracin (5 μg/ml), soyabean trypsin inhibitors (5 μg/ml), benzamidine HCL (5 μg/ml) and ovomucoid trypsin inhibitor (5 μg/ml)) using a 20 ml tissue grinder with Teflon® pestle and glass chamber. The nuclei were pelleted by centrifugation in JA - 21 centrifuge tubes at 800 × g for 10 min at 4°C using a JA-21 rotor in a Beckman centrifuge. The supernatants were transferred into fresh JA-21 centrifuge tubes and centrifuged at 45,000 × g for 30 min at 4°C. The pellet was homogenised in 20 ml homogenisation buffer (50 mM Tris-citrate, pH 7.4, 5 mM EDTA, 5 mM EGTA, 1 mM PMSF, bacitracin (5 μg/ml), soyabean trypsin inhibitors (5 μg/ml), benzamidine HCL (5 μg/ml) and ovomucoid trypsin inhibitor (5 μg/ml)) using a 20 ml tissue grinder with Teflon® pestle and glass chamber. The P2 fraction was collected by centrifugation at 45,000 × g for 30 min at 4°C. The pellets were resuspended in homogenisation buffer using a tight 7 ml Wheaton Dounce glass-glass homogeniser to give ~ 1.5 mg protein/ml. The proteins were snap frozen and stored at -20°C until analysis by immunoblotting, Section 2.2.2.11.

CHAPTER 3

RESULTS I

DISCUSSION I

3.1 RATIONALE

A systematic study of the associations between the PSD-95 MAGUK family and the major NR1/NR2 NMDA receptor subtypes

As described in Chapter 1, the association between PSD-95 and NMDA receptors has been shown to confer many properties onto the NMDA receptor. For example, the co-expression of PSD-95 was shown to result in the clustering of NMDA receptors (Kim *et al.*, 1996), the association of PSD-95 with Tac-NR2B chimeras regulated their cell surface expression via inhibition of internalization (Roche *et al.*, 2001), it facilitates phosphorylation and dephosphorylation via src, fyn and pyk2 tyrosine kinases and PTPξ tyrosine phosphatase (Natazawa *et al.*, 2001; Kalia and Salter, 2003; Seabold *et al.*, 2004), PSD-95 controls the calpain-mediated cleavage of NR2B subunits (Dong *et al.*, 2004), it inhibits protein kinase C-mediated potentiation of NR1/NR2A and NR1/NR2B NMDA receptors (Yamada *et al.*, 1999; 2002; Lin *et al.*, 2006), PSD-95 contributes to the cell surface expression of NMDA receptors via controlling the export of NR1-3a subunits from the endoplasmic reticulum (Standley *et al.*, 2000) and PSD-95 is thought to modulate the gating of NR1/NR2A NMDA receptors (Rutter and Stephenson 2002; Lin *et al.*, 2004). Lastly, when NR1-1a/NR2A or NR1-1a/NR2B NMDA receptors were co-expressed with PSD-95α there was a selective, ES(D/E)V dependent enhancement of NR2A and NR2B subunits respectively (Rutter and Stephenson, 2000). This enhancement of NR2A and NR2B subunit expression in the presence of PSD-95 was demonstrated to be translated into an enhanced cell surface expression of NR1/NR2A and NR1/NR2B NMDA receptors (Yamada *et al.*, 1999; 2002; Rutter *et al.*, 2002; Lin *et al.*, 2004).

PSD-95 is the prototypic member of the PSD-95 MAGUK family, Section 1.7. The family also includes chapsyn-110, SAP97 and SAP102. All previous studies have focused primarily on the interactions between PSD-95 and NR2A- or NR2B-containing NMDA receptors. The NR2A - NR2D subunits all contain the ES(D/E)V PSD-95 binding motif at their C-termini suggesting each subunit has the ability to interact with each PSD-95 MAGUK (Kornau *et al.*, 1996). However, to date only two studies have investigated the

interaction of NR2C and NR2D C-terminal domains with members of the PSD-95 MAGUK family. Mi *et al.* (2004) demonstrated that the C-terminal region of NR2D was able to interact with PSD-95 in spinal neurons. Using a yeast two-hybrid approach, Chen *et al.* (2006) demonstrated that the NR2C C-terminal domain is able to interact with both PSD-95 and SAP102. A summary of the known interactions between the PSD-95 MAGUK family and the NR2 subunits are shown in Table 1.2.

As seen from Table 1.2, knowledge is incomplete for the interactions of the PSD-95 MAGUK family with the major subclasses of NMDA receptors. Therefore a systematic study of the associations between the PSD-95 MAGUK family and the major NR1/NR2 NMDA receptor subtypes was carried out following their co-expression in HEK 293 cells. Each combination was expressed in a heterologous system and immunoprecipitation assays were performed. The use of a heterologous system had the advantage of expressing a homogenous population of NMDA receptors and PSD-95 MAGUK proteins. As mentioned previously, the co-expression of PSD-95α with NR1/NR2A or NR1/NR2B NMDA receptors resulted in a selective enhancement of NR2A or NR2B subunits (Rutter and Stephenson, 2000). The remaining members of the PSD-95 MAGUK family were investigated to assess if similar properties were elicited on all of the NR2 subunits. Rutter *et al.* (2002) and Lin *et al.* (2004) demonstrated an enhancement of cell surface expression of NR1/NR2A and NR1/NR2B NMDA receptors when co-expressed with PSD-95 in HEK 293 cells. Therefore cell surface expression studies were carried out to investigate if each PSD-95 MAGUK affected the cell surface expression of NR1/NR2A or NR1/NR2B NMDA receptors. Lastly, the role of the N-terminal domain of PSD-95 and the ESDV motif on NR2A and NR2B subunits was examined by NMDA receptor cell surface expression studies.

3.2 RESULTS

3.2.1 Expression of the PSD-95 MAGUK family clones

In addition to PSD-95, the other members of the PSD-95 MAGUK family are; chapsyn-110, SAP97 and SAP102. To ensure the proteins could be successfully expressed, HEK 293 cells were transfected with PSD-95α$^{c\text{-}Myc}$, chapsyn-110$^{c\text{-}Myc}$, SAP97 or SAP102$^{c\text{-}Myc}$ clones and cell homogenates were prepared. The resulting cell homogenates were analysed by immunoblotting using either anti-c-Myc or anti-SAP97 (115-133) antibodies, as appropriate. Representative immunoblots showing the expression of PSD-95α$^{c\text{-}Myc}$, chapsyn-110$^{c\text{-}Myc}$, SAP97 or SAP102$^{c\text{-}Myc}$ are shown in Figure 3.1.

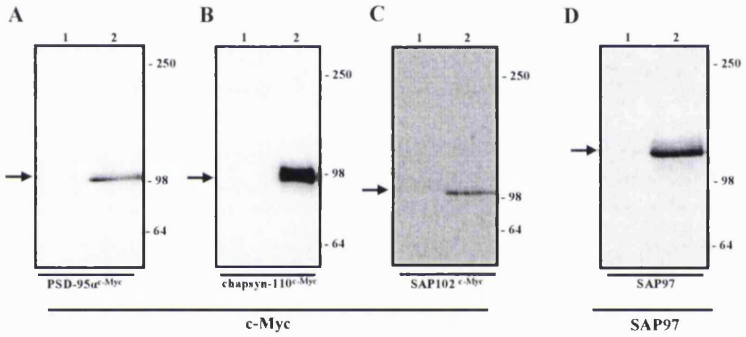

Figure 3.1 Verification of expression of PSD-95 MAGUKs

HEK 293 cells were transfected with PSD-95α$^{c\text{-}Myc}$, chapsyn-110$^{c\text{-}Myc}$, SAP97 and SAP102$^{c\text{-}Myc}$ clones. Cell homogenates were prepared and analysed by immunoblotting using either anti-c-Myc or anti-SAP97 (115-133) antibodies, as indicated. Lane 1 = untransfected HEK 293 cell homogenates, lane 2 = PSD-95 MAGUK expressing HEK 293 cell homogenates. Arrows denote: **A**, PSD-95α$^{c\text{-}Myc}$; **B**, chapsyn-110$^{c\text{-}Myc}$; **C**, SAP102$^{c\text{-}Myc}$ and **D**, SAP97. The positions of the molecular weight markers (kDa) are indicated on the right hand side.

Each protein was successfully expressed in HEK 293 cells as demonstrated by immunoreactive bands corresponding to the predicted size of each protein, i.e. PSD-95α$^{c\text{-}Myc}$, M_r = 102 ± 1 kDa (n = 22); chapsyn-110$^{c\text{-}Myc}$, M_r = 91 ± 5 kDa (n = 12); SAP97, M_r = 121 ± 5 kDa (n = 12) and SAP102$^{c\text{-}Myc}$, M_r = 110 ± 5 kDa (n = 12).

3.2.2 Demonstration of the co-immunoprecipitation of each major sub-class of NMDA receptor with each PSD-95 MAGUK

The aim of the following section was to investigate if each major NR1/NR2 NMDA receptor sub-type co-immunoprecipitates with each PSD-95 MAGUK following their

respective co-expression in a heterologous expression system i.e. HEK 293 cells. The same method was followed for each combination. HEK 293 cells were co-transfected with NR1/NR2 NMDA receptor clones in the presence and absence of each PSD-95 MAGUK, cell homogenates were prepared, detergent-solubilised and the detergent-soluble fraction was used for the immunoprecipitation. The immunoprecipitations were carried out using anti-NR1 C2 or non-immune antibodies as the control, Section 2.2.2.12. The resulting immune and non-immune pellets were dissolved in SDS PAGE sample buffer (40 µl) and the samples were divided as; 8 µl of immune or non-immune pellet was analysed by immunoblotting for NR1 detection, 10 µl for NR2 detection and 12 µl for PSD-95 MAGUK detection. Anti-NR1 C2, anti-NR2A (1381-1394), anti-NR2A/B (1435-1445), anti-NR2C/D (1307-1323), anti-SAP97 (115-133) or anti-c-Myc antibodies were used, as appropriate. In each respective immunoblot, immunoreactive bands were observed at the predicted molecular weight for each protein, i.e. NR1-1a subunits, M_r = 117 ± 7 kDa (n = 34); NR2A subunits, M_r = 177 ± 6 kDa (n = 36); NR2B subunits, M_r = 181 ± 11 (n = 36); NR2C subunits, M_r = 136 ± 4 kDa (n = 36); NR2D subunits, M_r = 155 ± 5 kDa (n = 36) and the molecular weights of PSD-95α$^{c\text{-}Myc}$, chapsyn-110$^{c\text{-}Myc}$, SAP97 and SAP-102$^{c\text{-}Myc}$ were the same in Section 3.2.1. Figures in Section 3.2.2 show only the area of the immunoblot containing the immunoreactive bands. All subsequent results will display the entire immunoblot.

3.2.2.1 Demonstration of the co-immunoprecipitation of NR1-1a/NR2A NMDA receptor complexes with PSD-95α$^{c\text{-}Myc}$, chapsyn-110$^{c\text{-}Myc}$, SAP97 and SAP102$^{c\text{-}Myc}$ following their co-expression in HEK 293 cells

Immunoprecipitation assays were carried out as described in Section 3.2.2. Representative immunoblots are shown in Figure 3.2. Immunoreactive bands corresponding to either NR1-1a subunits, NR2A subunits, PSD-95α$^{c\text{-}Myc}$, chapsyn-110$^{c\text{-}Myc}$, SAP97 or SAP-102$^{c\text{-}Myc}$ were present in the respective detergent-solubilised fractions. NR1-1a and NR2A subunits were both present in the immune pellets but were absent from the non-immune pellets thereby showing that they had both been specifically co-immunoprecipitated. The resulting immune pellets from detergent-solubilised HEK 293 cell homogenates expressing NR1-1a/NR2A/PSD-95α$^{c\text{-}Myc}$, NR1-1a/NR2A/chapsyn-110$^{c\text{-}Myc}$, NR1-1a/NR2A/SAP97 and

NR1-1a/NR2A/SAP102$^{c\text{-}Myc}$ showed immunoreactive bands corresponding to PSD-95α$^{c\text{-}Myc}$, chapsyn-110$^{c\text{-}Myc}$, SAP97 or SAP-102$^{c\text{-}Myc}$. Therefore PSD-95α$^{c\text{-}Myc}$, chapsyn-110$^{c\text{-}Myc}$, SAP97 and SAP-102$^{c\text{-}Myc}$ were found to co-immunoprecipitate with NR1-1a/NR2A NMDA receptor complexes following their co-expression in HEK 293 cells.

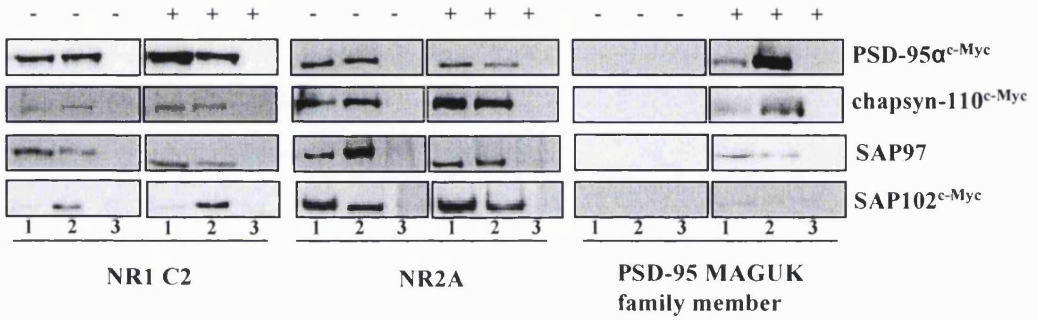

Figure 3.2 Demonstration by immunoprecipitation that NR1-1a/NR2A NMDA receptors co-immunoprecipitate with PSD-95α$^{c\text{-}Myc}$, chapsyn-110$^{c\text{-}Myc}$, SAP97 and SAP102$^{c\text{-}Myc}$

HEK 293 cells were transfected with NR1-1a/NR2A NMDA receptor clones ± PSD-95α$^{c\text{-}Myc}$, ± chapsyn-110$^{c\text{-}Myc}$, ± SAP97 and ± SAP-102$^{c\text{-}Myc}$. HEK 293 cell homogenates were collected 24 h post-transfection, detergent-solubilised and the detergent-soluble fractions used for immunoprecipitations assays using either affinity-purified anti-NR1 C2 or control non-immune antibodies. Gel lanes are identical in each immunoblot, lane 1 = detergent-soluble fraction; lane 2 = immune pellet and lane 3 = non-immune pellet. Immunoblots were analysed using anti-NR1 C2, anti-NR2A (1381-1394), anti-SAP97 (115-133) or anti-c-Myc antibodies, as indicated. The immunoblots are representative of at least n = 2 immunoprecipitations from n = 2 independent transfections.

3.2.2.2 Demonstration of the co-immunoprecipitation of NR1-1a/NR2B NMDA receptor complexes with PSD-95α$^{c\text{-}Myc}$, chapsyn-110$^{c\text{-}Myc}$, SAP97 or SAP102$^{c\text{-}Myc}$ following their co-expression in HEK 293 cells

Immunoprecipitation assays were carried out as described in Section 3.2.2. Representative immunoblots are shown in Figure 3.3. Immunoreactive bands corresponding to either NR1-1a subunits, NR2B subunits, PSD-95α$^{c\text{-}Myc}$, chapsyn-110$^{c\text{-}Myc}$, SAP97 or SAP-102$^{c\text{-}Myc}$ were present in the respective detergent-solubilised fractions. NR1-1a and NR2B subunits were both present in each of the respective immune pellets but were absent from the non-immune pellets showing that they had been specifically co-immunoprecipitated. The resulting immune pellets from detergent-solubilised HEK 293 cell homogenates expressing NR1-1a/NR2B/PSD-95α$^{c\text{-}Myc}$, NR1-1a/NR2B/chapsyn-110$^{c\text{-}Myc}$, NR1-1a/NR2B/SAP97 and NR1-1a/NR2B/SAP102$^{c\text{-}Myc}$ showed immunoreactive bands corresponding to PSD-95α$^{c\text{-}}$

^{Myc}, chapsyn-110$^{c\text{-}Myc}$, SAP97 or SAP-102$^{c\text{-}Myc}$. Therefore PSD-95α$^{c\text{-}Myc}$, chapsyn-110$^{c\text{-}Myc}$, SAP97 and SAP-102$^{c\text{-}Myc}$ were found to co-immunoprecipitate with NR1-1a/NR2B NMDA receptor complexes following their co-expression in HEK 293 cells.

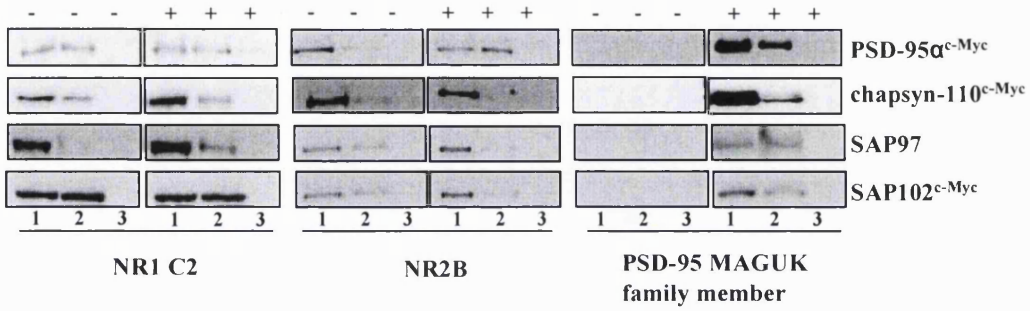

Figure 3.3 Demonstration by immunoprecipitation that NR1-1a/NR2B NMDA receptors co-immunoprecipitate with PSD-95α$^{c\text{-}Myc}$, chapsyn-110$^{c\text{-}Myc}$, SAP97 and SAP102$^{c\text{-}Myc}$

HEK 293 cells were transfected with NR1-1a/NR2B NMDA receptor clones ± PSD-95α$^{c\text{-}Myc}$, ± chapsyn-110$^{c\text{-}Myc}$, ± SAP97 and ± SAP-102$^{c\text{-}Myc}$. HEK 293 cell homogenates were collected 24 h post-transfection, detergent-solubilised and the detergent-soluble fractions used for immunoprecipitations assays using either affinity-purified anti-NR1 C2 or control non-immune antibodies. Gel lanes are identical in each immunoblot, lane 1 = detergent-soluble fraction; lane 2 = immune pellet and lane 3 = non-immune pellet. Immunoblots were analysed using anti-NR1 C2, anti-NR2A/B (1435-1445), anti-SAP97 (115-133) or anti-c-Myc antibodies, as indicated. The immunoblots are representative of at least n = 2 immunoprecipitations from n = 2 independent transfections.

It was noticed that the intensity of the immune pellet for NR2B subunits was always less than the detergent-soluble fraction when compared to the NR2A subunit detergent-soluble and NR2A subunit immune pellets. The immunoreactive species in the absence of the PSD-95 MAGUK were quantified and a ratio was taken from the detergent-soluble fraction to the immune pellet for NR2A and NR2B subunits. The ratio for NR2A subunits was 0.93 ± 0.13 and for NR2B subunits was 0.36 ± 0.08. (n = 8). There was a significant decrease in the immunoreactivity for the immune pellet when comparing the ratio of NR2A subunits with NR2B subunits ($p < 0.025$).

3.2.2.3 Demonstration of the co-immunoprecipitation of NR1-1a/NR2C NMDA receptor complexes with PSD-95α$^{c\text{-}Myc}$, chapsyn-110$^{c\text{-}Myc}$, SAP97 or SAP102$^{c\text{-}Myc}$ following their co-expression in HEK 293 cells

Immunoprecipitation assays were carried out as described in Section 3.2.2. Representative immunoblots are shown in Figure 3.4.

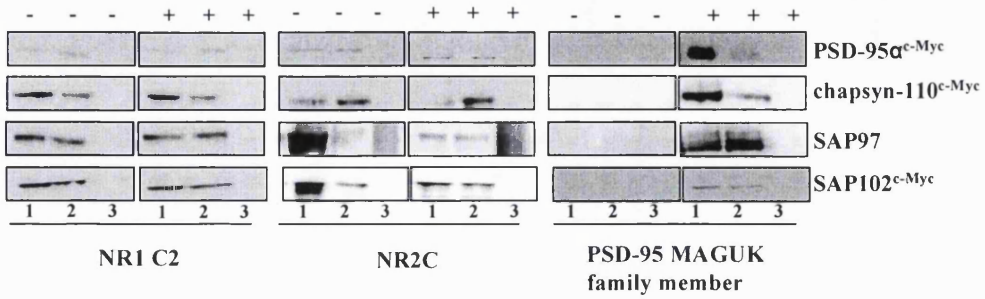

Figure 3.4 Demonstration by immunoprecipitation that NR1-1a/NR2C NMDA receptors co-immunoprecipitate with PSD-95α$^{c\text{-}Myc}$, chapsyn-110$^{c\text{-}Myc}$, SAP97 and SAP102$^{c\text{-}Myc}$

HEK 293 cells were transfected with NR1-1a/NR2C NMDA receptor clones ± PSD-95α$^{c\text{-}Myc}$, ± chapsyn-110$^{c\text{-}Myc}$, ± SAP97 and ± SAP-102$^{c\text{-}Myc}$. HEK 293 cell homogenates were collected 24 h post-transfection, detergent-solubilised and the detergent-soluble fractions used for immunoprecipitations assays using either affinity-purified anti-NR1 C2 or control non-immune antibodies. Gel lanes are identical in each immunoblot, lane 1 = detergent-soluble fraction; lane 2 = immune pellet and lane 3 = non-immune pellet. Immunoblots were analysed using anti-NR1 C2, anti-NR2C/D (1307-1323), anti-SAP97 (115-133) or anti-c-Myc antibodies, as indicated. The immunoblots are representative of at least n = 3 immunoprecipitations from n = 3 independent transfections.

Immunoreactive bands corresponding to either NR1-1a subunits, NR2C subunits, PSD-95α$^{c\text{-}Myc}$, chapsyn-110$^{c\text{-}Myc}$, SAP97 or SAP-102$^{c\text{-}Myc}$ were present in the respective detergent-solubilised fractions. NR1-1a subunits and NR2C subunits were present in the immune pellets but absent from the non-immune pellets showing that they had been specifically co-immunoprecipitated. The resulting immune pellets from detergent-solubilised HEK 293 cell homogenates expressing NR1-1a/NR2C/PSD-95α$^{c\text{-}Myc}$, NR1-1a/NR2C/chapsyn-110$^{c\text{-}Myc}$, NR1-1a/NR2C/SAP97 and NR1-1a/NR2C/SAP102$^{c\text{-}Myc}$ showed immunoreactive bands corresponding to PSD-95α$^{c\text{-}Myc}$, chapsyn-110$^{c\text{-}Myc}$, SAP97 or SAP-102$^{c\text{-}Myc}$. Therefore PSD-95α$^{c\text{-}Myc}$, chapsyn-110$^{c\text{-}Myc}$, SAP97 and SAP-102$^{c\text{-}Myc}$ were all found to co-immunoprecipitate with NR1-1a/NR2C NMDA receptor complexes following their co-expression in HEK 293 cells.

3.2.2.4 Demonstration of the co-immunoprecipitation of NR1-1a/NR2D NMDA receptor complexes with PSD-95α$^{c\text{-}Myc}$, chapsyn-110$^{c\text{-}Myc}$, SAP97 or SAP102$^{c\text{-}Myc}$ following their co-expression in HEK 293 cells

Immunoprecipitation assays were carried out as described in Section 3.2.2. Representative immunoblots are shown in Figure 3.5.

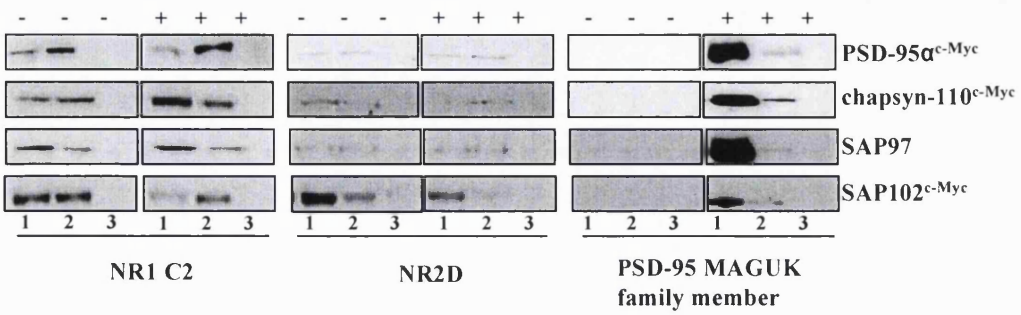

Figure 3.5 Demonstration by immunoprecipitation that NR1-1a/NR2D NMDA receptors co-immunoprecipitate with PSD-95α$^{c\text{-}Myc}$, chapsyn-110$^{c\text{-}Myc}$, SAP97 and SAP102$^{c\text{-}Myc}$

HEK 293 cells were transfected with NR1-1a/NR2D NMDA receptor clones ± PSD-95α$^{c\text{-}Myc}$, ± chapsyn-110$^{c\text{-}Myc}$, ± SAP97 and ± SAP-102$^{c\text{-}Myc}$. HEK 293 cell homogenates were collected 24 h post-transfection, detergent-solubilised and the detergent-soluble fractions used for immunoprecipitations assays using either affinity-purified anti-NR1 C2 or control non-immune antibodies. Gel lanes are identical in each immunoblot, lane 1 = detergent-soluble fraction; lane 2 = immune pellet and lane 3 = non-immune pellet. Immunoblots were analysed using anti-NR1 C2, anti-NR2C/D (1307-1323), anti-SAP97 (115-133) or anti-c-Myc antibodies, as indicated. The immunoblots are representative of at least n = 3 immunoprecipitations from n = 3 independent transfections.

Immunoreactive bands corresponding to either NR1-1a subunits, NR2D subunits, PSD-95α$^{c\text{-}Myc}$, chapsyn-110$^{c\text{-}Myc}$, SAP97 or SAP-102$^{c\text{-}Myc}$ were present in the respective detergent-solubilised fractions. NR1-1a subunits and NR2D subunits were present in the respective immune pellets but were absent from the non-immune pellets thus showing that NR1-1a subunits co-immunoprecipitate with NR2D subunits. The resulting immune pellets from detergent-solubilised HEK 293 cell homogenates expressing NR1-1a/NR2D/PSD-95α$^{c\text{-}Myc}$, NR1-1a/NR2D/chapsyn-110$^{c\text{-}Myc}$, NR1-1a/NR2D/SAP97 and NR1-1a/NR2D/SAP102$^{c\text{-}Myc}$ showed immunoreactive bands corresponding to PSD-95α$^{c\text{-}Myc}$, chapsyn-110$^{c\text{-}Myc}$, SAP97 or SAP-102$^{c\text{-}Myc}$. Therefore PSD-95α$^{c\text{-}Myc}$, chapsyn-110$^{c\text{-}Myc}$, SAP97 and SAP-102$^{c\text{-}Myc}$ were found to co-immunoprecipitate with NR1-1a/NR2D NMDA receptor complexes following their co-expression in HEK 293 cells.

3.2.3 Differential enhancement of expression for the major NMDA receptor subunits when co-expressed with each PSD-95 MAGUK

Since all the major NR1/NR2 NMDA receptor subclasses were shown to co-immunoprecipitate with each PSD-95 MAGUK, the effect on the total expression was examined. As described earlier, co-expression of PSD-95α with NR1/NR2A or NR1/NR2B NMDA receptors results in a selective enhancement of NR2A and NR2B

subunits but the NR1 subunit expression remains unchanged, (Rutter and Stephenson, 2000). Quantitative immunoblotting was carried out to investigate if all PSD-95 MAGUK family members had a similar effect on the expression levels of each NR2 subunit. HEK 293 cells were co-transfected with NR1/NR2 NMDA receptor clones in the presence and absence of each PSD-95 MAGUK, cell homogenates were prepared and analysed by immunoblotting using either anti-NR1-C2, anti-NR2A (1381-1394), anti-NR2A/B (1435-1445), anti-NR2C/D (1307-1323), anti-SAP97 (115-133) or anti-c-Myc antibodies, as appropriate, Section 2.2.2.11.

For each NR1/NR2 NMDA receptor ± PSD-95 MAGUK n = 3 transfections were carried out. To ensure the results were reproducible, triplicate samples were applied per gel lane for each combination and the immunoblots were replicated at least n = 2 within each individual transfection. A number of methods were employed to ensure that identical amounts of protein were applied per gel lane. Firstly HEK 293 cells were sub-cultured (always from the same progeny) to give a comparable cell number per flask. Secondly the protein concentration of the resulting cell homogenates was measured using the Bio-Rad protein assay, Section 2.2.2.15. All results are expressed as the ratio immunoreactivity + PSD-95 MAGUK /immunoreactivity - PSD-95 MAGUK.

3.2.3.1 Reproduction of the selective enhanced expression of NR2A and NR2B subunits following co-expression in HEK 293 cells with PSD-95α$^{c\text{-}Myc}$

Before new combinations of NR1/NR2 NMDA receptors ± PSD-95 MAGUK were investigated, it was necessary to replicate the enhanced expression for NR2A and NR2B subunits when NR1-1a/NR2A and NR1-1a/NR2B NMDA receptors were co-expressed with PSD-95α$^{c\text{-}Myc}$. Representative immunoblots are shown in Figure 3.6. Co-expression of PSD-95α$^{c\text{-}Myc}$ resulted in no significant change in the expression levels of NR1-1a subunits for both NR1-1a/NR2A and NR1-1a/NR2B NMDA receptor combinations, which is in agreement with the results demonstrated by Rutter and Stephenson (2000). In contrast a fold enhancement of 2.8 ± 0.4 ($p < 0.001$, n = 3) for NR2A subunits and 2.5 ± 0.4 ($p < 0.01$, n = 3) for NR2B subunits was observed. These values are comparable to those reported by Rutter and Stephenson (2000) i.e. 2.9 ± 1.1 for NR2A subunits and 3.4 ± 1.4

for NR2B subunits. A histogram to summarise the fold enhancement of expression for NR1-1a, NR2A and NR2B subunits in the presence of PSD-95α$^{c\text{-}Myc}$ are shown in Figure 3.7.

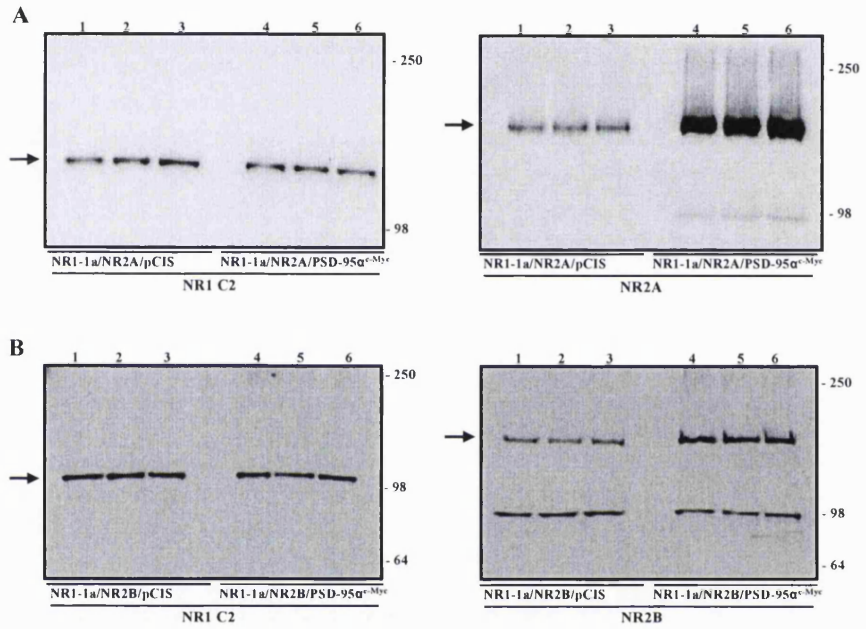

Figure 3.6 Immunoblots demonstrating the effect of PSD-95α$^{c\text{-}Myc}$ on expression levels of NR1-1a/NR2A and NR1-1a/NR2B NMDA receptor subunits following their co-expression HEK 293 cells

HEK 293 cells were transfected with NR1-1a/NR2A and NR1-1a/NR2B NMDA receptor clones ± PSD-95α$^{c\text{-}Myc}$. HEK 293 cell homogenates were collected 24 h post-transfection and subjected to quantitative immunoblotting. Immunoblots were analysed using anti-NR1 C2, anti-NR2A (1381-1394) or anti-NR2A/B (1435-1445) antibodies, as indicated. **A**. For each immunoblot, lanes 1-3 = triplicate samples of NR1/NR2A/pCIS and lanes 4-6 = triplicate samples of NR1/NR2A/PSD-95α$^{c\text{-}Myc}$. **B**. For each immunoblot, lanes 1-3 = triplicate samples of NR1/NR2B/pCIS and lanes 4-6 = triplicate samples of NR1/NR2B/PSD-95α$^{c\text{-}Myc}$. Arrows denote the position of NR1-1a, NR2A and NR2B subunits. The immunoblots are representative of n = 3 independent transfections. The positions of the molecular weight markers (kDa) are shown on the right.

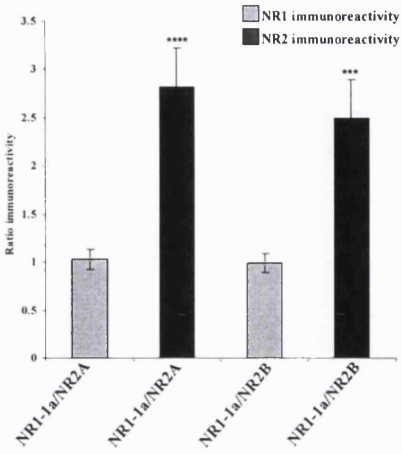

Figure 3.7 Histogram summarising the effect of PSD-95α$^{c\text{-}Myc}$ on expression levels of NR1-1a/NR2A and NR1-1a/NR2B NMDA receptor subunits following their co-expression in HEK 293 cells

HEK 293 cell homogenates expressing NR1-1a/NR2A and NR1-1a/NR2B NMDA receptors ± PSD-95α$^{c\text{-}Myc}$ were subjected to quantitative immunoblotting using anti-NR1 C2, anti-NR2A (1381-1394) or anti-NR2A/B (1435-1445) antibodies. Results are expressed as the fold enhancement, i. e. immunoreactivity + PSD-95α$^{c\text{-}Myc}$/ immunoreactivity - PSD-95α$^{c\text{-}Myc}$. The histogram is a summary of the mean fold enhancement ± SEM for each combination. The results expressed in the histogram are the mean fold enhancement from n = 3 independent transfections (**** = $p < 0.001$, *** = $p < 0.01$).

3.2.3.2 Differential enhancement of expression of NR2A subunits following the co-expression of chapsyn-110$^{c\text{-}Myc}$, SAP97 and SAP102$^{c\text{-}Myc}$ with NR1-1a/NR2A NMDA receptors in HEK 293 cells

HEK 293 cell homogenates expressing NR1-1a/NR2A NMDA receptors in the presence or absence of chapsyn-110$^{c\text{-}Myc}$, SAP97 and SAP102$^{c\text{-}Myc}$ were prepared and the methods outlined in Section 3.2.3 were followed. Representative blots are shown in Figure 3.8. The expression of NR1-1a subunits again showed no statistically significant change in expression in the presence of each PSD-95 MAGUK. Co-expression with chapsyn-110$^{c\text{-}Myc}$ resulted in a statistically significant enhanced expression of 1.6 ± 0.2 ($p < 0.005$, n = 3) for NR2A subunits. However, the co-expression with SAP97 or SAP102$^{c\text{-}Myc}$ gave no significant change in NR2A subunit expression. Values were SAP97 1.1 ± 0.1 ($p < 0.1$, n = 3) and SAP102$^{c\text{-}Myc}$ 1.0 ± 0.1 ($p < 0.1$, n = 3) fold change of NR2A subunit expression. A histogram to summarise the fold enhancement in the presence of each PSD-95 MAGUK is shown in Figure 3.9.

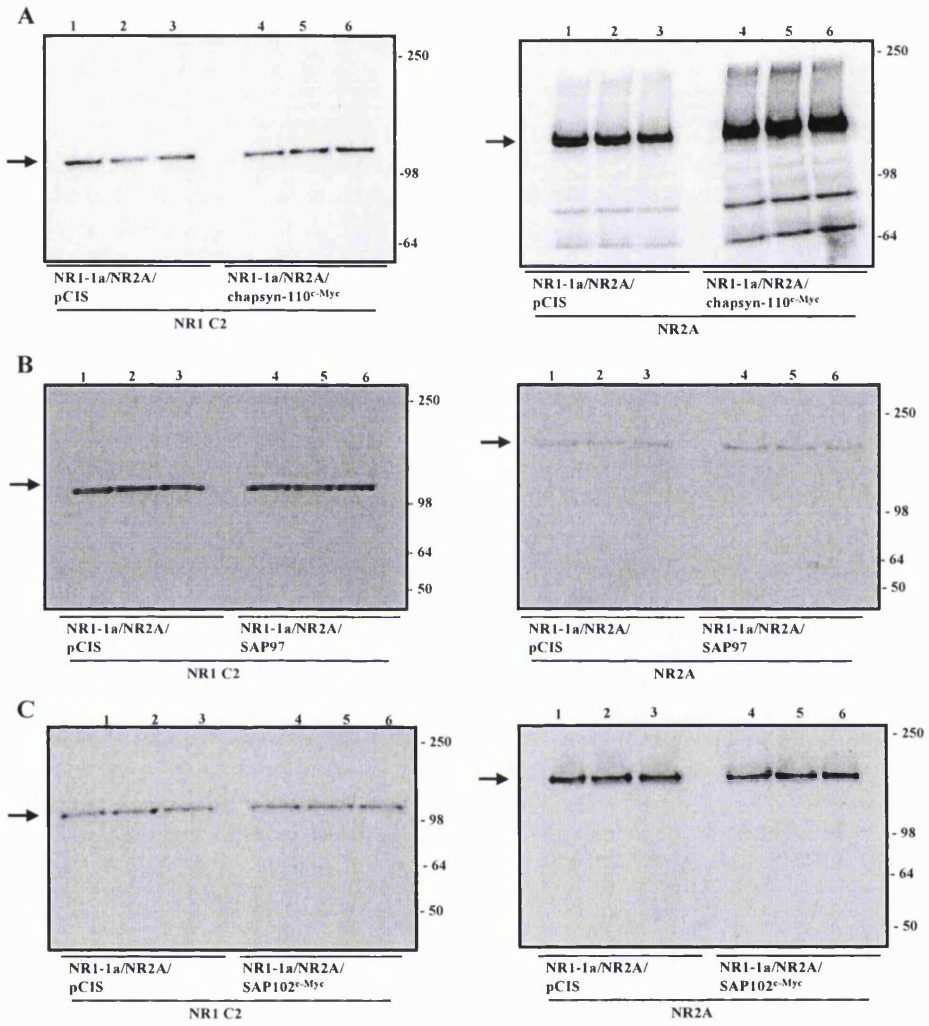

Figure 3.8 Immunoblots demonstrating the effect of chapsyn-110$^{c\text{-}Myc}$, SAP97 and SAP102$^{c\text{-}Myc}$ on expression levels of NR1-1a/NR2A NMDA receptor subunits following their co-expression in HEK 293 cells

HEK 293 cells were transfected with NR1-1a/NR2A NMDA receptor clones ± chapsyn-110$^{c\text{-}Myc}$, ± SAP97 and ± SAP102$^{c\text{-}Myc}$. HEK 293 cell homogenates were collected 24 h post-transfection and subjected to quantitative immunoblotting. Immunoblots were analysed using anti-NR1 C2 or anti-NR2A (1381-1394) antibodies, as indicated. For each immunoblot, lanes 1-3 = triplicate samples of NR1/NR2A/pCIS and lanes 4-6 = triplicate samples of NR1/NR2A/PSD-95 MAGUK. **A**, chapysn-110$^{c\text{-}Myc}$; **B**, SAP97 and **C**, SAP102$^{c\text{-}Myc}$. Arrows denote the positions of either NR1-1a or NR2A subunits. The positions of the molecular weight markers (kDa) are shown on the right. The immunoblots are representative of n = 3 independent transfections.

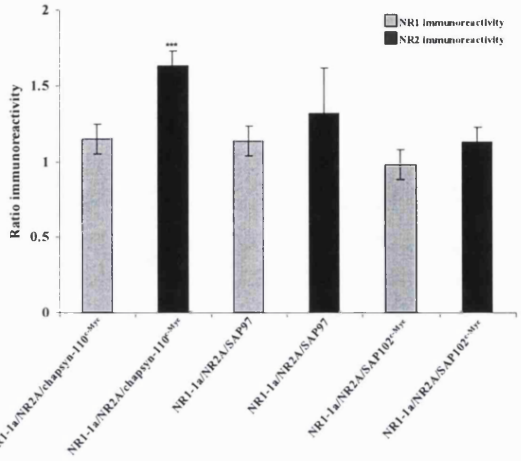

Figure 3.9 Histogram summarising the effect of chapsyn-110$^{c\text{-}Myc}$, SAP97 and SAP102$^{c\text{-}Myc}$ on expression levels of NR1-1a/NR2A NMDA receptor subunits following their co-expression in HEK 293 cells

HEK 293 cell homogenates expressing NR1-1a/NR2A NMDA receptors ± chapsyn-110$^{c\text{-}Myc}$, ± SAP97 and ± SAP102$^{c\text{-}Myc}$ were subjected to quantitative immunoblotting using anti-NR1 C2 or NR2A (1381-1394) antibodies. Results are expressed as a fold enhancement, i. e. immunoreactivity + PSD-95 MAGUK/ immunoreactivity - PSD-95 MAGUK. The histogram is a summary of the mean fold enhancement ± SEM for each combination. The results expressed in the histogram are the mean fold enhancement from n = 3 independent transfections (*** = $p < 0.005$).

3.2.3.3 Differential enhancement of expression of NR2B subunits following the co-expression of chapsyn-110$^{c\text{-}Myc}$, SAP97 and SAP102$^{c\text{-}Myc}$ with NR1-1a/NR2B NMDA receptors in HEK 293 cells

HEK 293 cell homogenates expressing NR1-1a/NR2B NMDA receptors in the presence or absence of chapsyn-110$^{c\text{-}Myc}$, SAP97 and SAP102$^{c\text{-}Myc}$ were prepared and the methods outlined in Section 3.2.3 were followed. Representative immunoblots are shown in Figure 3.10. The expression of NR1-1a subunits showed no statistically significant change in expression in the presence of each PSD-95 MAGUK. Co-expression of chapsyn-110$^{c\text{-}Myc}$ resulted in a statistically significant enhanced expression of 1.8 ± 0.3 ($p < 0.01$, n = 3) for NR2B subunits. However co-expression with SAP97 or SAP102$^{c\text{-}Myc}$ resulted in no significant change in NR2B subunit expression. Values were SAP97 1.1 ± 0.1 ($p < 0.1$, n = 3) and SAP102$^{c\text{-}Myc}$ 1.1 ± 0.0 ($p < 0.1$, n = 3) fold change in NR2B subunit expression. A histogram summarising the fold enhancement in the presence of each PSD-95 MAGUK is shown in Figure 3.11.

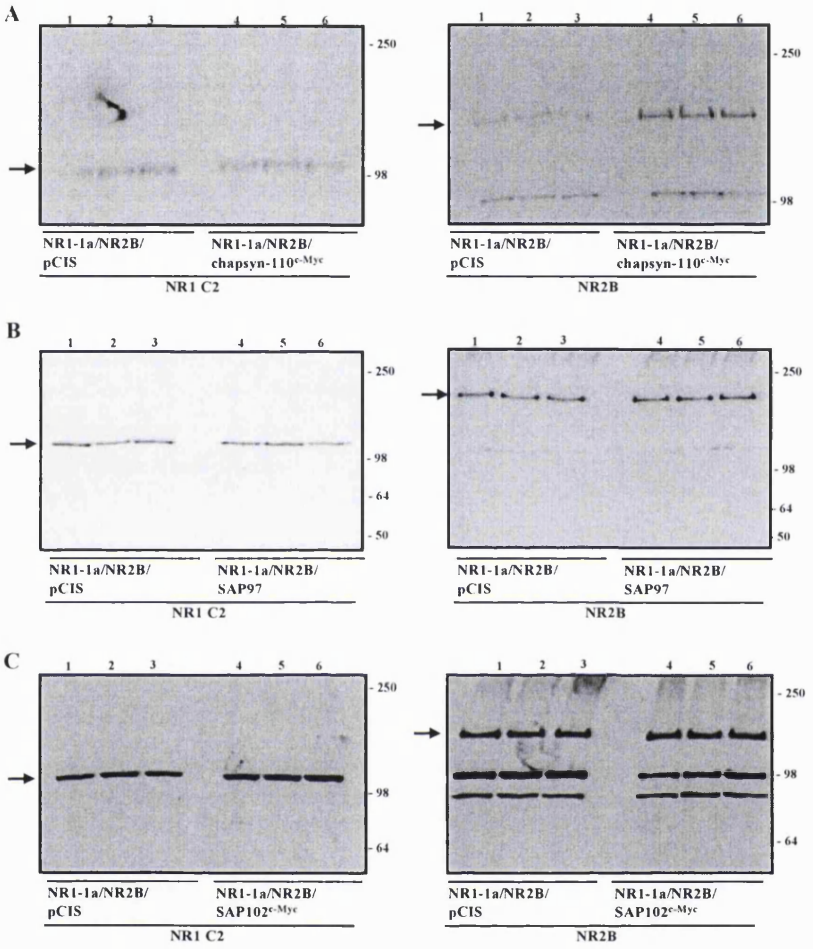

Figure 3.10 Immunoblots demonstrating the effect of chapsyn-110$^{c\text{-}Myc}$, SAP97 and SAP102$^{c\text{-}Myc}$ on expression levels of NR1-1a/NR2B NMDA receptor subunits following their co-expression in HEK 293 cells

HEK 293 cells were transfected with NR1-1a/NR2B NMDA receptor clones ± chapsyn-110$^{c\text{-}Myc}$, ± SAP97 and ± SAP102$^{c\text{-}Myc}$. HEK 293 cell homogenates were prepared 24 h post-transfection and subjected to quantitative immunoblotting. Immunoblots were analysed using anti-NR1 C2 or anti-NR2A/B (1435-1445) antibodies, as indicated. For each immunoblot, lanes 1-3 = triplicate samples of NR1/NR2B/pCIS and lanes 4-6 = triplicate samples of NR1/NR2B/PSD-95 MAGUK. **A**, chapysn-110$^{c\text{-}Myc}$; **B**, SAP97 and **C**, SAP102$^{c\text{-}Myc}$. Arrows denote the positions of NR1-1a or NR2B subunits. The positions of the molecular weight markers (kDa) are shown on the right. The immunoblots are representative of n = 3 independent transfections.

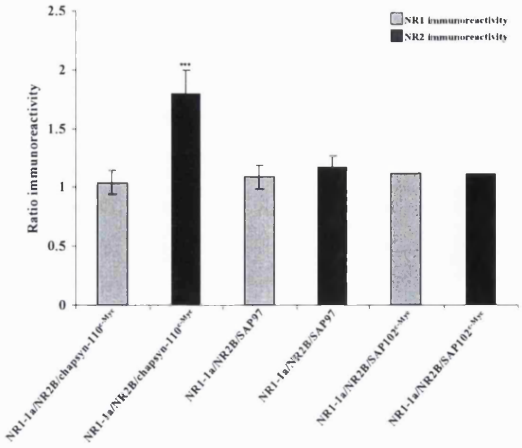

Figure 3.11 Histogram summarising the effect of chapsyn-110$^{c\text{-}Myc}$, SAP97 and SAP102$^{c\text{-}Myc}$ on expression levels of NR1-1a/NR2B NMDA receptor subunits following their co-expression in HEK 293 cells
HEK 293 cell homogenates expressing NR1-1a/NR2B NMDA receptors ± chapsyn-110$^{c\text{-}Myc}$, ± SAP97 and ± SAP102$^{c\text{-}Myc}$ were subjected to quantitative immunoblotting using anti-NR1 C2 or anti-NR2A/B (1435-1445) antibodies. Results are expressed as a fold enhancement, i. e. immunoreactivity + PSD-95 MAGUK/ immunoreactivity - PSD-95 MAGUK. The histogram is a summary of the mean fold enhancement ± SEM for each combination. The results expressed in the histogram are the mean fold enhancement from n = 3 independent transfections (*** = $p < 0.01$).

3.2.3.4 Co-expression of PSD-95α$^{c\text{-}Myc}$, chapsyn-110$^{c\text{-}Myc}$, SAP97 and SAP102$^{c\text{-}Myc}$ with NR1-1a/NR2C NMDA receptors does not result in enhancement of NR2C subunit expression following their co-expression in HEK 293 cells

HEK 293 cell homogenates expressing NR1-1a/NR2C NMDA receptors in the presence and absence of PSD-95α$^{c\text{-}Myc}$, chapsyn-110$^{c\text{-}Myc}$, SAP97 and SAP102$^{c\text{-}Myc}$ were prepared and the methods outlined in Section 3.2.3 were followed. Representative immunoblots are shown in Figure 3.12. There was no significant enhancement in expression for either NR1-1a or NR2C subunits in the presence of each PSD-95 MAGUK. A histogram summarising the results when NR1-1a/NR2C NMDA receptors were co-expressed with each PSD-95 MAGUK is shown in Figure 3.13

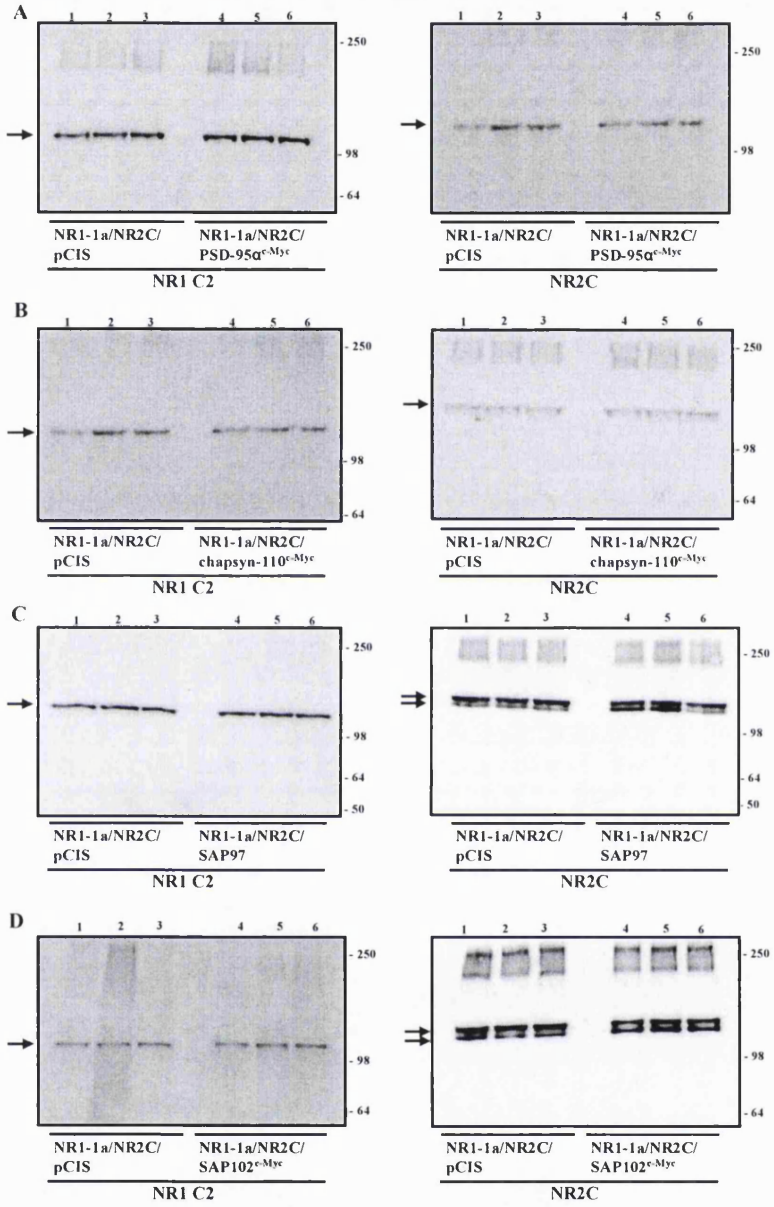

Figure 3.12 Immunoblots demonstrating the effect of PSD-95α$^{c\text{-}Myc}$, chapsyn-110$^{c\text{-}Myc}$, SAP97 and SAP102$^{c\text{-}Myc}$ on expression levels of NR1-1a/NR2C NMDA receptor subunits following their co-expression in HEK 293 cells

HEK 293 cells were transfected with NR1-1a/NR2C NMDA receptor clones ± PSD-95α$^{c\text{-}Myc}$, ± chapsyn-110$^{c\text{-}Myc}$, ± SAP97 and ± SAP102$^{c\text{-}Myc}$. HEK 293 cell homogenates were collected 24 h post-transfection and subjected to quantitative immunoblotting. Immunoblots were analysed using anti-NR1 C2 or anti-NR2C/D (1307-1323) antibodies, as indicated. For each immunoblot, lanes 1-3 = triplicate samples of NR1/NR2C/pCIS and lanes 4-6 = triplicate samples of NR1/NR2C/PSD-95 MAGUK. **A,** PSD-95α$^{c\text{-}Myc}$; **B,** chapysn-110$^{c\text{-}Myc}$; **C**, SAP97 and **D**, SAP102$^{c\text{-}Myc}$. Arrows denote the positions of either NR1-1a or NR2C subunits. The positions of the molecular weight markers (kDa) are shown on the right. The immunoblots are representative of n = 3 independent transfections.

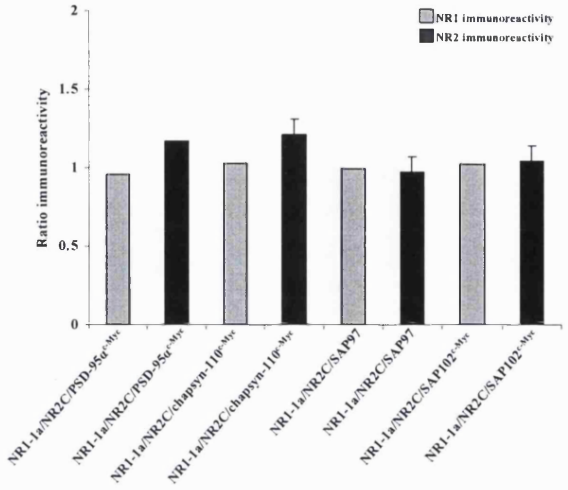

Figure 3.13 Histogram to summarise effect of PSD-95α$^{c\text{-}Myc}$, chapsyn-110$^{c\text{-}Myc}$, SAP97 and SAP102$^{c\text{-}Myc}$ on expression levels of NR1-1a/NR2C NMDA receptor subunits following their co-expression in HEK 293 cells

HEK 293 cell homogenates expressing NR1-1a/NR2C NMDA receptors ± PSD-95α$^{c\text{-}Myc}$, ± chapsyn-110$^{c\text{-}Myc}$, ± SAP97 and ± SAP102$^{c\text{-}Myc}$ were subjected to quantitative immunoblotting using anti-NR1 C2 or anti-NR2C/D (1307-1323) antibodies. Results are expressed as a fold enhancement, i. e. immunoreactivity + PSD-95 MAGUK/ immunoreactivity - PSD-95 MAGUK. The histogram is a summary of the mean fold enhancement ± SEM for each combination. The results expressed in the histogram are the mean fold enhancement from n = 3 independent transfections.

It was observed that only in the presence and absence of SAP-97 or SAP102$^{c\text{-}Myc}$ an immunoreactive doublet for NR2C subunits was detected. The molecular weights of these bands were 132 ± 6 kDa and 122 ± 5 kDa (± SD, n = 30, $p < 0.0005$). The lower molecular weight band was not observed in the presence and absence of both PSD-95α$^{c\text{-}Myc}$ and chapsyn-110$^{c\text{-}Myc}$. Additionally in immunoprecipitation assays the size of the NR2C subunit immunoprecipitated was always the M_r 132 kDa species.

3.2.3.5 Co-expression of PSD-95α$^{c\text{-}Myc}$, chapsyn-110$^{c\text{-}Myc}$, SAP97 and SAP102$^{c\text{-}Myc}$ with NR1-1a/NR2D NMDA receptors does not result in enhancement of NR2D subunit expression following their co-expression in HEK 293 cells

HEK 293 cell homogenates expressing NR1-1a/NR2D NMDA receptors in the presence and absence of PSD-95α$^{c\text{-}Myc}$, chapsyn-110$^{c\text{-}Myc}$, SAP97 and SAP102$^{c\text{-}Myc}$ were prepared and the methods outlined in Section 3.2.3 were followed. Representative immunoblots are shown in Figure 3.14.

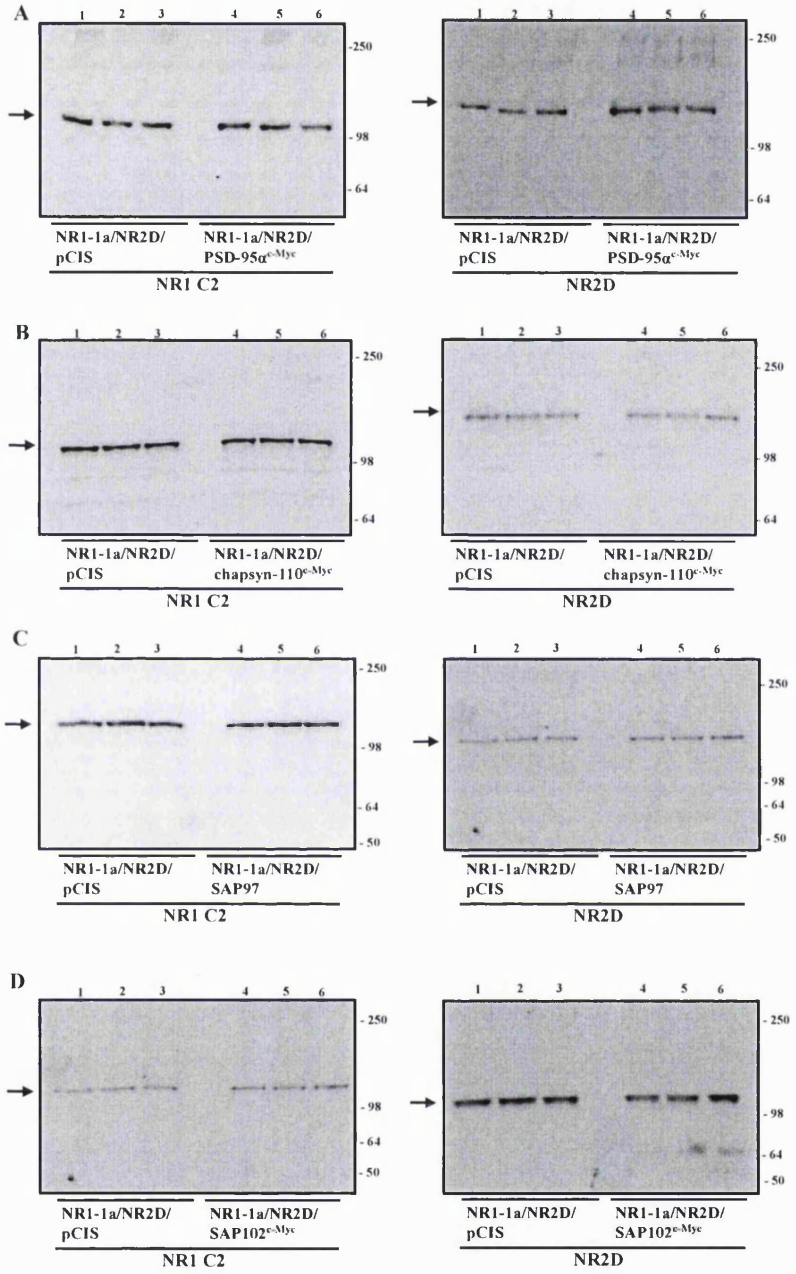

Figure 3.14 Immunoblots demonstrating the effect of PSD-95α$^{c\text{-}Myc}$, chapsyn-110$^{c\text{-}Myc}$, SAP97 and SAP102$^{c\text{-}Myc}$ on expression levels of NR1-1a/NR2D NMDA receptor subunits following their co-expression in HEK 293 cells

HEK 293 cells were transfected with NR1-1a/NR2D NMDA receptor clones ± PSD-95α$^{c\text{-}Myc}$, ± chapsyn-110$^{c\text{-}Myc}$, ± SAP97 and ± SAP102$^{c\text{-}Myc}$. HEK 293 cell homogenates were prepared 24 h post-transfection and subjected to quantitative immunoblotting. Immunoblots were analysed using anti-NR1 C2 or anti-NR2C/D (1307-1323) antibodies, as indicated. For each immunoblot, lanes 1-3 = triplicate samples of NR1/NR2D/pCIS and lanes 4-6 = triplicate samples of NR1/NR2D/PSD-95 MAGUK. **A,** PSD-95α$^{c\text{-}Myc}$; **B,** chapysn-110$^{c\text{-}Myc}$; **C**, SAP97 and **D**, SAP102$^{c\text{-}Myc}$. Arrows denote the position of NR1-1a or NR2D subunits. The positions of the molecular weight markers (kDa) are shown on the right. The immunoblots are representative of n = 3 independent transfections.

No significant enhancement in expression was observed for either NR1-1a or NR2D subunits in the presence of each PSD-95 MAGUK. A histogram summarising the results when NR1-1a/NR2D NMDA receptors were co-expressed with each PSD-95 MAGUK is shown in Figure 3.15.

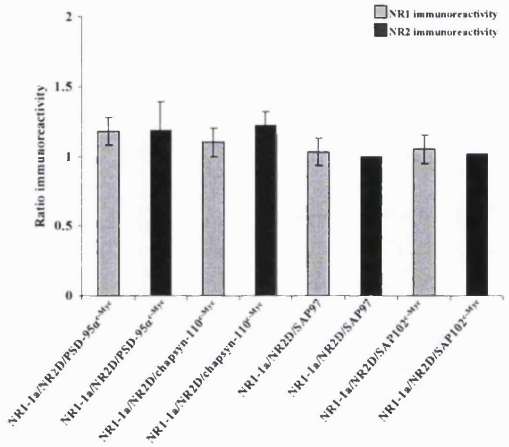

Figure 3.15 Histogram summarising the effect of PSD-95α$^{c\text{-}Myc}$, chapsyn-110$^{c\text{-}Myc}$, SAP97 and SAP102$^{c\text{-}Myc}$ on expression levels of NR1-1a/NR2D NMDA receptor subunits following their co-expression HEK 293 cells

HEK 293 cell homogenates expressing NR1-1a/NR2D NMDA receptors ± PSD-95α$^{c\text{-}Myc}$, ± chapsyn-110$^{c\text{-}Myc}$, ± SAP97 and ± SAP102$^{c\text{-}Myc}$ were subjected to quantitative immunoblotting using anti-NR1 C2 or anti-NR2C/D (1307-1323) antibodies. Results are expressed as a fold enhancement, i. e. immunoreactivity + PSD-95 MAGUK / immunoreactivity - PSD-95 MAGUK. The histogram is a summary of the mean fold enhancement ± SEM for each combination. The results expressed in the histogram are the mean fold enhancement from n = 3 independent transfections.

3.2.4 Generation of antibodies directed against NR2A extracellular determinants

The co-expression of PSD-95α with NR1/NR2B NMDA receptors resulted in an enhanced cell surface expression in HEK 293 cells (Rutter *et al.*, 2002). Recently Lin *et al.* (2004) showed an enhancement of cell surface expression of NR1/NR2A NMDA receptors in the presence of PSD-95 following their co-expression in HEK 293 cells. Thus to investigate further the properties that the PSD-95 MAGUK family elicits on NR1/NR2A NMDA receptor cell surface expression, antibodies directed against NR2A extracellular determinants were generated. The NR2A 44-58 Cys peptide was coupled to thyroglobulin and used to immunise a New Zealand white rabbit, Section 2.2.2.15.1. The resulting anti-NR2A (44-58) antibodies were purified on a NR2A (44-58) peptide affinity column, Section 2.2.2.16.3, and characterised as described below.

To characterise the new anti-NR2A (44-58) antibodies it was necessary to ensure that they are specific to NR2A subunits and that they do not cross-react with the other NR2 subunits. Thus, HEK 293 cells were transfected with either NR1-1a/NR2A, NR1-1a/NR2B, NR1-1a/NR2C or NR1-1a/NR2D NMDA receptor clones. HEK 293 cell homogenates were prepared and analysed by immunoblotting. Representative immunoblots for the characterisation of anti-NR2A (44-58) antibodies are shown in Figure 3.16.

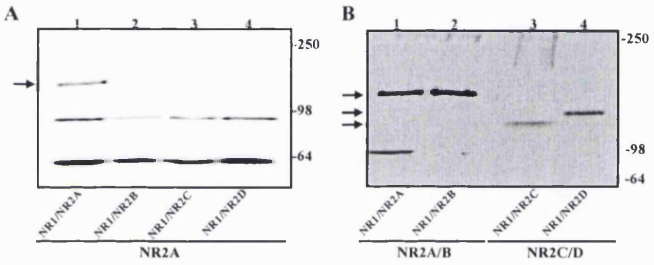

Figure 3.16 Demonstration of the specificity of anti-NR2A (44-58) antibodies for NR2A subunits and not the other NR2 subunits

HEK 293 cells were transfected with NR1-1a/NR2A, NR1-1a/NR2B, NR1-1a/NR2C and NR1-1a/NR2D NMDA receptor clones and cell homogenates were prepared 24 h post-transfection and analysed by immunoblotting. **A**. Immunoblotting with anti-NR2A (44-58) antibodies. The arrow denotes the position of NR2A, M_r = 180 kDa. **B**. Immunoblotting with either anti-NR2A/B (1435-1445) or anti-NR2C/D (1307-1323) antibodies, as indicated. Arrows denote the positions of NR2A, M_r = 180 kDa; NR2B, M_r = 180 kDa; NR2C, M_r = 135 kDa and NR2D, M_r = 155 kDa subunits. The immunoblots are representative of n = 3 independent transfections.

Anti-NR2A (44-58) antibodies showed a specific immunoreactive band with M_r = 180 kDa which corresponded to the predicted molecular weight for NR2A subunits. The anti-NR2A (44-58) antibodies did not recognise any of the other NR2 subunits. To ensure the other receptor combinations were successfully expressed identical immunoblots were carried out in parallel and probed with anti-NR2A/B (1435-1445) and anti-NR2C/D (1307-1323) antibodies, as appropriate. Immunoreactive bands corresponding to NR2A, NR2B, NR2C or NR2D subunits were detected. Therefore anti-NR2A (44-58) antibodies specifically recognised NR2A subunits when expressed in HEK 293 cells and did not cross-react with either NR1-1a, NR2B, NR2C or NR2D subunits.

As an additional control, NR2A (-/-) and wild-type mouse brains were used to further characterise the anti-NR2A (44-58) antibodies. P2 fractions were prepared from NR2A (-/-) and wild-type mouse brains and analysed by immunoblotting using anti-NR2A (44-58) and anti-NR2A/B (1435-1445) antibodies, Section 2.2.2.17. Representative immunoblots are shown in Figure 3.17. It was found that anti-NR2A (44-58) antibodies recognised an immunoreactive bands with a M_r = 180 kDa in wild-type P2 fractions which was absent in NR2A (-/-) P2 fractions. To demonstrate NR2B subunits were present in the NR2A (-/-) P2 fractions, identical immunoblots were carried out in parallel and probed with anti-NR2A/B (1435-1445) antibodies. Immunoreactive bands are observed at M_r = 180 kDa showing NR2B subunit expression was present in the NR2A (-/-) and wild-type P2 fractions. Therefore anti-NR2A (44-58) antibodies specifically recognise NR2A subunits in mouse brain P2 fractions.

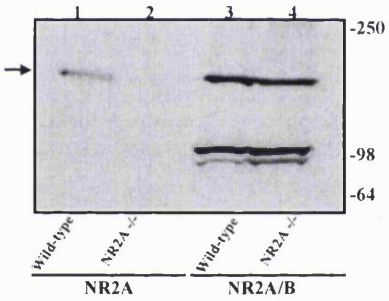

Figure 3.17 Demonstration of the specificity of anti-NR2A (44-58) antibodies recognising native NR2A subunits in P2 fractions from mouse brain

P2 fractions were prepared from NR2A (-/-) and wild-type mouse brains and analysed by immunoblotting using anti-NR2A (44-58) or anti-NR2A/B (1435-1445) antibodies, as indicated. The arrow denotes the position of NR2A or NR2B subunits. The positions of the molecular weight markers (kDa) are shown on the right. Results are representative of n = 3 immunoblots.

Lastly, to show that anti-NR2A (44-58) antibodies could recognise the NR2A subunit in its native conformation and additionally would not cross-react with NR2B subunits, cell surface ELISA assays were carried out. HEK 293 cells were transfected with NR1/NR2A or NR1/NR2B NMDA receptor clones on duplicate tissue culture grade 24 well plates, Section 2.2.2.14. One plate was incubated with anti-NR2A (44-58) antibodies and the second plate was incubated with anti-NR2B (46-60) antibodies. An example of the results

gained is shown in Figure 3.18. The anti-NR2B (46-60) antibodies gave a specific absorbance for HEK 293 cells expressing NR1-1a/NR2B NMDA receptors but not for cells expressing NR1-1a/NR2A NMDA receptors. Therefore anti-NR2B (46-60) antibodies were specific for NR1-1a/NR2B NMDA receptors. The anti-NR2A (44-58) antibodies gave a specific absorbance for HEK 293 cells expressing NR1-1a/NR2A NMDA receptors but not for cells expressing NR1-1a/NR2B NMDA receptors. Thus anti-NR2A (44-58) antibodies specifically recognised NR1-1a/NR2A NMDA receptors when expressed in HEK 293 cells.

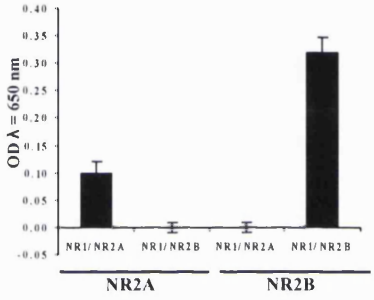

Figure 3.18 Generation and characterisation of new anti-NR2A antibodies directed to an NR2A extracellular epitope

HEK 293 cells were transfected with NR1-1a/NR2A and NR1-1a/NR2B NMDA receptor clones. ELISA assays were performed 24 h post-transfection using anti-NR2A (44-58) or anti-NR2B (46-60) antibodies, as indicated. The histogram shows the mean specific absorbance's gained from triplicate samples and is representative of n = 3 independent transfections.

In addition to raising antibodies in rabbits, a sheep was immunised with the anti-NR2A (44-58 Cys) peptide conjugated to thyroglobulin. The antibodies were affinity-purified using a NR2A (44-58) peptide affinity column and were characterised by immunoblotting and cell surface ELISA studies, as described above. An illustrative immunoblot is shown in Figure 3.19. The sheep anti-NR2A (44-58) antibodies showed an immunoreactive band with a M_r = 180 kDa which corresponded to the predicted molecular weight of NR2A subunits. Cell surface ELISA assays for NR1-1a/NR2A NMDA receptors were conducted to compare the rabbit and the sheep anti-NR2A (44-58) antibodies. A summary of the results gained is shown in Figure 3.19. Both the rabbit and sheep anti-NR2A (44-58) antibodies recognised

the NR1-1a/NR2A NMDA receptors. The rabbit anti-NR2A (44-58) antibodies gave a slightly higher signal: noise ratio.

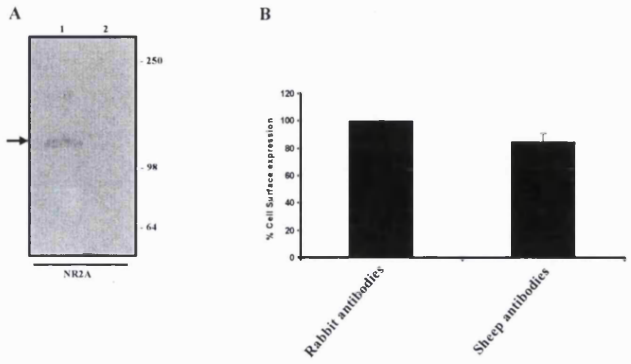

Figure 3.19 Characterisation of sheep anti-NR2A (44-58) antibodies

HEK 293 cells were transfected with NR1-1a/NR2A NMDA receptor clones and cell homogenates were prepared 24 h post-transfection and analysed by immunoblotting. **A**. Immunoblotting with sheep anti-NR2A (44-58) antibodies. Lane 1 = NR1-1a/NR2A, lane 2 = untransfected cell homogenates. The arrow denotes the position of NR2A subunit, M_r = 180 kDa species. The positions of the molecular weight markers (kDa) are shown on the right. **B**. HEK 293 cells were transfected with NR1-1a/NR2A NMDA receptor clones and ELISA assays were performed 24 h post-transfection using rabbit anti-NR2A (44-58) or sheep anti-NR2A (44-58) antibodies. Results are normalised to the absorbance from the rabbit anti-NR2A (44-58) antibodies (± range). The histogram is representative of n = 2 independent transfections.

In all future studies the rabbit anti-NR2A (44-58) antibodies were used. This was predominantly due to the high background gained with the available anti-sheep secondary antibodies.

3.2.5 Differential enhancement of cell surface expression of NR1-1a/NR2A and NR1-1a/NR2B NMDA receptors induced by each PSD-95 MAGUK family member following co-expression in HEK 293 cells

Quantitative immunoblotting revealed that co-expression of NR1-1a/NR2A or NR1-1a/NR2B NMDA receptors with either PSD-95$\alpha^{c\text{-}Myc}$ or chapsyn-$110^{c\text{-}Myc}$ resulted in a selective enhancement of total NR2A and NR2B subunit expression (Rutter and Stephenson, 2000; Section 3.2.2). However co-expression of SAP97 and SAP$102^{c\text{-}Myc}$ with NR1-1a/NR2A or NR1-1a/NR2B NMDA receptors resulted in no change in total NR2A or

NR2B subunit expression (Section 3.2.2). Additionally, an enhancement of cell surface expression of NR1/NR2A (Lin *et al.*, 2004) and NR1/NR2B (Rutter *et al.*, 2002) NMDA receptors was observed when co-expressed with PSD-95 in HEK 293 cells. Therefore it was investigated if the enhancement found for the total NR2A and NR2B subunit expression was translated into an enhancement of cell surface expression for NR1/NR2A or NR1/NR2B NMDA receptors in the presence of each PSD-95 MAGUK. HEK 293 cells were transfected with NR1-1a/NR2A and NR1-1a/NR2B NMDA receptor clones in the presence or absence of PSD-95$\alpha^{c\text{-}Myc}$, chapsyn-$110^{c\text{-}Myc}$, SAP97 or SAP$102^{c\text{-}Myc}$ clones. Cell surface ELISA assays were performed using anti-NR2A (44-58) or anti-NR2B (46-60) antibodies, as appropriate, Section 2.2.2.14. Results are expressed as the fold enhancement, i.e. NR2 cell surface expression + PSD-95 MAGUK/NR2 cell surface expression - PSD-95 MAGUK.

3.2.5.1 Differential enhancement of cell surface expression of NR1-1a/NR2A NMDA receptors in the presence of PSD-95$\alpha^{c\text{-}Myc}$, chapsyn-110 $^{c\text{-}Myc}$, SAP97 and SAP102 $^{c\text{-}Myc}$ following their co-expression in HEK 293 cells

Cell surface ELISA assays were conducted as described in Section 3.2.5. A histogram summarising the cell surface expression for NR1-1a/NR2A NMDA receptors in the presence of each PSD-95 MAGUK is shown in Figure 3.20. Co-expression with PSD-95$\alpha^{c\text{-}Myc}$ and chapsyn-$110^{c\text{-}Myc}$ gave a statistically significant enhancement of NR1-1a/NR2A cell surface NMDA receptor expression. Values were PSD-95$\alpha^{c\text{-}Myc}$, 3.0 ± 0.3 ($p < 0.0005$, $n = 12$); chapsyn-$110^{c\text{-}Myc}$, 2.8 ± 0.5 ($p < 0.005$, $n = 6$). There was no significant change in expression observed in the presence of SAP97 or SAP$102^{c\text{-}Myc}$. Therefore an enhancement in the cell surface expression of NR1-1a/NR2A NMDA receptors in the presence of PSD-95α and chapsyn-110 was found. This is in agreement with Lin *et al.* (2004) who demonstrated that the co-expression of PSD-95 with NR1/NR2A NMDA receptors resulted in an increase in cell surface expression. In contrast no significant change in the cell surface expression for NR1-1a/NR2A NMDA receptors or the total expression of NR2A subunits in the presence of SAP97 or SAP$102^{c\text{-}Myc}$ was observed.

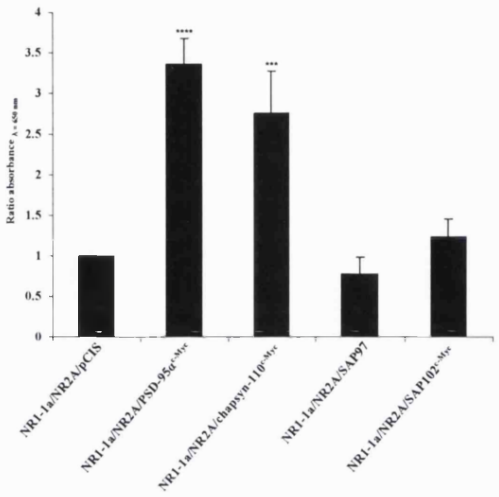

Figure 3.20 Cell surface expression of NR1-1a/NR2A NMDA receptors in the presence of PSD-95α$^{c\text{-}Myc}$, chapsyn-110$^{c\text{-}Myc}$, SAP97 and SAP102$^{c\text{-}Myc}$

HEK 293 cells were transfected with NR1-1a/NR2A NMDA receptor clones ± PSD-95α$^{c\text{-}Myc}$, ± chapsyn-110$^{c\text{-}Myc}$, ± SAP97 and ± SAP102$^{c\text{-}Myc}$. ELISA assays were performed 24 h post-transfection using anti-NR2A (44-58) antibodies. Results are expressed as the fold change in cell surface expression, i. e. NR2A cell surface expression + PSD-95 MAGUK/ NR2A cell surface expression - PSD-95 MAGUK. The histogram summarises the mean fold enhancement ± SEM for each combination. The results expressed in the histogram are the mean fold enhancement from at least n = 3 independent transfections (**** = $p < 0.0005$, *** = $p < 0.005$).

3.2.5.2 Differential enhancement of cell surface expression of NR1-1a/NR2B NMDA receptors in the presence of PSD-95α$^{c\text{-}Myc}$, chapsyn-110 $^{c\text{-}Myc}$, SAP97 and SAP102 $^{c\text{-}Myc}$ following their co-expression in HEK 293 cells

Cell surface ELISA assays were conducted as described in Section 3.2.5. A histogram summarising the cell surface expression for NR1-1a/NR2B NMDA receptors in the presence of each PSD-95 MAGUK is shown in Figure 3.21. Co-expression with PSD-95α$^{c\text{-}Myc}$ and chapsyn-110$^{c\text{-}Myc}$ resulted in a significant enhancement of NR1-1a/NR2B NMDA receptor cell surface expression. Values were PSD-95α$^{c\text{-}Myc}$, 2.69 ± 0.37 ($p < 0.0005$, n = 8) and chapsyn-110$^{c\text{-}Myc}$, 2.61 ± 0.45 ($p < 0.01$, n = 5). Co-expression of SAP97 or SAP102$^{c\text{-}Myc}$ resulted in no statistically significant change in cell surface expression. Therefore an enhancement was observed for the cell surface expression of NR1-1a/NR2B NMDA receptors in the presence of PSD-95α$^{c\text{-}Myc}$ and chapsyn-110$^{c\text{-}Myc}$. This is in agreement to Rutter *et al.* (2002) who demonstrated that the co-expression of PSD-95 with NR1/NR2B NMDA receptors resulted in an increase in cell surface expression. In contrast no

significant change in the cell surface expression for NR1-1a/NR2B NMDA receptors or the total expression of NR2B subunits in the presence of SAP97 or SAP102$^{c\text{-}Myc}$ was observed.

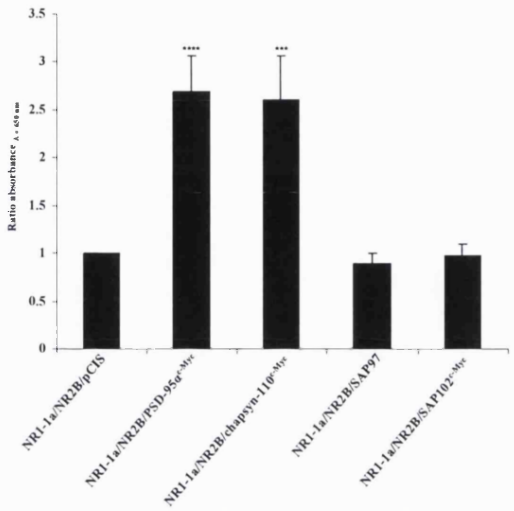

Figure 3.21 Cell surface expression of NR1-1a/NR2B NMDA receptors in the presence of PSD-95α$^{c\text{-}Myc}$, chapsyn-110$^{c\text{-}Myc}$, SAP97 or SAP102$^{c\text{-}Myc}$

HEK 293 cells were transfected with NR1-1a/NR2B NMDA receptor clones ± PSD-95α$^{c\text{-}Myc}$, ± chapsyn-110$^{c\text{-}Myc}$, ± SAP97 and ± SAP102$^{c\text{-}Myc}$. ELISA assays were performed 24 h post-transfection using anti-NR2B (46-60) antibodies. Results are expressed as the fold enhancement, i. e. NR2B cell surface expression + PSD-95 MAGUK/ NR2B cell surface expression - PSD-95 MAGUK. The histogram summarises the mean fold enhancement ± SEM for each combination. The results expressed in the histogram are the mean fold enhancement from at least n = 3 independent transfections (**** = $p < 0.0005$, *** = $p < 0.01$).

3.2.6 Investigation of the role of the NR2A and NR2B subunit C-terminal ESDV motif on the enhanced cell surface expression induced by PSD-95α$^{c\text{-}Myc}$

The ESDV motif present on the C-terminal of NR2A and NR2B subunits were shown to mediate the interaction with PSD-95 (Niethammer *et al.*, 1996). The deletion of this ESDV motif, thereby generating NR2A^{TRUNC} and NR2B^{TRUNC} subunits is thought to disrupt this interaction, although see Section 5. Rutter and Stephenson (2000) demonstrated that the PSD-95 induced enhancement of total NR2A and NR2B subunit expression was dependent upon the C-terminal ESDV PSD-95 binding motif. Since the enhancement of total NR2A and NR2B subunit expression in the presence of PSD-95α was demonstrated to be translated into an enhancement of cell surface expression of NR1/NR2A and NR1/NR2B NMDA receptors, the cell surface expression of NR1-1a/NR2A^{TRUNC} or NR1-

1a/NR2B^{TRUNC} NMDA receptors in the presence and absence of PSD-95$\alpha^{c\text{-}Myc}$ was investigated by cell surface ELISA studies. HEK 293 cells were transfected with wild-type NMDA receptor clones (NR1-1a/NR2A or NR1-1a/NR2B) and the corresponding truncated NMDA receptor clones (NR1-1a/NR2A^{TRUNC} or NR1-1a/NR2B^{TRUNC}) in the presence and absence of PSD-95$\alpha^{c\text{-}Myc}$. The ELISA assay was carried out using anti-NR2A (44-58) or anti-NR2B (46-60) antibodies, as appropriate, Section 2.2.2.14. Results are expressed as the fold enhancement, i.e. NR2 cell surface expression + PSD-95/ NR2 cell surface expression - PSD-95.

There was a significant decrease of 58 ± 9 % in the cell surface expression for NR1-1a/NR2A^{TRUNC} NMDA receptors was observed when compared to cell surface expression of NR1-1a/NR2A NMDA receptors ($p < 0.005$, $n = 3$). Additionally, there was a significant decrease of 34 ± 7 % in the cell surface expression for NR1-1a/NR2B^{TRUNC} NMDA receptors observed when compared to the expression of NR1-1a/NR2B NMDA receptors ($p < 0.025$, $n = 3$). A histogram summarising the results is shown in Figure 3.22. Rutter (2001) demonstrated that NR2A^{TRUNC} and NR2B^{TRUNC} subunits were expressed at a similar level to the NR2A or NR2B subunits respectively. Therefore the differences observed for the cell surface expression cannot be due to the level of the expressed NR2 subunits, rather the properties elicited by the ESDV motif. Interestingly, there was a significant difference in the cell surface expression of NR1-1a/NR2A^{TRUNC} receptors ($p < 0.05$) when compared to NR1-1a/NR2B^{TRUNC} NMDA receptors cell surface expression.

As observed before, the co-expression of PSD-95$\alpha^{c\text{-}Myc}$ with NR1-1a/NR2A and NR1-1a/NR2B NMDA receptors resulted in a significant enhancement of their cell surface expression. However there was no significant change in the cell surface expression for NR1-1a/NR2A^{TRUNC} or NR1-1a/NR2B^{TRUNC} NMDA receptors in the presence of PSD-95$\alpha^{c\text{-}Myc}$ ($p < 0.1$). A histogram summarising of the results gained are shown in Figure 3.23.

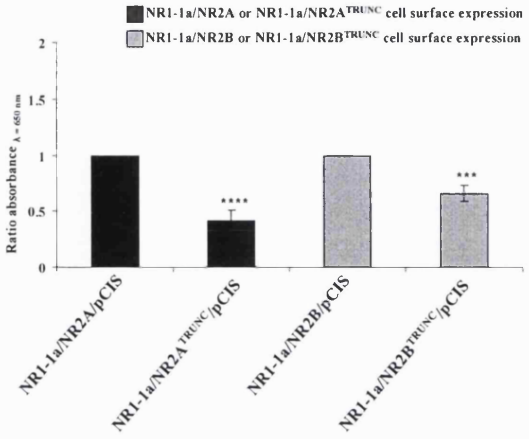

Figure 3.22 Cell surface expression of NR1-1a/NR2A^{TRUNC} and NR1-1a/NR2B^{TRUNC} NMDA receptors
HEK 293 cells were transfected with NR1-1a/NR2A, NR1-1a/NR2A^{TRUNC}, NR1-1a/NR2B and NR1-1a/NR2B^{TRUNC} NMDA receptor clones. ELISA assays were performed 24 h post-transfection using anti-NR2A (44-58) or anti-NR2B (46-60) antibodies, as appropriate. The results are expressed as the fold change i. e. NR2^{TRUNC} cell surface expression / NR2 cell surface expression. The histogram summarises the mean fold enhancement ± SEM for each combination. The results expressed in the histogram are the mean fold enhancement from at least n = 3 independent transfections (**** = $p < 0.0005$, *** = $p < 0.025$).

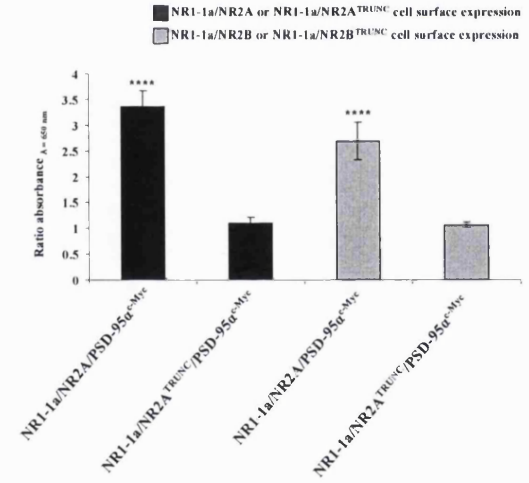

Figure 3.23 Cell surface expression of NR1-1a/NR2A^{TRUNC} and NR1-1a/NR2B^{TRUNC} NMDA receptors in the presence of PSD-95α$^{c\text{-}Myc}$
HEK 293 cells were transfected with NR1-1a/NR2A, NR1-1a/NR2A^{TRUNC}, NR1-1a/NR2B and NR1-1a/NR2B^{TRUNC} NMDA receptor clones ± PSD-95α$^{c\text{-}Myc}$. ELISA assays were performed 24 h post-transfection using anti-NR2A (44-58) or anti-NR2B (46-60) antibodies, as appropriate. The results are expressed as the fold change i. e. NR2 cell surface expression + PSD-95α$^{c\text{-}Myc}$/ NR2 cell surface expression - PSD-95α$^{c\text{-}Myc}$. The histogram summarises the mean fold enhancement ± SEM for each combination. The results expressed in the histogram are the mean fold enhancement from at least n = 3 independent transfections (**** = $p < 0.0005$, *** = $p < 0.025$).

3.2.7 A comparison of the effect of different N-terminal variants of PSD-95 has on NR1-1a/NR2A NMDA receptor cell surface expression following their co-expression in HEK 293 cells

PSD-95α enhanced the cell surface expression of the NR1-1a/NR2A NMDA receptors following their co-expression in HEK 293 cells (Lin *et al.*, 2004; Section 3.2.5.1). The N-terminal domain of PSD-95α was shown to be essential for clustering of NMDA receptors (Hsueh *et al.*, 1997). PSD-95α is known to be palmitoylated at the N-terminus on cysteine residues 3 and/or 5 (Topinka and Bredt, 1998; El-Husseini *et al.*, 2000). A palmitoylation dead mutant was generated by mutating the cysteine residues 3 and 5 of PSD-95α into serine residues, creating PSD-95α^{C3S,C5S} (Rutter, 2001). When NR1-1a/NR2A or NR1-1a/NR2B NMDA receptors were co-expressed with PSD-95α^{C3S,C5S} the fold enhancement of total NR2A or NR2B subunit expression was greatly reduced (Rutter, 2001). PSD-95β has an alternative protein interaction domain, the L27 domain present at the N-terminus which is a 53 amino acid insert replacing the palmitoylated cysteine residues (Chetkovich *et al.*, 2002). Papadakis (2004) demonstrated by quantitative immunoblotting that the co-expression of NR1/NR2A and NR1/NR2B NMDA receptors with PSD-95β resulted in a selective enhancement of total NR2A and NR2B subunit expression. To investigate the influence the N-terminal region of PSD-95 plays on the NR1-1a/NR2A NMDA receptor enhanced cell surface expression, cell surface expression studies were carried out in the presence of the different PSD-95 clones.

HEK 293 cells were transfected in parallel with NR1-1a/NR2A NMDA receptor clones in the presence and absence of PSD-95α$^{c\text{-}Myc}$, PSD-95α^{C3S,C5S} and PSD-95β. Cell surface ELISA assays were carried out using anti-NR2A (44-58) antibodies, Section 2.2.2.14. The results are expressed as the fold enhancement; NR2A cell surface expression + PSD-95/ NR2A cell surface expression - PSD-95. A histogram summarising the results is shown in Figure 3.24. In agreement with previous findings, there was a significant enhancement of NR1-1a/NR2A NMDA receptor cell surface expression in the presence of PSD-95α$^{c\text{-}Myc}$, 3.0 ± 0.3 ($p < 0.0005$, $n = 5$), Section 3.2.5.1. In addition, PSD-95β and PSD-95α^{C3S,C5S} both enhanced the cell surface expression of NR1-1a/NR2A NMDA receptors, 1.9 ± 0.1 ($p < 0.0005$, $n = 5$) and 1.5 ± 0.1 ($p < 0.025$, $n = 3$), respectively. When comparing the

resulting increase of cell surface expression of NR1-1a/NR2A NMDA receptors elicited by the different PSD-95 isoforms, the resulting enhancement was significantly less when co-expressed with PSD-95β ($p < 0.01$) and PSD-95$\alpha^{C3S,C5S}$ ($p < 0.005$) compared to PSD-95α. There was a significant decrease in the resulting enhancement when co-expressing PSD-95$\alpha^{C3S,C5S}$ compared to PSD-95β ($p < 0.025$).

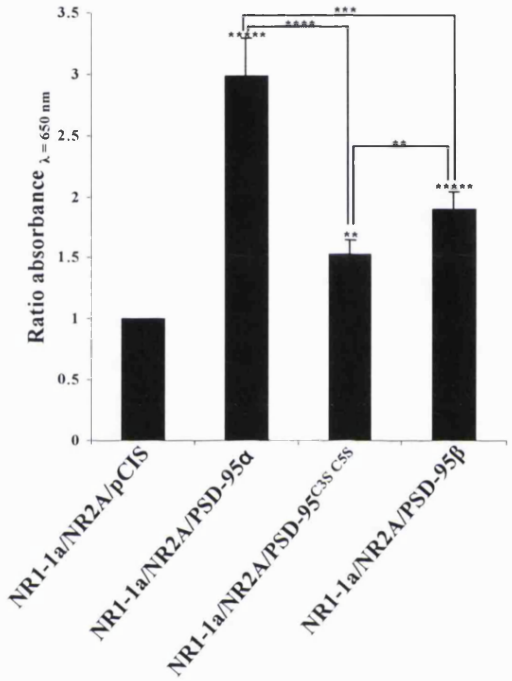

Figure 3.24 Cell surface expression of NR1-1a/NR2A NMDA receptors in the presence of PSD-95$\alpha^{c\text{-}Myc}$, PSD-95β and PSD-95$\alpha^{C3S,C5S}$

HEK 293 cells were transfected with NR1-1a/NR2A NMDA receptor clones ± PSD-95$\alpha^{c\text{-}Myc}$, ± PSD-95β and ± PSD-95$\alpha^{C3S,C5S}$. ELISA assays were performed 24 h post-transfection using anti-NR2A (44-58) antibodies. Results are expressed as the fold enhancement, i. e. NR2A cell surface expression + PSD-95/ NR2A cell surface expression - PSD-95. The histogram summarises the mean fold enhancement ± SEM for each combination. The results expressed in the histogram are the mean fold enhancement from at least n = 3 independent transfections (***** = $p < 0.0005$, **** = $p < 0.025$, *** = $p < 0.01$, * = $p<0.025$).

3.2.8 Endogenous expression of SAP97 and SAP102 in HEK 293 cells demonstrated by immunoblotting

SAP102 had no effect on the total expression of NR2A and NR2B subunits nor the cell surface expression of NR1-1a/NR2A and NR1-1a/NR2B NMDA receptors, Sections

3.2.3.2 and 3.2.5.1. A possible explanation may be that SAP102 was found to be endogenously expressed in HEK 293 cells (Sans *et al.*, 2003; Lin *et al.*, 2004). To investigate if SAP102 is endogenously expressed in the HEK 293 cells, cells were sham-transfected or transfected with SAP102$^{c\text{-}Myc}$ clones. Cell homogenates were prepared and subjected to immunoblotting using either anti-c-Myc or anti-SAP102 (83-100) antibodies, as appropriate. Representative immunoblots are shown in Figure 3.25.

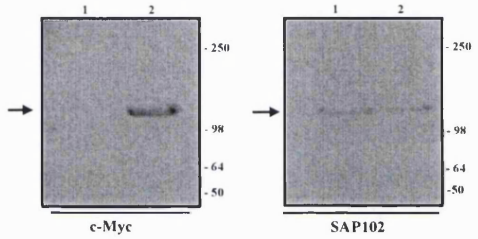

Figure 3.25 Investigation of the endogenous expression of SAP-102 in HEK 293 cells

HEK 293 cells were transfected with pCIS (empty vector) or SAP102$^{c\text{-}Myc}$ clones, cell homogenates were prepared 24 h post-transfection and analysed by immunoblotting using anti-SAP102 (83-100) or anti-c-Myc antibodies, as indicated. Lanes are identical in each immunoblot where lane 1 = pCIS transfected and lane 2 = SAP102$^{c\text{-}Myc}$ exogenously expressing. The arrows denote the position of SAP102, M_r = 110. Protein molecular weight standards (kDa) are shown on the right. Immunoblots are representative of n = 2 independent transfections.

When probing with anti-c-Myc antibodies, SAP102$^{c\text{-}Myc}$ expressing HEK 293 cells showed an immunoreactive band corresponding to the predicted molecular weight of SAP102 which was absent in the sham-transfected HEK 293 cell homogenate. However when probed with anti-SAP102 (83-100) antibodies, immunoreactive bands corresponding to SAP102 were observed for both exogenously SAP102$^{c\text{-}Myc}$ expressing and sham-transfected HEK 293 cell homogenates. Therefore in agreement with Sans *et al.* (2003) and Lin *et al.* (2004), SAP102 is expressed endogenously in HEK 293 cells.

The co-expression of SAP97 resulted in no significant change in either the cell surface expression of NR1-1a/NR2A or NR1-1a/NR2B NMDA receptors or the total NR2A and NR2B subunit expression. SAP97, like SAP102, was shown to be endogenously expressed in HEK 293 cells (Cai *et al.*, 2006). To investigate if SAP97 is endogenously expressed, HEK 293 cells were sham-transfected or transfected with SAP97 clones, cell homogenates were prepared and analysed by immunoblotting using anti-SAP97 (115-133) antibodies.

An representative immunoblot is shown in Figure 3.26. SAP97 expressing HEK 293 cells showed an immunoreactive band corresponding to the predicted molecular weight of SAP97 which was absent in the sham-transfected HEK 293 cell homogenates.

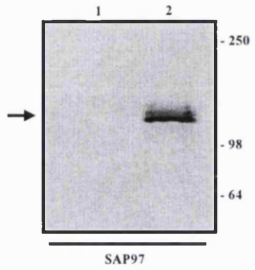

Figure 3.26 Investigation of the endogenous expression of SAP97 in HEK 293 cells
HEK 293 cells were transfected with pCIS (empty vector) or SAP97 clones, cell homogenates were prepared 24 h post-transfection and analysed by immunoblotting using anti-SAP97 (115-133) antibodies, as indicated. Lanes are identical in each immunoblot where lane 1 = pCIS transfected and lane 2 = SAP97 exogenously expressing. The arrow denotes the position of SAP97, M_r = 120. Protein molecular weight standards (kDa) are shown on the right. Immunoblots are representative of n = 2 independent transfections.

3.2.9 Co-immunoprecipitation of endogenous SAP102 in HEK 293 cells following co-expression of NR1-1a/NR2A NMDA receptors

SAP102 was shown to be expressed endogenously in HEK 293 cells (Sans *et al.*, 2003; Lin *et al.*, 2004; Section 3.2.8). Further, endogenously expressed SAP102 in HEK 293 cells was demonstrated to associate with NR1/NR2B NMDA receptors (Sans *et al.*, 2003). Therefore to investigate the possible association of NR1-1a/NR2A NMDA receptors with endogenous SAP102, immunoprecipitation assays were carried out. HEK 293 cells were transfected with NR1-1a/NR2A NMDA receptor clones, cell homogenates prepared, detergent-solubilised and the detergent-soluble fraction used to conduct immunoprecipitation assays using anti-NR1 C2 or non-immune antibodies, Section 2.2.2.12. The immune and non-immune pellets were analysed by immunoblotting with anti-NR2A (1381-1394) or anti-SAP102 (83-100) antibodies, as appropriate. Representative immunoblots are shown in Figure 3.27.

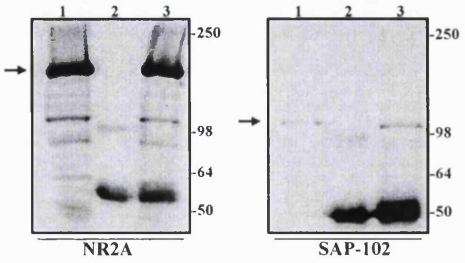

Figure 3.27 Co-immunoprecipitation of endogenous SAP-102 with NR1-1a/NR2A NMDA receptors following their co-expression in HEK 293 cells

HEK 293 cells were transfected with NR1-1a/NR2A NMDA receptor clones, cell homogenates were collected 24 h post-transfection, detergent-solubilised and used to conduct immunoprecipitation assays using anti-NR1 C2 or control non-immune antibodies. Immunoblots were analysed using anti-NR2A (1381-1394) and anti-c-Myc antibodies, as indicated. Gel lanes are identical in each immunoblot, lane 1 = detergent-soluble fraction, lane 2 = non-immune pellet and lane 3 = immune pellet. The arrows denote the positions of NR2A subunits and SAP102. Protein molecular weight standards (kDa) are shown on the right. The immunoblots are representative of n = 3 immunoprecipitations from n = 3 independent transfections.

Both NR2A subunits and SAP102 were present in the detergent-soluble fractions showing each protein was successfully detergent-solubilised. The immune pellets showed immunoreactive bands for both NR2A subunits and SAP102 which were absent from the non-immune pellet. Therefore NR1-1a/NR2A NMDA receptor complexes were found to co-immunoprecipitate with endogenous SAP102 present in HEK 293 cells. This is in agreement with the finding that NR1/NR2B NMDA receptors associate with endogenous SAP102 in HEK 293 cells as demonstrated by Sans *et al.* (2003).

3.2.10 Investigation into the role endogenous SAP102 expression plays on the cell surface enhancement of NR1-1a/NR2A and NR1-1a/NR2B NMDA receptors on the presence of PSD-95α$^{c\text{-}Myc}$ and tat-peptides following their co-expression in HEK 293 cells

SAP102 was shown to be endogenously expressed in HEK 293 cells and co-immunoprecipitated with NR1-1a/NR2A NMDA receptors (Sans *et al.*, 2003; Lin *et al.*, 2004; Section 3.2.8; Section 3.2.9). The co-expression of exogenous SAP102$^{c\text{-}Myc}$ did not result in any significant change in the cell surface expression of NR1-1a/NR2A and NR1-1a/NR2B NMDA receptors or the total NR2A or NR2B subunit expression. Lin *et al.* (2004) demonstrated a slight decrease in NMDA receptor currents when expressing NR1/NR2A NMDA receptors in HEK 293 cells in the presence of a 10 amino acid peptide

corresponding to the distal C-terminal of NR2A subunits. This suggested that the endogenous SAP102 in HEK 293 cells plays a role in the cell surface expression of NR1/NR2A NMDA receptors. Therefore it was investigated if the endogenous expression of SAP102 meant the system was saturated and thus no further change in the cell surface expression would be observed. ELISA assays were carried out in the presence of either tat-NR2B or tat-scrambled. These peptides are cell-permeable due to the attachment of the cell-membrane transduction domain of the human immunodeficiency virus-type 1 (HIV-1) Tat protein (YGRKKRRQRRR; Aarts *et al.*, 2002). The tat-NR2B peptide corresponded to the last 9 amino acids of the NR2B subunit, i.e. YGRKKRRQRRR-KLSSIESDV. A tat-scrambled peptide was used as a control and had the sequence RRRQRRKKRGY. HEK 293 cells were transfected with NR1-1a/NR2A and NR1-1a/NR2B NMDA receptor clones in the presence or absence of PSD-95$\alpha^{c\text{-}Myc}$. One hour prior to the start of the assay, HEK 293 cells were incubated with tat-NR2B, tat-scrambled peptides or HBS buffer control. Cell surface ELISA assays were carried out using anti-NR2A (44-58) or anti-NR2B (46-60) antibodies, as appropriate, Section 2.2.2.14. The cell surface expression of NR1-1a/NR2A and NR1-1a/NR2B NMDA receptors were normalised to receptors incubated in HBS buffer control, Figure 3.28. There was no significant change in the cell surface expression of NR1-1a/NR2A or NR1-1a/NR2B NMDA receptors in the presence of either the tat-NR2B or tat-scramble peptides.

The co-expression of PSD-95$\alpha^{c\text{-}Myc}$ resulted in a significant enhancement of the cell surface expression of NR1-1a/NR2B NMDA receptors in the presence of the HBS buffer control, 1.7 ± 0.2 ($\pm$ range, $p < 0.01$, $n = 2$) and the tat-scrambled peptides 1.5 ± 0.0 ($p < 0.01$, $n = 2$). However when co-expressed with PSD-95$\alpha^{c\text{-}Myc}$, there was no significant enhancement of NR1-1a/NR2B NMDA receptors in the presence of the tat-NR2B peptides, 0.9 ± 0.2 ($p < 0.5$, $n = 2$). In contrast, co-expression with PSD-95$\alpha^{c\text{-}Myc}$ resulted in a significant enhancement of the cell surface expression for NR1-1a/NR2A receptors when incubated with either the HBS buffer control, 2.2 ± 0.1 ($\pm$ range, $p < 0.001$, $n = 2$); tat-scrambled peptides, 2.1 ± 0.2 ($p < 0.001$, $n = 2$) and tat-NR2B peptides 1.9 ± 0.2 ($\pm$ range, $p < 0.001$, $n = 2$). A histogram summarising the results is shown in Figure 3.29.

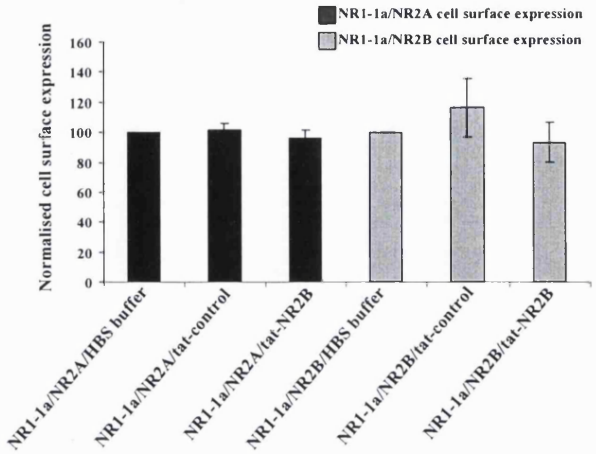

Figure 3.28 Cell surface expression of NR1-1a/NR2A and NR1-1a/NR2B NMDA receptors in the presence tat-control and tat-NR2B peptides

HEK 293 cells were transfected with NR1-1a/NR2A and NR1-1a/NR2B NMDA receptor clones. Tat-control and tat-NR2B peptides were incubated for one hour prior to the start of the assay. ELISA assays were performed 24 h post-transfection using anti-NR2A (44-58) and anti-NR2B (46-60) antibodies. Results are normalised to the HBS buffer control values. The histogram summarises the normalised cell surface expression ± range for each combination. The results expressed in the histogram are the mean fold enhancement from n = 2 independent transfections.

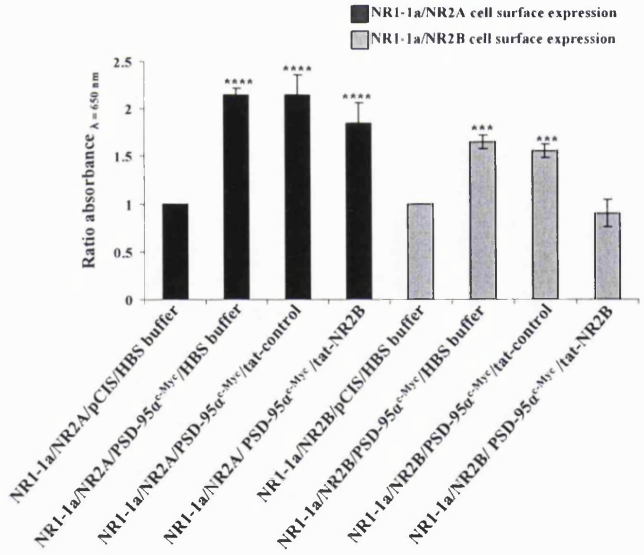

Figure 3.29 Cell surface expression of NR1-1a/NR2A and NR1-1a/NR2B NMDA receptors ± PSD-95αc-Myc in the presence tat-control and tat-NR2B peptides

HEK 293 cells were transfected with NR1-1a/NR2A and NR1-1a/NR2B NMDA receptor clones. Tat-control and tat-NR2B peptides were incubated for one hour prior to the start of the assay. ELISA assays were performed 24 h post-transfection using anti-NR2A (44-58) antibodies. Results are expressed as the fold change in cell surface expression, i. e. NR2A cell surface expression + PSD-95 MAGUK/ NR2A cell surface expression - PSD-95 MAGUK. The histogram summarises the normalised cell surface expression ± range for each combination. The results expressed in the histogram are the mean fold enhancement from n = 2 independent transfections (**** = $p < 0.001$, *** = $p < 0.01$).

3.3 DISCUSSION

As summarised in Table 1.2, the knowledge of the associations between NMDA receptor subtypes and the PSD-95 MAGUK family was incomplete. Thus in this chapter a systematic study of the association between the NMDA receptor subtypes and the PSD-95 MAGUK family was carried out. It has been shown that in a heterologous model system all of the NMDA receptor subtypes associate with each member of the PSD-95 MAGUK family. It is shown here for the first time in this chapter the association between NR1/NR2C and NR1/NR2D NMDA receptor complexes and PSD-95α, chapsyn-110, SAP97 and SAP102. A differential interaction was observed when measuring both the total subunit expression and the cell surface expression. In the presence of PSD-95α and chapsyn-110 there was a selective enhancement of the total expression of NR2A and NR2B subunits, whilst NR1-1a subunit total expression remained the same. However, in the presence of SAP97 and SAP102 the total expression of NR1-1a, NR2A and NR2B subunits remained the same. These results were found to be translated into the cell surface expression i.e. an enhanced cell surface expression of NR1-1a/NR2A and NR1-1a/NR2B NMDA receptors in the presence of PSD-95α and chapsyn-110 but not in the presence of SAP97 and SAP102. In contrast to these results, the co-expression of each PSD-95 MAGUK did not change the total expression of NR1-1a, NR2C and NR2D subunits.

It is perhaps not surprising that all of the NMDA receptor subtypes were found to associate with each PSD-95 MAGUK. As mentioned previously in Chapter 1, each NR2 subunit has the distal C-terminal ES(E/D)V PDZ domain consensus binding sequence. Further, it is known that NR2A and NR2B C-terminal domains interact predominantly via the PSD-95 PDZII domain (Niethammer *et al.*, 1996). This domain is highly conserved between all the PSD-95 MAGUK family members. For example, the amino acid identities of the PDZII domains when compared to PSD-95 are; chapsyn-110 = 80 %; SAP97 = 86 % and SAP102 = 46 %. Thus each PSD-95 MAGUK protein had the ability to associate with the NMDA receptor subtypes. However, this study utilised a model system which may not be representative of the NMDA receptor/PSD-95 MAGUK protein-protein interactions that occur *in vivo*. For example NR2B subunits and SAP102 are expressed at high levels

neonatally, whilst NR2A subunits, PSD-95 and PSD-93 are expressed at high levels in the mature brain (Wang *et al.*, 1995; Dunah *et al.*, 1996; Portera-Cailliau *et al.*, 1996; Sans *et al.*, 2000). Thus it has been suggested there is a preference for the formation of NR2A/PSD-93, NR2A/PSD-95 and NR2B/SAP102 complexes (Sans *et al.*, 2000; Losi *et al.*, 2003). In addition, NR2D-containing receptors are thought to be extra-synaptic (Brickley *et al.*, 2001), and therefore may not associate with PSD-95 which is thought to mainly reside in the post-synaptic density (Cho *et al.*, 1992).

The observed enhancement of the total NR2A and NR2B subunit expression and cell surface expression of NR1/NR2 receptors in the presence of PSD-95 is thought to be due to two possible mechanisms. Firstly, the enhancement is thought to be due to a decrease in the receptor turnover. For example, co-expression of PSD-95 with $K_v1.4$ potassium ion channels was found to result in a decrease in the receptor turnover (Jugloff *et al.*, 2000). Secondly, it was hypothesised that PSD-95 may protect NMDA receptors from degradation (Rutter and Stephenson, 2000). For example, the cleavage of NR2A subunits by calpain resulted in a decrease in the number of recombinant NR1/NR2A NMDA receptors present at the cell surface (Guttmann *et al.*, 2002). However, PSD-95 protected NR2A and NR2B subunits from this selective cleavage by calpain in HEK 293 cells (Dong *et al.*, 2004). Therefore the selective enhancement of NR2A and NR2B subunits could be due to these mechanisms. However, the expression of NR1-1a subunits did not change in the presence of each PSD-95 MAGUK. This may be due to the presence of the intracellular pool of NR1 subunits identified in the ER (Chazot and Stephenson, 1997b). As the NR2 subunits are thought to be the rate limiting factor in the assembly of NMDA receptors, this ER pool of NR1 subunits may assemble with the newly synthesised NR2 subunits (Prybylowski *et al.*, 2002), thus resulting in no change in the total expression of NR1 subunits.

As mentioned above, a differential interaction was observed with regards to both the total subunit and cell surface expression of NR1-1a/NR2A and NR1-1a/NR2B NMDA receptors in the presence of each PSD-95 MAGUK, i.e. an enhancement of cell surface expression when co-expressed with PSD-95 and chapsyn-110 versus no change in cell surface expression when co-expressed with SAP97 and SAP102. This suggested that NR1-

1a/NR2A and NR1-1a/NR2B receptors are differentially regulated by the different members of the PSD-95 MAGUK family. A possible explanation for these results is the endogenous expression of SAP97 and SAP102 in HEK 293 cells. The expression system may have been saturated with regards to SAP97 and SAP102. For example, Lin *et al.* (2004) demonstrated that the incubation of a peptide corresponding to the last 10 amino acids of NR2A subunits with recombinant NR1/NR2A NMDA receptors in HEK 293 cells resulted in a small decrease in the observed NMDA receptor current. This suggested that the endogenous SAP97 and SAP102 in HEK 293 cells played a role in the cell surface expression of NR1/NR2A NMDA receptors. However, it was found in this chapter that the incubation of tat-NR2B peptides with NR1-1a/NR2A and NR1-1a/NR2B NMDA receptors resulted in no significant change to their cell surface expression, which is in contrast to those demonstrated by Lin *et al.* (2004). This may be due to the methodology used; the ELISA assay may not be as sensitive for the measurement of cell surface expressed receptors compared to electrophysiological methods. Additionally, the co-expression of PSD-95 results in an increase in the cell surface expression of NR1-1a/NR2A and NR1-1a/NR2B NMDA receptors even though SAP102 is endogenously expressed in HEK 293 cells (Rutter *et al.*, 2002; Lin *et al.*, 2004). Both SAP102 and PSD-95 associate with the NR2A and NR2B domains via their PDZ domains (Niethammer *et al.*, 1996; Muller *et al.*, 1996). As mentioned previously, the PDZ domain interaction favours a distal C-terminal ESDV motif which is present on both NR2A and NR2B subunits. Therefore, as both SAP102 and PSD-95 compete for the same binding motif, it can be assumed that the endogenous expression of SAP102 in HEK 293 cells is not the reason why an enhancement of NR1-1a/NR2A and NR1-1a/NR2B NMDA receptor expression is not observed in the presence of exogenous SAP102. The endogenous expression of SAP97 as reported by Cai *et al.* (2006) could not be replicated, which may have been due to the antibodies used. Cai *et al.* (2006) demonstrated the endogenous expression of SAP97 in HEK 293 cells by immunoblotting with antibodies directed to amino acids 1 - 100 of SAP97. Here, the antibodies were raised against the rat variant, amino acids 115 – 133, of SAP97 and were found not to cross-react between different species. However, from the tat-peptide studies, which bind to PDZ domains indiscriminately, it can be deduced that the endogenous

expression of both SAP97 and SAP102 is not the reason why no effect was observed when exogenously expressed.

A possible explanation for these differences observed regarding the stabilisation of expression could be the divergent N-terminal domains found on the PSD-95 MAGUK proteins. PSD-95 and chaypsn-110 are palmitoylated at their N-terminal domains whilst SAP97 and SAP102 are not (El-Husseini *et al.*, 2000). This palmitoylation signal was found to be essential for the cell surface clustering of the potassium channel, $K_V1.4$, when co-expressed with PSD-95 or chapsyn-110 with the potassium channel, $K_V1.4$ in a heterologous system (El-Husseini *et al.*, 2000). However, palmitoylation dead mutants of both PSD-95 and chapsyn-110 abolished the formation of potassium channel, $K_V1.4$, clusters (El-Husseini *et al.*, 2000). Conversely, the co-expression of SAP97 or SAP102 resulted in the potassium channel, $K_V1.4$ forming perinuclear intracellular structures (El-Husseini *et al.*, 2000). Additionally, it was demonstrated that the co-expression of SAP97 and potassium channel, $K_V1.4$, resulted in a decrease in cell surface expression and the resulting intracellular clusters were co-localised with BiP, an ER marker (Tiffany *et al.*, 2000). Thus the association of the different PSD-95 family members resulted in the potassium channel, $K_V1.4$, having different sub-cellular localisations. This may be the same for the NMDA receptors, where they were clustered in the presence of PSD-95 or chapsyn-110 but formed intracellular clusters in the presence of SAP97 and SAP102. It would therefore be interesting to examine if intracellular clusters were formed when co-expressing NR1-1a/NR2A and NR1-1a/NR2B NMDA receptors with SAP97 and SAP102 in HEK 293 cells.

In contrast to the results found for NR1-1a/NR2A and NR1-1a/NR2B NMDA receptors, there was no change in the total subunit expression for NR2C or NR2D subunits. This may indicate a difference in the affinity between the PSD-95 MAGUK family and NR2C- or NR2D-containing NMDA receptors. Although the NMDA receptor complexes must be able to withstand the immunoprecipitation procedure, the PSD-95 MAGUK family may have a higher affinity for NR1-1a/NR2A or NR1-1a/NR2B NMDA receptor complexes in comparison to NR1-1a/NR2C and NR1-1a/NR2D NMDA receptor complexes. In

agreement with this hypothesis, Mi *et al.* (2003) demonstrated that the NR2D C-terminal domain had a lower affinity for PSD-95 compared to the NR2A C-terminal domain. Thus this has possible implications regarding the stabilisation or degradation of NR2C- and NR2D-containing NMDA receptors. As mentioned previously, PSD-95 is thought to either stabilise or protect the receptor from degradation. If these subtypes of receptor are not regulated in the same manner as those containing NR2A or NR2B subunits, this may mean that there are either different regulatory mechanisms in place or that their turnover is higher.

The co-expression of each PSD-95 variant resulted in a significant enhancement in the cell surface expression of NR1-1a/NR2A NMDA receptors. However, the resulting increase generated by PSD-95β and PSD-95α^{C3S,C5S} was significantly less when compared to PSD-95α. Therefore, the palmitoylation signal of PSD-95 was found not to be essential for the enhanced cell surface expression of NR1-1a/NR2A NMDA receptors. This result is in agreement with Craven *et al.* (1999) who demonstrated for the normal clustering and localisation of PSD-95 required the presence of the palmitoylation signal, PDZI domain, PDZII domain and a C-terminal sequence (residues 13-25 of the C-terminal). In contrast it was demonstrated that the synaptic localisation of PSD-95 was dependent on the cysteine residues being present (Craven *et al.*, 1999; Firestein *et al.*, 2000). Therefore further experiments could be carried out in neurones prepared from PSD-95$^{-/-}$ knock-out mice to test the cell surface expression of NMDA receptors in the presence of the above different PSD-95 variants.

As a control, NR1-1a/NR2A^{TRUNC} and NR1-1a/NR2B^{TRUNC} NMDA receptors were used to investigate their cell surface expression in the absence of the ESDV motif. Surprisingly, there was a significant decrease in the cell surface expression of NR1-1a/NR2A^{TRUNC} and NR1-1a/NR2B^{TRUNC} NMDA receptors when compared to their respective wild-type receptors. It was previously demonstrated that the NR2A^{TRUNC} and NR2B^{TRUNC} subunits were expressed at the same level as wild-type NR2A and NR2B subunits (Rutter, 2001). Therefore the observed different cell surface expression was due to the deletion of the ESDV motif. In agreement to these results, Lin *et al.* (2004) demonstrated that NR1-

1a/NR2A^{TRUNC} receptors resulted in a decrease of NMDA receptor currents in both HEK 293 cells and *Xenopus* oocytes. The ELISA assay used takes a 'snapshot' of the number of receptors present on the cell surface at a given time. Therefore these results could be interpreted either as the truncated NMDA receptors are trafficked to the cell surface at a lower rate or internalised at a higher rate when compared to the wild-type NMDA receptors. However, Lin *et al.* (2004) hypothesised that this finding was due to an alteration in the intrinsic channel property of NR1-1a/NR2A^{TRUNC} NMDA receptors. It was thought that there was a reduced delivery of receptors or a 'normal' number of receptors were trafficked to the cell membrane but were incorrectly assembled rendering them inactive (Lin *et al.*, 2004). The above data suggests that there is a reduced delivery of NR1-1a/NR2A^{TRUNC} NMDA receptors to the cell surface.

In summary the major finding reported in this chapter are:-

- NR1-1a/NR2A, NR1-1a/NR2B, NR1-1a/NR2C and NR1-1a/NR2D NMDA receptor complexes were all found to associate with each PSD-95 MAGUK member by co-immunoprecipitation following their co-expression in HEK 293 cells.
- As previously demonstrated by Rutter and Stephenson (2000), a selective enhancement of total NR2A and NR2B subunit expression in the presence of PSD-95α, in NR1-1a/NR2A or NR1-1a/NR2B NMDA receptor combinations was found. Chapsyn-110 was also found to elicit a selective enhancement of total NR2A and NR2B subunit expression when co-expressed with NR1-1a/NR2A and NR1-1a/NR2B NMDA receptors. This enhancement of total subunit expression was found to be translated into an increased cell surface expression of both NR1-1a/NR2A and NR1-1a/NR2B NMDA receptors when co-expressed with PSD-95α and chapsyn-110.
- In contrast to PSD-95α and chapsyn-110, SAP97 and SAP102 did not enhance the NR2A or NR2B subunit expression or the cell surface expression of NR1-1a/NR2A and NR1-1a/NR2B NMDA receptors.
- PSD-95α, chapsyn-110, SAP97 and SAP102 had no significant effect on the total expression level of NR2C or NR2D subunits in NR1-1a/NR2C and NR1-1a/NR2D NMDA receptor combinations.

- The PSD-95 induced enhancement of NR1-1a/NR2A and NR1-1a/NR2B NMDA receptors was found to be dependent on the distal C-terminal ESDV motif.
- Both PSD-95$^{C3S, C5S}$ and PSD-95β enhanced the cell surface expression of NR1-1a/NR2A NMDA receptors albeit at a lower level when compared to PSD-95α.

CHAPTER 4

RESULTS II

DISCUSSION II

4.1 RATIONALE

A study into the regulation of the interaction between PSD-95 and NR1/NR2A NMDA receptors by a putative PKA phosphorylation site

As discussed in Chapter 1, phosphorylation of the NMDA receptor NR2 subunits have been demonstrated to affect their binding with the PSD-95 MAGUK family of proteins. Firstly, casein kinase II (CK2) was shown to phosphorylate the serine residue, S1480, present in the ESDV motif of the NR2B subunit C-termini (Chung *et al.*, 2004). This phosphorylation of S1480 was shown to disrupt the interaction between NR2B subunits and PSD-95 or between NR2B and SAP102 (Chung *et al.*, 2004). Secondly, a phosphomimetic mutation of the serine present in the NR2A subunit ESDV motif, S1462E, abolished the PSD-95 potentiation of recombinant NR1/NR2A NMDA receptors (Lin *et al.*, 2006). Lastly, S1244 in the NR2C C-terminus has been shown to be phosphorylated by both PKA and PKC (Chen *et al.*, 2006). In contrast to the above described results, a phosphomimetic point mutation of the NR2C subunits, i.e. S1244E, still behaved as wild-type with respect to NR2C subunit association with PSD-95 or SAP102 (Chen *et al.*, 2006). However, outside-out patches of NR1/NR2C S1244E NMDA receptors expressed in HEK 293 cells showed an acceleration in the channel activation and decay kinetics of the response thus demonstrating that phosphorylation at S1244 affected ion channel gating (Chen *et al.*, 2006).

The sub-cellular localisation of the PSD-95 MAGUK family is also regulated by phosphorylation. Phosphorylation of S39 of SAP97 by CaMKII results in an altered localisation. The non-phosphorylated form of SAP97 is found in the cytoplasm whereas the phosphorylated form is localised in dendritic spines (Mauceri *et al.*, 2004). Mutating this residue resulted in the SAP97 associated protein, GluR1 re-localising from synapses to the cell soma (Mauceri *et al.*, 2004). Recently phosphorylation was shown to be the driving force for the translocation of NR2A/SAP97 complexes from the ER (Mauceri *et al.*, 2007). The phosphorylation of S232 of SAP97 by CaMKII was shown to disrupt the interaction between SAP97 and NR2A subunits thereby facilitating the localisation of NR2A containing NMDA receptors to the postsynaptic membrane (Gardoni *et al.*, 2003;

Mauceri *et al.*, 2007). The interaction of SAP97 with GluR1 subunits remained unaffected by S232 phosphorylation (Gardoni *et al.*, 2003). Similarly phosphorylation of PSD-95 on S73 by CaMKII resulted in the disruption of the association between PSD-95 and NR2A subunits but not between PSD-95 and NR2B subunits (Gardoni *et al.*, 2006). Thus phosphorylation of both the PSD-95 MAGUK or the respective binding partners regulates receptor-scaffold protein-protein interactions at synapses.

Each NR2 subunit has the PKA consensus sequence, (R/K) (R/K) X(X) (S/T), at their C-terminus, Figure 4.1.

NR2A 1451 - RRVYKKMP**S**I*ESDV*
NR2B 1469 - GHVYEKL**SS**I*ESDV*
NR2C 1226 - SCTWRRI**SS**L*ESEV*
NR2D 1309 - RRG**S**AHFSSL*ESEV*

Figure 4.1 The predicted protein kinase A (PKA) sites present at the distal NR2 subunit C-termini
The ten distal C-terminus amino acids of each NR2 subunit are shown. The PSD-95 ES(D/E)V motifs are shown in italics. The predicted PKA phosphorylation sites are shown in bold.

Indeed, Trinidad *et al.* (2006) showed by mass spectrometry that NR2A S1459 and NR2B S1476 and S1477 are phosphorylated *in vivo*. These serine residues are adjacent to the PSD-95 ESDV binding motif, suggesting a possible regulation by phosphorylation of the interaction between PSD-95 and NR2A or NR2B subunits. As discussed above, phosphorylation of the C-termini of interacting proteins influences their association with the PSD-95 MAGUK family of proteins. Therefore the possibility that the NR2A subunit putative PKA phosphorylation site plays a role in the association between NR2A subunits and PSD-95 was investigated. The approach taken was to generate a kinase dead mutant, i.e. $NR2A^{S1459A}$ and to characterise its association with PSD-95 by immunoprecipitation and cell surface trafficking experiments.

4.2 RESULTS

4.2.1 Generation of NR2A^{S1459A} mutant

To investigate the possible function of the putative PKA phosphorylation site, serine 1459 of the NR2A subunit was mutated into an alanine residue by *in vitro* site-directed mutagenesis generating NR2A^{S1459A} subunits, Section 2.2.1.2.10. Nucleotide sequencing of the NR2A^{S1459A} clone confirmed the correct mutation was generated with no additional mutations on the NR2A clone.

4.2.2 Characterisation of NR1-1a/NR2A^{S1459A} NMDA receptors by quantitative immunoblotting and cytotoxicity assays

Future studies required similar expression levels of NR2A^{S1459A} subunits and wild-type NR2A subunits to allow for comparisons between NR1-1a/NR2A and NR1-1a/NR2A^{S1459A} NMDA receptors. To investigate the expression level of NR2A^{S1459A} subunits, HEK 293 cells were transfected with NR1-1a/NR2A and NR1-1a/NR2A^{S1459A} NMDA receptor clones, cell homogenates were prepared and the resulting cell homogenates analysed by quantitative immunoblotting using anti-NR1 C2 or anti-NR2A (1381-1394) antibodies, Section 2.2.2.11. Representative immunoblots are shown in Figure 4.2.

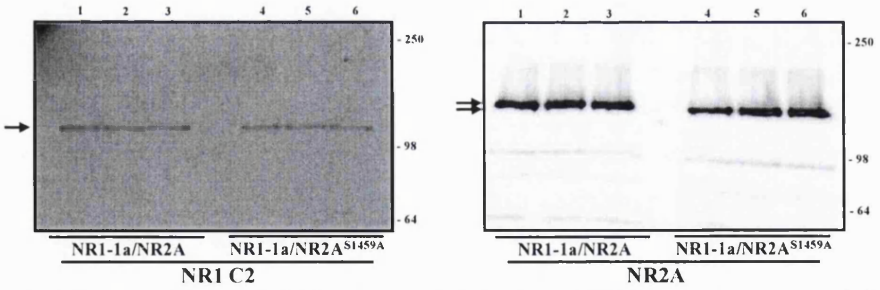

Figure 4.2 Immunoblotting demonstrating the expression of NR1-1a/NR2A and NR1-1a/NR2A^{S1459A} NMDA receptor subunits following their co-expression in HEK 293 cells

HEK 293 cells were transfected with NR1-1a/NR2A and NR1-1a/NR2A^{S1459A} NMDA receptor clones. Cell homogenates were prepared 24 h post-transfection and analysed by quantitative immunoblotting using anti-NR1 C2 or anti-NR2A (1381-1394) antibodies, as indicated. Lanes 1-3 = triplicate samples NR1-1a/NR2A and lanes 4-6 = triplicate samples NR1-1a/NR2A^{S1459A}. Arrows denote either NR1-1a subunits or NR2A subunits. The positions of the protein molecular weight markers (kDa) are shown on the right. The immunoblots are representative from n = 3 transfections.

A histogram summarising the fold change in expression level of NR1-1a and NR2A^{S1459A} subunits is shown in Figure 4.3. Results are expressed as a ratio of the immunoreactivity of NR1-1a/NR2A^{S1459A} receptors /immunoreactivity of NR1-1a/NR2A receptors. There was no significant change in the expression levels of NR1-1a and NR2A^{S1459A} subunits when compared to NR1-1a and NR2A subunits. Interestingly, a significant decrease in the molecular weight of NR2A^{S1459A} subunits was observed when compared to wild-type NR2A subunits, i.e. NR2A M_r = 172 ± 3 kDa (n = 15); NR2A^{S1459A} M_r = 167 ± 4 kDa ($p < 0.0005$, n = 15).

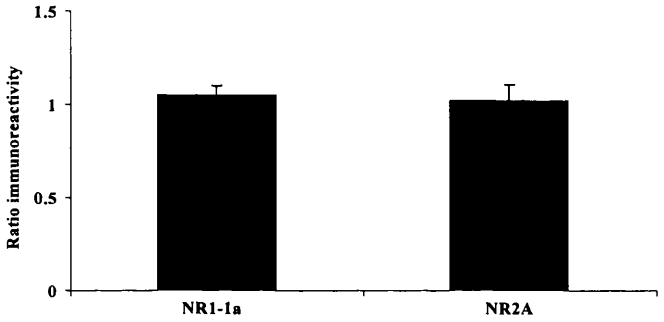

Figure 4.3 Histogram summarising quantitative immunoblotting of NR1-1a/NR2A and NR1-1a/NR2A^{S1459A} NMDA receptor subunits following their co-expression in HEK 293 cells

HEK 293 cells were transfected with NR1-1a/NR2A and NR1-1a/NR2A^{S1459A} NMDA receptor clones. Cell homogenates were prepared 24 h post-transfection and analysed by quantitative immunoblotting using anti-NR1 C2 or anti-NR2A (1381-1394) antibodies. Results are expressed as the fold change, i. e. immunoreactivity of NR1-1a/NR2A receptors/ immunoreactivity of NR1-1a/NR2A^{S1459A} receptors. The histogram is a summary of the mean fold change ± SEM for each combination. The results expressed in the histogram are the mean fold enhancement from n = 3 independent transfections.

As mentioned previously, the co-expression of NR1 and NR2 subunits in a heterologous cell line in the absence of an NMDA receptor antagonist results in cytotoxicity. This provided a useful measure to assess if functional NMDA receptors are formed (Cik *et al.*, 1993). Therefore to investigate if the co-expression of NR1-1a and NR2A^{S1459A} subunits resulted in the formation of functional NMDA receptors, HEK 293 cells were transfected in parallel with NR1-1a/NR2A and NR1-1a/NR2A^{S1459A} NMDA receptor clones and cytotoxicity assays were carried out, Section 2.2.2.7. A histogram summarising the cytotoxicity results from co-expression of NR1-1a/NR2A and NR1-1a/NR2A^{S1459A} NMDA receptors are shown in Figure 4.4.

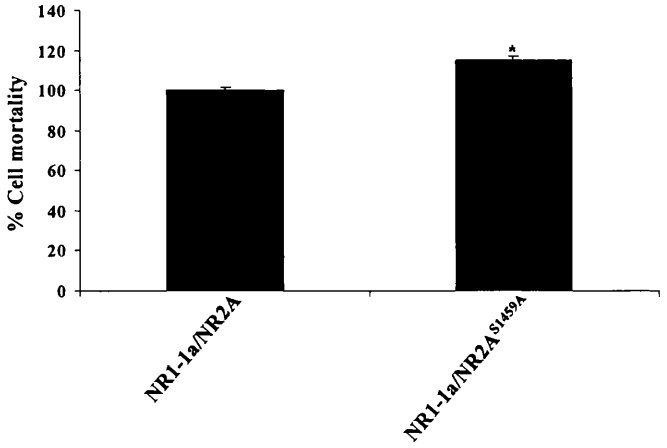

Figure 4.4 Histogram summarising the cytotoxicity resulting from the co-expression of NR1-1a/NR2A and NR1-1a/NR2A^{S1459A} NMDA receptors in HEK 293 cells

HEK 293 cells were transfected with NR1-1a/NR2A and NR1-1a/NR2A^{S1459A} NMDA receptor clones. Cytotoxicity was determined as in Section 2.2.2.7. . Results were normalised to the wild-type NR1-1a/NR2A NMDA receptor. The histogram summarises the mean cytotoxicity from n = 3 independent transfections (* $p < 0.0005$).

The cytotoxicity results were normalised to the cytotoxicity obtained for NR1-1a/NR2A NMDA receptors. There was a significant increase in the cytotoxicity observed for NR1-1a/NR2A^{S1459A} NMDA receptors when compared to NR1-1a/NR2A NMDA receptors ($p < 0.0005$, $n = 3$). Therefore, the co-expression of NR1-1a/NR2A^{S1459A} NMDA receptors in HEK 293 cells results in the formation of functional receptors. The increase cell cytotoxicity suggests that the phosphorylation of S1459 may affect the NMDA receptor channel properties. However, the cytotoxicity assays are not as sensitive compared to electrophysiological methods.

4.2.3 Demonstration of the association of NR1-1a and NR2A^{S1459A} subunits by co-immunoprecipitation following their co-expression in HEK 293 cells

To demonstrate the association of NR1-1a subunits with NR2A^{S1459A} subunits, immunoprecipitation assays were performed. HEK 293 cells were transfected with NR1-1a/NR2A and NR1-1a/NR2A^{S1459A} NMDA receptor clones, cell homogenates were prepared, detergent-solubilised and the detergent-soluble fractions used for immunoprecipitation assays. Immunoprecipitations were carried out using either anti-NR1 C2 or non-immune antibodies, Section 2.2.2.12. The resulting immune and non-immune pellets were analysed by immunoblotting using anti-NR1 C2 or anti-NR2A

(1381-1394) antibodies, as appropriate. Representative immunoblots are shown in Figure 4.5.

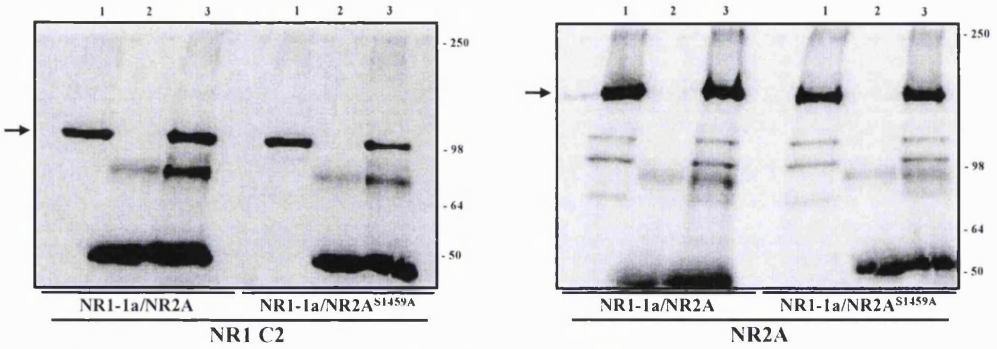

Figure 4.5 Demonstration by immunoprecipitation the association of NR1-1a subunits with NR2A^{S1459A} subunits following their co-expression in HEK 293 cells

HEK 293 cells were transfected with NR1-1a/NR2A and NR1-1a/NR2A^{S1459A} NMDA receptor clones. Cell homogenates were prepared 24 h post-transfection, detergent-solubilised and immunoprecipitations were carried out using anti-NR1 C2 or non-immune antibodies. The resulting immune and non-immune pellets were analysed by immunoblotting using anti-NR1 C2 or anti-NR2A (1381-1394) antibodies, as indicated. The gel layout is the same for each immunoblot, lane 1 = detergent-soluble fraction, lane 2 = non-immune pellet and lane 3 = immune pellet. Arrows denote NR1-1a subunits and NR2A subunits. The positions of the protein molecular weight markers (kDa) are shown on the right. The immunoblots are representative of n = 3 immunoprecipitations from n = 3 independent transfections.

Immunoreactive bands corresponding to the correct molecular weight for the NR1-1a, NR2A or NR2A^{S1459A} subunits were present in the corresponding detergent-soluble fractions demonstrating each subunit was successfully detergent-solubilised. The solubility of NR1-1a/NR2A and NR1-1a/NR2A^{S1459A} NMDA receptors was compared. The immunoreactivity from cell homogenates and detergent-soluble fractions were quantified. The results were then expressed as the percentage detergent-solubilised, i.e. immunoreactivity of detergent-soluble fraction/immunoreactivity of cell homogenate × 100. The NR1-1a/NR2A^{S1459A} NMDA receptor percentage solubility was not significantly different to the wild-type receptor, i.e. NR1-1a/NR2A 53 ± 18 % and NR1-1a/NR2A^{S1459A} 54 ± 21 % (± range, n = 2, $p < 0.1$). The immune pellet contained an immunoreactive band corresponding to NR1-1a subunits, which was absent from the non-immune pellet thus demonstrating the immunoprecipitation was successful. Also present in the immune pellets but absent from the non-immune pellets were NR2A and NR2A^{S1459A} subunits. The ~ 50 kDa immunoreactive bands present in both immune and non-immune pellet lanes are antibody heavy chains used for the immunoprecipitations.

Therefore NR2A and NR2A^{S1459A} subunits were found to co-immunoprecipitate with NR1-1a subunits following their co-expression in HEK 293 cells.

4.2.4 Cell surface expression of NR1-1a/NR2A and NR1-1a/NR2A^{S1459A} NMDA receptor complexes following their co-expression in HEK 293 cells

To investigate if the putative S1459 PKA phosphorylation site played a role in the cell surface expression of NR1-1a/NR2A^{S1459A} NMDA receptors, cell surface ELISA assays were carried out, Section 2.2.2.13. HEK 293 cells were transfected in parallel with NR1-1a/NR2A and NR1-1a/NR2A^{S1459A} NMDA receptor clones and cell surface ELISA assays were carried out using anti-NR2A (44-58) antibodies. A summary of the fold change in cell surface expression is shown in Figure 4.6.

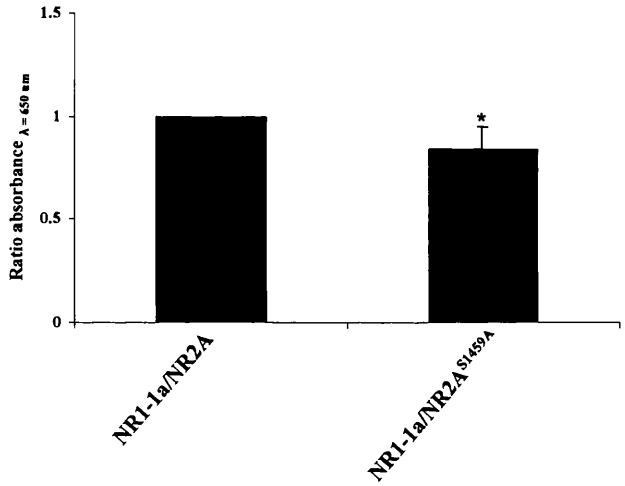

Figure 4.6 Cell surface expression studies of NR1-1a/NR2A and NR1-1a/NR2A^{S1459A} NMDA receptors following their co-expression in HEK 293 cells

HEK 293 cells were transfected with NR1-1a/NR2A and NR1-1a/NR2A^{S1459A} NMDA receptor clones. ELISA assays were performed 24 h post-transfection using anti-NR2A (44-58) antibodies. The results are expressed as a fold change in cell surface expression, i.e. NR2A^{S1459A} cell surface expression/NR2A cell surface expression. The histogram summarises the mean fold change ± SEM for each combination. The results expressed in the histogram are the mean fold enhancement from n = 5 independent transfections (* = $p < 0.025$).

The results are expressed as a fold change in cell surface expression, i.e. NR2A^{S1459A} cell surface expression/NR2A cell surface expression. There was a significant 15 ± 5 % decrease in the cell surface expression of NR1-1a/NR2A^{S1459A} NMDA receptors when compared to wild-type NR1-1a/NR2A NMDA receptors ($p < 0.025$, n = 5).

4.2.5 Cell surface expression of NR1-1a/NR2A and NR1-1a/NR2A^{S1459A} NMDA receptor complexes following their co-expression in HEK 293 cells in the presence of forskolin

The finding that the expression of cell surface NR1-1a/NR2A^{S1459A} NMDA receptors were decreased compared to wild-type receptors implied that phosphorylation on S1459 is required to either maintain cell surface expression or promote the forward trafficking of the receptors. Therefore forskolin, an activator of the enzyme adenylate cyclase, was used to drive the equilibrium to favour phosphorylation state. It was necessary to dissolve forskolin in DMSO, therefore initially cell surface ELISA assays were performed to establish if the presence of 0.1 % (v/v) DMSO effected the trafficking of NR1-1a/NR2A NMDA receptors and the PSD-95α$^{c\text{-}Myc}$ induced enhancement of cell surface expression. HEK 293 cells were transfected with NR1-1a/NR2A NMDA receptor clones in the presence and absence of PSD-95α$^{c\text{-}Myc}$. HEK 293 cells were incubated for 24 h post-transfection in the presence of 0.1 % (v/v) DMSO or 0.1 % (v/v) HBS buffer control and the ELISA assay carried out using anti-NR2A (44-58) antibodies. A summary of the results are shown in Figure 4.7. The results are expressed as the fold change in the presence of 0.1 % (v/v) DMSO, i.e. NR2A cell surface expression + 0.1 % (v/v) DMSO/ NR2A cell surface expression 0.1 % (v/v) HBS buffer control. There was no significant change observed in cell surface expression of either NR1-1a/NR2A NMDA receptors or the PSD-95 induced enhancement of NR1-1a/NR2A NMDA receptor cell surface expression in the presence of 0.1 % (v/v) DMSO. Therefore it was established that 0.1 % (v/v) DMSO can be used in the ELISA assay to dissolve forskolin.

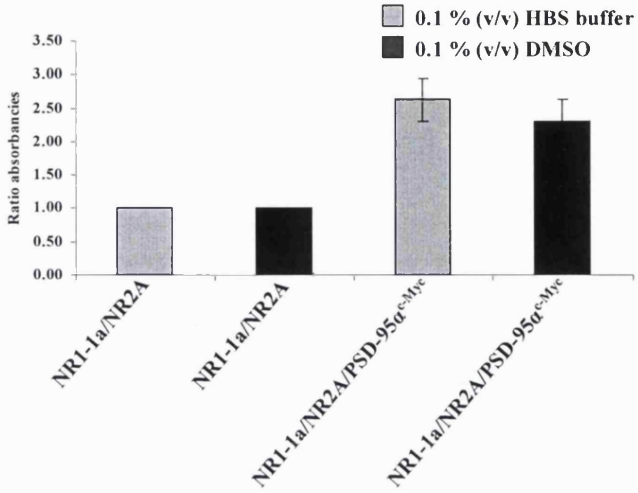

Figure 4.7 Cell surface expression studies of NR1-1a/NR2A NMDA receptors in the presence and absence of PSD-95α$^{c\text{-}Myc}$ when HEK 293 cells are cultured in the presence of 0.1 (v/v) % DMSO

HEK 293 cells were transfected with NR1-1a/NR2A NMDA receptor clones ± PSD-95α$^{c\text{-}Myc}$. Cells were incubated with 0.1 % (v.v) DMSO or 0.1 % (v/v) HBS buffer for 24 h. ELISA assays were performed 24 h post-transfection using anti-NR2A (44-58) antibodies. Results are expressed as the fold enhancement in the presence and absence of 0.1 % (v/v) DMSO, i.e. NR2A cell surface expression 0.1 % (v/v) DMSO/ NR2A cell surface expression 0.1 % (v/v) HBS buffer. The enhancement in the presence of PSD-95 was expressed as NR2A cell surface expression + PSD-95α$^{c\text{-}Myc}$ / NR2A cell surface expression - PSD-95α$^{c\text{-}Myc}$. The histogram summarises the mean fold enhancement ± SEM for each combination. The results expressed in the histogram are the mean fold enhancement from at n = 2 independent transfections.

HEK 293 cells were transfected with NR1-1a/NR2A and NR1-1a/NR2A^{S1459A} NMDA receptors and forskolin, 20 μM, or 0.1 % (v/v) DMSO solvent control were incubated 30 min prior to carrying out the cell surface ELISA assays using anti-NR2A (44-58) antibodies. A histogram summarising the mean cell surface expression is shown in Figure 4.8. The results are expressed as a fold change in the presence of forskolin, i.e. NR2A cell surface expression + forskolin/NR2A cell surface expression – forskolin. As observed previously there was a significant decrease in the cell surface expression of NR1-1a/NR2A^{S1459A} NMDA receptors. However, the resulting decrease in the cell surface expression of NR1-1a/NR2A^{S1459A} NMDA receptors in the presence of solvent control, DMSO was greater when compared to in the absence of DMSO, i.e. 33 ± 2 % ($p < 0.0005$, $n = 5$) in the presence of DMSO compared to 15 ± 5 % ($p < 0.025$, $n = 5$, Section 4.2.5.) in the absence of DMSO. However no further significant decrease in the

cell surface expression of NR1-1a/NR2A^{S1459A} NMDA receptors in the presence of forskolin was found. In contrast, forskolin resulted in a significant decrease in cell surface expression of NR1-1a/NR2A NMDA receptors, ~ 23 ± 8 % ($p < 0.025$, $n = 5$).

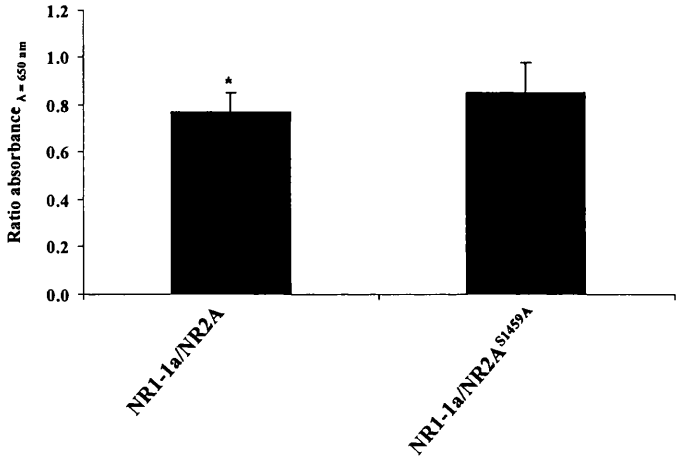

Figure 4.8 Cell surface expression of NR1-1a/NR2A or NR1-1a/NR2A^{S1459A} NMDA receptors in the presence of forskolin

HEK 293 cells were transfected with NR1-1a/NR2A and NR1-1a/NR2A^{S1459A} NMDA receptor clones. Cells were incubated with 20 μM forskolin or 0.1 % (v/v) DMSO for 20 min prior to start of ELISA assay. ELISA assays were performed 24 h post-transfection using anti-NR2A (44-58) antibodies. The results are expressed as the fold change in the presence of forskolin, i.e. NR2A cell surface expression + forskolin/NR2A cell surface expression – forskolin. The histogram summarises the mean fold enhancement ± SEM for each combination. The results expressed in the histogram are the mean fold enhancement from $n = 5$ independent transfections (* $p < 0.025$).

4.2.6 Demonstration of the co-immunoprecipitation of NR1-1a/NR2A and NR1-1a/NR2A^{S1459A} NMDA receptor complexes with PSD-95α$^{c\text{-}Myc}$ following their co-expression in HEK 293 cells

To investigate the association between NR1-1a/NR2A^{S1459A} NMDA receptors with PSD-95α$^{c\text{-}Myc}$ immunoprecipitation assays were carried out. HEK 293 cells were transfected with NR1-1a/NR2A and NR1-1a/NR2A^{S1459A} NMDA receptor clones in the presence and absence of PSD-95α$^{c\text{-}Myc}$, cell homogenates were prepared, detergent-solubilised and the detergent-soluble fraction was used for immunoprecipitation assays. Immunoprecipitations were carried out using anti-NR1 C2 or non-immune antibodies, Section 2.2.2.12. The resulting immune and non-immune pellets were analysed by immunoblotting using anti-NR2A (1381-1394) or anti-c-Myc antibodies, as appropriate Representative immunoblots are shown in Figure 4.9.

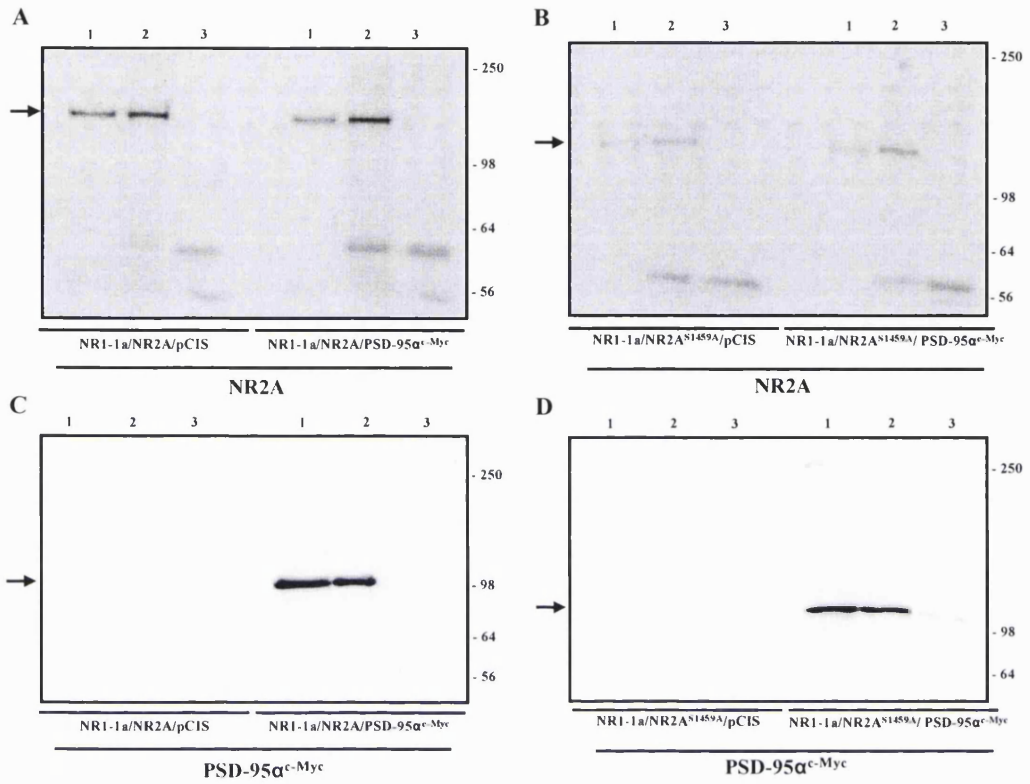

Figure 4.9 Association of NR1-1a/NR2A and NR1-1a/NR2A^{S1459A} NMDA receptors with PSD-95α$^{c\text{-}Myc}$ demonstrated by co-immunoprecipitation assays following their co-expression in HEK 293 cells

HEK 293 cells were transfected with NR1-1a/NR2A and NR1-1a/NR2A^{S1459A} NMDA receptor clones ± PSD-95α$^{c\text{-}Myc}$. Cell homogenates were prepared 24 h post-transfection, detergent-solubilised and immunoprecipitations were carried out using anti-NR1 C2 or non-immune antibodies. The resulting immune and non-immune pellets were analysed by immunoblotting using anti-NR2A (1381-1394) or anti-c-Myc antibodies, as indicated. The gel layout is the same for each immunoblot, lane 1 = detergent-soluble fraction, lane 2 = immune pellet and lane 3 = non-immune pellet. **A.C**. NR1-1a/NR2A receptors. **B.D**. NR1-1a/NR2A^{S1459A} NMDA receptors. Arrows denote NR2A subunits and PSD-95α$^{c\text{-}Myc}$. The positions of the protein molecular weight markers (kDa) are shown on the right. The immunoblots are representative of n = 3 immunoprecipitations from n = 3 independent transfections.

The detergent-soluble fractions contained immunoreactive bands corresponding to the molecular weights of NR2A and NR2A^{S1459A} subunits and PSD-95α$^{c\text{-}Myc}$. The immune pellets contained a specific immunoreactive band for NR2A and NR2A^{S1459A} subunits or PSD-95α$^{c\text{-}Myc}$ which were all absent in the respective non-immune pellets. The ~ 50 kDa immunoreactive bands present in both the immune and non-immune pellet lanes are antibody heavy chains used for the immunoprecipitations. It can be concluded from these results that NR1-1a/NR2A and NR1-1a/NR2A^{S1459A} NMDA receptor complexes were

found to co-immunoprecipitate with PSD-95α$^{c\text{-}Myc}$ following their co-expression in HEK 293 cells

4.2.7 The association of NR1-1a/NR2A and NR1-1a/NR2A^{S1459A} NMDA receptors with PSD-95α$^{c\text{-}Myc}$ in the presence of forskolin demonstrated by co-immunoprecipitation assays following their co-expression in HEK 293 cells

To investigate if phosphorylation of S1459 on NR2A subunits affects its association with PSD-95α$^{c\text{-}Myc}$, forskolin was incubated with the transfected cells prior to the start of each immunoprecipitation. HEK 293 cells were transfected with NR1-1a/NR2A or NR1-1a/NR2A^{S1459A} NMDA receptor clones in the presence of PSD-95α$^{c\text{-}Myc}$. The transfected HEK 293 cells were incubated with 20 μM forskolin or 0.1 % (v/v) DMSO solvent control for 30 min prior to harvesting the cells. All subsequent steps were performed in the presence of phosphatase inhibitors. Cell homogenates were prepared, detergent-solubilised and the detergent-soluble fraction used for immunoprecipitation assays using anti-NR1 C2 or non-immune antibodies, Section 2.2.2.12. The resulting immune and non-immune pellets were analysed by immunoblotting using anti-NR2A (1381-1394) or anti-c-Myc, as appropriate. Representative immunoblots are shown in Figure 4.10. Immunoreactive bands corresponding to NR2A and NR2A^{S1459A} subunits or PSD-95α$^{c\text{-}Myc}$ were present in the detergent-soluble fraction. NR2A, NR2A^{S1459A} subunits and PSD-95α$^{c\text{-}Myc}$ were also present in the respective immune pellets but absent from the respective non-immune pellets. Thus in the presence of forskolin NR1-1a/NR2A and NR1-1a/NR2A^{S1459A} NMDA receptor complexes were found to co-immunoprecipitate with PSD-95α$^{c\text{-}Myc}$ following their co-expression in HEK 293 cells.

The detergent-soluble and immune pellet immunoreactive bands were quantified and the immune pellet pixel units were corrected according to the corresponding detergent-soluble fraction pixel units. As determined in Section 4.2.4, there was no significant difference in the observed solubility between NR1-1a/NR2A and NR1-1a/NR2A^{S1459A} NMDA receptors. The results were expressed as a ratio of the expression of PSD-95 immunoreactivity + forskolin/ immunoreactivity - forskolin. The resulting fold changes were; 0.72 ± 0.08 for NR1-1a/NR2A and 0.87 ± 0.06 for NR1-1a/NR2A^{S1459A} NMDA

receptors (± range, n = 2). Therefore phosphorylation at S1459 on the NR2A subunit was shown to result in a greater decrease in NR2A/PSD-95 association, i.e. a 28 ± 8 % decrease in the association between NR2A/PSD-95 compared to 13 ± 6 % decrease in the association between NR2A^{S1459A}/PSD-95.

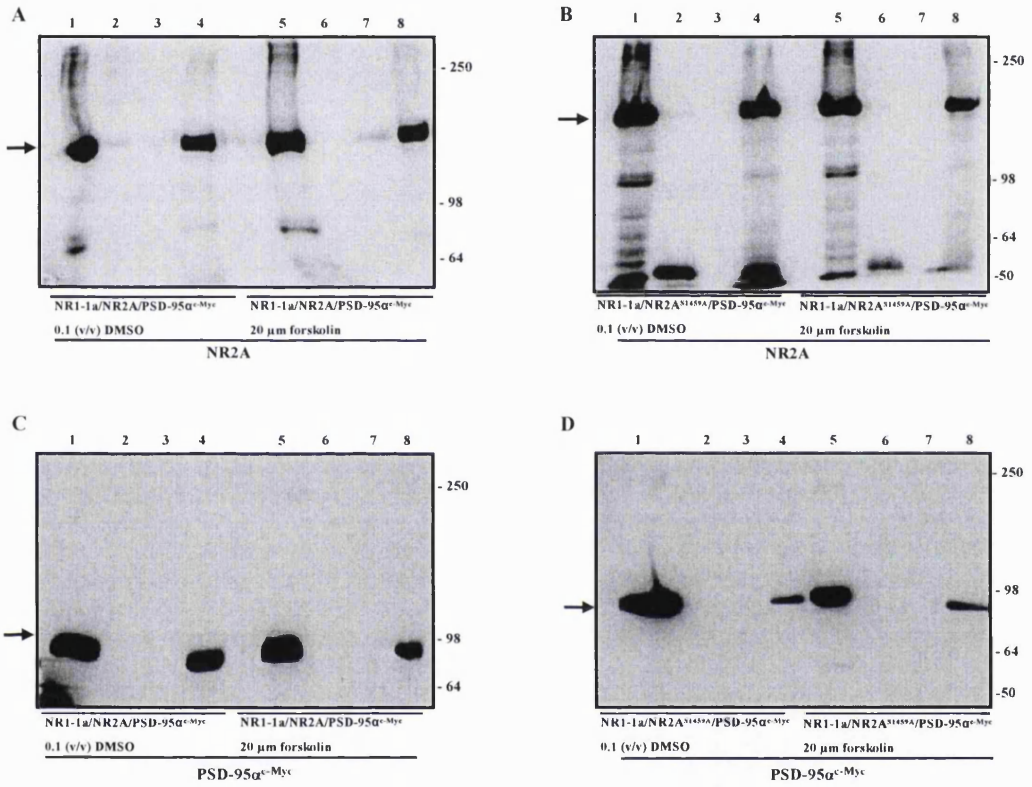

Figure 4.10 Demonstration by immunoprecipitation that NR1-1a/NR2A and NR1-1a/NR2A^{S1459A} NMDA receptors associate with PSD-95α$^{c\text{-}Myc}$ in the presence of forskolin following their co-expression in HEK 293 cells

HEK 293 cells were transfected with NR1-1a/NR2A and NR1-1a/NR2A^{S1459A} NMDA receptor clones + PSD-95α$^{c\text{-}Myc}$. Cells were incubated with 20 μM forskolin or 0.1 % (v/v) DMSO for 20 min prior to harvesting. Cell homogenates were prepared 24 h post-transfection, detergent-solubilised and immunoprecipitations were conducted using anti-NR1 C2 or non-immune antibodies. The resulting immune and non-immune pellets were analysed by immunoblotting using anti-NR2A (1381-1394) or anti-c-Myc antibodies, as indicated. **A. C**. NR1-1a/NR2A/PSD-95α$^{c\text{-}Myc}$ **B. D**. NR1-1a/NR2A^{S1459A}/PSD-95α$^{c\text{-}Myc}$. The gel layout is the same for each immunoblot. Lanes 1, 5 = detergent-soluble fraction; lanes 2, 6 = non-immune pellet; lanes 3, 7 = empty and lanes 4, 8 = immune pellet. Arrows denote NR2A subunits and PSD-95α$^{c\text{-}Myc}$. The positions of the protein molecular weight markers (kDa) are shown on the right. The immunoblots are representative of n = 2 immunoprecipitations from n = 2 independent transfections.

4.2.8 Co-Expression of PSD-95α$^{c\text{-}Myc}$ with NR1-1a/NR2A and NR1-1a/NR2A^{S1459A} NMDA receptors results in a selective enhancement of NR2A subunit expression following their co-expression in HEK 293 cells

The co-expression NR1-1a/NR2A NMDA receptors with PSD-95α$^{c\text{-}Myc}$ resulted in a selective enhancement of NR2A subunit expression whilst the expression of NR1-1a subunits remained unchanged (Rutter and Stephenson, 2000; Section 3.2.3). To investigate if the co-expression of PSD-95 with NR1-1a/NR2A^{S1459A} NMDA receptor subunits also resulted in a selective enhancement of NR2A^{S1459} subunit expression, HEK 293 cells were transfected with NR1-1a/NR2A and NR1-1a/NR2A^{S1459A} NMDA receptor clones in the presence and absence of PSD-95α$^{c\text{-}Myc}$, cell homogenates were prepared and quantitative immunoblotting was performed using anti-NR1 C2 or anti-NR2A (1381-1394) antibodies, as appropriate., Section 2.2.2.11. Representative immunoblots are shown in Figure 4.11. A histogram summarising the results from the co-expression with PSD-95α$^{c\text{-}Myc}$ and NR1-1a/NR2A or NR1-1a/NR2A^{S1459A} NMDA receptors is shown in Figure 4.12. The results were expressed as a ratio enhancement, i.e. immunoreactivity + PSD-95α$^{c\text{-}Myc}$ /immunoreactivity - PSD-95α$^{c\text{-}Myc}$. There was no significant change observed for the NR1-1a subunit expression for both NR1-1a/NR2A and NR1-1a/NR2A^{S1459A} NMDA receptor combinations. As previously observed there was a significant enhancement of NR2A subunit expression, 1.8 ± 0.1 ($p < 0.025$, $n = 3$). Similarly there was a significant enhancement of NR2A^{S1459A} subunit expression, 1.9 ± 0.1 ($p < 0.01$, $n = 3$). However, there was no statistically significant difference when comparing the PSD-95 induced enhancement of NR2A and NR2A^{S1459A} subunit expression ($p < 0.1$).

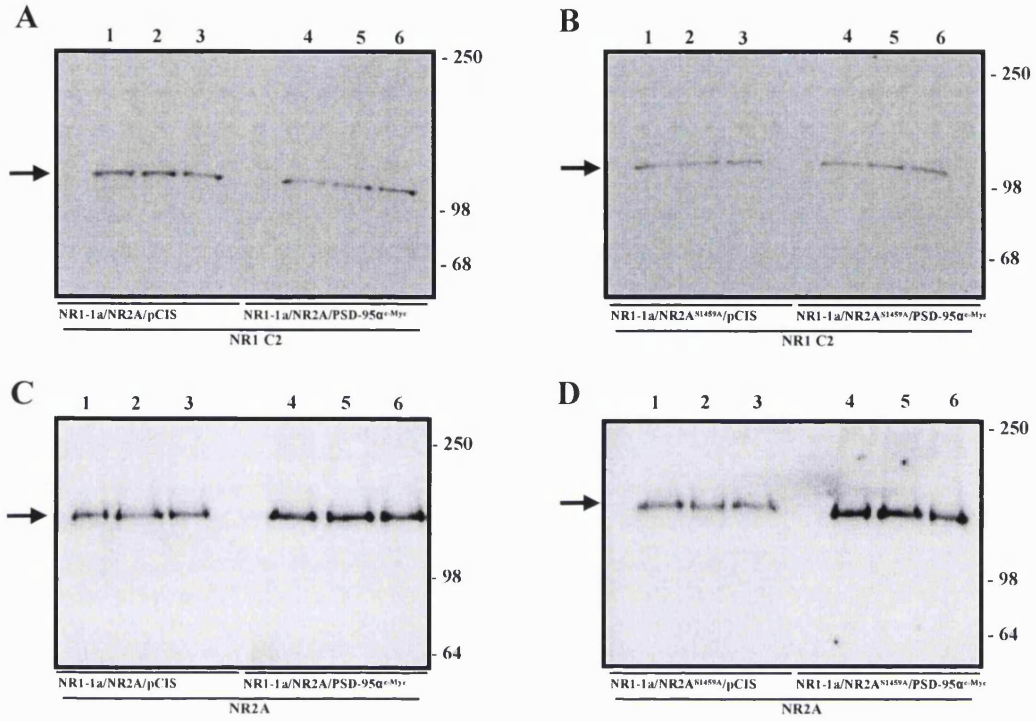

Figure 4.11 Immunoblots demonstrating the effect of PSD-95α$^{c\text{-}Myc}$ on expression levels of NR1-1a/NR2A or NR1-1a/NR2A^{S1459A} NMDA receptor subunits following their co-expression in HEK 293 cells

HEK 293 cells were transfected with NR1-1a/NR2A and NR1-1a/NR2A^{S1459A} NMDA receptor clones ± PSD-95α$^{c\text{-}Myc}$. Cell homogenates were prepared 24 h post-transfection and analysed by quantitative immunoblotting using anti-NR1 C2 or anti-NR2A (1381-1394) antibodies, as indicated. Lanes 1-3 = triplicate samples - PSD-95α$^{c\text{-}Myc}$ and lanes 4-6 = triplicate samples + PSD-95α$^{c\text{-}Myc}$. **A C**. NR1-1a/NR2A NMDA receptors. **B**. **D**. NR1-1a/NR2A^{S1459A} NMDA receptors. Arrows denote either NR1-1a subunits or NR2A subunits. The positions of the protein molecular weight markers (kDa) are shown on the right. The immunoblots are representative from n = 3 transfections.

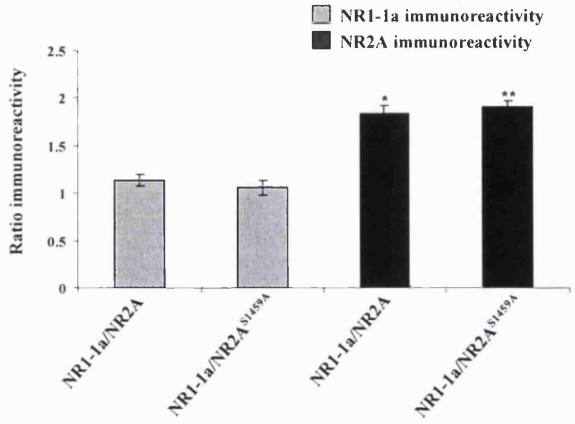

Figure 4.12 Histogram summarising the effect of PSD-95α$^{c\text{-}Myc}$ on expression levels of NR1-1a/NR2A or NR1-1a/NR2A^{S1459A} NMDA receptor subunits following their co-expression in HEK 293 cells

HEK 293 cells were transfected with NR1-1a/NR2A and NR1-1a/NR2A^{S1459A} NMDA receptor clones ± PSD-95α$^{c\text{-}Myc}$ Cell homogenates were prepared 24 h post-transfection and analysed by quantitative immunoblotting using anti-NR1 C2 or anti-NR2A (1381-1394) antibodies. Results are expressed as the fold change, i. e. immunoreactivity + PSD-95α$^{c\text{-}Myc}$/ immunoreactivity - PSD-95α$^{c\text{-}Myc}$. The histogram is a summary of the mean fold change ± SEM for each combination. The results expressed in the histogram are the mean fold enhancement from n = 3 independent transfections (* = $p < 0.025$; ** = $p < 0.01$)..

4.2.9 Cell surface expression studies of NR1-1a/NR2A and NR1-1a/NR2A^{S1459A} NMDA receptors in the presence and absence of PSD-95α$^{c\text{-}Myc}$ following their co-expression in HEK 293 cells

PSD-95α$^{c\text{-}Myc}$ resulted in a selective enhancement of NR2A^{S1459A} subunit expression which was comparable to the PSD-95-induced enhancement observed for wild-type NR2A subunits, Section 4.2.8. The total enhancement of NR2A subunit expression was found to be translated into an increase in the NR1/NR2A NMDA receptor cell surface expression in the presence of PSD-95α (Lin *et al.*, 2004; Section 3.2.5). Therefore to investigate whether the cell surface expression of NR1-1a/NR2A^{S1459A} NMDA receptors is enhanced in the presence of PSD-95α$^{c\text{-}Myc}$, cell surface ELISA assays were carried out, Section 2.2.2.13. HEK 293 cells were transfected with NR1-1a/NR2A and NR1-1a/NR2A^{S1459A} NMDA receptor clones in parallel in the presence and absence of PSD-95α$^{c\text{-}Myc}$ and ELISA assays performed using anti-NR2A (44-58) antibodies. A summary of the fold change in cell surface expression is shown in Figure 4.13. The results are expressed as the fold enhancement, i.e. NR2A cell surface expression + PSD-95/NR2A

cell surface expression – PSD-95. The co-expression of PSD-95$\alpha^{c\text{-}Myc}$ resulted in a significant enhancement of cell surface expression for both NR1-1a/NR2A ($p < 0.005$, $n = 5$) and NR1-1a/NR2A^{S1459A} ($p < 0.005$, $n = 5$) NMDA receptors. However, the resulting PSD-95$\alpha^{c\text{-}Myc}$ induced enhancement of cell surface expression for NR1-1a/NR2A^{S1459A} NMDA receptors was significantly greater than that observed for wild-type NR1-1a/NR2A NMDA receptors, i.e. an additional 90 ± 38 % further increase in NR1-1a/NR2A^{S1459A} NMDA receptors cell surface expression ($p < 0.05$, $n = 5$).

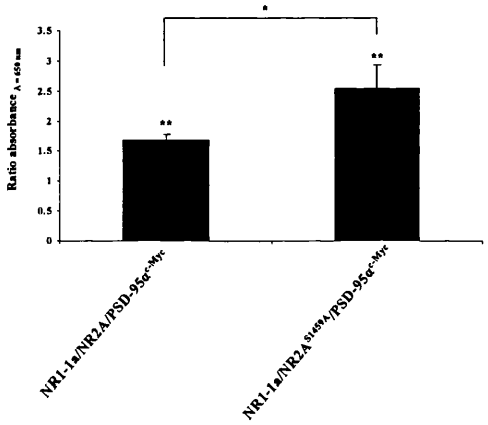

Figure 4.13 Cell surface expression studies of NR1-1a/NR2A and NR1-1a/NR2A^{S1459A} NMDA receptors in the presence of PSD-95$\alpha^{c\text{-}Myc}$ following their co-expression in HEK 293 cells

HEK 293 cells were transfected with NR1-1a/NR2A and NR1-1a/NR2A^{S1459A} NMDA receptor clones ± PSD-95$\alpha^{c\text{-}Myc}$. ELISA assays were performed 24 h post-transfection using anti-NR2A (44-58) antibodies. Results are expressed as the fold enhancement, i. e. NR2A cell surface expression + PSD-95/ NR2A cell surface expression - PSD-95. The histogram summarises the mean fold enhancement ± SEM for each combination. The results expressed in the histogram are the mean fold enhancement from $n = 5$ independent transfections (* = $p < 0.05$, ** = $p < 0.005$).

4.2.10 Cell surface expression of NR1-1a/NR2A and NR1-1a/NR2A^{S1459A} NMDA receptors in the presence and absence of PSD-95$\alpha^{c\text{-}Myc}$ in the presence of forskolin following their co-expression in HEK 293 cells

Immunoprecipitation assays in the presence of forskolin demonstrated a 15 % greater decrease in the association between PSD-95$\alpha^{c\text{-}Myc}$ and NR1-1a/NR2A NMDA receptors in comparison to NR1-1a/NR2A^{S1459A} NMDA receptors. Thus to investigate if this is translated into a change in cell surface expression of NR1-1a/NR2A and NR1-1a/NR2A^{S1459A} NMDA receptors when the equilibrium is shifted to favour the

phosphorylated state, cell surface ELISA assays were carried out in the presence of forskolin, Section 2.2.2.13. HEK 293 cells were transfected with NR1-1a/NR2A or NR1-1a/NR2A^{S1459A} NMDA receptor clones in the presence and absence of PSD-95α$^{c\text{-}Myc}$. Forskolin, 20 μM or 0.1 % (v/v) DMSO were incubated 30 min prior to the measure of cell surface NMDA receptor expression by ELISA assays using anti-NR2A (44-58) antibodies. A histogram summarising the results is shown in Figure 4.14. The results are expressed as a fold enhancement for NR2A cell surface expression + PSD-95 + forskolin/NR2A cell surface expression + PSD-95 - forskolin.

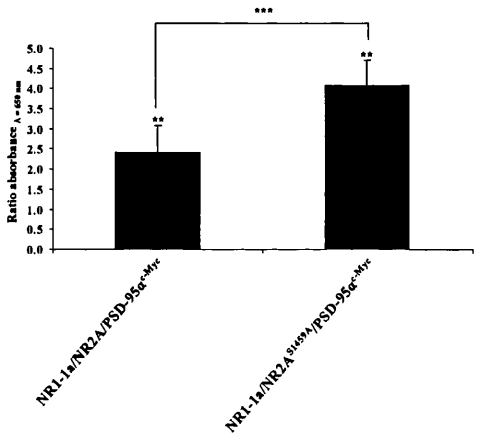

Figure 4.14 Cell surface expression of NR1-1a/NR2A or NR1-1a/NR2A^{S1459A} NMDA receptors in the presence and absence of PSD-95α$^{c\text{-}Myc}$ in the presence of forskolin

HEK 293 cells were transfected with NR1-1a/NR2A and NR1-1a/NR2A^{S1459A} NMDA receptor clones ± PSD-95α$^{c\text{-}Myc}$. Cells were incubated with 20 μM forskolin or 0.1 % (v/v) DMSO for 20 min prior to start of ELISA assay. ELISA assays were performed 24 h post-transfection using anti-NR2A (44-58) antibodies. Results are expressed as the fold change, i. e. NR2A cell surface expression + PSD-95 + forskolin/ NR2A cell surface expression + PSD-95 - forskolin. The histogram summarises the mean fold enhancement ± SEM for each combination. The results expressed in the histogram are the mean fold enhancement from n = 5 independent transfections (** = $p < 0.05$, *** = $p < 0.005$).

There was a significant enhancement in the cell surface expression of NR1-1a/NR2A ($p < 0.05$) and NR1-1a/NR2A^{S1459A} ($p < 0.05$) NMDA receptors in the presence of PSD-95α$^{c\text{-}Myc}$ when incubated with forskolin. As previously observed, there was a significant further increase in the cell surface expression of NR1-1a/NR2A^{S1459A} NMDA receptor expression when compared to NR1-1a/NR2A NMDA receptors. However, the difference in the enhancement between NR1-1a/NR2A and NR1-1a/NR2A^{S1459A} NMDA receptors observed was greater to that found in Section 4.2.9, i.e. 160 ± 30 % ($p < 0.005$) increase

in the presence of forskolin and 90 ± 38 % ($p < 0.05$) increase with no solvent control. There was no significant change in the PSD-95$\alpha^{c\text{-}Myc}$ induced enhancement of cell surface expression of both NR1-1a/NR2A and NR1-1a/NR2A^{S1459A} NMDA receptors in the presence of forskolin ($p < 0.1$).

4.2.11 Differential co-immunoprecipitation of NR1-1a/NR2A and NR1-1a/NR2A^{S1459A} NMDA receptors with Rab 5 and calnexin following their co-expression in HEK 293 cells

Quantitative immunoblotting showed that NR2A and NR2A^{S1459A} subunits are expressed at similar levels, Section 4.2.2. However cell surface studies showed a significant ~ 15 % decrease in expression of NR1-1a/NR2A^{S1459A} NMDA receptors compared to NR1-1a/NR2A wild-type receptors. A similar selective enhancement of total NR2A and NR2A^{S1459A} subunit expression was observed in the presence of PSD-95. When co-expressed with PSD-95$\alpha^{c\text{-}Myc}$ there was a further enhancement of ~ 90 % for the cell surface expression of NR1-1a/NR2A^{S1459A} compared with NR1-1a/NR2A NMDA receptors. This suggests that NR1-1a/NR2A^{S1459A} NMDA receptors are either trafficked or stabilised at the cell surface differently to NR1-1a/NR2A NMDA receptors. It was therefore investigated whether NR1-1a/NR2A^{S1459A} NMDA receptors are either retained in the ER or internalised at a greater rate compared to NR1-1a/NR2A NMDA receptors. This was done by determining the association of NR1-1a/NR2A^{S1459A} and NR1-1a/NR2A NMDA receptors with Rab 5, an early endosomal marker, and calnexin, an ER marker. HEK 293 cells were transfected with NR1-1a/NR2A and NR1-1a/NR2A^{S1459A} NMDA receptor clones in the presence and absence of PSD-95$\alpha^{c\text{-}Myc}$, cell homogenates were prepared, detergent-solubilised and the detergent-soluble fraction was used for quantitative immunoprecipitation assays carried out using anti-NR1 C2 or non-immune antibodies, Section 2.2.2.12. The resulting immune and non-immune pellets were analysed by immunoblotting using anti-NR2A (1381-1394), anti-Rab5 or anti-calnexin antibodies. Representative immunoblots are shown in Figure 4.15.

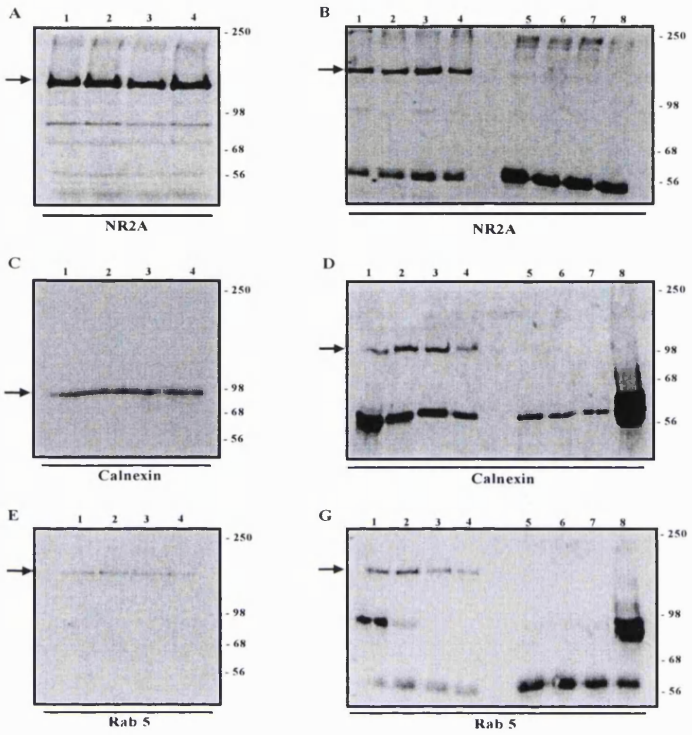

Figure 4.15 Immunoblots to illustrate the differential interaction of NR1-1a/NR2A and NR1-1a/NR2A^{S1459A} NMDA receptors with Rab 5 and calnexin following their co-expression in HEK 293 cells

HEK 293 cells were transfected with NR1-1a/NR2A and NR1-1a/NR2A^{S1459A} NMDA receptor clones ± PSD-95α$^{c\text{-}Myc}$. Cell homogenates were prepared 24 h post-transfection, detergent-solubilised and immunoprecipitations were carried out using anti-NR1 C2 or non-immune antibodies. The resulting immune and non-immune pellets were analysed by immunoblotting using anti-NR2A (1381-1394), anti-Rab5 or anti-calnexin antibodies, as indicated. **A. C. E.** Detergent-soluble fractions. **B.D.G.** Immune and non-immune pellets. The gel layout is the same for each immunoblot, lanes 1 - 4 = immune pellets, lanes 5 – 8 = non immune pellets. Lanes 1,5 = NR1-1a/NR2A/pCIS, lanes 2, 6 = NR1-1a/NR2A^{S1459A}/pCIS, lanes 3, 7 = NR1-1a/NR2A/ PSD-95α$^{c\text{-}Myc}$ and lanes 4, 8 = NR1-1a/NR2A^{S1459A}/ PSD-95α$^{c\text{-}Myc}$. Arrows denote NR2A subunits, Rab 5 or calnexin. The positions of the protein molecular weight markers (kDa) are shown on the right. The immunoblots are representative of n = 4 immunoprecipitations from n = 4 independent transfections.

The detergent-soluble fractions contained immunoreactive bands corresponding to the molecular weight of NR2A and NR2A^{S1459A} subunits, Rab 5 or calnexin (90 kDa and 170 kDa, respectively). Each immune pellet contained a specific band for NR2A and NR2A^{S1459A} subunits, Rab 5 or calnexin which were all absent in the respective non-immune pellets. The ~ 50 kDa immunoreactive bands present in both the immune and non-immune pellet lanes are antibody heavy chains used for the immunoprecipitations. This thus demonstrates that NR1-1a/NR2A and NR1-1a/NR2A^{S1459A} NMDA receptor

complexes co-immunoprecipitate with Rab 5 and calnexin in HEK 293 cells. The immunoreactivity from the cell homogenates and detergent-soluble fractions were quantified. As mentioned previously, it was found that NR1-1a/NR2A and NR1-1a/NR2A^{S1459A} NMDA receptor complexes had a similar level of solubility, thus these did not require adjustment, Section 4.2.4. As it is known that the NR2A and NR2A^{S1459A} subunits are expressed at the same level, the immune pellet pixel values for Rab 5 and calnexin were normalised to the NR2A or NR2A^{S1459A} subunit immune pellets, as appropriate. The results were then expressed as the fold change in the association of either Rab 5 or calnexin, i.e. immunoreactivity of immune pellet of Rab 5 or calnexin associated with NR1-1/NR2A^{S1459A} NMDA receptors / immunoreactivity of immune pellet of Rab 5 or calnexin associated with NR1-1/NR2A NMDA receptors. A histogram summarising the results is shown in Figure 4.16.

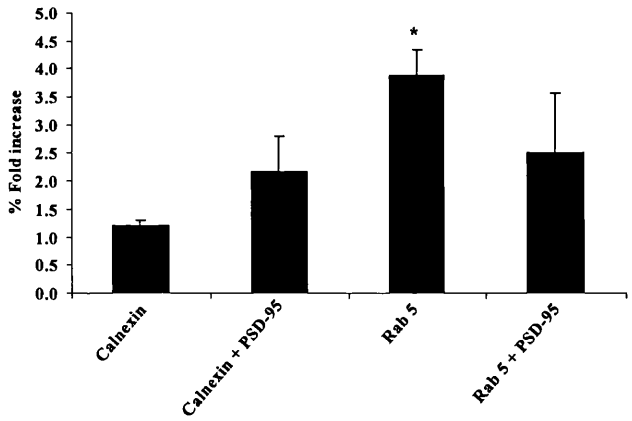

Figure 4.16 Histogram summarising the differential interaction of NR1-1a/NR2A and NR1-1a/NR2A^{S1459A} NMDA receptors with Rab 5 and calnexin following their co-expression in HEK 293 cells

HEK 293 cells were transfected with NR1-1a/NR2A or NR1-1a/NR2A^{S1459A} NMDA receptor clones ± PSD-95$\alpha^{c\text{-}Myc}$. Cell homogenates were prepared 24 h post-transfection, detergent-solubilised and immunoprecipitations were conducted using anti-NR1 C2 or non-immune antibodies. The resulting immune and non-immune pellets were analysed by immunoblotting using anti-NR2A (1381-1394), anti-Rab5 or anti-calnexin antibodies. Results are expressed as the fold change, i. e. immunoreactivity of NR1-1a/NR2A^{S1459A} receptors/ immunoreactivity of NR1-a/NR2A receptors. The histogram is a summary of the mean fold change ± SEM for each combination. The results expressed in the histogram are the mean fold enhancement from n = 4 independent transfection (* = $p < 0.005$).

It can been seen that there was a significant increase in the co-immunoprecipitation of Rab 5 with NR1-1a/NR2A^{S1459A} NMDA receptors in the absence of PSD-95 ($p < 0.005$, n = 4). There was no significant change in the co-immunoprecipitation of Rab 5 in the

presence of PSD-95α$^{c\text{-}Myc}$. Similarly, there was no significant change in the co-immunoprecipitation levels of calnexin with NR1-1a/NR2A^{S1459A} NMDA receptors in the presence or absence of PSD-95α$^{c\text{-}Myc}$.

4.3 DISCUSSION

In this chapter the role of a phosphorylation site, S1459 on NR2A subunits which is found close to the PSD-95 binding motif, was investigated with regards to the association between PSD-95 and NR1-1a/NR2A NMDA receptors. NR1-1a/NR2A^{S1459A} NMDA receptor complexes were found to co-immunoprecipitate with PSD-95$\alpha^{c\text{-}Myc}$. Co-immunoprecipitation assays in the presence of forskolin demonstrated a greater decrease in association between PSD-95 and NR1-1a/NR2A NMDA receptor complexes in comparison to NR1-1a/NR2A^{S1459A} NMDA receptor complexes. This implied that the phosphorylation of S1459 disrupts the association between NR2A subunits and PSD-95. The co-expression of PSD-95$\alpha^{c\text{-}Myc}$ with NR1-1a/NR2A^{S1459A} NMDA receptors resulted in a selective enhancement of the total NR2A^{S1459A} subunit expression. However, there was no significant difference in the resulting enhancement of NR2A subunits when compared to NR2A^{S1459A} subunits when NR1-1a/NR2A or NR1-1a/NR2A^{S1459A} NMDA receptors were co-expressed with PSD-95$\alpha^{c\text{-}Myc}$. As demonstrated by Lin *et al.* (2004) and in Section 3.2.5.1, the co-expression of PSD-95 with NR1/NR2A NMDA receptors resulted in an enhancement in cell surface expression. A significant enhancement was also observed for NR1-1a/NR2A^{S1459A} NMDA receptors in the presence of PSD-95$\alpha^{c\text{-}Myc}$. This enhancement of NR1-1a/NR2A^{S1459A} NMDA receptor cell surface expression was significantly greater when compared to the enhancement observed for wild-type NR1-1a/NR2A NMDA receptors. Therefore the association between PSD-95$\alpha^{c\text{-}Myc}$ and NR1-1a/NR2A NMDA receptors appears to be regulated by phosphorylation of S1459. Lastly, the cell surface studies in the presence of forskolin gave some peculiar results. The PSD-95$\alpha^{c\text{-}Myc}$ induced enhancement of cell surface expression for both NR1-1a/NR2A and NR1-1a/NR2A^{S1459A} NMDA receptors did not significantly change in the presence of forskolin. It was hypothesised that there would be a decrease in resulting PSD-95$\alpha^{c\text{-}Myc}$ induced enhancement of the cell surface expression of NR1-1a/NR2A NMDA receptors, as quantitative immunoprecipitations demonstrated that in the presence of forskolin a decrease was found for this association. Therefore these results do not correlate with those described above. Although the manufacturers guidelines were followed, it may be

that the forskolin was not given adequate time to take effect for cell surface studies. Further experiments could be attempted using different PKA activators or using cell membrane permeable cAMP to directly activate the PKA.

As described previously, the phosphorylation of serine or threonine residues close to the PDZ binding motifs have been shown to disrupt their association with the PSD-95 MAGUK family. For example, the phosphorylation of the serine present in the ESDV motif of NR2B subunits was found to disrupt their association with both PSD-95 and SAP102 (Chung *et al.*, 2004). In this chapter the results demonstrate that a phosphorylation site close to the ESDV motif of NR2A subunits is also able to disrupt this association. S1459 is conserved between the NR2 subunits. In contrast to these results, a phosphomimetic point mutation of S1244E of NR2C subunits, which is homologous to NR2A S1459, did not affect their association with PSD-95 or SAP102 (Chen *et al.*, 2006). This suggests that the NMDA receptor subtypes may be differentially regulated with regards to their association with the PSD-95 MAGUK family.

Interestingly during the characterisation of $NR2A^{S1459A}$ subunits, it was found that NR1-1a/$NR2A^{S1459A}$ NMDA receptors were expressed at the cell surface significantly less well compared to wild-type NR1-1a/NR2A NMDA receptors. The total expression of NR2A and $NR2A^{S1459A}$ subunits was shown to be expressed at similar levels by quantitative immunoblotting. Thus S1459 was thought to influence the cell surface expression of NR1-1a/$NR2A^{S1459A}$ NMDA receptors. The reduction in cell surface expression of NR1-1a/$NR2A^{S1459A}$ NMDA receptors was thought to be due to the receptors being retained in the ER or internalised at a higher rate when compared to wild-type receptors. Quantitative immunoprecipitations revealed an increase in the association between the early endosomal marker, Rab 5, and NR1-1a/$NR2A^{S1459A}$ NMDA receptors. This suggested that NR1-1a/$NR2A^{S1459A}$ NMDA receptors are internalised at a higher rate compared to wild-type receptors and that position S1459 should be phosphorylated for the maintenance of cell surface expression of NR1-1a/NR2A NMDA receptors. This hypothesis was further tested by incubating the cells with forskolin prior to the start of

cell surface NMDA receptor expression measurement. It was thought that in the presence of forskolin there would be either no change or an increase in the cell surface expression of NR1-1a/NR2A NMDA receptors. However, a significant decrease in the cell surface expression of NR1-1a/NR2A receptors was observed. To further test if this result is an anomaly or a true finding the cell surface ELISA assay should be carried out in the presence of other either direct or indirect PKA activators.

As mentioned above, the maintenance of cell surface expression of NR1-1a/NR2A NMDA receptors were dependent on the phosphorylation of S1459. A similar mechanism was identified for the regulation of GluR1-containing AMPA receptors. Man *et al.* (2007) demonstrated that phosphorylation of GluR1 S845 by PKA was required to maintain AMPA receptor cell surface expression. Further, this phosphorylation of S845 promoted receptor insertion and decreased the endocytosis of GluR1-containing AMPA receptors (Man *et al.*, 2007). Phosphorylation is also known to prevent the internalisation of NMDA receptors. For example, Vissel *et al.* (2001) demonstrated that activity-induced dephosphorylation of NR1 Y837 and NR2A Y842 allowed AP-2 binding which resulted in the internalisation of recombinant NR1/NR2A receptors. Indeed, S1459 is close to a putative internalisation motif, YKKM, on the NR2A C-terminal domain. The phosphorylation of S1459 close to this putative internalisation motif may serve to regulate the cell surface expression of NMDA receptors by inhibiting the binding of internalisation machinery. However, Lavezzari *et al.* (2004) demonstrated that the truncation of the last 11 amino acids from the NR2A C-terminal domain, i.e. removing both the ESDV and the YKKM motifs did not affect the Tac-NR2A$^{\Delta 11}$ chimera internalisation. Conversely, as discussed in Chapter 5, when deleting the last 24 amino acids from NR2A subunits there was a ~ 2 fold increase in cell surface expression for NR1-1a/NR2A$^{T1441\text{-}STOP}$ NMDA receptors. This suggested that the last 24 amino acids of the NR2A C-terminal domain regulate the cell surface expression, which is partly regulated by phosphorylation.

A possible model to explain all the above findings could be as follows. NMDA receptors are trafficked to the cell surface and are stabilised by their association with PSD-95 (Lin

et al., 2004). PSD-95 is known to associate with AKAP79/150 (Colledge *et al.*, 2000). AKAP79/150 is a scaffolding protein which associates with PKA, PKC and PP2B (Klauck *et al.*, 1996). Therefore PKA is brought into close proximity to the C-terminal domain of NR2A subunits and results in the phosphorylation of S1459. The phosphorylated S1459 of the NR2A C-terminal domain results in the dissociation of PSD-95. However, PSD-95 is anchored into to the cell membrane by a N-terminal palmitoylation modification (Topinka and Bredt, 1998). The PSD-95/AKAP79/150 complex may contain PP2B which would facilitate the dephosphorylation of S1459 on the NR2A C-terminal domain. The dephosphorylated S1459 on the NR2A C-terminal domain favours the internalisation of NR1/NR2A NMDA receptors. A diagram to summarise the possible role of phosphorylation on S1459 on NR2A subunits is shown in Figure 4.17. In favour of this model was the finding that a SAP97/AKAP79/150 complex brings PKA into close proximity to the human β1-adrenergic receptor which was found to facilitate its recycling once the ligand has bound (Gardner *et al.*, 2007). Therefore, once glutamate and glycine have bound to NMDA receptors, this may provide the signal to promote the phosphorylation of the C-terminal domains of NMDA receptors which facilitates their internalisation.

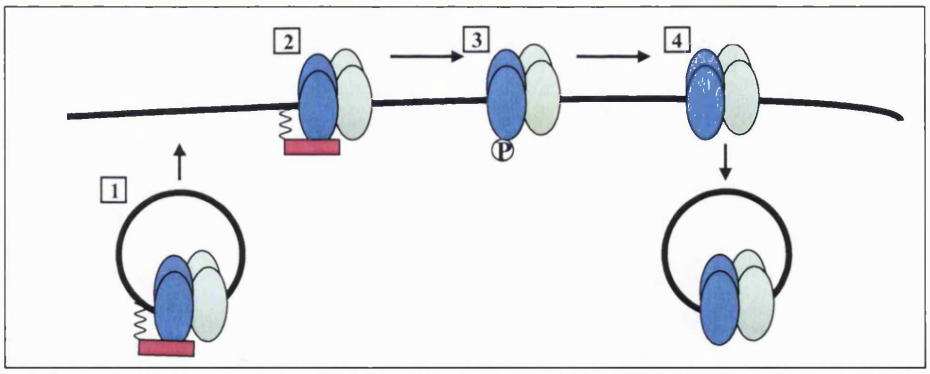

Figure 4.17 Schematic diagram depicting the role phosphorylation at S1459 on NR2A subunits may play in NR1-1a/NR2A NMDA receptor cell surface expression

1. NMDA receptors are trafficked to the cell surface.
2. PSD-95 enhances the expression of NR1-1a/NR2A NMDA receptors at the cell surface in HEK 293 cells.
3. The phosphorylation of S1459 on NR2A subunits causes the dissociation of PSD-95 from the NMDA receptor.
4. Once the NMDA receptor is dephosphorylated the receptor is primed for internalisation.

Additionally, during the characterisation of the NR2A^{S1459A} subunits it was found that there was a significant ~ 5 kDa decrease in the observed molecular weight. NR2A subunits may be phosphorylated at S1459 in HEK 293 cells which would increase their net negative charge. Therefore proportionally less SDS could bind to NR2A subunits when compared to NR2A^{S1459A} subunits. A comparative increase in the SDS binding would mean NR2A^{S1459A} subunits are mobile when analysed by SDS-PAGE thereby resulting in a difference in the apparent molecular weight. Additionally, cytotoxicity assays showed a significant increase in the cytotoxicity gained for the kinase dead NR1-1a/NR2A^{S1459A} NMDA receptors in comparison to NR1-1a/NR2A NMDA receptors. This is in contrast to Chen *et al.* (2006) who demonstrated using outside-out patches of recombinant NR1/NR2C S1244E NMDA receptors showed an acceleration in the channel activation and decay kinetics of the response. However, the cytotoxicity assay does not look at single channel function rather it provides a gross measure of receptor function. Therefore electrophysiological methods should be carried out to ascertain if NR1-1a/NR2A^{S1459A} NMDA receptors have different conductance properties compared to wild-type NMDA receptors.

In summary, in this chapter it was shown that:-

- NR1-1a/NR2A^{S1459A} NMDA receptors co-immunoprecipitated with PSD-95$\alpha^{c\text{-}Myc}$. This association between PSD-95$\alpha^{c\text{-}Myc}$ and NR1-1a/NR2A NMDA receptor complexes was found to be regulated by phosphorylation. In the presence of forskolin there was a greater decrease in the association between PSD-95$\alpha^{c\text{-}Myc}$ and NR1-1a/NR2A NMDA receptors compared to NR1-1a/NR2A^{S1459A} NMDA receptors.
- Co-expression of PSD-95$\alpha^{c\text{-}Myc}$ resulted in a significant enhancement of the total expression of NR2A and NR2A^{S1459A} subunits. However, this total PSD-95 induced enhancement of total expression of NR2A and NR2A^{S1459A} subunits was not significantly different.
- Cell surface studies of NR1-1a/NR2A^{S1459A} NMDA receptors in the presence of PSD-95$\alpha^{c\text{-}Myc}$ resulted in an enhancement of cell surface expression which was significantly greater than that observed with NR1-1a/NR2A NMDA receptors.

- NR1-1a/NR2A^{S1459A} NMDA receptors were found to be expressed significantly lower at the cell surface when compared to wild-type NR1-1a/NR2A NMDA receptors. NR1-1a/NR2A^{S1459A} NMDA receptors showed an increase in the co-immunoprecipitation with Rab 5, an early endosomal marker which suggested that NR1-1a/NR2A^{S1459A} NMDA receptors are internalised at a higher rate compared to NR1-1a/NR2A NMDA receptors.
- A ~ 5 kDa shift in the molecular weight of NR2A^{S1459A} subunits when compared to wild-type NR2A subunits was observed, suggesting that NR2A subunits are phosphorylated on S1459 in HEK 293 cells.
- NR1-1a/NR2A^{S1459A} NMDA receptors resulted in a cytotoxicity significantly different to wild-type NR1-1a/NR2A NMDA receptors which suggested that the channel properties may have been changed.

CHAPTER 5

RESULTS III

DISCUSSION III

5.1 RATIONALE

Investigations into the additional PSD-95 binding motif present in the NR2A and NR2B C-terminal domains

As discussed previously in the Chapter 1, the interaction between PSD-95 and NMDA receptors is thought to occur via the ESDV motif present on the distal C-terminus of NR2A and NR2B subunits (Kornau *et al.*, 1995; Niethammer *et al.*, 1996). However, it was demonstrated by Bassand *et al.* (1999) using a yeast two-hybrid interaction assay approach that a PSD-95/NR2A and SAP97/NR2A interaction still remained when the ESDV motif was removed. This interaction was completely abolished when the NR2A C-terminal domain was truncated at amino acid residue 1157 (Bassand *et al.*, 1999). Further, previous work by Rutter (2001) and Papadakis (2004) demonstrated that NR1-1a/NR2A^{TRUNC} NMDA receptors, i.e. NR2A subunits lacking the ESDV motif, were still able to co-immunoprecipitate with PSD-95 following their co-expression in HEK 293 cells. In addition, the removal of the last six amino acids from either the NR2A or NR2B C-terminal domain were found to result in a reduced delivery of NMDA receptors to synapses but no effects on their localisation (Barria and Malinow, 2002). This suggested that a mechanism independent to the ESDV motif can also deliver NMDA receptors to synapses, albeit at a lower rate. All these observations suggested that an additional PSD-95 binding site may be present in the NR2A subunit C-terminal domain. In contrast to the above findings, recombinant NR1/NR2B^{S1480A} NMDA receptors, i.e. ESDV $\rightarrow$ EADV, no longer co-immunoprecipitated with PSD-95 (Prybylowski *et al.*, 2005). This suggested a differential interaction between NR2A/PSD-95 and NR2B/PSD-95 complexes. In this chapter, the possible existence of additional PSD-95 binding motifs present in the NR2A and NR2B C-terminal domains was investigated.

5.2 RESULTS

5.2.1 Replication of the association of NR1-1a/NR2A^{TRUNC} NMDA receptors with PSD-95α$^{c\text{-}Myc}$ following their co-expression in HEK 293 cells

Rutter (2001) and Papadakis (2004) demonstrated that NR1-1a/NR2A^{TRUNC} NMDA receptors, i.e. deletion of the NR2A C-terminal ESDV, are able to co-immunoprecipitate with PSD-95α$^{c\text{-}Myc}$ following their co-expression in HEK 293 cells. To replicate this result HEK 293 cells were transfected with NR1-1a/NR2A and NR1-1a/NR2A^{TRUNC} NMDA receptor clones in the presence of PSD-95α$^{c\text{-}Myc}$, cell homogenates were prepared, detergent-solubilised and immunoprecipitations with anti-NR1 C2 or non-immune antibodies were carried out, Section 2.2.2.12. The immune and non-immune pellets were analysed by immunoblotting using anti-NR2A (1381-1394) or anti-c-Myc antibodies, as appropriate. Representative immunoblots are shown in Figure 5.1.

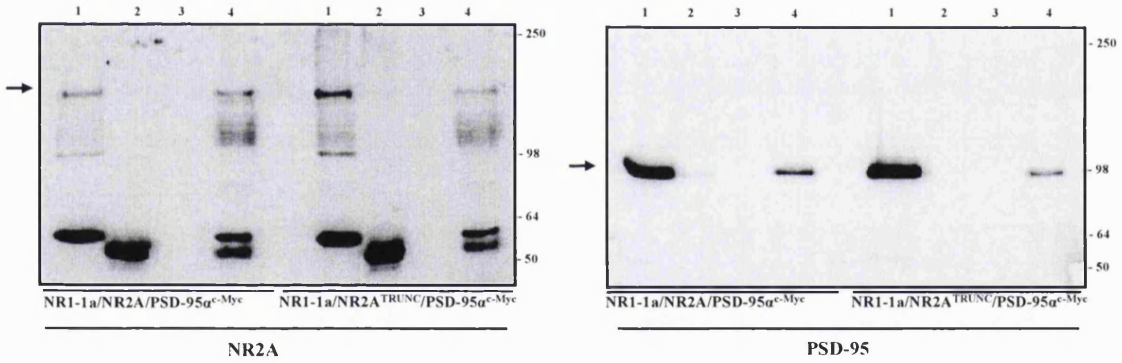

Figure 5.1 PSD-95 co-immunoprecipitates with NR1-1a/NR2A or NR1-1a/NR2A^{TRUNC} NMDA receptors following their co-expression in HEK 293 cells

HEK 293 cells were transfected with NR1-1a/NR2A and NR1-1a/NR2A^{TRUNC} NMDA receptor clones + PSD-95α$^{c\text{-}Myc}$. Cell homogenates were prepared 24 h post-transfection, detergent-solubilised and immunoprecipitations were carried out using anti-NR1 C2 or non-immune antibodies. The resulting immune and non-immune pellets were analysed by immunoblotting using anti-NR2A (1381-1394) or anti-c-Myc antibodies, as indicated. The gel layout is the same for each immunoblot, lane 1 = detergent-soluble fraction, lane 2 = non-immune pellet, lane 3 = empty and lane 4 = immune pellet. Arrows denote NR2A subunits and PSD-95α$^{c\text{-}Myc}$. The positions of the protein molecular weight markers (kDa) are shown on the right. The immunoblots are representative of n = 3 immunoprecipitations from n = 3 independent transfections.

The detergent-soluble fraction was found to contain immunoreactive bands corresponding to NR2A, NR2A^{TRUNC} subunits and PSD-95α$^{c\text{-}Myc}$ showing that each protein was successfully detergent-solubilised. The immune pellets contained NR2A, NR2A^{TRUNC}

subunits and PSD-95α$^{c\text{-}Myc}$ but each was absent from the non-immune pellets. The immunoprecipitations were carried out using anti-NR1 C2 antibodies and subsequent immunoblotting demonstrated that NR2A and PSD-95 were both present in the same complex. Therefore NR1-1a/NR2A^{TRUNC} NMDA receptor complexes were found to co-immunoprecipitate with PSD-95α$^{c\text{-}Myc}$ following their co-expression in HEK 293 cells and the initial findings of Rutter (2001) and Papadakis (2004) were replicated.

5.2.2 Generation of NR2B$^{FLAG/TRUNC}$ construct

Since NR1-1a/NR2A^{TRUNC} receptors were shown to associate with PSD-95, it was of interest to ascertain if the same was true for NR1-1a/NR2B^{TRUNC} receptors. Firstly it was necessary to test the available anti-NR2B antibodies for reactivity with NR2B^{TRUNC} subunits in immunoblots. HEK 293 cells were transfected with NR1-1a/NR2B and NR1-1a/NR2B^{TRUNC} NMDA receptors, cell homogenates were prepared and the resulting cell homogenates analysed by immunoblotting using anti-NR2B (44-58) and NR2A/B (1435-1445) antibodies. Representative immunoblots are shown in Figure 5.2.

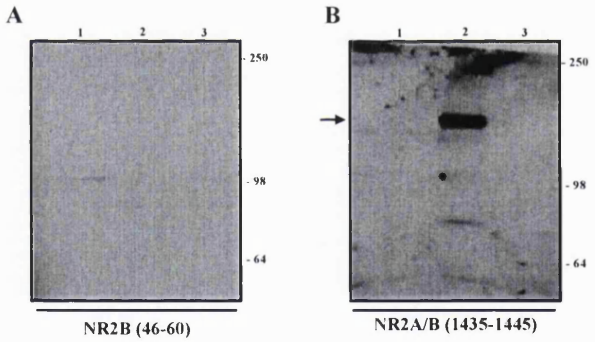

Figure 5.2 Reactivity of NR2B^{TRUNC} subunits with anti-NR2B antibodies

HEK 293 cells were transfected with NR1-1a/NR2B and NR1-1a/NR2B^{TRUNC} NMDA receptor clones. Cell homogenates were prepared 24 h post-transfection and analysed by immunoblotting using anti-NR2B (46-60) or anti-NR2A/B (1454-1464) antibodies, as indicated. Lanes 1 = untransfected cell homogenates; lanes 2 = NR1-1a/NR2B; and lanes 3 = NR1-1a/NR2B^{TRUNC}. The arrow denotes the position of NR2B subunits. The positions of the protein molecular weight markers (kDa) are shown on the right. The immunoblots are representative from n = 3 transfections.

Anti-NR2B (44-58) antibodies did not recognise either NR2B or NR2B^{TRUNC} subunits. The anti-NR2A/B (1454-1464) antibodies gave a specific immunoreactive band corresponding to NR2B subunits but they did not recognise NR2B^{TRUNC} subunits. Anti-NR2A/B antibodies are directed against NR2A amino acids 1454-1464, i.e. YKKMPSIESDV.

NR2A and NR2B subunits share a high amino acid sequence identity within this region and since the antibodies do not recognise $NR2B^{TRUNC}$ subunits, it can be concluded that the ESDV motif is essential for the antibodies to recognise the NR2B subunits. Note, to ensure $NR2B^{TRUNC}$ subunits were expressed, qualitative cytotoxicity assays were performed with NR1-1a/ $NR2B^{TRUNC}$ transfected HEK 293 cells and ~ 20 % cytotoxicity was obtained.

Available in the laboratory was an epitope tagged version of the NR2B subunit where the FLAG tag was inserted at amino acids 53-54 (Hawkins *et al.*, 1999). Thus, in the absence of useful antibodies that recognised both wild-type and truncated NR2B subunits, $NR2B^{FLAG/TRUNC}$ subunits were generated. A STOP codon was introduced at amino acid 1479 of the $NR2B^{FLAG}$ subunit. The $NR2B^{FLAG/TRUNC}$ clone was generated by *in vitro* site-directed mutagenesis, Section 2.2.1.2.10. Nucleotide sequencing of the $NR2B^{FLAG/TRUNC}$ clone confirmed the correct mutation was generated with no additional mutations.

5.2.3 Characterisation of NR1-1a/$NR2B^{FLAG/TRUNC}$ NMDA receptors by quantitative immunoblotting and cytotoxicity assays

To demonstrate that NR2B and $NR2B^{FLAG/TRUNC}$ NMDA receptor subunits were expressed at the same level, quantitative immunoblotting was performed, Section 2.2.2.11. HEK 293 cells were transfected with NR1-1a/$NR2B^{FLAG}$ and NR1-1a/$NR2B^{FLAG/TRUNC}$ NMDA receptor clones and cell homogenates were prepared. The resulting cell homogenates were analysed using either anti-NR1 C2 or anti-FLAG antibodies, as appropriate. Representative immunoblots are shown in Figure 5.3. There was no significant difference observed for the molecular weights of NR2B and $NR2B^{FLAG/TRUNC}$ subunits, i.e. $NR2B^{FLAG}$ subunits M_r = 167 ± 3 kDa (n = 15) and $NR2B^{FLAG/TRUNC}$ subunits M_r = 167 ± 3 (n = 15, $p < 0.1$). A histogram to summarise the relative expression of NR1-1a/$NR2B^{FLAG/TRUNC}$ NMDA receptor subunits is shown in Figure 5.4. No significant change in the expression level of either NR1-1a subunits or $NR2B^{FLAG/TRUNC}$ subunits compared to the wild-type subunits was observed.

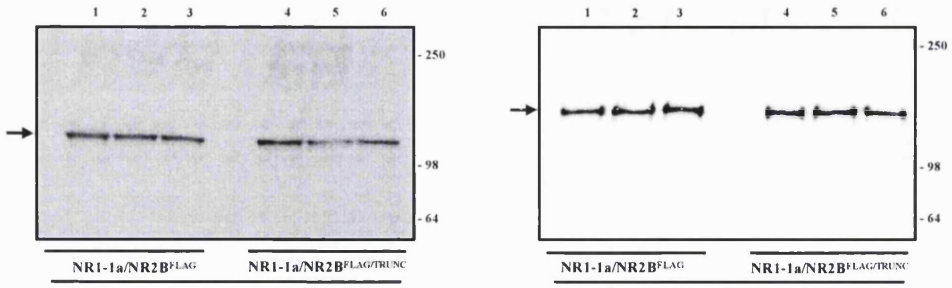

Figure 5.3 Quantitative immunoblotting of NR1-1a/NR2B^{FLAG} and NR1-1a/NR2B$^{FLAG/TRUNC}$ NMDA receptor subunits following their co-expression in HEK 293 cells

HEK 293 cells were transfected with NR1-1a/NR2B^{FLAG} and NR1-1a/NR2B$^{FLAG/TRUNC}$ NMDA receptor clones. Cell homogenates were prepared 24 h post-transfection and analysed by quantitative immunoblotting using anti-NR1 C2 or anti-FLAG antibodies, as indicated. Lanes 1-3 = triplicate samples of NR1-1a/NR2B^{FLAG} and lanes 4-6 = triplicate samples of NR1-1a/NR2B$^{FLAG/TRUNC}$. Arrows denote NR1-1a subunits or NR2B subunits. The positions of the protein molecular weight markers (kDa) are shown on the right. The immunoblots are representative from n = 3 transfections.

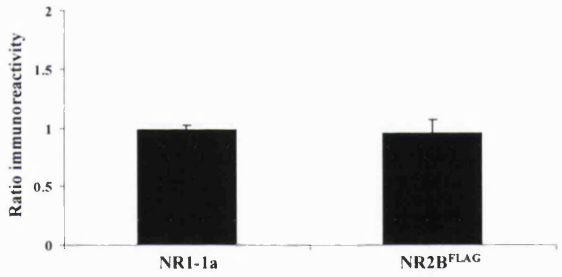

Figure 5.4 Histogram summarising the expression levels of NR1-1a/NR2B^{FLAG} and NR1-1a/NR2B$^{FLAG/TRUNC}$ NMDA receptor subunits following their co-expression in HEK 293 cells

HEK 293 cells were transfected with NR1-1a/NR2B^{FLAG} and NR1-1a/NR2B$^{FLAG/TRUNC}$ NMDA receptor clones. Cell homogenates were prepared 24 h post-transfection and analysed by quantitative immunoblotting using anti-NR1 C2 or anti-FLAG antibodies. Results are expressed as the fold change, i. e. immunoreactivity of NR1-1a/NR2B$^{FLAG/TRUNC}$ receptor subunits/ immunoreactivity of NR1-1a/NR2B^{FLAG} receptor subunits. The histogram is a summary of the mean fold change ± SEM for each combination. The results expressed in the histogram are the mean fold enhancement from n = 3 independent transfections.

As mentioned previously, cytotoxicity assays provide a means to show that functional NMDA receptors are expressed in HEK 293 cells. Therefore, cytotoxicity assays were carried out to demonstrate that NR2B$^{FLAG/TRUNC}$ subunits could co-assemble with NR1-1a subunits to form functional NMDA receptors, Section 2.2.2.7. HEK 293 cells were transfected in parallel with NR1-1a/NR2B^{FLAG} and NR1-1a/NR2B$^{FLAG/TRUNC}$ NMDA receptor clones. The transfected HEK 293 cells were cultured in the presence and absence

of the NMDA receptor antagonist, ketamine. Cytotoxicity assays were performed 20 h post-transfection. A summary of the cytotoxicity results are shown in Figure 5.5. Cytotoxicity results were normalised to NR1-1a/NR2B^{FLAG} NMDA receptor cytotoxicity. There was no significant difference in the resulting cytotoxicity gained for NR1-1a/NR2B$^{FLAG/TRUNC}$ NMDA receptors ($p < 0.1$, $n = 3$).

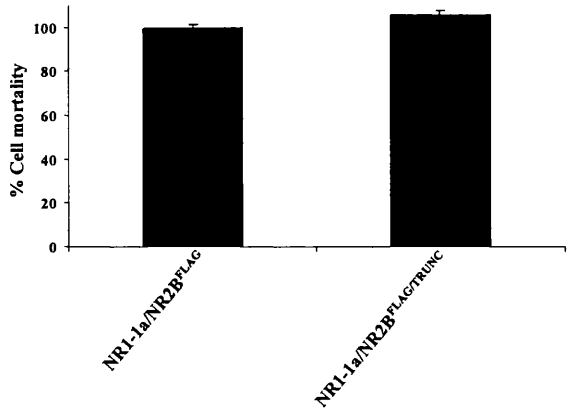

Figure 5.5 Histogram summarising cell cytotoxicity post-transfection for NR1-1a/NR2B^{FLAG} and NR1-1a/NR2B$^{FLAG/TRUNC}$ NMDA receptors

HEK 293 cells were transfected with NR1-1a/NR2B^{FLAG} and NR1-1a/NR2B$^{FLAG/TRUNC}$ NMDA receptor clones. Cytotoxicity was determined as in Section 2.2.2.7. Results are normalised to the wild-type NR1-1a/NR2B^{FLAG} NMDA receptor. The histogram summarises the mean cytotoxicity from n = 3 independent transfections.

5.2.4 Demonstration of the association between NR1-1a/NR2B$^{FLAG/TRUNC}$ NMDA receptors and PSD-95α$^{c\text{-}Myc}$ by co-immunoprecipitation following their co-expression in HEK 293 cells

To investigate if NR1-1a/NR2B$^{FLAG/TRUNC}$ NMDA receptors are able to associate with PSD-95α$^{c\text{-}Myc}$, immunoprecipitation assays were carried out. HEK 293 cells were transfected with NR1-1a/NR2B^{FLAG} and NR1-1a/NR2B$^{FLAG/TRUNC}$ NMDA receptor clones in the presence of PSD-95α$^{c\text{-}Myc}$, cell homogenates were prepared, detergent-solubilised and immunoprecipitations with anti-NR1 C2 and non-immune antibodies were carried out, Section 2.2.2.12. The resulting immune and non-immune pellets were analysed by immunoblotting with either anti-FLAG or anti-c-Myc antibodies, as appropriate. Representative immunoblots are shown in Figure 5.6.

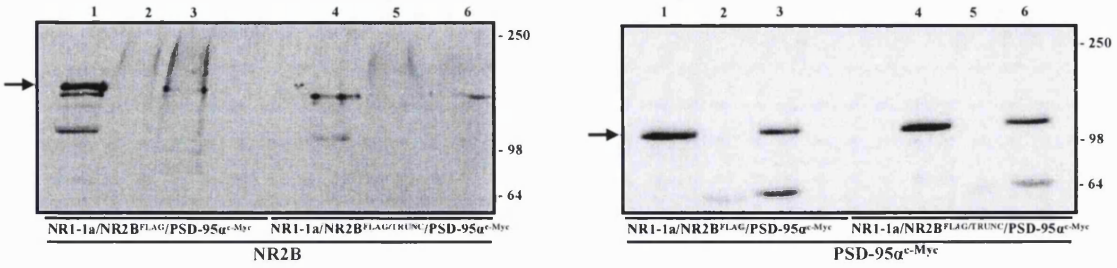

Figure 5.6 NR1-1a/NR2B^{FLAG} or NR1-1a/NR2B$^{FLAG/TRUNC}$ NMDA receptors co-immunoprecipitate with PSD-95α^{c-Myc} following their co-expression in HEK 293 cells

HEK 293 cells were transfected with NR1-1a/NR2B^{FLAG} and NR1-1a/NR2B$^{FLAG/TRUNC}$ NMDA receptor clones + PSD-95α^{c-Myc}. Cell homogenates were prepared 24 h post-transfection, detergent-solubilised and immunoprecipitations were carried out using anti-NR1 C2 or non-immune antibodies. The resulting immune and non-immune pellets were analysed by immunoblotting using anti-FLAG or anti-c-Myc antibodies, as indicated. The gel layout is the same for each immunoblot, lane 1 = detergent-soluble fraction, lane 2 = non-immune pellet and lane 3 = immune pellet. Arrows denote NR2B subunits and PSD-95α^{c-Myc}. The positions of the protein molecular weight markers (kDa) are shown on the right. The immunoblots are representative of n = 3 immunoprecipitations from n = 3 independent transfections.

Immunoreactive bands corresponding to NR2B^{FLAG}, NR2B$^{FLAG/TRUNC}$ subunits and PSD-95α^{c-Myc} were present in the detergent-soluble fraction thus showing that each protein was successfully detergent-solubilised. The immune pellets showed immunoreactive bands for NR2B^{FLAG} and NR2B$^{FLAG/TRUNC}$ subunits which were absent from the non-immune pellets showing an co-immunoprecipitation with NR1-1a subunits. Both immune pellets contained PSD-95α^{c-Myc} which was absent from the non-immune pellets. Therefore, NR1-1a/NR2B$^{FLAG/TRUNC}$ NMDA receptor complexes were found to co-immunoprecipitate with PSD-95α^{c-Myc} following their co-expression in HEK 293 cells.

5.2.5 Generation of NR2A$^{T1441-STOP}$ and NR2A$^{N1157-STOP}$ NMDA receptor subunits to identify additional PSD-95α^{c-Myc} interaction motifs

NR1-1a/NR2A^{TRUNC} and NR1-1a/NR2B$^{FLAG/TRUNC}$ NMDA receptor complexes were both found to co-immunoprecipitate with PSD-95α^{c-Myc} following their co-expression in HEK 293 cells. This demonstrated that PSD-95α^{c-Myc} can immunoprecipitate with NR1-1a/NR2A and NR1-1a/NR2B NMDA receptors in a distal C-terminal ESDV-independent manner (Rutter, 2001; Papadakis, 2004; Section 5.2.1; Section 5.2.4). As described earlier, Bassand *et al.* (1999) demonstrated using a yeast two-hybrid approach that the interaction with PSD-95 was abolished once the NR2A C-terminal domain was truncated to amino

acid N1157. The C-terminal domains of NR2A and NR2B subunits were aligned starting from amino acid 1157 to the C-terminus for each subunit to identify additional putative PSD-95 binding motifs common to both C-termini, Figure 5.7.

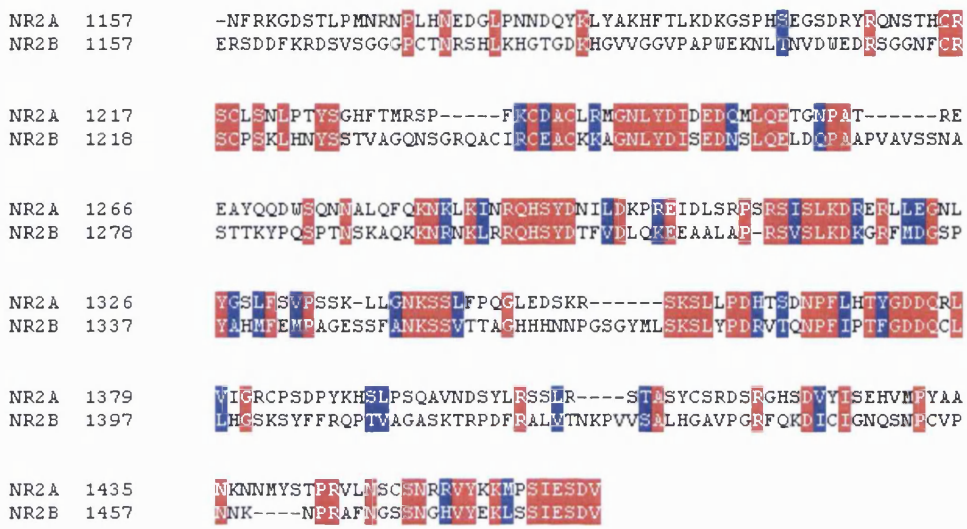

Figure 5.7 Alignment of NR2A amino acid residues 1157-1464 and NR2B amino acid residues 1157-1481

NR2A amino acid residues 1157-1464 and NR2B amino acid residues 1157-1481 were aligned using ClustalW (http://www.ch.embnet.org/software/ClustalW.html). Identical amino acids are shown in red ( ) and similar amino acids are shown in blue ( ). Overall there is 37 % amino acid identity and 51 % amino acid similarity. The last 24 amino acids share 58 % amino acid identity and 67 % amino acid similarity.

There is 37 % amino acid identity and 51 % amino acid similarity between NR2A and NR2B C-terminal domains over this region. The following deletion constructs were made:

1. The NR2A subunit was truncated to amino acid N1157 to serve a negative control for the interactions with PSD-95$\alpha^{c\text{-}Myc}$ (Bassand *et al.*, 1999).

2. Although it is not known if the NR2A and NR2B subunits interact with the same or different additional PSD-95 binding motifs, it was assumed initially that they interact via a similar motif. The last 24 amino acids of the NR2A and NR2B C-terminal domains share 58 % amino acid identify and 67 % amino acid similarity. Thus due to this high amino acid similarity a second truncation was made at amino acid NR2A T1441.

Thus truncations of the NR2A subunit were generated by creating STOP codons at amino acid N1157 and T1441 by *in vitro* site-directed mutagenesis generating NR2A$^{N1157\text{-}STOP}$ and NR2A$^{T1441\text{-}STOP}$ subunits, Section 2.2.1.2.10. Nucleotide sequencing of the NR2A$^{N1157\text{-}STOP}$ and NR2A$^{T1441\text{-}STOP}$ clones confirmed the correct mutation was generated with no additional mutations on the NR2A clone.

5.2.6 Characterisation of NR1-1a/NR2A$^{T1441\text{-}STOP}$ and NR1-1a/NR2A$^{N1157\text{-}STOP}$ NMDA receptors by quantitative immunoblotting and cytotoxicity assays

To examine if NR2A$^{T1441\text{-}STOP}$ and NR2A$^{N1157\text{-}STOP}$ subunits were expressed at the same level as wild-type NR2A subunits, quantitative immunoblotting was carried out, Section 2.2.2.11. HEK 293 cells were transfected with NR1-1a/NR2A, NR1-1a/NR2A$^{T1441\text{-}STOP}$ and NR1-1a/NR2A$^{N1157\text{-}STOP}$ NMDA receptor clones, cell homogenates were prepared and quantitative immunoblotting was carried out using either anti-NR1 C2 or anti-NR2A (44-58) antibodies, as appropriate. Representative immunoblots are shown in Figure 5.8.

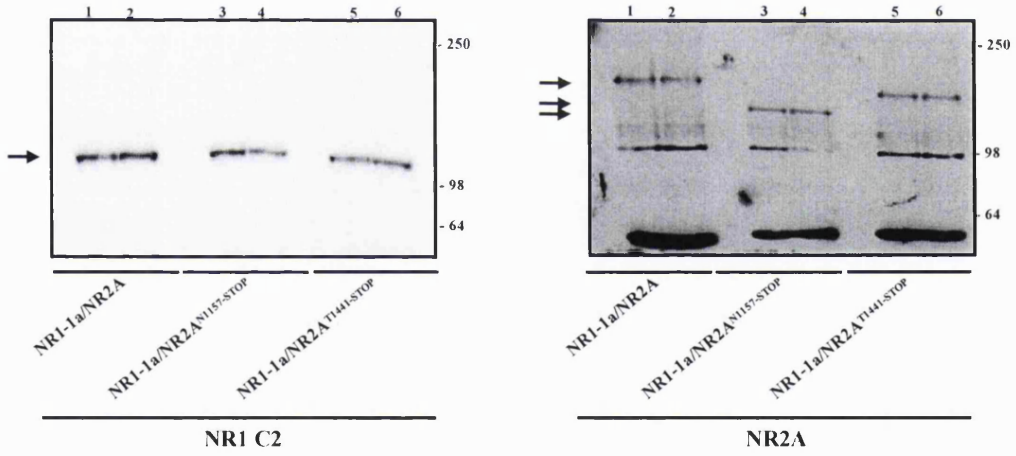

Figure 5.8 Quantitative immunoblotting of NR1-1a/NR2A, NR1-1a/NR2A$^{T1441\text{-}STOP}$ and NR1-1a/NR2A$^{N1157\text{-}STOP}$ NMDA receptors following their co-expression in HEK 293 cells

HEK 293 cells were transfected with NR1-1a/NR2A, NR1-1a/NR2A$^{T1441\text{-}STOP}$ and NR1-1a/NR2A$^{N1157\text{-}STOP}$ NMDA receptor clones. Cell homogenates were prepared 24 h post-transfection and analysed by quantitative immunoblotting using anti-NR1 C2 or anti-NR2A (44-58) antibodies, as indicated. Lanes 1-2 = duplicate samples of NR1-1a/NR2A; lanes 3-4 = duplicate samples of NR1-1a/NR2A$^{T1441\text{-}STOP}$ and lanes 4-6 = duplicate samples of NR1-1a/NR2A$^{N1157\text{-}STOP}$. Arrows denote NR1-1a or NR2A subunits. The positions of the protein molecular weight markers (kDa) are shown on the right. The immunoblots are representative from n = 3 transfections.

There was no significant change observed between the molecular weights of the wild-type NR2A and NR2A$^{T1441\text{-}STOP}$ subunits, i.e. NR2A subunits M_r = 180 ± 8 kDa (n = 14) and NR2A$^{N1441\text{-}STOP}$ subunits M_r = 174 ± 14 kDa (n = 14, $p < 0.1$). However, a significant change was observed between the molecular weights of the wild-type NR2A and NR2A$^{N1157\text{-}STOP}$ subunits, i.e. NR2A$^{N1157\text{-}STOP}$ M_r = 148 ± 14 kDa (n = 14, $p < 0.0005$). A summary of the expression levels for NR1-1a, NR2A$^{1441\text{-}STOP}$ and NR2A$^{1157\text{-}STOP}$ NMDA receptor subunits are shown in Figure 5.9. There was no significant change in the expression level of either NR2A$^{T1441\text{-}STOP}$ or NR2A$^{N1157\text{-}STOP}$ subunits observed when compared to NR2A subunits.

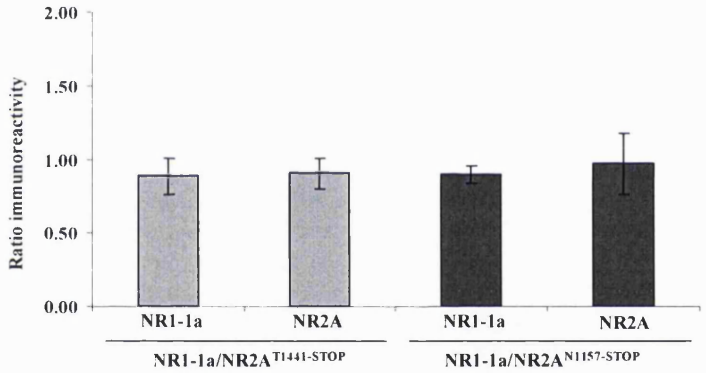

Figure 5.9 A histogram summarising the expression levels of NR1-1a/NR2A, NR1-1a/NR2A$^{T1441\text{-}STOP}$ and NR1-1a/NR2A$^{N1157\text{-}STOP}$ NMDA receptor subunits following their co-expression in HEK 293 cells

HEK 293 cells were transfected with NR1-1a/NR2A, NR1-1a/NR2A$^{T1441\text{-}STOP}$ and NR1-1a/NR2A$^{N1157\text{-}STOP}$ NMDA receptor clones. Cell homogenates were prepared 24 h post-transfection and analysed by quantitative immunoblotting using anti-NR1 C2 or anti-NR2A (44-58) antibodies. Results are expressed as the fold change, i. e. immunoreactivity of truncated NR1-1a/NR2A receptor subunits/ immunoreactivity of NR1-1a/NR2A receptor subunits. The histogram is a summary of the mean fold change ± SEM for each combination. The results expressed in the histogram are the mean fold enhancement from n = 3 independent transfections.

Cytotoxicity assays were performed to demonstrate that NR2A$^{T1441\text{-}STOP}$ and NR2A$^{N1157\text{-}STOP}$ subunits could both co-assemble with NR1-1a subunits to form functional NMDA receptors, Section 2.2.2.7. HEK 293 cells were transfected in parallel with NR1-1a/NR2A, NR1-1a/NR2A$^{T1441\text{-}STOP}$ and NR1-1a/NR2A$^{N1157\text{-}STOP}$ NMDA receptor clones. The transfected HEK 293 cells were cultured in the presence and absence of the NMDA

receptor antagonist, ketamine for 20 h post-transfection. A histogram to summarise the cytotoxicity results is shown in Figure 5.10. There was no significant difference in cytotoxicity post-transfection for NR1-1a/NR2A$^{T1441\text{-}STOP}$ ($p < 0.1$, $n = 3$) and NR1-1a/NR2A$^{N1157\text{-}STOP}$ ($p < 0.1$, $n = 3$) NMDA receptors. Therefore, the expression of NR1-1a/NR2A$^{T1441\text{-}STOP}$ and NR1-1a/NR2A$^{N1157\text{-}STOP}$ resulted in cell surface, functional NMDA receptors.

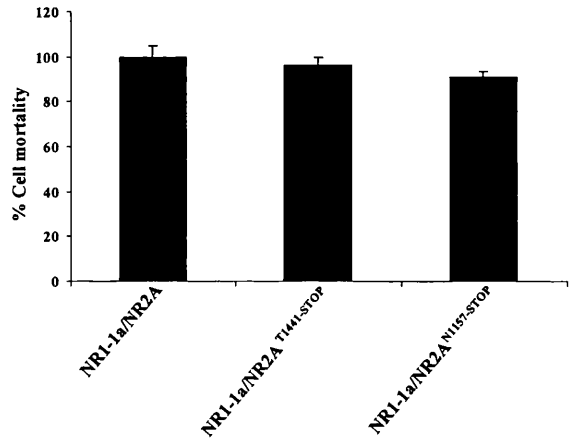

Figure 5.10 Histograms to summarise the cytotoxicity resulting from co-expression of NR1-1a/NR2A, NR1-1a/NR2A$^{T1441\text{-}STOP}$ and NR1-1a/NR2A$^{N1157\text{-}STOP}$ NMDA receptors in the absence of a NMDA receptor antagonist in HEK 293 cells

HEK 293 cells were transfected with NR1-1a/NR2A, NR1-1a/NR2A$^{T1441\text{-}STOP}$ and NR1-1a/NR2A$^{N1157\text{-}STOP}$ NMDA receptor clones. Cytotoxicity was determined as in Section 2.2.2.7. Results are normalised to the wild-type NR1-1a/NR2A NMDA receptor. The histogram summarises the mean cytotoxicity from n = 3 independent transfections.

5.2.7 Demonstration of an additional PSD-95α$^{c\text{-}Myc}$ interaction site present in the NR2A C-terminal domain by co-immunoprecipitation following the co-expression of NR1-1a/NR2A, NR1-1a/NR2A^{TRUNC}, NR1-1a/NR2A$^{T1441\text{-}STOP}$ and NR1-1a/NR2A$^{N1157\text{-}STOP}$ NMDA receptors with PSD-95α$^{c\text{-}Myc}$

To further localise the additional PSD-95 binding site (s) present on the NR2A C-terminal domain, immunoprecipitations were carried out with the newly generated NR2A subunit truncations. HEK 293 cells were transfected with NR1-1a/NR2A, NR1-1a/NR2A^{TRUNC}, NR1-1a/NR2A$^{T1441\text{-}STOP}$ and NR1-1a/NR2A$^{N1157\text{-}STOP}$ NMDA receptor clones in the presence of PSD-95α$^{c\text{-}Myc}$, cell homogenates were prepared, detergent-solubilised and immunoprecipitations carried out using anti-NR1 C2 or non-immune antibodies, Section 2.2.2.12. The resulting immune and non-immune pellets were analysed by immunoblotting

using anti-NR2A (44-58) or anti-c-Myc antibodies, as appropriate. Representative immunoblots are shown in Figure 5.11. It was found that the detergent-soluble fractions contained NR2A, NR2A^{TRUNC}, NR2A$^{T1441\text{-}STOP}$, NR2A$^{N1157\text{-}STOP}$ subunits and PSD-95α$^{c\text{-}Myc}$ thus showing that each protein was successfully detergent-solubilised. Each immune pellet contained an immunoreactive band present corresponding to the respective NR2A subunit demonstrating that they co-immunoprecipitate with the NR1-1a subunit. As previously demonstrated, an immunoreactive band was present for PSD-95α$^{c\text{-}Myc}$ from HEK 293 cells expressing either NR1-1a/NR2A or NR1-1a/NR2A^{TRUNC} NMDA receptors, Section 5.2.1. An immunoreactive band corresponding to PSD-95α$^{c\text{-}Myc}$ was present from HEK 293 cells expressing NR1-1a/NR2A$^{T1441\text{-}STOP}$ NMDA receptors. However, no immunoreactivity was present for PSD-95α$^{c\text{-}Myc}$ from HEK 293 cells expressing NR1-1a/NR2A$^{N1157\text{-}STOP}$ NMDA receptors. The ~ 50 kDa immunoreactive bands present in both immune and non-immune pellet lanes are antibody heavy chains used for the immunoprecipitations. It can therefore be concluded that PSD-95α$^{c\text{-}Myc}$ co-immunoprecipitated with NR1-1a/NR2A, NR1-1a/NR2A^{TRUNC}, NR1-1a/NR2A$^{T1441\text{-}STOP}$ but not NR1-1a/NR2A$^{N1157\text{-}STOP}$ NMDA receptor complexes following their co-expression in HEK 293 cells. Thus, the additional PSD-95 interaction sites (s) must be localised within amino acid residues 1157 -1441.

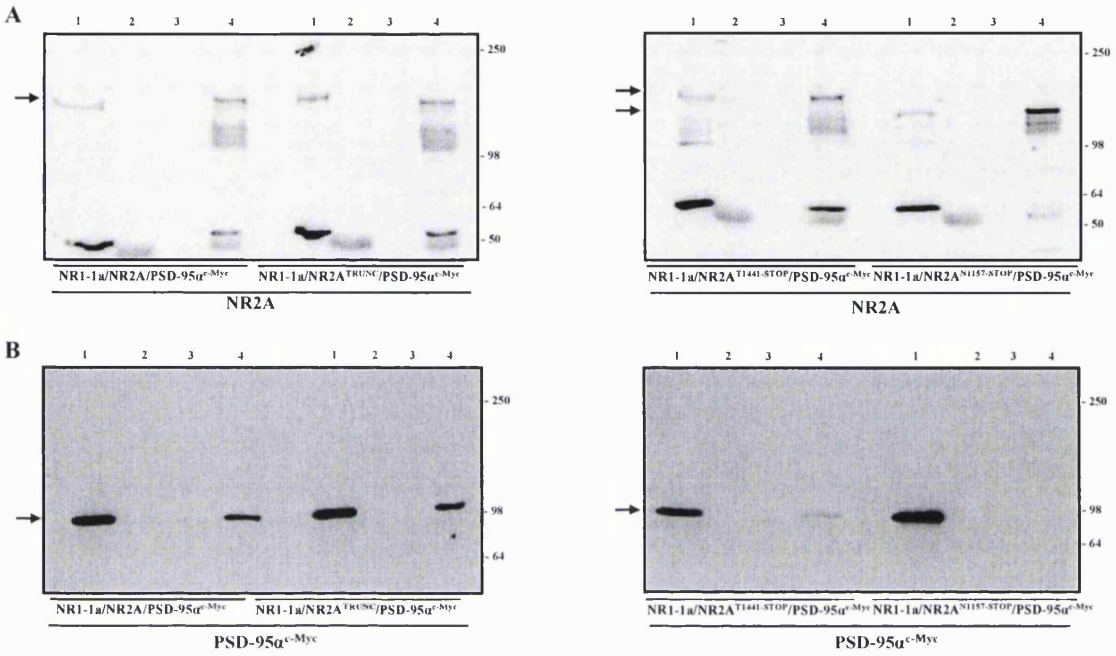

Figure 5.11 Demonstration of an additional PSD-95α$^{c\text{-}Myc}$ binding site when co-expressed with NR1-1a/NR2A, NR1-1a/NR2A^{TRUNC}, NR1-1a/NR2A$^{T1441\text{-}STOP}$ and NR1-1a/NR2A$^{N1157\text{-}STOP}$ NMDA receptors in HEK 293 cells

HEK 293 cells were transfected with NR1-1a/NR2A, NR1-1a/NR2A^{TRUNC}, NR1-1a/NR2A$^{T1441\text{-}STOP}$ and NR1-1a/NR2A$^{N1157\text{-}STOP}$ NMDA receptor clones + PSD-95α$^{c\text{-}Myc}$. Cell homogenates were prepared 24 h post-transfection, detergent-solubilised and immunoprecipitation assays were carried out using anti-NR1 C2 or non-immune antibodies. The resulting immune and non-immune pellets were analysed by immunoblotting using anti-NR2A (44-58) or anti-c-Myc antibodies, as indicated. The gel layout is the same for each immunoblot, lane 1 = detergent-soluble fraction, lane 2 = non-immune pellet, lane 3 = empty and lane 4 = immune pellet. Arrows denote NR2A subunits and PSD-95α$^{c\text{-}Myc}$. The positions of the protein molecular weight markers (kDa) are shown on the right. The immunoblots are representative of = 4 immunoprecipitations from n = 4 independent transfections.

5.2.8 Cell surface studies of NR1-1a/NR2A$^{T1441\text{-}STOP}$ and NR1-1a/NR2A$^{N1157\text{-}STOP}$ NMDA receptors following their expression in HEK 293 cells

The removal of the ESDV motif from NR2A subunits resulted in a significant 58 ± 9 % decrease in the cell surface expression of NR1-1a/NR2A^{TRUNC} NMDA receptors when compared to wild-type NR1-1a/NR2A receptors, Section 3.2.6. This demonstrated that the ESDV motif plays a role in the cell surface expression of NR1-1a/NR2A NMDA receptors. Additionally, a significant 15 ± 5 % decrease in the cell surface expression of NR1-1a/NR2A^{S1459A} NMDA receptors was also found, indicating that phosphorylation on S1459

is required for cell surface expression of wild-type NR1-1a/NR2A NMDA receptors, Section 4.2.7. It was therefore of interest to investigate the cell surface expression of NR1-1a/NR2A$^{T1441\text{-}STOP}$ and NR1-1a/NR2A$^{N1157\text{-}STOP}$ NMDA receptors following their co-expression in HEK 293 cells. HEK 293 cells were transfected in parallel with NR1-1a/NR2A, NR1-1a/NR2A^{TRUNC}, NR1-1a/NR2A$^{T1441\text{-}STOP}$ and NR1-1a/NR2A$^{N1157\text{-}STOP}$ NMDA receptor clones and cell surface ELISA assays were carried out using anti-NR2A (44-58) antibodies, Section 2.2.2.13. A histogram summarising the results is shown in Figure 5.12.

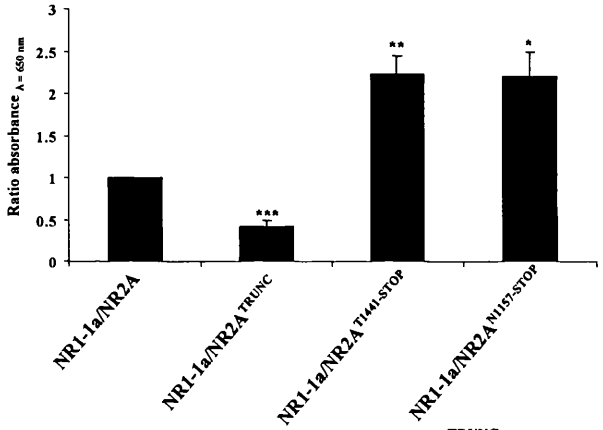

Figure 5.12 Cell surface studies of NR1-1a/NR2A, NR1-1a/NR2A^{TRUNC}, NR1-1a/NR2A$^{T1441\text{-}STOP}$ and NR1-1a/NR2A$^{N1157\text{-}STOP}$ NMDA receptors following their co-expression in HEK 293 cells

HEK 293 cells were transfected with NR1-1a/NR2A, NR1-1a/NR2A^{TRUNC}, NR1-1a/NR2A$^{T1441\text{-}STOP}$ and NR1-1a/NR2A$^{N1157\text{-}STOP}$ NMDA receptor clones. ELISA assays were performed 24 h post-transfection using anti-NR2A (44-58) antibodies. Results are expressed as the fold change of cell surface expression, i. e. truncated NR2A cell surface expression / wild-type NR2A cell surface expression. The histogram summarises the mean fold enhancement ± SEM for each combination. The results expressed in the histogram are the mean fold enhancement from n = 7 independent transfections (*** = $p < 0.001$, ** = $p < 0.005$. * = $p < 0.01$).

In agreement with results found previously, a significant decrease in the cell surface expression of NR1-1a/NR2A^{TRUNC} NMDA receptors was observed when compared to wild-type NR1-1a/NR2A NMDA receptors. However, it was found that there was a significant increase in the cell surface expression of both NR1-1a/NR2A$^{T1441\text{-}STOP}$ and NR1-1a/NR2A$^{N1157\text{-}STOP}$ NMDA receptors when compared to NR1-1a/NR2A NMDA receptors. A fold increase of 2.2 ± 0.2 ($p < 0.005$, n = 7) was observed for NR1-1a/NR2A$^{T1441\text{-}STOP}$ NMDA receptors and 2.2 ± 0.3 ($p < 0.01$, n = 7) was observed for NR1-1a/NR2A$^{N1157\text{-}STOP}$ NMDA receptors. There was no significant difference observed when comparing the cell

surface expression between NR1-1a/NR2A$^{T1441\text{-}STOP}$ and NR1-1a/NR2A$^{N1157\text{-}STOP}$ NMDA receptors.

5.2.9 Cell surface expression of NR1-1a/NR2A$^{T1441\text{-}STOP}$ and NR1-1a/NR2A$^{N1157\text{-}STOP}$ NMDA receptors in the presence and absence of PSD-95α$^{c\text{-}Myc}$

The co-expression of PSD-95α$^{c\text{-}Myc}$ with NR1-1a/NR2A NMDA receptors results in a significant enhancement of cell surface expression. This enhancement was abolished when the ESDV motif on NR2A subunits was removed. Therefore, the cell surface expression of NR1-1a/NR2A$^{T1441\text{-}STOP}$ and NR1-1a/NR2A$^{N1157\text{-}STOP}$ NMDA receptors in the presence of PSD-95α$^{c\text{-}Myc}$ following their co-expression in HEK 293 cells was investigated. HEK 293 cells were transfected in parallel with NR1-1a/NR2A, NR1-1a/NR2A^{TRUNC}, NR1-1a/NR2A$^{T1441\text{-}STOP}$ and NR1-1a/NR2A$^{N1157\text{-}STOP}$ NMDA receptor clones in the presence and absence of PSD-95α$^{c\text{-}Myc}$. Cell surface ELISA assays were carried out using anti-NR2A (44-58) antibodies, Section 2.2.2.13. A summary of the results are shown in Figure 5.13. In agreement with previous findings the co-expression of PSD-95α$^{c\text{-}Myc}$ with NR1-1a/NR2A NMDA receptors resulted in a significant enhancement of cell surface expression. NR1-1a/NR2A^{TRUNC} NMDA receptors in the presence of PSD-95α$^{c\text{-}Myc}$ gave no significant change in cell surface expression. Lastly, both NR1-1a/NR2A$^{T1441\text{-}STOP}$ and NR1-1a/NR2A$^{N1157\text{-}STOP}$ NMDA receptors also did not show a significant change in their cell surface expression in the presence of PSD-95α$^{c\text{-}Myc}$.

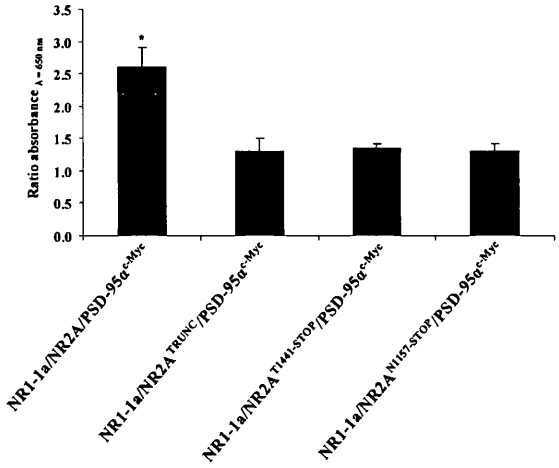

Figure 5.13 Cell surface studies of NR1-1a/NR2A, NR1-1a/NR2A^{TRUNC}, NR1-1a/NR2A$^{T1441\text{-}STOP}$ and NR1-1a/NR2A$^{N1157\text{-}STOP}$ NMDA receptors in the presence and absence of PSD-95α$^{c\text{-}Myc}$ following their co-expression in HEK 293 cells

HEK 293 cells were transfected with NR1-1a/NR2A, NR1-1a/NR2A^{TRUNC}, NR1-1a/NR2A$^{T1441\text{-}STOP}$ and NR1-1a/NR2A$^{N1157\text{-}STOP}$ NMDA receptor clones ± PSD-95α$^{c\text{-}Myc}$. ELISA assays were performed 24 h post-transfection using anti-NR2A (44-58) antibodies. Results are expressed as the fold enhancement, i. e. NR2A cell surface expression + PSD-95/ NR2A cell surface expression - PSD-95. The histogram summarises the mean fold enhancement ± SEM for each combination. The results expressed in the histogram are the mean fold enhancement from n = 5 independent transfections (* = $p < 0.005$).

5.3 DISCUSSION

The aim of this chapter was to investigate the location of an additional PSD-95 binding site within the NR2A and NR2B C-terminal domains. It was previously found that NR1-1a/NR2A^{TRUNC} NMDA receptor complexes associate with PSD-95$\alpha^{c\text{-}Myc}$ following their co-expression in HEK 293 cells (Rutter, 2001; Papadakis, 2004; Section 5.2.1). In this chapter it was shown that NR1-1a/NR2B$^{FLAG/TRUNC}$ NMDA receptor complexes are also able to associate with PSD-95$\alpha^{c\text{-}Myc}$. Thus both NR1/NR2A and NR1/NR2B NMDA receptors are able to associate with PSD-95 in a distal ESDV-independent mechanism. The location of additional PSD-95 binding motif (s) was further refined to be between amino acids 1157 – 1441 of the NR2A C-terminal domain.

The identification that PSD-95 associates to a site independent to the distal ESDV motif may play an important role in the regulation of these subtypes of NMDA receptors. Although the stoichiometry of the association between PSD-95 and NR2A subunits is not known, the identification of an additional PSD-95 binding site suggested that multiple copies of PSD-95 could associate with one NR2A subunit. This could have implications in terms of receptor cell surface stability. It is known that PSD-95 stabilises the cell surface expression of Tac-NR2B by decreasing their internalisation (Roche *et al.*, 2001). Therefore if more molecules of PSD-95 are able to bind onto these receptor subtypes this could result in their stabilisation. It would be interesting to determine if the NR2C and NR2D subunits also contain additional PSD-95 motifs. This may be why the differential enhancement of expression was observed in Chapter 3, between NR2A/NR2B versus NR2C/NR2D subunits when co-expressed with PSD-95 and chapsyn-110. If two or more molecules of PSD-95 bind to NR2A/NR2B subunits but not to NR2C/NR2D subunits, it may mean that PSD-95 is able to stabilise the expression of the former by a greater extent. For example, by protecting them further from cleavage by degradative enzymes such as calpain.

As mentioned previously in Chapter 1, PSD-95 contains 3 PDZ domains, an SH3 domain and a GK-like kinase domain. PSD-95 was shown to preferentially interact via the PDZII domain with the distal C-terminal ESDV binding motif (Niethammer *et al.*, 1996). Further

analysis of the NR2A C-terminal domain between amino acids 1157-1441 identified three putative PSD-95 binding sites, which are highlighted in Figure 5.14.

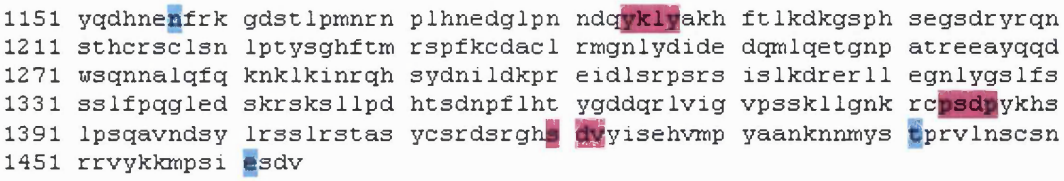

Figure 5.14 Prediction of additional PSD-95 binding motif present in amino acids 1157-1441 region of the NR2A C-termini

The additional PSD-95 binding motif was identified being present within amino acids 1157-1441 of NR2A subunits. Highlighted in ▯ = sites where STOP codons were introduced, ▯ = putative additional PSD-95 binding sites.

Firstly, amino acids 1420-1422 of the NR2A C-terminal are a putative internal PDZ domain binding consensus motif, SDV. It was demonstrated that PSD-95 favored the interaction with distal C-terminal ligands (Songyang *et al.*, 1997; Lim *et al.*, 2002). However, TRP calcium channels were found to associate with the PDZ domain-containing protein INAD via an internal PDZ domain binding motif (Shieh and Zhu, 1996). Therefore demonstrating that PDZ domains are able to bind to internal motifs, suggesting that PSD-95 may also be able to associate with NR2A or NR2B C-terminal domains in a similar fashion. Secondly, there are two putative SH3 domain consensus binding motifs. Both a typical and atypical SH3 domain binding motifs are present within this region, PXXP and YXXY respectively (where X is any amino acid, amino acids 1383-1387 and 1184-1187 respectively, for review see Kay *et al.,* 2000). The SH3 domain of PSD-95 and the NR2A C-terminal domain were shown not to associate by a yeast two-hybrid approach (Niethammer *et al.*, 1996). However, it is known that PSD-95 contains many protein interaction domains which work synergistically with each other (Long *et al.,* 2003). The SH3 domain is known to form in an intramolecular interaction with the GK-like domain (Shin *et al.*, 2000; Tavares *et al.*, 2001). Thus the PSD-95 SH3 domain conformation *in vivo* may differ from the conformation it adopts when expressed in isolation in yeast two-hybrid studies resulting in different binding affinities. Lastly, both the putative PDZ and SH3 domain binding motifs have a glycine residue upstream from their consensus sequences. Glycine is a planar amino acid which may form a 'kink' in the polypeptide exposing the amino acids to form the binding site. Therefore, further truncations could be

generated at amino acid residues 1184, 1383 and 1420 of the NR2A subunit and immunoprecipitations performed to investigate their association with PSD-95.

In contrast to the results found in this chapter, Prybylowski *et al.* (2005) demonstrated NR1-1a/NR2B^{S1480A} NMDA receptors no longer co-immunoprecipitated with PSD-95 following their co-expression in HEK 293 cells. Prybylowski *et al.* (2005) solubilised their transfected HEK 293 cells using 1 % (v/v) deoxycholate whilst the detergent-solubilisation methods employed for immunoprecipitations here were 1 % (v/v) Triton X-100 and 240 mM NaCl. Thus the solubilisation conditions utilised are less harsh and may detect relatively weaker interactions. Additionally, Prybylowski *et al.* (2005) transfected their HEK 293 cells in a ratio of 5NR1: 10NR2B: 1PSD-95 whilst the ratio used in the above experiments was 2.5NR1: 7.5NR2B: 10PSD-95. This aroused suspicion that the association detected may be an artefact. However, no association was observed with the negative control, i.e. NR1-1a/NR2A$^{N1157\text{-}STOP}$ NMDA receptors did not co-immunoprecipitate with PSD-95, suggesting that the interactions determined are not due to over-expression of PSD-95.

Interestingly NR1-1a/NR2A$^{T1441\text{-}STOP}$ and NR1-1a/NR2A$^{N1157\text{-}STOP}$ NMDA receptors both resulted in a significant ~ 2 fold increase in their cell surface expression when compared to wild-type NR1-1a/NR2A NMDA receptors. The total expression NR2A$^{T1441\text{-}STOP}$ and NR2A$^{N1157\text{-}STOP}$ subunits was not significantly different to the total expression the wild-type NR2A subunits. Thus, the last 24 amino acids of the NR2A C-terminal domain appears to contain an interplay of motifs which regulate the cell surface expression of NR1-1a/NR2A NMDA receptors. As found previously in Chapter 3, NR1-1a/NR2A^{TRUNC} NMDA receptors had a significant decrease in their cell surface expression demonstrating that the ESDV motif is required for normal cell surface expression. The observation that a reduced expression of NR1-1a/NR2A^{TRUNC} NMDA receptors are expressed at the cell surface is in agreement with Roche *et al.* (2001) and Lavezzari *et al.* 2004, who demonstrated that the deletion of the last four amino acids, i.e. ESDV, resulted in a decrease in the Tac-NR2A$^{\Delta 7}$ and Tac-NR2B$^{\Delta 7}$ cell surface expression. This decrease in cell surface expression of Tac-NR2B$^{\Delta 7}$ was due to an internalization motif, YEKL, which is adjacent to the last four

amino acids of the NR2B subunits (Roche *et al.*, 2001; Lavezzari *et al.*, 2003). This tyrosine is conserved within the NR2A subunit where a putative internalization motif is present, YKKM. However in contrast to the findings in this chapter, the deletion of the last 11 amino acids on the NR2A C-terminal domain, i.e. both the ESDV and YKKM motifs, resulted in no change in the cell surface expression of Tac-NR2A$^{\Delta 11}$ chimeras suggesting that this YKKM motif does not play a role in the cell surface expression of NR1/NR2A receptors (Lavezzari *et al.*, 2004). In the above experiments a full length receptor was expressed whilst Lavezzari *et al.* (2004) used Tac-NR2A chimeras which may explain the discrepancy between the results. In addition the experiments by Lavezzari *et al.* (2004) were performed in Hela cells, which may not have similar endogenous scaffolding proteins when compared to HEK 293 cells. Lastly, instead of the YKKM motif, there may be a novel internalization motif present within the last 24 amino acids of the NR2A subunit. Therefore, there are regulatory signals present on the distal C-terminal domain of NR2A subunits which regulates the cell surface expression of NR1-1a/NR2A NMDA receptors in HEK 293 cells. These signals should be further investigated by the generation of additional truncations to locate which amino acids which are responsible for the maintenance of NR1-1a/NR2A NMDA receptors cell surface expression.

In summary, in this chapter it was shown that:-

- NR1-1a/NR2B$^{FLAG/TRUNC}$, like NR1-1a/NR2A^{TRUNC}, NMDA receptors were found to still co-immunoprecipitate with PSD-95$\alpha^{c\text{-}Myc}$ following their co-expression in HEK 293 cells. The additional PSD-95 interaction motif (s) is located between amino acids 1157 – 1441 of the NR2A C-terminal domain.
- A significant enhancement in the cell surface expression was observed for NR1-1a/NR2A$^{T1441\text{-}STOP}$ and NR1-1a/NR2A$^{N1157\text{-}STOP}$ NMDA receptors when compared to wild-type NR1-1a/NR2A NMDA receptors. This suggested that the distal C-terminal domain of NR2A subunits plays a role in the regulation of their cell surface expression.

CHAPTER 6

RESULTS IV

DISCUSSION IV

6.1 RATIONALE

6.1.1 Identification of specific NR2D subunit protein interactors

As discussed in the Chapter 1, the NR2 subunit family members are considered the modulatory subunits of NMDA receptors. They are thought to influence the pharmacological properties, receptor localisation and the downstream intracellular signalling pathways to which the receptor is coupled. The predicted C-terminal domains of the NR2 subunits are ~ 400 – ~ 600 amino acids in length and are highly divergent. This gives many opportunities for unique protein interaction sites on each of the NR2 subunits that mediate receptor trafficking and signalling. For example, mutant mice expressing NR2 subunits lacking their C-terminal domain demonstrated specific phenotypes: transgenic animals in which the wild-type NR2A subunits were replaced by NR2A C-terminal domain deleted subunits had impaired synaptic plasticity and contextual memory: transgenic animals in which the wild-type NR2B subunits were replaced by NR2B C-terminal domain deleted subunits resulted in death perinatally (Sprengel *et al.*, 1998). These findings suggested that the C-terminal domain of each NR2 subunit contributes to the linkage of downstream signalling pathways.

As shown in Section 3, NR1-1a/NR2D NMDA receptor complexes were found to immunoprecipitate with each of the PSD-95 MAGUK family of proteins following their co-expression in HEK 293 cells. However, no change in the total expression of NR2D subunits was observed when NR1-1a/NR2D NMDA receptors were co-expressed with each PSD-95 MAGUK. This suggested that NR2D-containing receptors may interact differently with PSD-95 MAGUK proteins compared to NR2A- and NR2B-containing receptors. Indeed, it was demonstrated that the NR2D C-terminal domain associated with a lower affinity to PSD-95 compared to the NR2A C-terminal domain (Mi *et al.*, 2004). Further, NR2D-containing NMDA receptors have been shown to be localised in extrasynaptic sites suggesting that they may not associate with the PSD-95 MAGUK family *in vivo* (Brickley *et al.*, 2003). NR2D-containing receptors may therefore have a different set of interacting proteins to traffic and regulate this NMDA receptor subtype.

Analysis of the NR2D C-terminal domain amino acid sequence revealed many potential protein domain interaction motifs, these were as follows:

1. **SH3 consensus motifs.** SH3 domains are common protein interaction domains which is ~ 60 amino acids in length. They are found in a variety of proteins such as tyrosine kinases, scaffolding proteins and adaptor proteins. The consensus sequence for the SH3 domain binding is PXXP (where X is any amino acid). The NR2D C-terminal domain contains 10 PXXP motifs compared to only 1 found in the NR2A C-terminal domain, 5 in the NR2B C-terminal domain and 4 in the NR2C C-terminal domain.
2. **Tryptophan-tryptophan (WW) consensus motif.** WW domains are 38 amino acids in length and are named after two conserved tryptophan residues which are found between 20-22 amino acids apart in the consensus sequence. The consensus sequence for WW domains is PPXX. Both the NR2C and NR2D C-terminal domains contain 1 predicted WW domain. NR2A and NR2B C-terminal domains do not have a WW domain consensus sequence.
3. **Internalisation consensus motifs.** Internalisation motifs have been characterised for NR2A and NR2B subunits. The distal C-terminal YEKL motif for NR2B subunits and a LL motif for NR2A subunits were shown to play a role in the internalisation of Tac-NR2A and Tac-NR2B chimeras, respectively (Roche *et al.*, 2001; Lavezzari *et al.*, 2003; Lavezzari *et al.*, 2004). The NR2D C-terminal domain contains 2 YXXL and 3 LL internalisation motifs.
4. **ER retention consensus motifs.** The ER retention RRR motif is well characterised for the NR1 subunit (Standley *et al.*, 2000; Scott *et al.*, 2001; Xia *et al.*, 2001). However, no ER retention motifs have not yet been successfully identified for NR2 subunits. The NR2D C-terminal domain contains 4 RXR motifs. An ER export motif was identified of the NR2A and NR2B subunits, which was found to be an overlapping motif EHL/HDLF present at the start of the C-terminal domains (Hawkins *et al.*, 2004; Yang *et al.*, 2007). This motif is conserved for each NR2 subunit.

5. **Tyrosine kinase interaction motifs**. It was found that amino acids 866-1064 of the NR2D C-terminal domain associate with the tyrosine kinase c-Abl (Glover *et al.*, 2000).

The amino acid sequence of the predicted NR2D C-terminal domain is shown in Figure 6.1 where internalisation, ER retention, WW and SH3 consensus sequences are highlighted. A yeast two-hybrid screen was therefore carried out with the purpose of the identification of NR2D subunit interacting proteins.

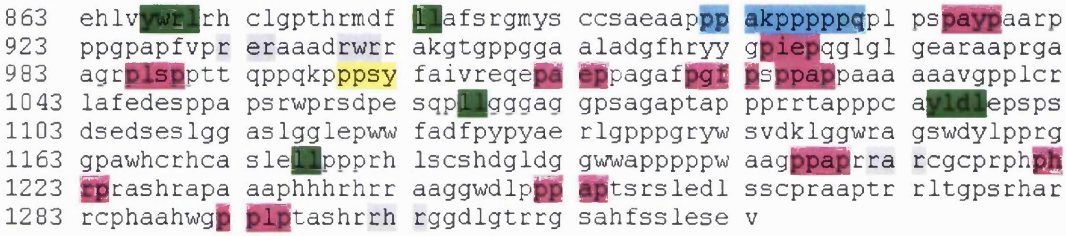

Figure 6.1 The amino acid sequence of the C-terminal domain of NR2D subunits

The C-terminal domain of NR2D subunits was predicted by Ikeda *et al.* (1992) and additionally by carrying out a SMART analysis using the program found at http://smart.embl-heidelberg.de. The amino acids highlighted in green are predicted internalisation consensus sequences, amino acids highlighted in grey are putative ER retention motifs, yellow are predicted WW domain, amino acids highlighted in pink are the PXXP SH3 binding motif and the amino acids highlighted in blue is the region predicted to interact with the tyrosine kinase c-Abl (Glover *et al.*, 2000).

6.1.2 Introduction to yeast two-hybrid system

The GAL4 transcription factor has two functional domains namely the DNA-binding domain and the activation domain. The DNA-binding domain binds to an upstream activation sequence (UAS) which is near the transcription promoter whilst the activation domain forms the transcription complex made from accessory proteins. Each domain maintains its function even if the other domain has been deleted (Keegan *et al.*, 1986). Transcription is initiated when the DNA-binding domain and activation domain are in close proximity, this discovery became the basis of the yeast two-hybrid system (Fields and Song, 1989; for review see Fields and Sternglanz, 1994). Expression vectors have been designed which contain the cDNA for either the DNA-binding or activation domain. The whole or portion of a protein of interest can be genetically fused to either domain. The

fusion protein containing the DNA-binding domain is termed the bait whilst the fusion protein containing the activation domain is termed the prey.

AH109 and Y187 yeast cell lines have been engineered to be unable to grow in media lacking the amino acids leucine (Leu) and tryptophan (Trp). Therefore, the expression vectors also contain nutritional selective markers for leucine and tryptophan. Thus regardless of whether the proteins of interest interact with each other; yeast cell growth will be observed on -Leu/-Trp selective dropout plates indicating successful co-transformation of both the DNA-binding domain and the activation domain containing vectors into the yeast cells. Figure 6.2 summarises the yeast two-hybrid system.

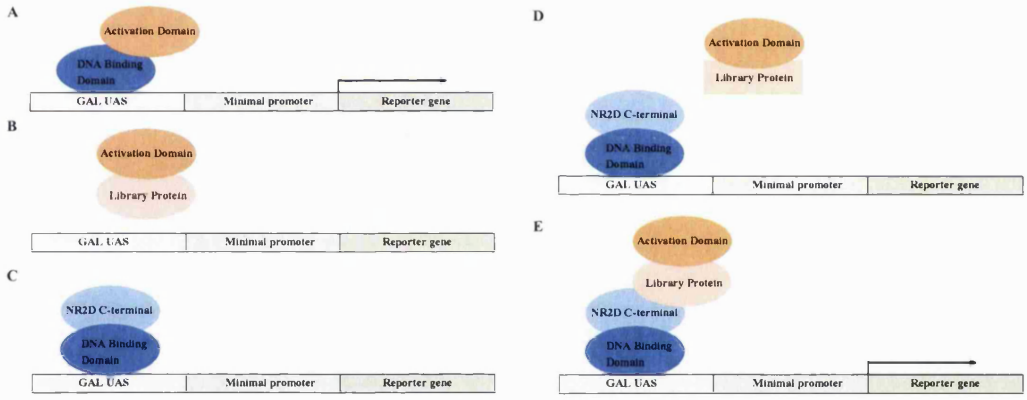

Figure 6.2 A diagram summarising the GAL4 yeast two-hybrid system

As shown in the above diagram, when the DNA-binding domain and activation domain are in close proximity this activates transcription, **A**. The expression of a DNA-binding domain, **B**, or a activation domain, **C**, alone does not activate transcription. The co-expression of a bait and prey which do no interact also results in no activation in transcription, **D**. However the co-expression of a bait and prey which do show an interaction brings the activation and DNA-binding domain into close proximity thus activating transcription, **E**.

AH109 and Y187 yeast cell lines also have an inactivated GAL4 gene. This allows reporter genes to be under the control of the GAL4 gene. If the proteins of interest interact with each other this results in the DNA-binding domain being in close proximity to the activation domain resulting in an activation of transcription of the reporter genes. The GAL4 yeast two-hybrid system has four reporter genes, which are summarised in Figure 6.3. Two of the reporter genes are nutritional, i.e. histidine (His) and adenine (Ade). Thus

-Leu/-Trp/-His/-Ade selective dropout plates lack these nutrients so the yeast cells have to synthesise these by activation of the reporter genes demonstrating an interaction. The remaining two markers are for the α- and β-galactosidase enzyme, which produces a blue phenotype in the presence of X-gal. The activation of transcription results in yeast cell growth being observed on -Leu/-Trp/-His/-Ade selective dropout plates. However if the proteins of interest do not interact with each other, the DNA-binding domain and activation domain are not positioned in close enough proximity to activate transcription and no yeast cell growth would be observed on -Leu/-Trp/-His/-Ade selective dropout plates.

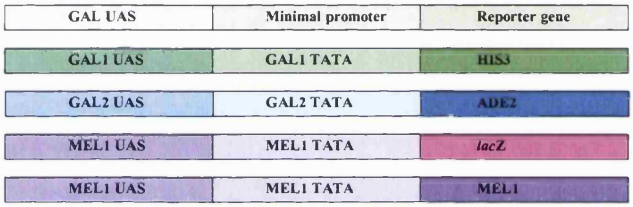

Figure 6.3 The reporter genes used in the yeast two-hybrid system

The yeast two-hybrid system has four reporter genes, as depicted above. When the DNA-binding domain and the activation domain are in close proximity this results in transcription. Two of the reporter genes are nutritional markers, i.e. His and Ade which are both under the control different promoter sequences. The β- and α-galactosidase enzymes are encoded by the *lacZ* and MEL1 genes, respectively and the expression of each enzyme is under the control of the MEL1 UAS. The above diagram is adapted from the 'Yeast Methods Handbook' by Clontech

6.2 RESULTS

6.2.1 Generation and characterisation of pGBKT7NR2D and pGBKT7NR2D^{TRUNC} constructs

6.2.1.1 Generation of pGBKT7NR2D and pGBKT7NR2D^{TRUNC} constructs

The numbering of the NR2D C-terminal domain was predicted by Ikeda *et al.* (1992) and also checked using the simple modular architecture research tool program (SMART analysis, http://smart.embl-heidelberg.de). Therefore, the NR2D C-terminal domain was amplified from nucleotide numbers 2587 – 3969, which corresponds to amino acid residues 863 – 1323. Primers were designed to amplify the NR2D C-terminal domain using pcDNANR2D as the template DNA. However, due to problems amplifying this region additional primers were designed and tested, as shown in Section 2.1.8. The C-terminal domain was successfully PCR amplified using forward primer 2 and reverse primer 2, Section 2.2.1.2.6. The NR2D C-terminal domain that was amplified corresponded to amino acids 864 – 1323. This does not include the first amino acid of the predicted C-terminal domain, which disrupts the EHL/HLFY motif identified as ER export motifs for NR2A and NR2B subunits (Hawkins *et al.*, 2004; Yang *et al.*, 2007).

The resulting PCR product was subsequently analysed by flat bed agarose gel electrophoresis, Section 2.2.1.2.2. A specific band was observed with a size of ~ 1.3 kB which corresponded to the predicted size of the NR2D C-terminal domain. This PCR product was PCR purified, restriction endonuclease digested and ligated into a restriction endonuclease digested, dephosphorylated pGBKT7 vector, Sections 2.2.1.2.7 – 2.2.1.2.9. The ligated products were then transformed into DH5α *E.coli* cells and amplified by mini-preparations of plasmid DNA, Sections 2.2.1.1.3 and 2.2.1.1.7. The resulting amplified plasmid DNA was restriction endonuclease digested and analysed by flat bed agarose gel electrophoresis to ensure an insert of the correct size was present, Section 2.2.1.2.1 and 2.2.1.2.2. Lastly the clone was sent for DNA nucleotide sequencing to ensure the insert was in frame with the DNA-binding domain and was the correct sequence, Section 2.2.1.2.3, Appendix 2.5.

The NR2D C-terminal domain contains the ES(D/E)V PSD-95 MAGUK motif, therefore to investigate if the identified interactors from the yeast two-hybrid screen interacted in a ES(D/E)V dependent manner the last 6 amino acids were deleted. The last 6 amino acids of the NR2D C-terminal domain were deleted by the introduction of a STOP codon at amino acid 1318. *In vivo* site-directed mutagenesis was performed using pGBKT7NR2D as the template, Section 2.2.1.2.10. The resulting clone was sent for DNA nucleotide sequencing to ensure the correct mutation was present and no additional mutations were generated.

6.2.1.2 Expression of NR2D and NR2D^{TRUNC} C-terminal domains following their expression in AH109 yeast cells

To ensure both NR2D and NR2D^{TRUNC} C-terminal domains were successfully expressed, AH109 yeast cells were transformed with pGBKT7, pGBKT7NR2D or pGBKT7NR2D^{TRUNC}, proteins were extracted and subsequently analysed by immunoblotting using anti-c-Myc antibodies, Sections 2.2.1.3.3, 2.2.1.3.4 and 2.2.1.3.9. Representative immunoblots are shown in Figure 6.4. No immunoreactive bands were observed in the untransformed yeast cell protein extraction lanes. Immunoreactive bands are present for the size of the correct predicted DNA-binding domain at AH109 yeast cells transformed with pGBKT7, 39 ± 1 kDa (n = 6). Immunoreactive bands at the correct predicted molecular weight for both the NR2D and NR2D^{TRUNC} C-terminal domains were observed, i.e. NR2D, 87 ± 6 kDa (± SD, n = 6) and NR2D^{TRUNC}, 84 ± 3 kDa (n = 6). Thus, the constructs were successfully expressed following their transformation in AH109 yeast cells.

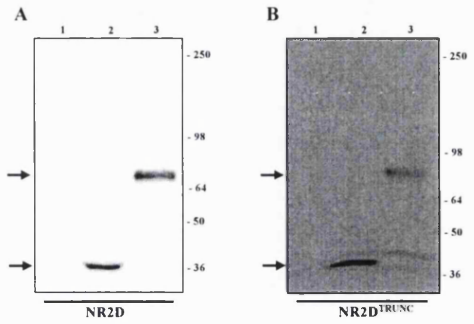

Figure 6.4 Immunoblots to demonstrate the expression of NR2D and NR2D^{TRUNC} C-terminal domains following their expression in AH109 yeast cells

A single colony of AH109 yeast cells pre-transformed with NR2D, NR2D^{TRUNC} or pGBKT7 clones were used to inoculate separate 5 ml of -Trp selective media cultures and grown at 30°C for 48 h at 250 rpm. Proteins were extracted from the resulting yeast cell pellets and analysed by immunoblotting using anti-c-Myc antibodies. The gel layout is the same for each immunoblot, lane 1 = untransformed AH109 yeast cell protein extractions, lane 2 = pGBKT7 and lane 3 = **A**. NR2D and **B**. NR2D^{TRUNC}. Arrows denote the positions of either the DNA-binding domain, NR2D or NR2D^{TRUNC} C-terminal domains. The molecular weight markers are shown on the right hand side. The immunoblots are representative of n = 3 independent transformations.

6.2.1.3 Co-Expression of pGBKT7NR2D or pGBKT7NR2D^{TRUNC} with pGADT7 to test for auto-activation of reporter genes

Both NR2D and NR2D^{TRUNC} C-terminal domains were successfully expressed in AH109 yeast cells. Before the cDNA mouse brain library screening could be carried out it was necessary to ensure the expression of NR2D and NR2D^{TRUNC} C-terminal domains did not auto-activate the reporter genes when co-transformed with an empty vector, pGADT7. Auto-activation refers to the activation of the reporter genes in the absence of a positive protein interaction, i.e. the bait is able to activate reporter genes when transformed with an empty vector. Therefore, AH109 yeast cells were co-transformed with pGBKT7NR2D or pGBKT7NR2D^{TRUNC} clones in the presence of pGADT7, Sections 2.2.1.3.3 and 2.2.1.3.4. A positive control was included alongside all test co-transformations, i.e. pVA3-1 and pTD1-1. As a negative control the empty vectors pGBKT7 and pGADT7 were co-transformed and additionally pVA3-1 and pTD1-1 were each co-transformed with the corresponding empty vector, i.e. pVA3-1/pGADT7 and pTD1-1/PGBKT7. The resulting transformed yeast cells were incubated for 5 days at 30°C and the subsequent colonies were counted.

As shown in Table 6.1, all co-transformations were successful due to the presence of yeast colonies on the -Leu/-Trp selective medium plates. As expected there was yeast cell growth when co-transforming the positive controls, pVA3-1/pTD1-1 on -Leu/-Trp/-His/-Ade selective medium plates, demonstrating a protein-protein interaction is activating the reporter genes. The negative controls did not show any yeast cell growth on -Leu/-Trp/-His/-Ade selective medium plates. Lastly both pGBKT7NR2D and pGBKT7NR2D^{TRUNC} did not show any yeast cell growth on the -Leu/-Trp/-His/-Ade selective medium plates. Thus it was found that the expression of both the NR2D and NR2D^{TRUNC} C-terminal domains in AH109 yeast cells did not auto-activate the reporter genes and therefore can be used for further study.

Activation domain construct	**DNA-binding domain construct**	**-Leu/-Trp selective medium**	**-Leu/-Trp/-His/-Ade selective medium**
pGADT7	pGBKT7NR2D	+	-
pGADT7	pGBKT7NR2D^{TRUNC}	+	-
pTD1-1	pVA3-1	+	+
pGADT7	pVA3-1	+	-
pTD1-1	pGBKT7	+	-
pGADT7	pGBKT7	+	-

Table 6.1 Characterisation of NR2D and NR2D^{TRUNC} C-terminal domains following their co-expression with pGADT7 in AH109 yeast cells

AH109 yeast cells were co-transformed with NR2D or NR2D^{TRUNC} clones and pGADT7. The manufacturer's positive control clones, pTD1-1 and pVA3.1 were co-expressed and each positive control clone was co-expressed alongside an empty vector, i.e. pGBKT7 or pGADT7, as appropriate. Yeast cell colonies were counted 5 days after transformation, where - = no yeast growth, + = yeast growth.

6.2.2 Library screening using pGBKT7NR2D as bait

6.2.2.1 Library screening using pGBKT7NR2D as bait

The NR2D C-terminal domain was shown to be successfully expressed in yeast cells and did not auto-activate the reporter genes. Therefore a yeast two-hybrid cDNA mouse brain library scale screen was carried out to identify novel protein interactions with the NR2D C-terminal domain. For the library screening, a sequential transformation approach was taken to allow the transformation of the mouse brain cDNA library to be the limiting factor, i.e. instead of 2 plasmids having to be co-transformed into AH109 yeast cells, pGBKT7NR2D will already by pre-transformed in the yeast cells, allowing the transformation of the library

plasmids to be limiting factors. A summary of the screening method is shown in Figure 2.3. Before the library scale transformation was performed, the cDNA mouse brain library was titred in yeast cells to calculate the amount of plasmid DNA required to ensure that each clone was represented a minimum of 3 times thereby allowing rare clones to be represented in the screen, Section 2.2.1.3.5.2. Once the library was successfully titred, a library scale screen was carried out as in Section 2.2.1.3.5.3. Yeast colonies which appeared on the -Leu/-Trp/-His/-Ade selective medium plates were picked and subsequently grown on fresh -Leu/-Trp/-His/-Ade selective medium plates. A yeast colony which had grown on -Leu/-Trp/-His/-Ade selective medium plates after having been re-streaked a total of three times was considered a putative positive interactor. The library screen resulted in ~ 240 putative positive interactors which were divided into strong or weak interactions depending on when yeast cell growth was observed. Colonies which appeared 3-5 days after transformation were considered strong interactors and those which appeared 5-7 days were called weak interactors. A yeast mating strategy was carried out to test the specificity of the putative positive interactors.

6.2.2.2 Verification of putative positive interactors with the NR2D C-terminal domain via yeast mating assays

The yeast mating strategy had the advantage of saving both time and resources allowing a larger number of putative positive interactions to be screened. From the original ~ 240 putative positive interactors, 60 strong and 60 weak interactors were randomly selected and the yeast mating strategy was carried out to verify if the clones specifically interacted with the NR2D C-terminal domain, Section 2.2.1.3.7.

As previously described in the Section 2, yeast cells were segregated to obtain a homogenous population of AH109 yeast cells containing theoretically only the cDNA mouse brain library clone and these were subsequently mated with Y187 yeast cells pre-transformed with either:

1. pGBKT7NR2D to test if the putative positive interactor still interacted with the NR2D C-terminal domain.

2. pGBKT7 to test if the putative positive interactor resulted in the auto-activation of reporter genes.
3. pVA3-1 to test if the putative positive interactor bound indiscriminately to other proteins.

As a positive control, AH109 yeast cells pre-transformed with pTD1-1 were mated with Y187 yeast cells pre-transformed with pVA3-1. A negative control was carried out by mating AH109 cells pre-transformed with pGAD10 and Y187 yeast cells pre-transformed with pVA3-1. From the 60 strong and 60 weak interactors, diploid yeast cell growth was observed on all of the -Leu/-Trp selective medium plates thus demonstrating the yeast mating assays were successful. Diploid yeast cell growth was observed on -Leu/-Trp/-His/-Ade selective medium plates for the positive control but not for the negative control. From the 120 putative positive clones screened it was found that 20 clones were true positive interactors with the NR2D C-terminal domain following their co-expression in yeast. From the 20 identified, 19 were from the strong interactor group, whilst 1 was thought of as a weak interactor in the yeast two-hybrid system. The strong interactor clones were numbers 1, 2, 3, 6, 11, 14, 15, 26, 27, 37, 38, 40, 41, 43, 45, 47, 49, 52 and 55. The weak interactor clone was number 44.

Plasmid DNA was extracted from the 20 positive interactors and transformed into *DH5α E.coli* cells. From the transformed *DH5α E.coli* cells, three individual colonies were picked, amplified by a mini-preparation of plasmid DNA and the insert size analysed by restriction endonuclease digestion and subsequently separated by flat bed agarose gel electrophoresis, Sections 2.2.1.2.1, 2.2.1.2.2, 2.2.1.3.8, 2.2.1.1.5 and 2.2.1.1.7. Each positive interactor was analysed in triplicate because, unlike bacteria, yeast are able to replicate multiple plasmid DNAs. Table 6.2 shows a summary of the resulting insert sizes gained for the positive clones.

Clone Number	Calculated insert size (bp)
1	~ 1000
2	~ 1000
3	~ 900
6	~ 1750
11	~ 1000
14	~ 1000
15	~ 1000
26	~ 2700
27	~ 1400
37	~ 1700
38	~ 1000
40	~ 1100
41	~ 1100
43	~ 1500
44	~ 1250
45	~ 1250
47	~ 1500
49	~ 3000
52	~ 1000
55	~ 750

Table 6.2 Identification of the insert size for the positive cDNA mouse brain library interactors

AH109 yeast cells containing the identified positive cDNA mouse brain library interactor plasmids were grown as patches on -Leu selective plates and grown at 30°C until cell growth was observed. Plasmid DNA was extracted from AH109 yeast cells, transformed into DH5α *E.coli* by electroporation and mini-preparations of plasmid DNA were carried out. The plasmid DNA was then analysed by restriction endonuclease digestion and subsequently separated by flat bed agarose gel electrophoresis. The resulting insert sizes were calculated and are shown in the above table. Each insert was present in at least n = 2 of the n = 3 separate clones analysed per positive interactor.

6.2.2.3 Determination of interactions between the positive interactors with NR2D^{TRUNC} C-terminal domain

The 20 identified positive interactors of the NR2D C-terminal domain were further characterised to investigate if the interaction was mediated by the PDZ domain consensus ESEV motif. Thus AH109 yeast cells pre-transformed with the positive interactor were mated with Y187 yeast cells pre-transformed with NR2D, NR2D^{TRUNC}, pGBKT7 or pVA3-1. Appropriate positive and negative controls were carried out in parallel, as discussed in Section 6.2.2.2. A summary of the yeast mating results is shown in Table 6.3. There was diploid yeast cell growth on all of the -Leu/-Trp selective medium plates thus demonstrating the yeast mating assays were successful. Yeast cell growth was observed on -Leu/-Trp/-His/-Ade selective media plates for diploids expressing pVA3-1 and pTD1-1 but absent from diploids expressing pGBKT7 and pVA3-1. All of the positive clones, except clone 45, were found to interact with the NR2D^{TRUNC} C-terminal domain.

Clone number	Diploid cell growth on -Leu/-Trp selective medium				Diploid cell growth on -Leu/-Trp/-His/-Ade selective medium			
	NR2D	NR2D^{TRUNC}	pGBKT7	pVA3-1	NR2D	NR2D^{TRUNC}	pGBKT7	pVA3-1
1	+	+	+	+	+	+	-	-
2	+	+	+	+	+	+	-	-
3	+	+	+	+	+	+	-	-
6	+	+	+	+	+	+	-	-
11	+	+	+	+	+	+	-	-
14	+	+	+	+	+	+	-	-
15	+	+	+	+	+	+	-	-
26	+	+	+	+	+	+	-	-
27	+	+	+	+	+	+	-	-
37	+	+	+	+	+	+	-	-
38	+	+	+	+	+	+	-	-
40	+	+	+	+	+	+	-	-
41	+	+	+	+	+	+	-	-
43	+	+	+	+	+	+	-	-
44	+	+	+	+	+	+	-	-
45	+	+	+	+	+	+	-	-
47	+	+	+	+	+	+	-	-
49	+	+	+	+	+	+	-	-
52	+	+	+	+	+	+	-	-
55	+	+	+	+	+	+	-	-
pTD1-1	+	+	+	+	-	-	-	+
pGAD10	+	+	+	+	-	-	-	-

Table 6.3 A summary of the yeast mating assays with the NR2D^{TRUNC} C-terminal domain to test the specificity of the interaction

AH109 yeast cells pre-transformed with the cDNA mouse brain library positive interactor were mated with Y187 yeast cells pre-transformed with NR2D, NR2D^{TRUNC}, pGBKT7 and pVA3-1. As a positive control AH109 yeast cells pre-transformed with pTD1-1 were mated with Y187 yeast cells pre-transformed with pVA3-1. A negative control was carried out by mating AH109 cells pre-transformed with pGAD10 and Y187 yeast cells pre-transformed with pVA3-1. The diploids were incubated for 5 days at 30°C and the resulting diploid colonies were counted. The above table summarises the diploid yeast cell growth observed on -Leu/-Trp and -Leu/-Trp/-His/-Ade selective medium, where - = no yeast growth, + = yeast growth. Results are representative of at least n = 2 independent yeast mating assays.

6.2.2.4 Nucleotide sequencing for the positive interactors

The positive interactors were sent for nucleotide sequencing using a primer which hybridised in the activation domain. During the synthesis of the library, the cDNA was cloned into the pACT2 vector via a common adaptor sequence. Therefore, when analysing the positive interactor cDNA sequences this adaptor sequence was not included in the analysis. For each positive interactor the nucleotide sequence was translated using the 'Translate' program (http://www.expasy.org/tools/dna.html). The positive interactor clones were analysed to ensure the sequence was in frame with the activation domain. Clones 1, 2, 3, 6, 14, 38, 43, 44 and 45 were found to be short peptide sequences in frame + 1. Thus no further analysis was carried out for these clones. Table 6.4 summarises the clones resulting in short peptide sequences.

Clone number	Peptide number in frame + 1
1	22
2	57
3	93
6	44
14	10
38	10
43	113
44	17
45	17

Table 6.4 A summary of the cDNA library clones resulting in short peptide sequences

The nucleotide sequences for clones 1, 2, 3, 6, 14, 38, 43, 44 and 45 were translated using the 'Translate' program available at http://www.expasy.org/tools/dna.html and found to be short peptide sequences. The above table summarises the number of amino acids in the + 1 frame.

The translation of clones 11, 15, 27, 37, 40, 41, 47, 49, 52 and 55 revealed they all had amino acid sequences which were in frame with the activation domain and database searching was carried out for these clones.

6.2.2.5 Nucleotide and amino acid sequence database searching for the positive interactors

Clones 11, 15, 27, 37, 40, 41, 47, 49, 52 and 55 were all found to be in frame with the activation domain therefore nucleotide and amino acid BLAST searches were carried out using the National Centre for Biotechnology Information (NCBI) database (www.ncbi.nlm.nih.gov/BLAST) to identify each clone. Their identities are summarised in Table 6.5. The yeast two-hybrid system is known for generating false positive interactions. The most common false positive interactors are summarised by Dr. Golemis's laboratory (http://www.fccc.edu/research/labs/golemis/InteractionTrapInWork.html). Clones 11, 15, 40, 41, 49, 52 and 55 were all found in the database and were therefore considered as false positives and no further analysis was carried out. Clones 26, 27, 37 and 47, shown in bold in Table 6.5, were each found to be in frame with the activation domain in the + 1 reading frame. Interestingly clones 37 and 47 both encoded the C-terminal binding protein but they encoded different but overlapping segments. There is an overlap of clones 37 and 47 of 63 amino acids, corresponding to residues 161-224. Therefore the C-terminal binding protein

is a good candidate for an interaction with NR2D subunits and requires further study to verify an *in vivo* association

Clone number	Identification	Accession	Amino acid residues	Percentage amino acid identity
11	Ribosomal L19 domain	BAE24733	2 - 213	99 %
15	Proteasome subunit alpha type 3	NP_035314	1 - 129	99 %
26	**Un-named protein**	**BAE31106**	**538 – 820**	**99.5 %**
27	**Cathepsin B**	**1701299A**	**163-339**	**96 %**
37	**C-terminal binding protein**	**NP_038530**	**161 - 306**	**100 %**
40	Leucine zipper, putative tumor suppressor 2	NP_663478	475 - 671	100 %
41	EGF containing fibulin-like extracellular matrix protein	Q8BPB5	290 - 493	100 %
47	**C-terminal binding protein**	**NP_038530**	**1 – 224**	**99.5 %**
49	Signal transducer and activator for transcription	NP_036879	1 – 203	100 %
52	Mitochondrial protein L19	NP_080766	2 - 213	100 %
55	Small nuclear ribonucleoprotein B	NP_033251	2 - 152	44 %

Table 6.5 A summary of the cDNA library clones which are predicted to be false positives

The nucleotide sequences for clones 11, 15, 27, 37, 40, 41, 47, 49, 52 and 55 were translated using the 'Translate' program available at http://www.expasy.org/tools/dna.html and then nucleotide and amino acid sequence database searches were carried out using NCBI database (www.ncbi.nlm.nih.gov/BLAST). The above table summarises the identity of clones 11, 15, 40, 41, 43, 49, 52 and 55 as being commonly observed false positives in the yeast two-hybrid system (http://www.fccc.edu/research/labs/golemis/InteractionTrapInWork.html).

6.3 DISCUSSION

A cDNA mouse brain yeast two-hybrid screen was carried out using the NR2D C-terminal domain as bait. From the putative positive interactors analysed four were found to be true interactors in the yeast two-hybrid system. These were an un-named protein, cathepsin B and two different overlapping clones of the C-terminal binding protein. The best candidate from the screen was the C-terminal binding protein, as two overlapping clones were found to interact with both the NR2D and NR2D^{TRUNC} C-terminal domains. Firstly, the interactions need to be verified in a heterologous cell line and *in vivo* i.e. the brain. Secondly, the interaction of the C-terminal binding proteins should be investigated in terms of its specificity, i.e. does it interact with the other NR2 subunits or is it a specific association with NR2D subunits. Due to time constraints these further investigations could not be carried out.

The C-terminal binding protein was first identified as an interactor with the adenovirus E1A proteins (Schaeper *et al.*, 1998). A conserved PLDLS motif in the E1A proteins mediates this interaction (Schaeper *et al.*, 1998). However, this PLDLS motif is not present in the NR2D C-terminal domain suggesting a different mode of interaction. The C-terminal binding protein was demonstrated to interact with nNOS by affinity chromatography using a GST fusion protein column containing the PDZ domain of nNOS (Riefler and Firestein, 2001). Although the C-terminal binding protein is thought to be a transcription co-repressor (Meloni *et al.*, 1999; Postigo and Dean, 1999), the binding of the C-terminal protein to nNOS caused a redistribution of the C-terminal binding protein from the nucleus to the cytoplasm (Riefler and Firestein, 2001). Therefore, it is interesting to speculate that the nNOS/C-terminal binding protein complex is targeted to NR2D-containing NMDA receptors. It currently known that nNOS associates with PSD-95 in the brain (Brenman *et al,* 1996). This association between PSD-95 and nNOS links NMDA receptors to a neurotoxicity pathway (Sattler *et al.*, 1999). NR2D-containing NMDA receptors may be differentially linked to nNOS via a PSD-95-independent mechanism which would be important in terms of neurotoxicity.

Interestingly, from the analysed putative positive interactors, the library screen did not identify any PSD-95 MAGUK family members. This was a surprising result as the PSD-95 MAGUK family are expressed at a high abundance in the brain and therefore one would expect PSD-95 to be present (Cho *et al.*, 1992). Additionally, amino acids 866-1064 of the NR2D C-terminal domain were found to interact with the tyrosine kinase c-Abl (Glover *et al.*, 2000), which was also not identified in the library screen. However not all the putative positive clones were analysed and therefore an un-analysed putative positive interactor may be one of the above mentioned proteins. Conversely, this could suggest that the conformation of the NR2D C-terminal domain in yeast does not resemble its natural conformation. To test this hypothesis the NR2D C-terminal domain should be co-expressed with PSD-95 in yeast cells and their interaction determined.

In summary, in this chapter it was shown that:-

- The NR2D C-terminal domain associates with an un-named protein, cathepsin B and two different overlapping clones of the C-terminal binding protein following their co-expression in yeast cells.

CHAPTER 7

FINAL DISCUSSION AND FUTURE PROSPECTS

The major aim of this thesis was to understand the role that the PSD-95 MAGUK family of scaffolding proteins plays on determining the number of cell surface expressed NMDA receptor subtypes and how this NMDA receptor/PSD-95 MAGUK association is regulated. This was an important question to ask since the number of surface expressed NMDA receptors is a fine balance between normal neuronal function and a pathogenic state. The identification of proteins associated with the NMDA receptor complex led to an understanding of the downstream NMDA receptor associated pathways (Husi and Grant 2001a, b; Collins *et al.*, 2005). From these studies it was deduced that PSD-95 behaves as a central 'hub' where it scaffolds many different proteins to the NMDA receptors. In addition, PSD-95 is involved in the clustering, prevention of internalisation and enhancement of the cell surface expression of NMDA receptors in heterologous cells and neurones, thus demonstrating the importance of this association between NMDA receptors and PSD-95.

In this thesis it was found that each NR1-1a/NR2 NMDA receptor subtype associates with each PSD-95 MAGUK. However differential effects were observed in terms of the subunit expression levels of the NMDA receptor subtypes and the PSD-95 MAGUK family. This raised questions as to whether the different NMDA receptor subtypes are regulated by the PSD-95 family in a similar manner. It is thought that there is a functional redundancy between the PSD-95 MAGUK family, for example SAP102 is up-regulated in PSD-95 and PSD-93 double knock-out mice, therefore SAP102 compensated for these deletions (Elias *et al.*, 2006). However, in this thesis the findings suggest that the different PSD-95 MAGUK family members play different roles in the maintenance of the cell surface expression of NMDA receptors. This is in agreement with the idea that each PSD-95 MAGUK has specific roles *in vivo*, for example, the cell surface expression of NMDA receptors was found to be reduced neurones prepared from PSD-93 knock-out mice (Tao *et al.*, 2003).

Although the NMDA receptor subtypes were found to associate with each PSD-95 MAGUK in this thesis, these experiments were carried out in a heterologous system and it is important to demonstrate that these NMDA receptor/PSD-95 MAGUK complexes exist

in vivo and whether the expression level of the scaffold proteins affects NMDA receptor cell surface expression. This could be achieved by measuring the cell surface expression of NMDA receptor subtypes in neurones cultured from knock-out mice when compared to wild-type animals. Additionally, siRNA could be employed to directly knock-down the expression of specific PSD-95 MAGUK proteins in neurones to access the properties that each PSD-95 MAGUK protein elicits onto each NMDA receptor subtype. Lastly, tat-peptides corresponding to the last 9 amino acids of NR2A/NR2B subunits could be used to inhibit the association between all the PSD-95 MAGUK family/NMDA receptors and therefore access the overall properties that the PSD-95 family elicits on the trafficking/stabilisation of NMDA receptors to the cell surface.

As mentioned in Chapter 1, the cell surface expression of NMDA receptors is dependent on many different motifs found within their C-terminal domains. In this thesis it was found that there are a number of regulatory signals present in the distal C-terminus of NR2A subunits. As described in Chapters 4 and 5, the cell surface expression of NR2A-containing NMDA receptors is regulated by phosphorylation and a putative internalisation motif. Further investigation is required to test if this putative internalisation motif plays a role in the regulation of the cell surface expression of NMDA receptors. It is interesting to speculate, that if this putative internalisation motif is found to influence the cell surface expression of NMDA receptors, the phosphorylation signal found close to this motif plays a role in their internalisation. It was similarly found that the phosphorylation of the identified internalisation motif on NR2B subunits maintained their cell surface expression (Nakazawa *et al.*, 2001). The differential regulation of NMDA receptor subtypes was further highlighted by the finding that a mutation of a serine residue on the NR2C subunits, which was in a homologous position to that of the above studies with NR2A subunits, did not result in a change in the cell surface expression of NR1/NR2C NMDA receptors. Thus although NR2A-containing NMDA receptors require phosphorylation at their distal C-terminus for the maintenance of their cell surface expression, NR2C-containing NMDA receptors do not. Further investigations should be carried out to investigate the contributions that these phosphorylation signals close to the PDZ interaction sites play in the regulation of the protein-protein interactions between the NMDA receptor subtypes and

the PSD-95 MAGUKs. The identification of the phosphorylation sites in the C-terminal domains of each subunit by Trinidad *et al.* (2006) allows for further point mutations to be generated and the subsequent characterisation of the receptor properties in terms of their association with scaffolding proteins and their cell surface expression.

Thus overall, this thesis has identified some regulatory mechanisms for the association of PSD-95 which are required for the maintenance of NMDA receptor cell surface expression. This is important as the association between NMDA receptors and the PSD-95 MAGUK family is thought to be a possible therapeutic target. For example, a peptide corresponding to the last 9 amino acids of NR2B subunits, i.e. the PDZ domain binding motif was found to disrupt the association between NMDA receptors and PDZ-containing proteins in cortical neurones (Aarts *et al.*, 2002). This disruption decreased the NMDA receptor elicited excitotoxicity but did not affect the NMDA receptor function (Aarts *et al.*, 2002). The incubation of these peptides prevented ischemic brain damage and was thought to be a possible stroke therapy (Aarts *et al.*, 2002). Further, inhalational anaesthetics were found to disrupt the interaction between NMDA receptors and PSD-95/PSD-93 by competing for the PDZ domain ligand binding site (Fang *et al.*, 2003). Therefore, further investigation into the determinants of the association between NMDA receptor subtypes and the PSD-95 MAGUK family of proteins which leads to their stabilisation, clustering, turnover and compartmentalisation may permit the design of specifically targeted therapeutics.

APPENDICES

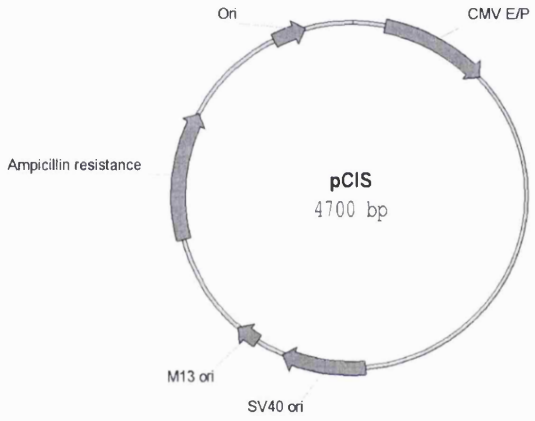

Appendix 2.1 Vector map of pCIS

The pCIS vector is shown above. The plasmid contains a bacterial origin of replication (Ori) and an ampicillin resistance marker, therefore allowing replication in bacteria. The expression of the protein in mammalian cells was under the control of the cytomegavirus promoter (CMV E/P). The pCIS vector was a gift from Dr.C. Gorman (Genentech, San Francisco, U.S.A).

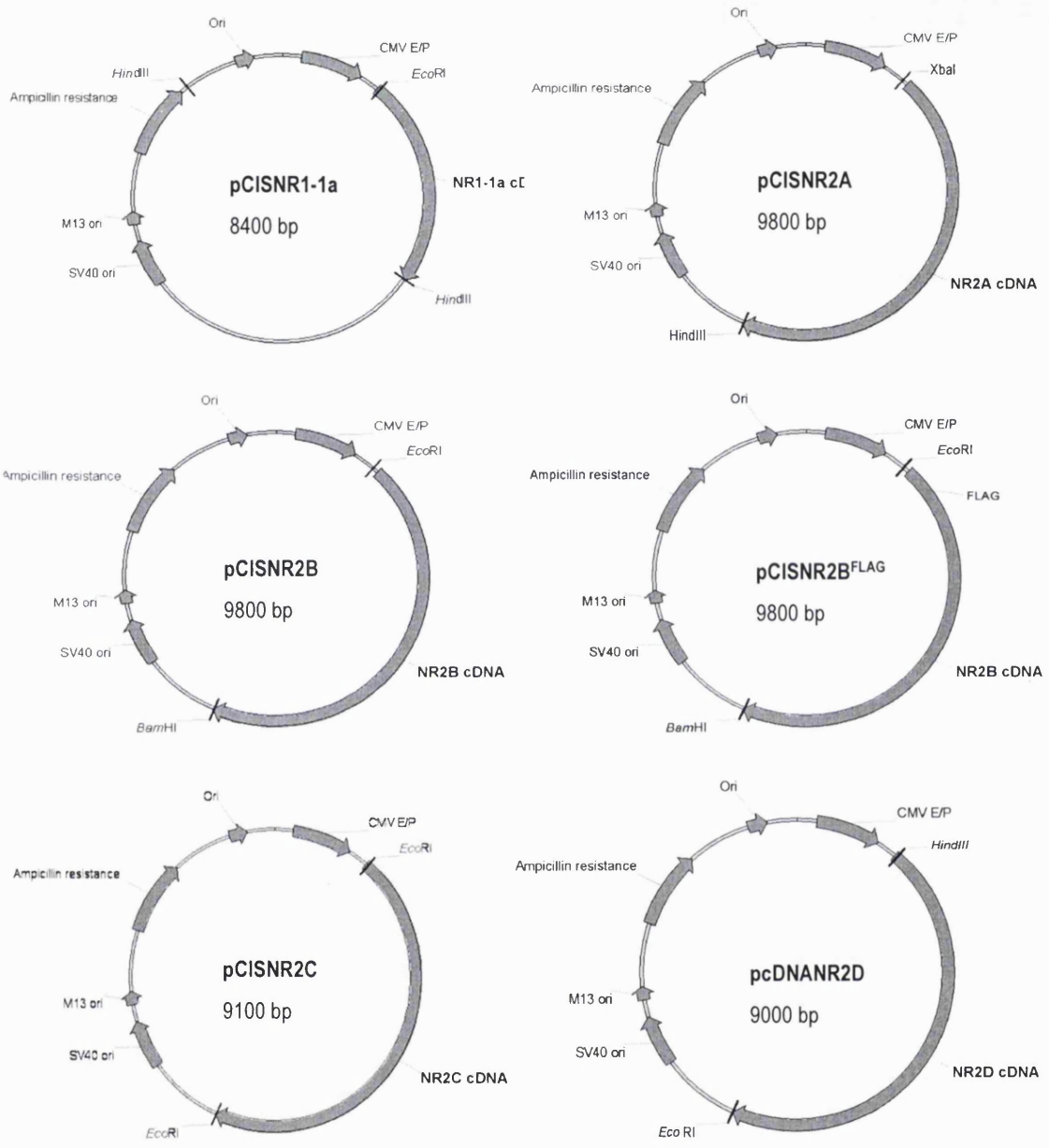

Appendix 2.2 Vector maps of the NMDA receptor subunit clones used for mammalian transfections

The pCISNR1-1a, pCISNR2A, pCISNR2B, pCISNR2B^{FLAG}, pCISNR2C and pcDNANR2D clones are shown above. Each plasmid contains a bacterial origin of replication (Ori) and an ampicillin resistance marker, therefore allowing the replication of each clone in bacteria. For expression of each protein in mammalian cells was under the control of the cytomegavirus promoter (CMV E/P). Clones were generated as described in Cik *et al*. (1993), Chazot *et al*. (1994), Hawkins *et al.* (1999) and Chopra *et al*. (2000).

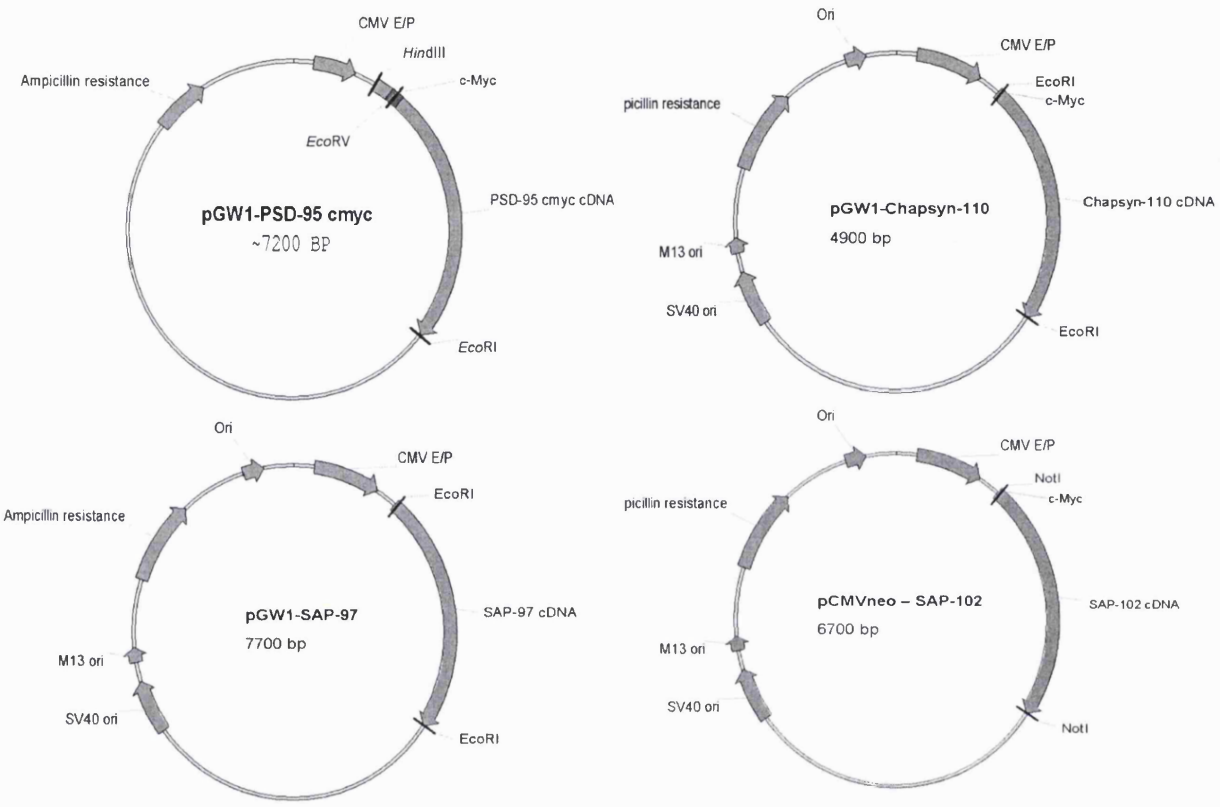

Appendix 2.3 Vector maps of the PSD-95 MAGUK family clones used for mammalian transfections

The pGW1-PSD-95, pGW1-chapsyn-110, pGW1-SAP97 and pCMVneo-SAP102 are shown above. As seen in the above vector maps, each clone contains a bacterial origin of replication (Ori) and an ampicillin resistance marker, therefore allowing the replication of each clone in bacteria. For expression of each protein in mammalian cells, each plasmid contains the cytomegavirus promoter (CMV E/P). Clones were a kind gift from Dr. M. Sheng (MIT, USA).

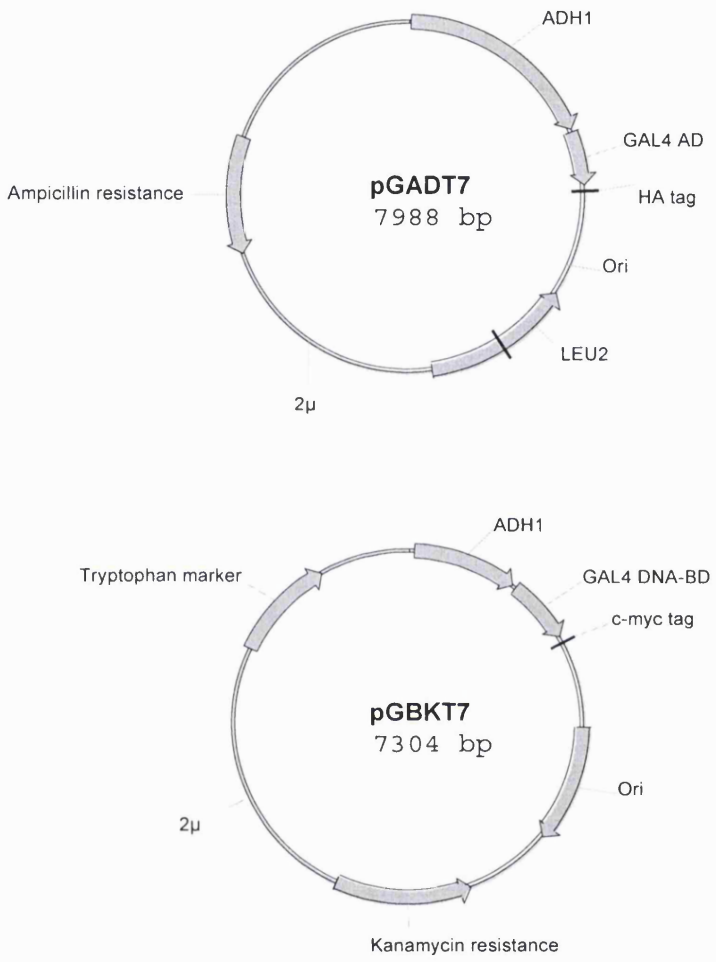

Appendix 2.4 Vector maps of pGADT7 and pGBKT7
Above are the vector maps for pGADT7 and pGBKT7. To facilitate their amplification in *E.coli* cells, the cloning vectors contained an origin of replication and a kanamycin or ampicillin resistance marker. To facilitate their replication in yeast cells, the vectors contained a μ2 origin of replication and a leucine or tryptophan marker. For expression of proteins cloned into the vectors they both contained the constitutive alcohol dehydrogenase (ADH1) promoter.

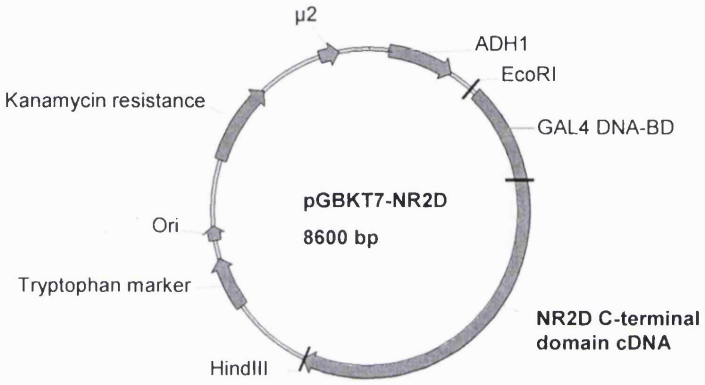

Appendix 2.5 Vector map for pGBKT7NR2D

Above is the vector map for pGBKT7NR2D. To facilitate the amplification of pGBKT7NR2D in E.coli cells, the cloning vector contained an origin of replication and a kanamycin resistance marker. To facilitate the replication in yeast cells, the vector contained a μ2 origin of replication and a tryptophan marker. For expression of the NR2D C-terminal domain, the vector contained the constitutive alcohol dehydrogenase (ADH1) promoter.

REFERENCES

Agatep, R., Kirkpatrick, R. D., Parchaliuk, D. L., Woods, R. A. and Gietz, R. D. (1998) Elsevier Trends Journals Technical Tips Online. Transformation of *Saccharomyces cerevisciae* by Lithium Acetate/Single-stranded Carrier DNA/Polyethylene Glycerol Protocol.

Akum, B. F., Chen, M., Gunderson, S. I., Riefler, G. M., Scerri-Hansen, M. M. and Firestein, B. L. (2004) Nat. Neurosci. 7, 145-152. Cypin regulates dendrite patterning in hippocampal neurons by promoting microtubule assembly.

Anson, L. C., Chen, P. E., Wyllie, D. J. A., Colquhoun, D. and Schoepfer, R. (1998) J. Neurosci. 18, 581-589. Identification of amino acid residues of the NR2A subunit that control glutamate potency in recombinant NR1/NR2A NMDA receptors.

Araki, K., Meguro, H., Kushiya, E., Takayama, C., Inoue, Y. and Mishina, M. (1993) Biochem. Biophys. Res. Commun. 197, 1267-1276.Selective expression of the glutamate receptor channel delta 2 subunit in cerebellar Purkinje cells.

Armstrong, N. and Gouaux, E. (2000) Neuron 28, 165-181. Mechanisms for activation and antagonism of an AMPA-sensitive glutamate receptor: crystal structures of the GluR2 ligand binding core.

Armstrong, N., Sun, Y., Chen, G. Q. and Gouaux, E. (1998) Nature 395, 913-917. Structure of a glutamate-receptor ligand-binding core in complex with kainate.

Awobuluyi, M., Yang, J., Ye, Y., Chatterton, J. E., Godzik, A., Lipton, S. A. and Zhang, D. (2007) Mol. Pharmacol. 71, 112-22. Subunit-specific roles of glycine-binding domains in activation of NR1/NR3 N-methyl-D-aspartate receptors.

Ayalon, G. and Stern-Bach, Y. (2001) Neuron 31, 103-113. Functional assembly of AMPA and kainate receptors is mediated by several discrete protein-protein interactions.

Ayalon, G., Segev, E., Elgavish, S. and Stern-Bach, Y. (2005) J. Biol. Chem. 280, 15053-15060. Two regions in the N-terminal domain of ionotropic glutamate receptor 3 form the subunit oligomerization interfaces that control subtype-specific receptor assembly.

Barria, A. and Malinow, R. (2002) Neuron 35, 345-353. Subunit-specific NMDA receptor trafficking to synapses.

Bassand, P., Bernard, A., Rafiki, A., Gaynet, D. and Khrestchatisky, M. (1999) Eur. J. Neurosci. 11, 2031-2043. Differential interaction of the tSXV motifs of the NR1 and NR2A NMDA receptor subunits with PSD-95 and SAP97.

Bécamel, C., Gavarini, S., Chanrion, B., Alonso, G., Galéotti, N., Dumuis, A., Bockaert, J. and Marin, P. (2004) J. Biol. Chem. 279, 20257-20266. The serotonin 5-HT_{2A} and 5-HT_{2C} receptors interact with specific sets of PDZ proteins.

Behe, P., Stern, P., Wyllie, D. J. A., Nassar, M. and Schoepfer, R. (1995) Proc. Natl. Acad. Sci. USA 262, 205-213. Determination of NMDA NR1 subunit copy number in recombinant NMDA receptors.

Bellaiche, Y., Radovic, A., Woods, D. F., Hough, C. D., Parmentier, M. L., O'Kane, C. J., Bryant, P. J. and Schweisguth, F. (2001) Cell 106, 355-366. The partner of inscuteable/Discs-large complex is required to establish planar polarity during asymmetric cell division in *Drosophila*.

Bence, M., Arbuckle, M. I., Dickson, K. S. and Grant, S. G. (2005) Brain Res. Mol. Brain Res. 133, 143-152. Analyses of murine postsynaptic density-95 identify novel isoforms and potential translational control elements.

Benveniste, M. and Mayer, M. L. (1991) Biophys. J. 59, 560-573. Kinetic analysis of antagonist action at N-methyl-D-aspartic acid receptors. Two binding sites each for glutamate and glycine.

Bettler, B., Boulter, J., Hermans-Borgmeyer, I., O'Shea-Greenfield, A., Deneris, E. S., Moll, C., Borgmeyer, U., Hollmann, M. and Heinemann, S. (1990) Neuron 5, 583-595. Cloning of a novel glutamate receptor subunit, GluR5: expression in the nervous system during development. Neuron 5, 583-595

Bettler, B., Egebjerg, J., Sharma, G., Pecht, G., Hermans-Borgmeyer, I., Mol, C., Stevens, C. F. and Heinemann, S. (1992) Neuron 8, 257-265. Cloning of a putative glutamate receptor: a low affinity kainate-binding subunit.

Bi, X., Rong, Y., Chen, J., Dang, S., Wang, Z. and Baudry, M. (1998) Brain Res. 790, 245-253. Calpain-mediated regulation of NMDA receptor structure and function.

Blahos, J. and Wenthold. R. J. (1996) J. Biol. Chem. 271, 15669-15674. Relationship between N-methyl-D-aspartate receptor NR1 splice variants and NR2 subunits.

Bliss, T. V. P. and Collingridge, G. L. (1993) Nature 361, 31-39. A synaptic model of memory: long-term potentiation in the hippocampus.

Boeckers, T. M. (2006) Cell and Tissue Research. 326, 409-422. The postsynaptic density.

Bonifacino, J. S. and Traub, L. M. (2003). Annu. Rev. Biochem. 72, 395-447. Signals for sorting of transmembrane proteins to endosomes and lysosomes.

Brenman, J. E., Chao, D. S., Gee, S. H., McGee, A. W., Craven, S. E., Santillano, D. R., Wu, Z., Huang, F., Xia, H., Peters, M. F., Froehner, S. C. and Bredt D. S. (1996b) Cell 84, 757-767. Interaction of nitric oxide synthase with the post-synaptic density protein PSD-95 and α1-syntrophin mediated by PDZ domains.

Brenman, J. E., Christopherson, K. S., Craven, S. E., McGee, A. W. and Bredt, D. S. (1996a) J. Neurosci. 16, 7407-7415. Cloning and characterisation of post-synaptic density 93, a nitric oxide synthase interacting protein.

Brickley, S. G., Misra, C., Mok, M. H., Mishina, M. and Cull-Candy, S. G. (2003) J. Neurosci. 23, 4958-4966. NR2B and NR2D subunits coassemble in cerebellar Golgi cells to form a distinct NMDA receptor subtype restricted to extrasynaptic sites.

Brimecombe, J. C., Boeckman, F. A. and Aienman, E. (1997) Proc. Nat. Acad. Sci. USA. 94, 11019-11024. Functional consequences of NR2 subunit composition in single recombinant N-methyl-D-aspartate receptors.

Brose, N., Gasic, P., Vetter, D. E., Sullivan, J. M. and Heinemann, S. F. (1993) J. Biol. Chem. 268, 22663-22671. Protein chemical characterisation and immunocytochemical localization of the NMDA receptor subunit NMDA R1.

Buller, A. L. and Monaghan, D. T. (1997) European Journal of Pharmacology. 320, 87-94. Pharmacological heterogeneity of NMDA receptors: characterization of NR1a/NR2D heteromers expressed in *Xenopus* oocytes.

Burnashev, N. Schoepfer, R., Monyer, H., Ruppersberg, J. P., Gunther, W., Seeburg, P. H. and Sakmann, B. (1992) Science 257, 1415-1419. Control by asparagine residues of calcium permeability and magnesium blockade in the NMDA receptor.

Cai, C., Li, H., Rivera, C. and Keinänen, K. (2006) J. Biol. Chem. 281, 4267 - 4273. Interaction between SAP97 and PSD-95, two MAGUK proteins involved in synaptic trafficking of AMPA receptors.

Carroll, R. C., Lissin, D. B., von Zastrow, M., Nicoll, R. A. and Malenka, R. C. (1999) Nat. Neurosci. 2, 454-460. Rapid redistribution of glutamate receptors contributes to long-term depression in hippocampal cultures.

Caruana, G. and Bernstein, A. (2001) Mol. Cell. Bio. 21, 1475-1483. Craniofacial dysmorphogenesis including cleft palate in mice with an insertional mutation in the *discs large* gene.

Chatterton. J. E., Awobuluyi, M., Premkumar, L. S., Takahashi, H., Talantova, M., Shin, Y., Cui, J., Tu, S., Sevarino, K. A., Nakanishi, N., Tong, G., Lipton, S. A. and Zhang, D. (2002) Nature 415, 793-798. Excitatory glycine receptors containing the NR3 family of NMDA receptor subunits.

Chazot P. L., Cik, M. and Stephenson F. A. (1996) Methods in Molecular Biology 128, 33-42. Transient expression of functional NMDA receptors in mammalian cells.

Chazot, P. L. and Stephenson, F. A. (1997a) J. Neurochem. 69, 2138- 2144. Molecular dissection of native mammalian forebrain NMDA receptors containing the NR1 C2 exon: direct demonstration of NMDA receptors comprising NR1, NR2A, and NR2B subunits within the same complex.

Chazot, P. L. and Stephenson, F. A. (1997b) J. Neurochem. 68, 507-516. Biochemical evidence for the existence of a pool of unassembled C2 exon-containing NR1 subunits of the mammalian forebrain NMDA receptor.

Chazot, P. L., Cik, M. and Stephenson, F. A. (1995) Mol. Membr. Biol. 12, 331-337. An investigation into the role of N-glycosylation in the functional expression of a recombinant heteromeric NMDA receptor.

Chazot, P. L., Cik, M., and Stephenson, F. A. (1992) J. Neurochem. 59, 1176-1178. Immunological detection of the NMDAR1 glutamate receptor subunit expressed in human embryonic kidney 293 cells and in rat brain.

Chazot, P. L., Coleman, S. K., Cik, M. And Stephenson, F. A. (1994) J. Biol. Chem. 269, 24403-24409. Molecular characterization of N-methyl-D-aspartate receptors expressed in mammalian cells yields evidence for the coexistence of three subunit types within a discrete receptor molecule.

Chazot, P.L., Reiss, C., Chopra, B. and Stephenson, F. A. (1998) Eur. J. Pharmacol. 353, 137-40. [3H]MDL 105,519 binds with equal high affinity to both assembled and unassembled NR1 subunits of the NMDA receptor.

Cheffings, C. M. and Colquhoun, D. (2000) J. Phyiol. 526, 481-491. Single channel analysis of a novel NMDA channel from Xenopus oocytes expressing recombinant NR1a, NR2A and NR2D subunits.

Chen, B-S., Braud, S., Badger II, J. D., Isaac, J. T. R. and Roche, K. W. (2006) J. Biol. Chem. 281, 16583 - 16590. Regulation of NR1/NR2C *N*-Methyl-D-aspartate (NMDA) receptors by phosphorylation.

Chen, H. J., Rojas-Soto, M., Oguni, A. and Kennedy, M. B. (1998) Neuron 20, 895-904. A synaptic Ras-GTPase activating protein (p135 SynGAP) inhibited by CaM kinase II.

Chen, L., Chetkovich, D. M., Petralia, R. S., Sweeney, N. T., Kawasaki, Y., Wenthold, R. J., Bredt, D. S. and Nicoll, R. A. (2000) Nature 408, 936-943. Stargazin regulates synaptic targeting of AMPA receptors by two distinct mechanisms.

Chetkovich, D. M., Bunn, R. C., Kuo, S. H., Kawasaki, Y., Kohwi, M. and Bredt, D. S. (2002) J. Neurosci. 22, 6415-6425. Postsynaptic targeting of alternative postsynaptic density-95 isoforms by distinct mechanisms.

Cho, K.-O., Hunt, C. A. and Kennedy, M. B. (1992) Neuron 9, 929-942. The rat brain post-synaptic density fraction contains a homolog of the drosophila discs-large tumor suppressor protein.

Choi, J., Ko, J., Park, E., Lee, J.R., Yoon, J., Lim, S. and Kim, E. (2002) J. Biol. Chem. 277, 12359-12363. Phosphorylation of stargazin by protein kinase A regulates its interaction with PSD-95.

Choi, Y. B. and Lipton, S. A. (1999) Neuron 23, 171-180. Identification and mechanism of action of two histidine residues underlying high-affinity Zn2+ inhibition of the NMDA receptor.

Chopra, B., Chazot, P. L., and Stephenson, F. A. (2000) Br. J. Pharmacol. 130, 65-72. Characterisation of the binding of two novel glycine site antagonists to cloned NMDA receptors: evidence for two pharmacological classes of antagonists.

Chung, H. J., Huang, Y. H., Lau, L. F. and Huganir, R. L. (2004) J. Neurosci. 24, 10248-10259. Regulation of the NMDA receptor complex and trafficking by activity-dependent phosphorylation of the NR2B subunit PDZ ligand.

Ciabarra, A. M., Sullivan, J. M., Gahn, L. G., Pecht, G., Heinemann, S. and Sevarino, K. A. (1995) J. Neurosci. 15, 6498-6508. Cloning and characterisation of chi-1: A developmentally regulated member of a novel class of the ionotropic glutamate receptor family.

Cik, M., Chazot, P. L. and Stephenson, F. A. (1993) Biochem. J. 15, 877-883. Optimal expression of cloned NMDAR1/NMDAR2A heteromeric glutamate receptors: a biochemical characterization.

Clements, J. D. and Westbrook, G. L. (1991) Neuron 7, 605-13. Activation kinetics reveal the number of glutamate and glycine binding sites on the N-methyl-D-aspartate receptor.

Coghlan, V. M., Perrino, B. A., Howard, M., Langeberg, L. K., Hicks, J. B., Gallatin, W. M. and Scott J. D. (1995) Science 267, 108-111. Association of protein kinase A and protein phosphatase 2B with a common anchoring protein.

Colledge, M., Dean, R. A., Scott, G. K., Langeberg, L. K., Huganir, R. L. and Scott J. D. (2000) Neuron 27, 107-119. Targeting of PKA to glutamate receptors through a MAGUK-AKAP complex.

Collins, M. O., Husi, H., Yu, L., Brandon, J. M., Anderson, C. N., Blackstock, W. P., Choudhary, J. S. and Grant, S. G. (2005) J. Neurochem. 97, 16-23. Molecular characterization and comparison of the components and multiprotein complexes in the postsynaptic proteome.

Conn, P. J. and Pin, J-P (1997) Ann. Rev. of Pharmacology and Toxicology 95, 787-793. Pharmacology and functions of metabotropic glutamate receptors.

Craven, S. E., El-Husseini, A. E. and Bredt, D. S. (1999) Neuron 22, 497-509. Synaptic targeting of the post-synaptic density protein PSD-95 mediated by lipid and protein motifs.

Cull-Candy, S. G., Brickley, S. G. and Farrant, M. (2001) Curr. Opin. Neurobiol. 11, 327-335. NMDA receptor subunits: diversity, development and disease.

Cuthbert, P. C., Stanford, L. E., Coba, M. P., Ainge, J. A., Fink, A. E., Opazo, P., Delgado, J. Y., Komiyama, N. H., O'Dell, T. J. and Grant, S. G. (2007) J. Neurosci. 27, 2673-2682. Synapse-associated protein 102/dlgh3 couples the NMDA receptor to specific plasticity pathways and learning strategies.

Dalva, M. B., Takasu, M. A., Lin, M. Z., Shamah, S. M., Hu, L., Gale, N. W. and Greenberg, M. E. (2000) Cell 103, 945-956. EphB receptors interact with NMDA receptors and regulate excitatory synapse formation.

Das, S., Sasaki, Y. F., Rothe, T., Premkumar, L. S., Takasu, M., Crandall, J. E., Dikkes, P., Conner, D. A., Rayudu, P. V., Cheung, W., Chen, H-S, V., Lipton, S. A. and Nakanishi, N. (1998) Nature 393, 377-381. Increased NMDA current and spine density in mice lacking the NMDA receptor subunit NR3A.

Deguchi, M., Hata, Y., Takeuchi, M., Ide, N., Hirao, K., Yao, I., Irie, M., Toyoda, A. and Takai, Y. (1998) J. Biol. Chem. 273, 26269-26272. BEGAIN (brain-enriched guanylate kinase-associated protein), a novel neuronal PSD-95/SAP90-binding protein.

Dingledine, R., Borges, K., Bowie, D. and Traynelis, S. F. (1999) Pharmacol. Rev. 51, 7-61. The glutamate receptor ion channels.

Dong, Y. N., Waxman, E. A. and Lynch, D. R. (2004) J. Neurosci. 24, 11035-11045. Interactions of postsynaptic density-95 and the NMDA receptor 2 subunit control calpain-mediated cleavage of the NMDA receptor.

Doyle, D. A., Lee, A., Lewis, J., Kim, E., Sheng, M. and MacKinnon, R. (1996) Cell 85, 1067-1076. Crystal structures of a complexed and peptide-free membrane protein-binding domain: molecular basis of peptide recognition by PDZ.

Dunah, A. W., Luo, J., Wang, Y. H., Yasuda, R. P. and Wolfe, B.B. (1998) Mol. Pharmacol. 53, 429-437. Subunit composition of N-methyl-D-aspartate receptors in the central nervous system that contain the NR2D subunit.

Dunah, A. W., Wyszynski, M., Martin, D. M., Sheng, M. and Standaert, D. G. (2000) Brain. Res. Mol. Brain. Res. 79, 77-87. Alpha-actinin-2 in rat striatum: localization and interaction with NMDA glutamate receptor subunits.

Dunah, A. W., Yasuda, R. P., Wang, Y.-H., Luo, J., Davila-Garcia, M., Gbadegesin, M., Vicini, S. and Wolfe, B. B. (1996) J. Neurochem. 67, 2335-2345. Regional and ontogenic expression of the NMDA receptor subunit NR2D protein in rat brain using a subunit-specific antibody.

Ebralidze, A. K., Rossi, D. J., Tonegawa, S. and Slater, N. T. (1996) J. Neurosci. 16, 5014-5025. Modification of NMDA receptor channels and synaptic transmission by targeted disruption of the NR2C gene.

Egebjerg, J., Bettler, B., Hermans-Borgmeyer, I. and Heinemann, S. (1991) Nature 351, 745-748. Cloning of a cDNA for a glutamate receptor subunit activated by kainate but not AMPA.

Ehlers, M. D., Fung, E. T., O'Brien, R. J. and Huganir, R. L. (1998) J. Neurosci. 18, 720-730. Splice variant-specific interaction of the NMDA receptor subunit NR1 with neuronal intermediate filaments.

Ehlers, M. D., Zhang, S., Bernhardt, J. P. and Huganir, R. L. (1996) Cell 84, 745-755. Inactivation of NMDA receptors by direct interaction of calmodulin with the NR1 subunit.

El-Husseini, A. E., Craven, S. E., Chetkovich, D. M., Firestein, B. L. Schnell, E., Aoki, C. and Bredt, D. S. (2000b) J. Cell Biol. 148, 159-171. Dual palmitoylation of PSD-95 mediates its vesiculotubular sorting, postsynaptic targeting, and ion channel clustering.

El-Husseini, A. E., Topinka, J. R., Lehrer-Graiwer, J. E., Firestein, B. L., Craven, S. E., Aoki, C. and Bredt, D. S. (2000a) J. Biol.Chem. 275, 23904-23910. Ion channel clustering by membrane-associated guanylate kinases. Differential regulation by N-terminal lipid and metal binding motifs.

Elias, G. M., Funke, L., Stein, V., Grant, S. G., Bredt, D. S. and Nicoll, R. A. (2006) Neuron 52, 307-320. Synapse-specific and developmentally regulated targeting of AMPA receptors by a family of MAGUK scaffolding proteins.

Farrant, M., Feldmeyer, D., Takahashi, T. and Cull-Candy, S. (1994) Nature 368, 335-339. NMDA-receptor channel diversity in the developing cerebellum.

Feng, B., Tse, H. W., Skifter, D. A., Morley, R., Jane, D. E. and Monaghan. D. T. (2004) Br. J. Pharmacol. 141, 508-516. Structure-activity analysis of a novel NR2C/NR2D-preferring NMDA receptor antagonist: 1-(phenanthrene-2-carbonyl) piperazine-2,3-dicarboxylic acid.

Fields, S. and Song, O-K. (1989) Nature. 340, 245-246. A Novel Genetic System to Detect Protein-Protein Interactions.

Fields, S. and Sternglanz, R. (1994) Trends in Genetics 10, 286-291. The two-hybrid system: an assay for protein-protein interactions.

Fiorentini, C., Gardoni, F., Spano, P., Di Luca, M. and Missale, C. (2003) J. Biol. Chem. 278, 20196-20202. Regulation of dopamine D1 receptor trafficking and desensitization by oligomerization with glutamate N-methyl-D-aspartate receptors.

Firestein, B. L., Craven, S. E. and Bredt, D. B. (2000) Neuroreport 11, 3479 - 3484. Postsynaptic targeting of MAGUKs mediated by distinct N-terminal domains.

Flint, A. C., Maisch, U. S., Weishaupt, J. H., Kriegstein, A. R. and Monyer, H. (1997) J. Neurosci. 17, 2469-2476.NR2A subunit expression shortens NMDA receptor synaptic currents in developing neocortex.

Forrest, D., Yuzaki, M., Soares, H. D., Ng, L., Luk, D. C., Sheng, M., Stewart, C. L., Morgan, J. I., Connor, J. A. and Curran, T. (1994) Neuron 13, 325-338. Targeted disruption of NMDA receptor 1 gene abolishes NMDA response and results in neonatal death.

Foucaud, B., Laube, B., Schemm, R., Kreimeyer, A., Goeldner, M. and Betz, H. (2003) J. Biol. Chem. 278, 24011-24017. Structural model of the N-methyl-D-aspartate receptor glycine site probed by site-directed chemical coupling.

Fukaya, M., Kato, A., Lovett, C., Tonegawa, S. and Watanabe, M. (2003) Proc. Natl. Acad. Sci. USA 100, 4855-4860. Retention of NMDA receptor NR2 subunits in the lumen of endoplasmic reticulum in targeted NR1 knockout mice.

Furukawa, H. and Gouaux, E. (2003) EMBO J. 22, 2873-2885. Mechanisms of activation, inhibition and specificity: crystal structures of the NMDA receptor NR1 ligand-binding core.

Furukawa, H., Singh, S. K., Mancusso, R. and Gouaux, E. (2005) Nature. 438, 185-192. Subunit arrangement and function in NMDA receptors.

Furuyashiki, T., Fujisawa, K., Fujita, A., Madaule, P., Uchino, S., Mishina, M., Bito, H. and Narumiya, S. (1999) J. Neurosci. 19, 109-118. Citron, a Rho-target, interacts with PSD-95/SAP-90 at glutamatergic synapses in the thalamus.

Gallagher, M. J., Huang, H., Pritchett, D. B. and Lynch, D. R. (1996) J. Biol. Chem. 271, 9603-9611. Interactions between ifenprodil and the NR2B subunit of the N-methyl-D-aspartate receptor.

Garcia, E. P., Mehta, S., Blair, L. A., Wells, D. G., Shang, J., Fukushima, T., Fallon, J. R., Garner, C. C. and Marshall, J. (1998) Neuron 21, 727-739. SAP90 binds and clusters kainate receptors causing incomplete desensitization.

Garcia, R. A., Vasudevan, K. and Buonanno, A. (2000) Proc. Natl. Acad. Sci. USA 97, 3596-3601. The neuregulin receptor ErbB-4 interacts with PDZ-containing proteins at neuronal synapses.

Gardner, L. A., Tavalin, S. J., Goehring, A. S., Scott, J. D. and Bahouth, S. W. (2007) J. Biol. Chem. 281, 33537-33553. AKAP79-mediated targeting of the cyclic AMP-dependent protein kinase to the beta1-adrenergic receptor promotes recycling and functional resensitization of the receptor.

Gardoni, F., Mauceri, D., Fiorentini, C., Bellone, C., Missale, C., Cattabeni, F. and Di Luca, M. (2003) J. Biol. Chem. 278, 44745-44752. CaMKII-dependent phosphorylation regulates SAP97/NR2A interaction.

Gardoni, F., Polli, F., Cattabeni, F. and Di Luca, M. (2006) Eur. J. Neurosci. 24, 2694-2704. Calcium-calmodulin-dependent protein kinase II phosphorylation modulates PSD-95 binding to NMDA receptors.

Garner, C. C., Nash, J. and Huganir. R. L. (2000) Trends Cell Biol. 10, 274-280. PDZ domains in synapse assembly and signalling.

Gietz, R. D., Triggs-Raine, B., Robbins, A., Graham, K. C. and Woods, R. A. (1997) Mol. Cell Biochem. 172, 67-79. Identification of proteins that interact with a protein of interest: applications of the yeast two-hybrid system.

Gingrich, J. R., Pelkey, K. A., Fam, S. R., Huang, Y., Petralia, R. S., Wenthold, R. J. and Salter, M. W. (2004) Proc. Natl. Acad. Sci. USA. 101, 6237-6242. Unique domain anchoring of Src to synaptic NMDA receptors via the mitochondrial protein NADH dehydrogenase subunit 2.

Glover, R. T., Angiolieri, M., Kelly, S., Monaghan, D. T., Wang, J. Y. J., Smithgall, T.E. and Buller, A. L. (2000) J. Biol. Chem. 275, 12725-12729. Interaction of the *N*-Methyl-D-Aspartic acid receptor NR2D subunit with the c-Abl tyrosine kinase.

Gomperts, S. N., Rao, A., Craig, A. M, Malenka, R. C. and Nicoll, R. A. (1998) Neuron 21, 1443-1451. Postsynaptically silent synapses in single neuron cultures.

Grant, E. R., Bacskai, B. J., Anegawa, N. J., Pleasure, D. E. and Lynch, D. R. (1998) J. Neurochem. 71, 1471-1481. Opposing contributions of NR1 and NR2 to protein kinase C modulation of NMDA receptors.

Grimwood, S., Le Bourdellès, B. and Whiting, P. J. (1995) J. Neuorochem. 64, 525-530. Recombinant human NMDA homomeric NR1 receptors expressed in mammalian cells form a high-affinity glycine antagonist binding site.

Groc, L., Heine, M., Cousins, S. L., Stephenson, F. A., Lounis, B., Cognet, L. and Choquet, D. (2006) Proc. Natl. Acad. Sci. USA. 103, 18769-18774. NMDA receptor surface mobility depends on NR2A-2B subunits.

Guillaud, L., Setou, M. and Hirokawa, N. (2003) J. Neurosci. 23, 131-140. KIF17 dynamics and regulation of NR2B trafficking in hippocampal neurons.

Guttmann, R. P., Baker, D. L., Seifert, K. M., Cohen, A. S., Coulter, D. A. and Lynch, D. R. (2001) J. Neurochem. 78, 1083-1093. Specific proteolysis of the NR2 subunit at multiple sites by calpain.

Guttmann, R. P., Sokol, S., Baker, D. L., Simpkins, K. L., Dong, Y. and Lynch, D. R. (2002) J. Pharmacol. Exp. Ther. 302, 1023-1030. Proteolysis of the N-methyl-d-aspartate receptor by calpain in situ.

Hardingham, G. E., Fukunaga, Y. and Bading, H. (2002) Nat. Neurosci. 5, 405-414. Extrasynaptic NMDARs oppose synaptic NMDARs by triggering CREB shut-off and cell death pathways.

Hawkins, L. M., Chazot, P. L. and Stephenson, F. A. (1999) J. Biol. Chem. 274, 27211-27218. Biochemical evidence for the co-association of three N-methyl-D-aspartate (NMDA) R2 subunits in recombinant NMDA receptors.

Hawkins, L. M., Prybylowski, K., Chang, K., Moussan, C., Stephenson, F. A. and Wenthold, R. J. (2004) J. Biol. Chem. 279, 28903-28910. Export from the endoplasmic reticulum of assembled N-methyl-D-aspartic acid receptors is controlled by a motif in the C terminus of the NR2 subunit.

Herb, A., Burnashev, N., Werner, P., Sakmann, B., Wisden, W. and Seeburg, P. H. (1992) Neuron 8, 775-785. The KA-2 subunit of excitatory amino acid receptors shows widespread expression in brain and forms ion channels with distantly related subunits.

Hirai, H., Kirsch, J., Laube, B., Betz, H. and Kuhse, J. (1996) Proc. Natl. Acad. Sci. USA. 93, 6031-6036. The glycine binding site of the N-methyl-D-aspartate receptor subunit NR1: identification of novel determinants of co-agonist potentiation in the extracellular M3-M4 loop region.

Hoe, H. S., Pocivavsek, A., Chakraborty, G., Fu, Z., Vicini, S., Ehlers, M. D. and Rebeck, G. W. (2006) J. Biol. Chem. 281, 3425-3431. Apolipoprotein E receptor 2 interactions with the N-methyl-D-aspartate receptor.

Hollmann, M., O'Shea-Greenfield, A., Rogers, S. and Heinemann, S. (1989) Nature 342, 643-648. Cloning by functional expression of a member of the glutamate receptor family.

Hsueh, Y. P. and Sheng, M. (1999) J. Biol. Chem. 274, 532-536. Requirement of N-terminal cysteines of PSD-95 for PSD-95 multimerization and ternary complex formation, but not for binding to potassium channel Kv1.4.

Hsueh, Y.P., Kim, E. and Sheng, M. (1997) Neuron. 18, 803-814. Disulfide-linked head-to-head multimerization in the mechanism of ion channel clustering by PSD-95.

Huang, Y. Z., Won, S., Ali, D. W., Wang, Q., Tanowitz, M., Du, Q. S., Pelkey, K. A., Yang, D. J., Xiong, W. C., Salter, M. W. and Mei, L. (2000) Neuron 26, 443-455. Regulation of neuregulin signaling by PSD-95 interacting with ErbB4 at CNS synapses.

Huh, K.-H. and Wenthold, R. J. (1999) J. Biol. Chem. 274, 151-157. Turnover analysis of glutamate receptors identifies a rapidly degraded pool of the N-methyl-D-aspartate receptor subunit, NR1, in cerebellar granule cells.

Hung, A. Y. and Sheng, M. (2002) J. Biol. Chem. 277, 5699-5702. PDZ domains: structural modules for protein complex assembly.

Husi, H. and Grant, S. G. (2001a) Trends Neurosci. 24, 259-266. Proteomics of the nervous system.

Husi, H. and Grant, S. G. (2001b) J. Neurochem. 77, 281-291. Isolation of 2000-kDa complexes of N-methyl-D-aspartate receptor and postsynaptic density 95 from mouse brain.

Ikeda, K., Araki, K., Takayama, C., Inoue, Y., Yagi, T., Aizawa, S. and Mishina, M. (1995) Brain. Res. Mol. Brain Res. 33, 61-71. Reduced spontaneous activity of mice defective in the epsilon 4 subunit of the NMDA receptor channel.

Ikeda, K., Nagasawa, M., Mori, H., Araki, K. and Sakimura, K. (1992) FEBS Lett. 313, 34-38. Cloning and expression of the epsilon4 subunit of the NMDA receptor channel.

Inagaki, S., Ohoka, Y., Sugimoto, H., Fujioka, S., Amazaki, M., Kurinami, H., Miyazaki, N., Tohyama, M. and Furuyama, T. (2001) J. Biol. Chem. 276, 9174-9181. Sema4c, a transmembrane semaphorin, interacts with a post-synaptic density protein, PSD-95.

Irie, M., Hata, Y., Takeuchi, M., Ichtchenko, K., Toyoda, A., Hirao, K., Takai, Y., Rosahl, T. W. and Sudhof, T. C. (1997) Science 277, 1511-1515. Binding of neuroligins to PSD-95.

Isaac, J.T.R. (2003) Neuropharmacology. 45, 450-460. Postsynaptic silent synapses: evidence and mechanisms.

Ishii, T., Moriyoshi, K., Sugihara, H., Sakurada, K., Kadotani, H., Yokoi, M., Akazawa, C., Shigemoto, R., Mizuno, N., Masu, M. and Nakanishi, S. (1993) J. Biol. Chem. 268, 2863-2843. Molecular characterisation of a family of the N-methyl-D-aspartate receptor subunits.

Ivanov, A., Pellegrino, C., Rama, S., Dumalska, I., Salyha, Y., Ben-Ari, Y. and Medina, I. (2006) J. Physiol. 572, 789-798. Opposing role of synaptic and extrasynaptic NMDA receptors in regulation of the extracellular signal-regulated kinases (ERK) activity in cultured rat hippocampal neurons.

Jugloff, D. G. M., Khanna, R., Schlichter, L. C. and Jones, O. T. (2000) J. Biol. Chem. 275, 1357-1364. Internalisation of the Kv1.4 potassium channel is suppressed by clustering interactions with PSD-95.

Kadotani, H., Hirano, T., Masugi, H., Nakamura, K., Nakao, K., Katsuki, M. and Nakanishi, S. (1996) J. Neurosci. 16, 7859-7867. Motor discoordination results from combined gene disruption of the NMDA receptor NR2A and NR2C subunits, but not from single disruption of the NR2A or NR2C subunit.

Kalia, L. V. and Salter, M. W. (2003) Neuropharmacology. 45, 720-728. Interactions between Src family protein tyrosine kinases and PSD-95.

Kalia, L. V., Pitcher, G. M., Pelkey, K. A. and Salter, M. W. (2006) *EMBO J.* 25, 4971-4982. PSD-95 is a negative regulator of the tyrosine kinase Src in the NMDA receptor complex.

Kato, A., Rouach, N., Nicoll, R. A. and Bredt, D. S. (2005) Proc. Natl. Acad. Sci. USA. 102, 5600-5605. Activity-dependent NMDA receptor degradation mediated by retrotranslocation and ubiquitination.

Kay, B. K., Williamson, M. P. and Sudol, M. (2000) FASEB J. 14, 231-241. The importance of being proline: the interaction of proline-rich motifs in signaling proteins with their cognate domains.

Keegan, L., Gill, G. and Ptashne, M. (1986) Science 231, 699-704. Separation of DNA binding from the transcription-activating function of a eukaryotic regulatory protein.

Keinanen, K., Wisden, W., Sommer, B., Werner, P., Herb, A., Verdoorn, T. A., Sakmann, B. and Seeburg, P. H. (1990) Science 249, 556-560. A family of AMPA-selective glutamate receptors.

Kendrick S. J., Lynch, D. R. and Pritchett, D. B. (1996) J. Neurochem. 67, 608- 616. Characterisation of glutamate binding sites in receptors assembled from transfected NMDA receptor subunits.

Kew, J. N., Richards, J. G., Mutel, V. and Kemp, J. A. (1998) J. Neurosci. 18, 1935-1943. Developmental changes in NMDA receptor glycine affinity and ifenprodil sensitivity reveal three distinct populations of NMDA receptors in individual rat cortical neurons.

Kim, E., Cho, K. O., Rothschild, A. and Sheng, M. (1996) Neuron 17, 103-113. Heteromultimerization and NMDA receptor-clustering activity of Chapsyn-110, a member of the PSD-95 family of proteins.

Kim, E., Naisbitt, S., Hsueh, Y.-P., Rao, A., Rothschild, A., Craig, A. M. and Sheng, M. (1997) J. Cell Biol. 136, 669-678. GKAP, novel synaptic protein that interacts with the guanylate kinase-like domain of the PSD- 95/SAP90 family of channel clustering molecules.

Kim, E., Niethammer, M., Rothschild, A., Jan, Y.N. and Sheng, M. (1995) Nature. 378, 85-88. Clustering of Shaker-type K+ channels by interaction with a family of membrane-associated guanylate kinases.

Kim, M. J., Dunah, A. W., Wang, Y. T. and Sheng, M. (2005) Neuron 46, 745-760. Differential roles of NR2A- and NR2B-containing NMDA receptors in Ras-ERK signaling and AMPA receptor trafficking.

Kistner, U., Wenzel, B. M., Veh, R. W., Cases-Langhoff, C., Garner, A. M., Appeltauer, U., Voss, B., Gundelfinger, E. D. and Garner, C. C. (1993) J. Biol. Chem. 268, 4580-4583. SAP90, a rat pre-synaptic protein related to the product of the Drosophila tumor suppressor gene dlg-A.

Kiyama, Y., Manabe, T., Sakimura, K., Kawakami, F., Mori, H. and Mishina, M. (1998) J Neurosci. 18, 6704-6712. Increased thresholds for long-term potentiation and contextual learning in mice lacking the NMDA-type glutamate receptor ε1 subunit.

Klauck, T. M., Faux, M. C., Labudda, K., Langeberg, L. K., Jaken, S. and Scott, J. D. (1996) Science. 271, 1589 – 1592. Coordination of three signalling enzymes by AKAP79, a mammalian scaffold protein.

Kornau, H.-C., Schenker, L. T., Kennedy, M. B. and Seeburg, P. H. (1995) Science 269, 1737-1740. Domain interaction between NMDA receptor subunits and the post-synaptic density protein PSD-95.

Kuryatov, A., Laube, B., Betz, H. and Kuhse, J. (1994) Neuron 12, 1291-1300. Mutational analysis of the glycine-binding site of the NMDA receptor: structural similarity with bacterial amino acid-binding proteins.

Kutsuwada, T., Kashiwabucki, N., Mori, H., Sakimura, K., Kushiya, E., Araki, K., Meguro, H., Masaki, H., Kumanishi, T., Arakawa, M. and Mishina, M. (1992) Nature 358, 36-41. Molecular diversity of the NMDA receptor channel.

Kutsuwada, T., Sakimura, K., Manabe, T., Takayama, C., Katakura, N., Kushiya, E., Natsume, R., Watanabe, M., Inoue, Y., Yagi, T., Aizawa, S., Arakawa, M., Takahashi, T., Nakamura, Y., Mori, H. and Mishina, M. (1996) Neuron 16, 333-344. Impairment of suckling response, trigeminal neuronal pattern formation, and hippocampal LTD in NMDA receptor ε2 subunit mutant mice.

Laube, B., Hirai, H., Sturgess, M., Betz, H. and Kuhse, J. (1997) Neuron 18, 493-503. Molecular determinants of agonist discrimination by NMDA receptor subunits: analysis of the glutamate binding site on the NR2B subunit.

Laube, B., Kuhse, J. and Betz, H. (1998) J. Neurosci. 18, 2954-2961. Evidence for a tetrameric structure of recombinant NMDA receptors.

Laurie, D. J., Bartke, I., Schoepfer, R., Naujoks, K. and Seeburg, P. H. (1997) Brain Res. Mol. Brain Res. 51, 23-32. Regional, developmental and interspecies expression of the four NMDAR2 subunits, examined using monoclonal antibodies.

Laurie, D. J., Putzke, J., Zieglgansberger, W., Seeburg, P. H. and Tolle, T. R. (1995) Mol. Brain Res. 32, 94-108. The distribution of splice variants of the NMDAR1 subunit mRNA in adult rat brain.

Lavezzari, G., McCallum, J., Dewey, C. M. and Roche, K. W. (2004) J. Neurosci. 24, 6383-6391. Subunit-specific regulation of NMDA receptor endocytosis.

Lavezzari, G., McCallum, J., Lee, R. and Roche, K.W. (2003) Neuropharmacology. 45, 729-737. Differential binding of the AP-2 adaptor complex and PSD-95 to the C-terminus of the NMDA receptor subunit NR2B regulates surface expression.

Lee, F. J., Xue, S., Pei, L., Vukusic, B., Chery, N., Wang, Y., Wang, Y. T., Niznik, H. B., Yu, X. M. and Liu, F. (2002) Cell 111, 219-230. Dual regulation of NMDA receptor functions by direct protein-protein interactions with the dopamine D1 receptor.

Lee, F.J., Xue, S., Pei, L., Vukusic, B., Chery, N., Wang, Y., Wang, Y. T., Niznik, H. B., Yu, X. M. and Liu, F. (2002) Cell 111,219-230. Dual regulation of NMDA receptor functions by direct protein-protein interactions with the dopamine D1 receptor.

Leonoudakis, D., Mailliard, W., Wingerd, K., Clegg, D. and Vandenberg, C. (2001) J. Cell Sci. 114, 987-998. Inward rectifier potassium channel Kir2.2 is associated with synapse-associated protein SAP97.

Li, J. H., Wang, Y. H., Wolfe, B. B., Krueger, K. E., Corsi, L., Stocca, G. and Vicini, S. (1998) Eur. J. Neurosci. 10, 1704-1715. Developmental changes in localization of NMDA receptor subunits in primary cultures of cortical neurons.

Li, Y., Erzurumlu, R. S., Chen, C., Jhaveri, S. and Tonegawa, S. (1994) Cell 76, 427-437. Whisker-related neuronal patterns fail to develop in the trigeminal brainstem nuclei of NMDAR1 knockout mice.

Liao, D., Hessler, N. A. and Malinow, R. (1995) Nature 375, 400-404. Activation of postsynaptically silent synapses during pairing-induced LTP in CA1 region of hippocampal slice.

Liao, D., Zhang, X., O'Brien, R., Ehlers, M. D. and Huganir, R. L. (1999) Nat. Neurosci. 2, 37-43. Regulation of morphological postsynaptic silent synapses in developing hippocampal neurons.

Lim, I. A., Hall, D. D. and Hell, J. W. (2002) J. Biol. Chem. 277, 21697-21711. Selectivity and promiscuity of the first and second PDZ domains of PSD-95 and synapse-associated protein 102.

Lin, J. W., Wyszynski, M., Madhavan, R., Sealock, R., Kim, J. U. and Sheng, M. (1998) J. Neurosci. 18, 2017-2027. Yotiao, a novel protein of neuromuscular junction and brain that interacts with specific splice variants of NMDA receptor subunit NR1.

Lin, Y., Jover-Mengual, T., Wong, J., Bennett, M. V. and Zukin, R. S. (2006) Proc. Natl. Acad. Sci. USA. 103, 19902-19907. PSD-95 and PKC converge in regulating NMDA receptor trafficking and gating.

Lin, Y., Skeberdis, V. A., Francesconi, A., Bennett, M. V. and Zukin, R. S. (2004) J. Neurosci. 24, 10138-10148. Postsynaptic density protein-95 regulates NMDA channel gating and surface expression.

Lipschutz, J. H. and Mostov, K. E. (2002) Curr. Biol. 12, R212-R214. Exocytosis: the many masters of the exocyst.

Lisman, J. (2001a) Encyclopedia of Life Science. Long-term depression and depotentiation.

Lisman, J. E. and McIntyre, C.C. (2001b) Curr. Biol. 11, 788-791. Synaptic plasticity: a molecular memory switch.

Lisman, J., Schulman, H. And Cline, H. (2002) Nature Rev. Neurosci. 3, 175 - 190. The molecular basis of CaMKII function in synaptic and behavioural memory.

Liu, L., Wong, T. P., Pozza, M. F., Lingenhoehl, K., Wang, Y., Sheng, M., Auberson Y. P. and Wang, Y. T. Science 304 (2004), pp. 1021–1024. Role of NMDA receptor subtypes in governing the direction of hippocampal synaptic plasticity.

Long, J. F., Tochio, H., Wang, P., Fan, J. S., Sala, C., Niethammer, M., Sheng, M. and Zhang. M. (2003) J. Mol. Biol. 327, 203-14. Supramodular structure and synergistic target binding of the N-terminal tandem PDZ domains of PSD-95.

Losi, G., Prybylowski, K., Fu, Z., Luo, J., Wenthold, R. J. and Vicini, S. (2003) J. Physiol. 548, 21-29. PSD-95 regulates NMDA receptors in developing cerebellar granule neurons of the rat.

Lund, A. H., Duch, M. and Pederson, F. S. (1996) Nucleic Acids Res. 24, 800-801. Increased cloning efficiency by temperature-cycle ligation.

Luo, J., Wang, Y., Yasuda, R. P., Dunah, A. W. and Wolfe, B. B. (1997) Mol. Pharmacol. 51, 79-86. The majority of N-methyl-D-aspartate receptor complexes in adult rat cerebral cortex contain at least three different subunits (NR1/NR2A/NR2B).

Lynch, D. R. and Guttmann, R. P. (2001) Curr. Drug Targets 2, 215-231. NMDA receptor pharmacology: perspectives from molecular biology.

Madry, C., Mesic, I., Bartholomaus, I., Nicke, A., Betz, H. and Laube, B. (2007) Biochem. Biophys. Res. Commun. 354, 102-8. Principal role of NR3 subunits in NR1/NR3 excitatory glycine receptor function.

Malenka, R. C. and Nicoll, R. A. (1997) Neuron 19, 473-476. Silent synapses speak up.

Man, H-Y., Sekine-Aizawa, Y. and Huganir, R. L. (2007) Proc. Natl. Acad. Sci. USA. 104, 3579-3584. Regulation of α-amino-3-hydroxy-5-methyl-4-isoxazolepropionic acid receptor trafficking through PKA phosphorylation of the Glu receptor 1 subunit.

Margeta-Mitrovic, M., Jan, Y. N. and Jan, L. Y. (2000) Neuron 27, 97-106. A trafficking checkpoint controls GABA(B) receptor heterodimerization.

Matsuda, K., Kamiya, Y., Matsuda, S. and Yuzaki, M. (2002) Mol. Brain Res. 100, 43-52. Cloning and characterization of a novel NMDA receptor subunit NR3B: a dominant subunit that reduces calcium permeability.

Mattar, P. A., Holmes, K. D. and Dekaban, G. A. (2005) Neuroscience 132, 281-298. The NR1-4 C-terminus interferes with N-methyl-D-aspartate receptor-mediated excitotoxicity: evidence against a typical T/SXV-PDZ interaction.

Mauceri, D., Cattabeni, F., Di Luca, M. and Gardoni, F. (2004) J. Biol. Chem. 279, 23813-23821. Calcium/calmodulin-dependent protein kinase II phosphorylation drives synapse-associated protein 97 into spines.

Mauceri, D., Gardoni, F., Marcello, E. and Di Luca, M. (2007) J. Neurochem. 100, 1032-1046. Dual role of CaMKII-dependent SAP97 phosphorylation in mediating trafficking and insertion of NMDA receptor subunit NR2A.

Mayer, M. L. (2006) Nature 440, 456-462. Glutamate receptors at atomic resolution.

Mayer, M. L., Westbrook, G. L. and Guthrie, P. B. (1984) Nature 309, 261-263. Voltage-dependent block by Mg^{2+} of NMDA responses in spinal cord neurones.

Mayer, M.L. (2005) Curr. Opin. Neurobiol. 15, 282-288. Glutamate receptor ion channels.

McBain, C. J. and Mayer, M. L. (1994) Physiol. Rev. 74, 723-360. N-methyl-D-aspartic acid receptor structure and function.

McIlhinney, R. A. J., Le Bourdellès, B., Molnar, E., Tricaud, N., Streit, P. and Whiting, P. J. (1998) Neuropharmacology 37, 1355-1367. Assembly, intracellular targeting and cell surface expression of the human N-methyl-D-aspartate receptor subunits NR1a and NR2A in transfected cells.

Meddows, E., Le, Bourdellès, B., Grimwood, S., Wafford, K., Sandhu, S., Whiting, P. and McIlhinney, R. A. (2001) J. Biol. Chem. 276, 18795-18803. Identification of molecular determinants that are important in the assembly of N-methyl-D-aspartate receptors.

Meguro, H., Mori, H., Araki, K., Kushiya, E., Kutsuwada, T., Yamazaki, M., Kumanishi, T., Arakawa, M., Sakimura, K. and Mishina, M. (1992) Nature 357, 70-74. Functional characterisation of a heteromeric NMDA receptor channel expressed from cloned cDNAs.

Meloni, A. R., Smith, E. J. and Nevins, J. R. (1999) Proc. Natl. Acad. Sci. USA. 96, 9574-9579. A mechanism for Rb/p130-mediated transcription repression involving recruitment of the CtBP corepressor.

Mi, R., Sia, G-M., Rosen, K., Tang, X., Moghekar, A., Black, J. L., McEnery, M., Huganir, R. L. and O'Brien, R. J. (2004) Neuron 44, 335-349. AMPA receptor-dependent clustering of synaptic NMDA receptors is mediated by stargazin and NR2A/B in spinal neurons and hippocampal interneurons.

Migaud, M., Charlesworth, P., Dempster, M., Webster, L. C., Watabe, A. M., Makhinson, M., He, Y., Ramsay, M. F., Morris, R. G., Morrison, J. H., O'Dell, T. J. and Grant, S. G. (1998) Nature 396, 433-439. Enhanced long-term potentiation and impaired learning in mice with mutant postsynaptic density-95 protein.

Misra, C., Brickley, S. G., Farrant, M. and Cull-Candy, S. G. (2000) J. Physiol. 524, 147-162. Identification of subunits contributing to synaptic and extrasynaptic NMDA receptors in Golgi cells of the rat cerebellum.

Mohrmann, R., Hatt, H. and Gottmann, K. (2000) Neuroreport 11, 1203-1208. Developmental regulation of subunit composition of extrasynaptic NMDA receptors in neocortical neurones.

Mohrmann, R., Kohr, G., Hatt, H., Sprengel, R. and Gottmann, K. (2002) J. Neurosci. Res. 68, 265-275. Deletion of the C-terminal domain of the NR2B subunit alters channel properties and synaptic targeting of N-methyl-D-aspartate receptors in nascent neocortical synapses.

Mok, H., Shin, H., Kim, S., Lee, J. R., Yoon, J. and Kim, E. (2002) J. Neurosci. 22, 5253-5258. Association of the kinesin superfamily motor protein KIF1Balpha with postsynaptic density-95 (PSD-95), synapse-associated protein-97, and synaptic scaffolding molecule PSD-95/discs large/zona occludens-1 proteins.

Momiyama, A., Feldmeyer, D. and Cull-Candy, S. G. (1996) J. Physiol. 494, 479-492. Identification of a native low-conductance NMDA channel with reduced sensitivity to Mg2+ in rat central neurones.

Monyer, H., Burnashev, N., Laurie, D. J., Sakmann, B. and Seeburg, P. H. (1994) Neuron 12, 529-540. Developmental and regional expression in the rat brain and functional properties of four NMDA receptors.

Monyer, H., Sprengel, R., Schoepfer, R., Herb, A., Higuchi, M., Lomeli, H., Burnashev, N., Sakmann, B. and Seeburg, P. H. (1992) Science 256, 1217-1221. Heteromeric NMDA receptors: Molecular and functional distinction of subtypes.

Montgomery, J.M., Zamorano, P.L. and Garner C.C. (2004) Cell. Mol. Life. Sci, 61, 911-929. MAGUKs in synapse assembly and function: an emerging view.

Mori, H., Manabe, T., Watanabe, M., Satoh, Y., Suzuki, N., Toki, S., Nakamura, K., Yagi, T., Kushiya, E., Takahashi, T., Inoue, Y., Sakimura, K. and Mishina, M. (1998) Neuron 21, 571-580. Role of the carboxy-terminal region of the GluRepsilon2 subunit in synaptic localization of the NMDA receptor channel.

Mori, H., Yamakura, T., Masaki, H. and Mishina, M. (1993) Neuroreport 4, 519-522. Involvement of the carboxyl-terminal region in modulation by TPA of the NMDA receptor channel.

Moriyoshi, K., Masu, M., Ishii, T., Shigemoto, R., Mizuno, N. and Nakanishi, S. (1991) Nature 354, 31-37. Molecular cloning and characterisation of the rat NMDA receptor.

Muller, B. M., Kistner, U., Kindler, S., Chung, W. J., Kuhlendahl, S., Fenster, S. D., Lau, L.-F., Veh, R. W., Huganir, R. L., Gundelfinger, E. D. and Garner, C. C. (1996) Neuron 17, 255-265. SAP102, a novel postsynaptic protein that interacts with NMDA receptor complexes in vivo.

Muller, B. M., Kistner, U., Veh, R. W., Cases-Langhoff, C., Becker, B., Gundelfinger, E. D. and Garner, C. C. (1995) J. Neurosci. 15, 2354-2366. Molecular characterisation and spatial distribution of SAP97, a novel presynaptic protein homologous to SAP90 and the Drosophila discs-large tumor suppressor protein.

Murata, Y., Doi, T., Taniguchi, H. and Fujiyoshi, Y. (2005) Biochem. Biophys. Res. Commun. 327, 183-191. Proteomic analysis revealed a novel synaptic proline-rich membrane (PRR7) associated with PSD-95 and NMDA receptor.

Naisbitt, S., Kim, E., Tu, J. C., Xiao, B., Sala, C., Valtschanoff, J., Weinberg, R. J., Worley, P. F. and Sheng, M. (1999) Neuron 23, 569-582. Shank, a novel family of post-synaptic density proteins that binds to the NMDA receptor/PSD-95/GKAP complex and cortactin.

Nakazawa, T., Komai, S., Tezuka, T., Hisatsune, C., Umemori, H., Semba, K., Mishina, M., Manabe, T. and Yamamoto, T. (2001) J. Biol. Chem. 276, 693-699. Characterization of Fyn-mediated tyrosine phosphorylation sites on GluR epsilon 2 (NR2B) subunit of the N-methyl-D-aspartate receptor.

Nehring, R. B., Wischmeyer, E., Döring, F., Veh, R. W., Sheng, M. and Karschin, A. (2000) J. Neurosci. 20, 156-162. Neuronal inwardly rectifying K^+ channels differentially couple to PDZ proteins of the PSD-95/SAP90 family.

Neithammer, M., Kim, E. and Sheng, M. (1996) J. Neurosci. 16, 2157-2163. Interaction between the C terminus of NMDA receptor subunits and multiple members of the PSD-95 family of membrane-associated guanylate kinases.

Neithammer, M., Valtschanoff, J. G., Kapoor, T. M., Allison, D. W., Weinberg, R. J., Craig, A. M. and Sheng, M. (1998) Neuron 20, 693-707. CRIPT, a novel post-synaptic protein that binds to the third PDZ domain of PSD-95/SAP90.

Neyton, J. and Paoletti, P. (2006) J. Neurosci. 26, 1331-1333. Relating NMDA receptor function to receptor subunit composition: limitations of the pharmacological approach.

Nishi, M., Hinds, H., Lu, H. P., Kawata, M. and Hayashi, Y. (2001) J. Neurosci. 21, RC185. Motoneuron-specific expression of NR3B, a novel NMDA-type glutamate receptor subunit that works in a dominant-negative manner.

Noel, J., Ralph, G. S., Pickard, L., Willimans, J., Molnar, E., Uney, J. B., Collingridge, G. L. and Henley, J.M. (1999) Neuron 23, 365-376. Surface expression of AMPA receptors in hippocampal neurons is regulated by an NSF-dependent mechanism.

Nong, Y., Huang, Y. Q., Ju, W., Kalia, L. V., Ahmadian, G., Wang, Y. T. and Salter, M. W. (2003) Nature 422, 302-307. Glycine binding primes NMDA receptor internalization.

Oh, B. H., Pandit, J., Kang, C. H., Nikaido, K., Gokcen, S., Ames, G. F. and Kim, S. H. (1993) J. Biol. Chem. 268, 11348-11355. Three-dimensional structures of the periplasmic lysine/arginine/ornithine-binding protein with and without a ligand.

Okabe, S., Miwa, A. and Okade, H. (1999) J. Neurosci. 19, 7781-7792. Alternative splicing of the C-terminal domain regulates cell surface expression of the NMDA receptor NR1 subunit.

Olsen, O. and Bredt, D. S. (2003) J. Biol. Chem. 278, 6873-6878. Functional analysis of the nucleotide binding domain of membrane-associated guanylate kinases.

Pak, D. T., Yang, S., Rudolph-Correia, S., Kim, E. and Sheng, M. (2001) Neuron 31, 289-303. Regulation of dendritic spine morphology by SPAR, a PSD-95-associated RapGAP.

Paoletti, P., Ascher, P. and Neyton, J. (1997) J Neurosci 17, 5711–5725. High-affinity zinc inhibition of NMDA NR1-NR2A receptors.

Paoletti, P. and Neyton, J. (2007) Curr. Opin. Pharmacol. 7, 39-47. NMDA receptor subunits: function and pharmacology.

Papadakis, M. (2004) Assembly and trafficking of NMDA receptors: a biochemical approach. PhD thesis, School of Pharmacy, University of London, U. K.

Papadakis, M., Hawkins, L. M., and Stephenson, F. A. (2004) J. Biol. Chem. 279, 14703-14712. Appropriate NR1-NR1 disulfide-linked homodimer formation is requisite for efficient expression of functional, cell surface N-methyl-D-aspartate NR1/NR2 receptors.

Passafaro, M., Sala, C., Niethammer, M. and Sheng, M. (1999) Nat. Neurosci. 2, 1063 – 1069. Microtubule binding by CRIPT and its potential role in the synaptic clustering of PSD-95.

Pei, L., Lee, F. J., Moszczynska, A., Vukusic, B. and Liu, F. (2004) J. Neurosci. 24, 1149-1158. Regulation of dopamine D1 receptor function by physical interaction with the NMDA receptors.

Penzes, P., Johnson, R. C., Sattler, R., Zhang, X., Huganir, R. L., Kambampati, V., Mains, R. E. and Eipper, B. A. (2001) Neuron 29, 229-242. The neuronal Rho-GEF Kalirin-7 interacts with PDZ domain-containing proteins and regulates dendritic morphogenesis.

Perin-Dureau, F., Rachline, J., Neyton, J. and Paoletti, P. (2002) J. Neurosci. 22, 5955-5965. Mapping the binding site of the neuroprotectant ifenprodil on NMDA receptors.

Pickard, L., Noel, J., Henley, J.M., Collingridge, G.L. and Molnar, E. (2000) J. Neurosci. 20, 7922-7931. Developmental changes in synaptic AMPA and NMDA receptor distribution and AMPA receptor subunit composition in living hippocampal neurons.

Portera-Cailliau, C., Price, D. L. and Martin, L. J. (1996) J. Neurochem. 66, 692-700. N-methyl-D-aspartate receptor proteins NR2A and NR2B are differentially distributed in the developing rat central nervous system as revealed by subunit-specific antibodies.

Postigo, A. A. and Dean, D. C. (1999) Mol. Cell Biol. 19, 7961-7971. Independent repressor domains in ZEB regulate muscle and T-cell differentiation.

Premkumar, L. S. and Auerbach, A. (1997) J. Gen. Physiol. 110, 485-502. Stoichiometry of recombinant *N*-methyl-D-aspartate receptor channels inferred from single-channel current patterns.

Prybylowski, K., Chang, K., Sans, N., Kan, L., Vicini, S. and Wenthold, R. J. (2005) Neuron 47, 845-57. The synaptic localization of NR2B-containing NMDA receptors is controlled by interactions with PDZ proteins and AP-2.

Prybylowski, K., Fu, Z., Losi, G., Hawkins, L. M., Luo, J., Chang, K., Wenthold, R. J. and Vicini, S. (2002) J. Neurosci. 22, 8902-8910. Relationship between availability of NMDA receptor subunits and their expression at the synapse.

Qiu, S., Hua, Y. L., Yang, F., Chen, Y. Z. and Luo. J. H. (2005) J. Biol. Chem. 280, 24923-24930. Subunit assembly of N-methyl-d-aspartate receptors analyzed by fluorescence resonance energy transfer.

Richmond, S. A., Irving, A. J., Molnar, E., McIlhinney, R. A., Michelangeli, F., Henley, J. M. and Collingridge, G. L. (1996) Neuroscience 4, 794-802. Localisation of the glutamate receptor subunit GluR1 on the surface of living and within cultured hippocampal neurons.

Riefler, G. M. and Firestein, B. L. (2001) J. Biol. Chem. 276, 48262-48268. Binding of neuronal nitric-oxide synthase (nNOS) to carboxyl-terminal-binding protein (CtBP) changes the localization of CtBP from the nucleus to the cytosol: a novel function for targeting by the PDZ domain of nNOS.

Robinson, R. S., Watts, C. and Zerial, M. (1996) Cell 84, 13-21. Membrane dynamics in endocytosis.

Roche, K. W., Standley, S., McCallum, J., Dune, Ly. C., Ehlers, M. D. and Wenthold, R. J. (2001) Nat. Neurosci. 4, 794-802. Molecular determinants of NMDA receptor internalization.

Roy, B. C., Kohu, K., Matsuura, K., Yanai, H. and Akiyama, T. (2002) Genes Cells. 7, 607-617. SPAL, a Rap-specific GTPase activating protein, is present in the NMDA receptor-PSD-95 complex in the hippocampus.

Rutter, A. R. (2001) Biochemical and pharmacological characterisation of the interaction between NMDA receptors and the scaffolding protein, PSD-95. PhD thesis, School of Pharmacy, University of London, U. K.

Rutter, A. R. and Stephenson, F. A. (2000) J. Neurochem. 75, 2501-2510. Coexpression of postsynaptic density-95 protein with NMDA receptors results in enhanced receptor expression together with a decreased sensitivity to L-glutamate.

Rutter, A. R., Freeman, F. M., and Stephenson, F. A. (2002) J. Neurochem. 81, 1298-1307. Further characterization of the molecular interaction between PSD-95 and NMDA receptors: the effect of the NR1 splice variant and evidence for modulation of channel gating.

Sakimura, K., Kutsuwada, T., Ito, I., Manabe, T., Takayama, C., Kushiya, E., Yagi, T., Aizawa, S., Inoue, Y., Sugiyama, H. and Mishina, M. (1995) Nature 373, 151-155. Reduced hippocampal LTP and spatial learning in mice lacking NMDA receptor ε1 subunit.

Sandhu, S., Grimwood, S., Mortishire-Smith, R. J., Whiting, P. J. and Le Bourdellès, B. (1999) J. Neurochem. 72, 1694-1698. Delineation of the structural determinants of the N-methyl-D-aspartate receptor glycine binding site.

Sans, N., Petralia, R. S., Wang, Y. X., Blahos, J 2nd., Hell, J. W. and Wenthold, R. J. (2000) J. Neurosci. 20, 1260-1271. A developmental change in NMDA receptor-associated proteins at hippocampal synapses.

Sans, N., Prybylowski, K., Petralia, R. S., Chang, K., Wang, Y. X., Racca, C., Vicini, S., and Wenthold, R. J. (2003) Nat. Cell Biol. 5, 520-530. NMDA receptor trafficking through an interaction between PDZ proteins and the exocyst complex.

Sans, N., Wang, P. Y., Du, Q., Petralia, R. S., Wang, Y. X., Nakka, S., Blumer, J. B., Macara, I.G. and Wenthold, R. J. (2005) Nat. Cell Biol. 7, 1179-1190. mPins modulates PSD-95 and SAP102 trafficking and influences NMDA receptor surface expression.

Sattler, R. and Tymianski, M. (2000) J. Mol. Med. 78, 3 - 13. Molecular mechanisms of calcium-dependent excitotoxicity.

Sattler, R., Xiong, Z., Lu, W.-Y., Hafner, M., MacDonald, J. F. and Tymianski, M. (1999) Science 284, 1845-1848. Specific coupling of NMDA receptor activation to nitric oxide neurotoxicity by PSD-95 protein.

Schaeper, U., Subramanian, T., Lim, L., Boyd, J.M. and Chinnadurai. G. (1998) J. Biol. Chem. 273, 8549-8552. Interaction between a cellular protein that binds to the C-terminal region of adenovirus E1A (CtBP) and a novel cellular protein is disrupted by E1A through a conserved PLDLS motif.

Schiestl, R. H. and Gietz, R. D. (1989) Curr. Genet. 16, 339-346. High efficiency transformation of intact yeast cells using single stranded nucleic acids as a carrier.

Schluter, O.M., Xu, W. and Malenka, R.C. (2006) Neuron. 51, 99-111. Alternative N-terminal domains of PSD-95 and SAP97 govern activity-dependent regulation of synaptic AMPA receptor function.

Schorge, S. and Colquhoun, D. (2003) J. Neurosci. 23, 1151-1158. Studies of NMDA receptor function and stoichiometry with truncated and tandem subunits.

Scott, D. B., Blanpied, T. A., Swanson, G. T., Zhang, C. and Ehlers, M. D. (2001) J. Neurosci. 21, 3063-3072. An NMDA receptor ER retention signal regulated by phosphorylation and alternative splicing.

Scott, D. B., Michailidis, I., Mu, Y., Logothetis, D. and Ehlers, M. D. (2004) J. Neurosci. 24, 7096-7109. Endocytosis and degradative sorting of NMDA receptors by conserved membrane-proximal signals.

Scott, L., Kruse, M. S., Forssberg, H., Brismar, H., Greengard, P. and Aperia, A. (2002) Proc. Natl. Acad. Sci. USA. 99, 1661-1664. Selective up-regulation of dopamine D1 receptors in dendritic spines by NMDA receptor activation.

Scott, L., Zelenin, S., Malmersjo, S., Kowalewski, J. M., Markus, E. Z., Nairn, A. C., Greengard, P., Brismar, H. and Aperia, A. (2006) Proc. Natl. Acad. Sci. USA. 103, 762-767. Allosteric changes of the NMDA receptor trap diffusible dopamine 1 receptors in spines.

Seabold, G. K., Burette, A., Lim, I. A., Weinberg, R. J. and Hell, J.W. (2003) J. Biol. Chem. 278, 15040-15048. Interaction of the tyrosine kinase Pyk2 with the N-methyl-D-aspartate receptor complex via the Src homology 3 domains of PSD-95 and SAP102.

Setou, M., Nakagawa, T., Seog, D. H. and Hirokawa, N. (2000) Science 288, 1796-1802. Kinesin superfamily motor protein KIF17 and mLin-10 in NMDA receptor-containing vesicle transport.

Sheng, M. and Pak, D. T. (2000) Annu. Rev. Physiol. 62, 755-778. Ligand-gated ion channel interactions with cytoskeletal and signaling proteins.

Sheng, M. and Sala, C. (2001) Annu. Rev. Neurosci. 24, 1-29. PDZ domains and the organization of supramolecular complexes.

Sheng, M., Cummings, J., Roldan, L. A., Jan, Y. N. and Jan, L. Y. (1994) Nature 368, 144-147. Changing subunit composition of heteromeric NMDA receptors during development of rat cortex.

Shieh, B. H. and Zhu, M. Y. (1996) Neuron 16, 991-998. Regulation of the TRP Ca2+ channel by INAD in Drosophila photoreceptors.

Shin, H., Hsueh, Y. P., Yang, F. C., Kim, E. and Sheng, M. (2000) J. Neurosci. 20, 3580-3587. An intramolecular interaction between Src homology 3 domain and guanylate kinase-like domain required for channel clustering by postsynaptic density-95/SAP90.

Silva, A. J., Paylor, R., Wehner, J. M. and Tonegawa, S. (1992) Science 257, 206-11. Impaired spatial learning in alpha-calcium-calmodulin kinase II mutant mice.

Silva, A. J., Stevens, C.F., Tonegawa, S. and Wang, Y. (1992) Science 257, 201-6. Deficient hippocampal long-term potentiation in alpha-calcium-calmodulin kinase II mutant mice.

Simpkins, K. L., Guttmann, R. P., Dong, Y., Chen, Z., Sokol, S., Neumar, R. W. and Lynch, D. R. (2003) J. Neurosci. 23, 11322-11331. Selective activation induced cleavage of the NR2B subunit by calpain.

Songyang, Z., Fanning, A. S., Fu, C., Xu, J., Marfatia, S. M., Chishti, A. H., Crompton, A., Chan, A. C., Anderson, J. M. and Cantley, L. C. (1997) Science 275, 73-77. Recognition of unique carboxyl-terminal motifs by distinct PDZ domains.

Sprengel, R., Suchanek, B., Amico, C., Brusa, R., Burnashev, N., Rozov, A., Hvalby, O., Jensen, V., Paulsen, O., Andersen, P., Kim, J. J., Thompson, R. F., Sun, W., Webster, L. C., Grant, S. G. N., Eilers, J., Konnerth, A., Li, J., McNamara, J. O. and Seeburg, P. H. (1998) Cell 92, 279-289. Importance of the intracellular domain of NR2 subunits for NMDA receptor function in vivo.

Standley, S. Roche, K. W., McCallum, J., Sans, N. and Wenthold, R. J. (2000) Neuron 28, 887-898. PDZ-domain suppression of an ER retention signal in NMDA receptor NR1 splice variants.

Steigerwald, F., Schulz, T. W., Schenker, L. T., Kennedy, M. B. Seeburg, P. H. and Kohr, G. (2000) J. Neurochem. 20, 4573-4581. C-terminal truncation of NR2A subunits impairs synaptic but not extra-synaptic localization of NMDA receptors.

Stephenson, F. A. (2001) Curr. Drug Targets 2, 233-239. Subunit characterization of NMDA receptors.

Stern, P., Behe, P., Schoepfer, R. and Colquhoun, D. (1992) Proc. Royal Soc. Lon. - B. Biological Sciences. 250, 271-277. Single-channel conductances of NMDA receptors expressed from cloned cDNAs: Comparison with native receptors.

Stocca, G. and Vicini, S. (1998) J. Physiol. 507, 13-24. Increased contribution of NR2A subunit to synaptic NMDA receptors in developing rat cortical neurons.

Strack, S. and Colbran, R. J. (1998) J. Biol. Chem. 273, 20689-20692. Autophosphorylation-dependent targeting of calcium/ calmodulin-dependent protein kinase II by the NR2B subunit of the N-methyl- D-aspartate receptor.

Sucher, N. J., Awobuluyi, M., Choi, Y. B. and Lipton, S. A. (1996) Trends. Pharmacol Sci. 17, 348-355. NMDA receptors: from genes to channels.

Takahshi, T., Feldmeyer, D., Suzuki, N., Onodera, K., Cull-Candy, S. G., Sakimura, K. and Mishina, M. (1996) J. Neurosci. 16, 4376-4382. Functional correlation of NMDA receptor ε subunits expression with the properties of single-channel and synaptic currents in the developing cerebellum.

Takeuchi, M., Hata, Y., Hirao, K., Toyoda, A., Irie, M. and Takai, Y. (1997) J. Biol. Chem. 272, 11943-11951. SAPAPs. A family of PSD-95/SAP90-associated proteins localized at postsynaptic density.

Takumi, Y., Matsubara, A., Rinvik, E. and Ottersen. O. P. (1999) Ann N Y Acad Sci. 868, 474-82. The arrangement of glutamate receptors in excitatory synapses.

Tao, Y. X., Rumbaugh, G., Wang, G. D., Petralia, R. S., Zhao, C., Kauer, F. W., Tao, F., Zhuo, M., Wenthold, R. J., Raja, S. N., Huganir, R. L., Bredt, D. S. and Johns, R. A. (2003) J. Neurosci. 23, 6703-6712. Impaired NMDA receptor-mediated postsynaptic function and blunted NMDA receptor-dependent persistent pain in mice lacking postsynaptic density-93 protein.

Tavares, G. A., Panepucci, E. H. and Brunger, A. T. (2001) Mol. Cell. 8, 1313-1325. Structural characterization of the intramolecular interaction between the SH3 and guanylate kinase domains of PSD-95.

Tezuka, T., Umemori, H., Akiyama, T., Nakanishi, S. and Yamamoto, T. (1999) Proc. Natl. Acad. Sci. USA. 96, 435-440. PSD-95 promotes Fyn-mediated tyrosine phosphorylation of the N-methyl-D-aspartate receptor subunit NR2A.

Thomas, C. G., Miller, A. J. and Westbrook, G. L. (2006) J. Neurophysiol. 95, 1727-1734. Synaptic and extrasynaptic NMDA receptor NR2 subunits in cultured hippocampal neurons.

Thompson, C. L., Drewery, D. L., Atkins, H. D. and Stephenson, F. A. (2000) Neurosci. Lett. 283, 85-88. Immunohistochemical localization of N-methyl-D-aspartate receptor NR1, NR2A, NR2B and NR2C/D subunits in the adult mammalian cerebellum.

Thompson, C. L., Drewery, D. L., Atkins, H. D., Stephenson, F. A. and Chazot, P. L. (2002) Brain Res. Mol. Brain Res. 102, 55-61. Immunohistochemical localization of N-methyl-D-aspartate receptor subunits in the adult murine hippocampal formation: evidence for a unique role of the NR2D subunit.

Tiffany, A. M., Manganas, L. N., Kim, E., Hsueh, Y. P., Sheng, M. and Trimmer, J. S. (2000) J. Cell Bio. 148, 147-58. PSD-95 and SAP97 exhibit distinct mechanisms for regulating K(+) channel surface expression and clustering.

Tingley, W. G., Roche, K. W., Thompson, A. K. and Huganir, R. L. (1993) Nature 364, 70-73. Regulation of NMDA receptor phosphorylation by alternative splicing of the C-terminal domain.

Topinka, J. R. and Bredt, D. S. (1998) Neuron 20, 125-134. N-terminal palmitoylation of PSD-95 regulates association with cell membranes and interaction with K^+ channel Kv1.4.

Tovar, K. R. and Westbrook, G. J. (1999) J. Neurosci. 19, 4180-4188. The incorporation of NMDA receptors with distinct subunit composition at nascent hippocampal synapses in vitro.

Tovar, K. R. and Westbrook, G. L. (2002) Neuron 34, 255-264. Mobile NMDA receptors at hippocampal synapses.

Townsend, M., Yoshii, A., Mishina, M. and Constantine-Paton, M. (2003) Proc. Natl. Acad. Sci. USA. 100, 1340-1345. Developmental loss of miniature N-methyl-D-aspartate receptor currents in NR2A knock mice.

Trinidad, J. C., Specht, C. G., Thalhammer, A., Schoepfer, R. and Burlingame, A. L. (2006) Mol. Cell Proteomics 5, 914-922. Comprehensive identification of phosphorylation sites in postsynaptic density preparations.

Vazhappilly, R. and Sucher, N. J. (2002) Neurosci. Lett. 318, 153-157. Turnover analysis of N-methyl-D-aspartate receptor subunit NR1 protein in PC12 cells.

Vissel, B., Krupp, J. J., Heinemann, S. F. and Westbrook, G. L. (2001) Nat. Neurosci. 4, 587-596. A use-dependent tyrosine dephosphorylation of NMDA receptors is independent of ion flux.

Wafford, K. A., Bain, C. J., Le Bourdelles, B., Whiting, P. J. and Kemp, J. A. (1993) Neuroreport. 4, 1347-1349. Preferential co-assembly of recombinant NMDA receptors composed of three different subunits.

Wafford, K. A., Kathoria, M., Bain, C. J., Marshall, G., Le Bourdelles, B., Kemp, J. A. and Whiting, P. J. (1995) Mol. Pharmacol. 47, 374-380. Identification of amino acids in the N-methyl-D-aspartate receptor NR1 subunit that contribute to the glycine binding site.

Wallace, R. B. Shaffer, J. Murphy, R. F., Bonner, J., Hirose, T. and Itakura, K. (1979) Nucleic Acids Res. 6, 3543-6357. Hybridization of synthetic oligodeoxyribonucleotides to Phi Chi 174 DNA: the effect of single base pair mismatch.

Wang, C-Y., Chang, K., Petralia, R. S., Wang, Y-X., Seabold, G. K. and Wenthold, R.J. (2006) J. Neurosci. 26: 2174-2183. A novel family of adhesion-like molecules that interacts with the NMDA receptor.

Wang, L., Piserchio, A. and Mierke. D. F. (2005) J. Biol. Chem. 280, 26992-6. Structural characterization of the intermolecular interactions of synapse-associated protein-97 with the NR2B subunit of N-methyl-D-aspartate receptors.

Wang, Y. H., Bosy, T. Z., Yasuda, R. P., Grayson, D. R., Vicini, S., Pizzorusso, T. and Wolfe, B. B. (1995) J. Neurochem. 65, 176-183. Characterization of NMDA receptor subunit-specific antibodies: distribution of NR2A and NR2B receptor subunits in rat brain and ontogenic profile in the cerebellum.

Wang, Y. T. and Salter, M. W. (1994) Nature 369, 233-235. Regulation of NMDA receptors by tyrosine kinases and phosphatases.

Wenzel, A., Scheurer, L., Kunzi, R., Fritschy, J. M., Mohler, H. and Benke, D. (1995) Neuroreport 29, 45-48. Distribution of NMDA receptor subunit proteins NR2A, 2B, 2C and 2D in rat brain.

Werner, P., Voigt, M., Keinanen, K., Wisden, W. and Seeburg. P. H. (1991) Nature 351, 742-744. Cloning of a putative high-affinity kainate receptor expressed predominantly in hippocampal CA3 cells.

Williams, K. (1993) Mol. Pharmacol. 44, 851-859. Ifenprodil discriminates subtypes of the N-methyl-D-aspartate receptor: selectivity and mechanisms at recombinant heteromeric receptors.

Williams, K. (1995) Neurosci. Lett. 184, 181-184. Pharmacological properties of recombinant *N*-methyl-D-aspartate (NMDA) receptors containing the epsilon4 (NR2D) subunit.

Williams, K., Chao, J., Kashiwagi, W., Masuko, T. and Igarashi, K. (1996) Mol. Pharmacol. 50, 701-708. Activation of N-methyl-D-aspartate receptors by glycine: role of an aspartate residue in the M3-M4 loop of the NR1 subunit.

Wong, R.W., Setou, M., Teng, J., Takei, Y. and Hirokawa, N. (2002) Proc. Natl. Acad. Sci. USA. 99, 14500-14505. Overexpression of motor protein KIF17 enhances spatial and working memory in transgenic mice.

Wood, M. W., VanDongen, H. M. A., and VanDongen, A. M. J. (1995) Proc. Natl. Acad. Sci. USA. 92, 4882-4886. Structural conservation of ion channel pathways in K^+ channels and glutamate receptors.

Wood, M. W., VanDongen, H. M. and VanDongen, A. M. (1997) J. Biol. Chem. 272, 3532-3537. An alanine residue in the M3-M4 linker lines the glycine binding pocket of the N-methyl-D-aspartate receptor.

Wyszynski, M., Kharazia, V., Shanghvi, R., Rao, A., Beggs, A. H., Craig, A. M., Weinberg, R. and Sheng, M (1998) J. Neurosci. 18, 1383-1392. Differential regional expression and ultrastructural localisation of α-Actinin-2, a putative NMDA receptor-anchoring protein, in rat brain.

Wyszynski, M., Lin, J., Rao, A., Nigh, E., Beggs, A. H., Craig, A. M., and Sheng, M. (1997) Nature 385, 439-442. Competitive binding of α-actinin and calmodulin to the NMDA receptor.

Xia, H., Hornby, Z. D., and Malenka, R. C. (2001) Neuropharmacology 41, 714-723. An ER retention signal explains differences in surface expression of NMDA and AMPA receptor subunits.

Yamada, Y., Chochi, Y., Takamiya, K., Sobue, K. and Inui, M. (1999) J. Biol. Chem. 274, 6647-6652. Modulation of the channel activity of the ε2/ζ1-subtype N-methyl-D-aspartate receptor by PSD-95.

Yamada, Y., Iwamoto, T., Watanabe, Y., Sobue, K. and Inui, M. (2002) J. Neurochem. 81, 758-764. PSD-95 eliminates Src-induced potentiation of NR1/NR2A-subtype NMDA receptor channels and reduces high-affinity zinc inhibition.

Yamazaki, M., Araki, K., Shibata, A. and Mishina, M. (1992) Biochem. Biophys. Res. Commun. 183, 886-892. Molecular cloning of a cDNA encoding a novel member of the mouse glutamate receptor channel family.

Yang, W., Zheng, C., Song, Q., Yang, X., Qiu, S., Liu, C., Chen, Z., Duan, S. and Luo, J. (2007) J. Biol. Chem. 282, 9269-92678. A three amino acid tail following the TM4 region of the N-methyl-D-aspartate receptor (NR) 2 subunits is sufficient to overcome endoplasmic reticulum retention of NR1-1a subunit.

Yao, I., Hata, Y., Ide, N., Hirao, K., Deguchi, M., Nishioka, H., Mizoguchi, A. and Takai, Y. (1999) J. Biol. Chem. 274, 11889-11896. MAGUIN, a novel neuronal membrane-associated guanylate kinase-interacting protein.

Zhang, J., Vinuela, A., Neely, M. H., Hallett, P. J., Grant, S. G., Miller, G. M., Isacson, O., Caron, M. G. and Yao, W. D. (2007) J. Biol. Chem. 282, 15778-15789. Inhibition of the Dopamine D1 Receptor Signaling by PSD-95.

Zhang, W., Vazquez, L., Apperson, M. and Kennedy, M. B. (1999) J. Neurosci. 19, 96-108. Citron binds to PSD-95 at glutamatergic synapses on inhibitory neurons in the hippocampus.

Zukin, R. S. and Bennett, M. V. L. (1995) Trends in Neurosci. 7, 306-313. Alternatively spliced isoforms of the NMDAR1 receptor subunit.

LIST OF PUBLICATIONS

PUBLICATIONS

Papers

- Groc, L., Heine, M., **Cousins, S.L.,** Stephenson, F.A., Lounis, B., Cognet, L. and Choquet, D. (2006) Proc. Natl. Acad. Sci USA. 103,18769-18774. NMDA receptor surface trafficking depends on NR2A/NR2B subunits.

Poster presentations

- **Cousins, S. L.**, Papadakis, M. and Stephenson, F. A. (2005) British Neurosci. Assoc. Abstr. 18, p30.08.
  Demonstration of association and modulation of NR1/NR2C and NR1/NR2D NMDA receptors with PSD-95.
- **Cousins, S. L.**, Papadakis, M. and Stephenson, F. A. (2005) Biochemical Society Focused Meeting, 'Molecular Determinants of Synaptic Function: Molecules and Models', University of Southampton
  Differential interaction of PSD-95 and Chapsyn-110 with NR1/NR2A, NR1/NR2B and NR1/NR2C, NR1/NR2D NMDA receptors.
- **Cousins, S. L.**, Papadakis, M. and Stephenson, F. A. (2006) Bioscience, Glasgow, UK.
  Differential interaction of NMDA receptor subtypes with the PSD-95 family of MAGUK proteins.
- **Cousins, S. L.**, Papadakis, M. and Stephenson, F. A. (2006) Society for Neuroscience.
  Differential interaction of NMDA receptor subtypes with the PSD-95 family of MAGUK proteins

NMDA receptor surface mobility depends on NR2A-2B subunits

Laurent Groc*†, Martin Heine*, Sarah L. Cousins‡, F. Anne Stephenson‡, Brahim Lounis§, Laurent Cognet§, and Daniel Choquet*

*Physiologie Cellulaire de la Synapse, Unité Mixte de Recherche (UMR) 5091, Centre National de la Recherche Scientifique (CNRS), Université Bordeaux 2, 33077 Bordeaux, France; §Centre de Physique Moléculaire Optique et Hertzienne, CNRS-UMR 5798, Université Bordeaux 1, 33405 Talence, France; and ‡School of Pharmacy, University of London, 29/39 Brunswick Square, London WC1N 1AX, United Kingdom

Edited by Richard L. Huganir, Johns Hopkins University School of Medicine, Baltimore, MD, and approved September 29, 2006 (received for review June 22, 2006)

The NR2 subunit composition of NMDA receptors (NMDARs) varies during development, and this change is important in NMDAR-dependent signaling. In particular, synaptic NMDAR switch from containing mostly NR2B subunit to a mixture of NR2B and NR2A subunits. The pathways by which neurons differentially traffic NR2A- and NR2B-containing NMDARs are poorly understood. Using single-particle and -molecule approaches and specific antibodies directed against NR2A and NR2B extracellular epitopes, we investigated the surface mobility of native NR2A and NR2B subunits at the surface of cultured neurons. The surface mobility of NMDARs depends on the NR2 subunit subtype, with NR2A-containing NMDARs being more stable than NR2B-containing ones, and NR2A subunit overexpression stabilizes surface NR2B-containing NMDARs. The developmental change in the synaptic surface content of NR2A and NR2B subunits was correlated with a developmental change in the time spent by the subunits within synapses. This suggests that the switch in synaptic NMDAR subtypes depends on the regulation of the receptor surface trafficking.

development | glutamate receptor | lateral mobility

NMDA receptors (NMDARs) are heterotetrameric cation channels composed of NR1 and NR2/3 subunits (1). NMDARs are assembled early in the endoplasmic reticulum, and both NR1 and NR2 subunits are necessary for their association and their successful cell surface targeting (2). In addition to glutamate and glycine, NMDARs require membrane depolarization to open with high probability (3), making this receptor a pre- and postsynaptic activity coincident detector involved in the induction of Hebbian synaptic plasticity. The functional properties of NMDARs depend also on the subunit composition, and such subunit heterogeneity of synaptic NMDARs is thought to play an important role during synaptic development, maturation, and plasticity processes (4). During synaptic development, the subunit composition of synaptic NMDARs changes from heterodimers containing predominantly NR2B subunits at early stages to heterodimers containing NR1/NR2B, NR1/NR2A, and NR1/NR2A/NR2B subunits at mature stage (1, 5–14). This change often is associated with the refinement of neuronal connections within cortical areas, although this model has been challenged and, thus, is likely incomplete (4). The pathways by which neurons differentially traffic NR2A- and NR2B-containing NMDARs remain, however, an open question of crucial importance to understand the shaping of synaptic maturation and plasticity.

Changes in NR2 subunit composition of NMDARs within synapses can be triggered by mechanisms that include differences in insertion (15), internalization (16, 17), and/or lateral diffusion. Interestingly, NMDARs diffuse laterally at the neuronal surface (18, 19). In immature neurons, synaptic NMDARs are replaced rapidly by extrasynaptic ones through lateral diffusion (18), suggesting that surface mobility of NMDARs may be involved in shaping mature NMDAR synaptic components. In this study, we investigated the surface mobility of NR2A- and NR2B-containing NMDARs by using single-particle and single-molecule approaches. To selectively discriminate between these NMDAR types, we used antibodies directed against specific extracellular epitopes of these two subunits. Our results indicate that the surface mobility of NR2A-containing NMDARs is much smaller than that of NR2B-containing ones. During neuronal maturation, the decreased contribution of synaptic surface NR2B-containing NMDARs correlated with decreases in synaptic stabilization of the more mobile NR2B-containing NMDARs.

Results

Specific Detection of NR2A and NR2B Subunits. To selectively track surface NR2A- and NR2B-containing NMDARs, polyclonal antibodies directed against extracellular epitopes of NR2A subunit was developed, and a previously described antibody directed against NR2B subunit were used (20, 21). As shown in Fig. 1*a*, the peptide sequences used for antibody production correspond to amino acid sequences in the N-terminal domain of the NR2 subunits. Importantly, an alignment of the two peptide sequences, peptide NR2A versus full-length NR2B and peptide NR2B versus full-length NR2A, show no amino acid sequence similarity. To test the specificity of the NR2A antibody, HEK293 cells were transfected with NR1/NR2A, NR1/NR2B, NR1/NR2C, or NR1/NR2D subunit cDNAs, total cell homogenates were prepared and analyzed by immunoblotting with either anti-NR2A (44–58) antibodies (Fig. 1*b*), anti-NR2A antibodies (1454–1464) (Fig. 1*c*) that recognize both NR2A and NR2B subunits, or anti-NR2D antibodies (1307–1323) (Fig. 1*c*) that recognize both NR2C and NR2D subunits (22). As shown in Fig. 1*b*, the anti-NR2A (44–58) antibody recognizes only recombinant NR2A subunits. To further test the antibody specificity, P2 fractions prepared from whole brain of either wild-type or NR2A (−/−) mice were analyzed by immunoblotting with anti-NR2A (44–58) or anti-NR2A (1454–1464) antibodies (Fig. 1*d*). As predicted, anti-NR2A (44–58) antibodies did not recognize a M_r 180-kDa immunoreactive species in the P2 fractions prepared from NR2A (−/−) mice (Fig. 1*d*). In an additional control, HEK293 cells were transfected with either NR1/NR2A or NR1/NR2B subunit cDNAs, and cell surface ELISAs were carried out, as described in ref. 21 by using either anti-NR2A (44–58) or anti-NR2B (42–60) antibodies (Fig. 1 *e* and *f*). It can be seen that anti-NR2A (44–58) antibodies recognize mostly cell surface-expressed NR2A subunits and anti-NR2B (42–60), NR2B subunits only (Fig. 1*e*). For total staining, the cells first were permeabilized

Author contributions: L.G. and D.C. designed research; L.G. and M.H. performed research; S.L.C., F.A.S., B.L., and L.C. contributed new reagents/analytic tools; L.G. analyzed data; and L.G. wrote the paper.

The authors declare no conflict of interest.

This article is a PNAS direct submission.

Abbreviations: IQR, interquartile range; NMDAR, NMDA receptor; QD, quantum dot.

†To whom correspondence should be addressed. E-mail: laurent.groc@u-bordeaux2.fr.

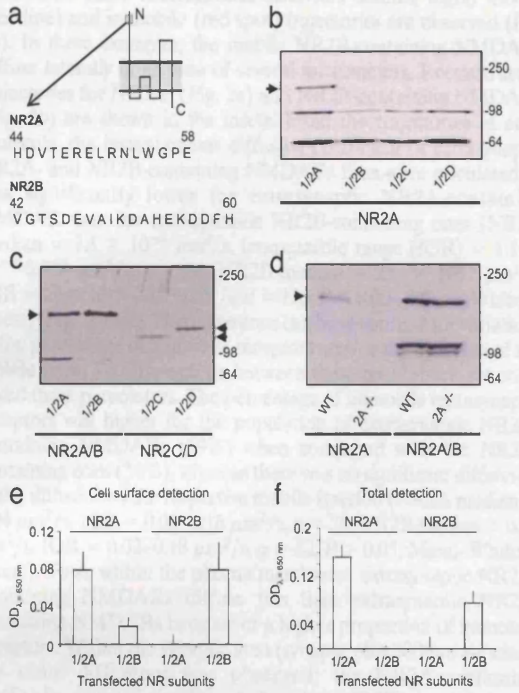

Fig. 1. Characterization of anti-NR2A and anti-NR2B antibodies. (*a*) Peptide sequences from the N-terminal domain of NR2A (44–58) and NR2B (42–60) subunits used to raise antibodies. (*b*) HEK293 cells were transfected with either NR1/NR2A, NR1/NR2B, NR1/NR2C, or NR1/NR2D subunit cDNAs. Cells were analyzed by immunoblotting with an anti-NR2A (44–58) antibody. Note the specific detection of NR2A subunit (arrow). (*c*) Using the same method as in *b*, NR2A, NR2B, NR2C, or NR2D subunit was detected by using either an anti-NR2A antibody (1454–1464) that recognizes both NR2A (M_r 180 kDa) and NR2B (M_r 180 kDa) subunits (left arrowhead in lanes 1 and 2) or an anti-NR2D antibody (1307–1323) that recognizes both NR2C (M_r 135 kDa, right lower arrowhead) and NR2D (150 kDa, right upper arrowhead) (lanes 3 and 4). The positions of molecular mass standards (kDa) are shown on the right. (*d*) P2 fractions were prepared from whole brain (15 μg of wet weight tissue applied per gel lane) of either wild-type (WT) or NR2A (−/−) mice and analyzed by immunoblotting with anti-NR2A (44–58) or anti-NR2A (1454–1464) antibodies. In lane 2, note that the anti-NR2A (44–58) antibody does not recognize an immunoreactive species in the P2 fractions prepared from NR2A (−/−) mice. (*e* and *f*) HEK293 cells were transfected with either NR1/NR2A or NR1/NR2B NMDA receptor subunit cDNAs and cell surface ELISAs carried out by using either anti-NR2A (44–58) or anti-NR2B (42–60) antibodies as indicated. It can be seen that anti-NR2A (44–58) antibodies recognize only cell surface-expressed NR2A subunits and anti-NR2B (42–60), NR2B subunits only (means ± SD for triplicate values, $n = 3$).

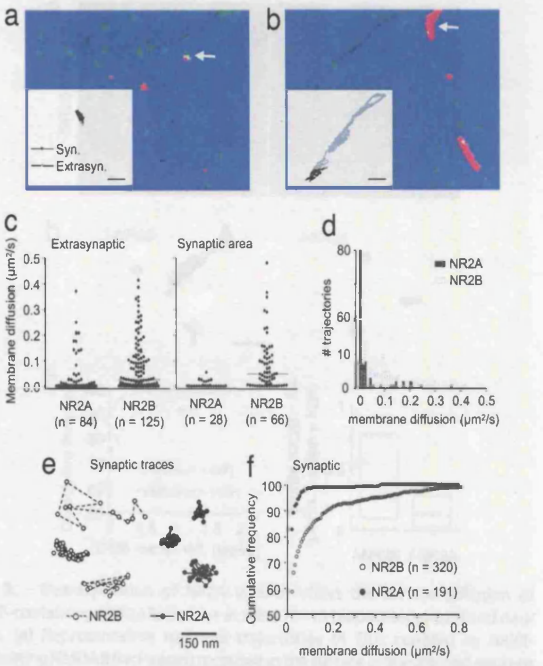

Fig. 2. Differential membrane diffusion of NR2A- and NR2B-containing NMDARs at the surface of D15 neurons. (*a* and *b*) Representative summed trajectories of QD coupled to NR2A- (*a*) and NR2B-containing (*b*) NMDARs. The green spots represent synaptic sites labeled with Mitotracker. The red traces represent the trajectory of QD–NR2 subunit complexes, with immobile complexes being exemplified by dot-like trajectory, whereas diffusing complexes are represented by extended line trajectories. (*c*) Scatter plot distributions of the instantaneous diffusion coefficient of NR2A- and NR2B-containing NMDARs in the extrasynaptic (*Left*) and the synaptic area (*Right*). The bar in each group represents the median value. (*d*) Superimposed distribution histograms of the instantaneous diffusion coefficient of NR2A- (filled bars) and NR2B- (hatched gray bars) containing NMDARs. Note the overlap for the low diffusion coefficients. (*e*) Examples of NR2A- (filled dots, full line) and NR2B-containing NMDAR (open dots, broken line) trajectories obtained by single-molecule approach within synapses (Scale bar: 150 nm.) (*f*) Cumulative distributions of the instantaneous diffusion coefficient of synaptic NR2A- (filled dots) and NR2B-containing (open dots) NMDARs. The first point of the distributions corresponds to the percentage of immobile receptors (bin size = 0.0075 $\mu m^2/s$). Note the higher percentage of immobile synaptic NR2A- (83%) when compared with NR2B-containing (59%) NMDARs.

with 0.25% Triton X-100, and then antibody was added for incubation. The same conclusion regarding antibody specificity was reached (Fig. 1*f*). Finally, we tested the specificity of antibodies by labeling live HEK cells double-transfected with the NR1 coupled to yellow fluorescent protein and either NR2A or NR2B subunit cDNAs. The presence of membrane NR2A subunits then was revealed by using the anti-NR2A (44–58) antibodies. We found that only NR1-positive HEK cells that were cotransfected with NR2A subunit cDNAs displayed NR2A subunit surface staining, whereas cells cotransfected with NR2B subunit cDNAs displayed no NR2A subunit surface staining (data not shown). All together, the data indicate that these newly generated anti-NR2A and anti-NR2B antibodies can be used in live cells to discriminate between surface-exposed NR2A or NR2B subunit, respectively.

Differential Surface Diffusion of NR2A- and NR2B-Containing NMDARs. Because NR2A- and NR2B-containing NMDARs have different surface distributions, we then measured and compared the surface mobility of both NR2A- and NR2B-containing NMDARs by using two approaches: (*i*) single-particle tracking based on the detection of quantum dots (QDs) and (*ii*) single-molecule tracking based on the detection of the single organic fluorophores, i.e., cyanine 3. QD-based tracking provides a unique tool for long-term recording of receptor surface diffusion because QDs are more photostable than organic dyes (19, 23). However, as reported in ref. 19, QD-based tracking may be biased to some extent within a confined space, so we also used the single-molecule approach to track synaptic receptors. To differentiate synaptic versus extrasynaptic receptors, synapses were labeled with the active mitochondria marker, Mitotracker (rhodamine derivative), which was shown to colocalize with the presynaptic synaptotagmin clusters (19, 24).

Representative summed trajectories recorded at days *in vitro* 15 and over a 60-s period time (reconstruction from image series acquired at 30 Hz rate), are shown in Fig. 3 *a* and *b*. The NR2A-containing NMDAR summed trajectories (a single red trace corresponds to the whole trajectory of a single QD–NR2A antibody complex) show that subunits are immobile or very slowly mobile in both synaptic (green spots) and extrasynaptic compartments (Fig. 2*a*). In contrast, the NR2B-containing NMDAR summed trajec-

tories show more heterogenous behaviors because highly mobile (red line) and immobile (red spot) trajectories are observed (Fig. 2*b*). In these examples, the mobile NR2B-containing NMDARs diffuse laterally in an area of several micrometers. Reconstructed trajectories for NR2A- (Fig. 2*a*) and NR2B-containing NMDARs (Fig. 2*b*) are shown in the insets. From the trajectories of each molecule, the instantaneous diffusion coefficient of extrasynaptic NR2A- and NR2B-containing NMDARs then were calculated. It was significantly lower for extrasynaptic NR2A-containing NMDAR than for extrasynaptic NR2B-containing ones (NR2A median = 7.5×10^{-4} $\mu m^2/s$, interquartile range (IQR) = 1.1×10^{-4}-0.013 $\mu m^2/s$, $n = 84$; NR2B median = 250×10^{-4} $\mu m^2/s$, IQR = 24×10^{-4}-0.115 $\mu m^2/s$, $n = 125$; $P < 0.001$, Mann–Whitney *U* test) (Fig. 2*c Left*). This difference can be accounted for variations in the percentage of immobile receptors and/or the diffusion of the mobile ones. To differentiate between these possibilities, we compared these parameters. The percentage of immobile extrasynaptic receptors was higher for the population of extrasynaptic NR2A-containing NMDARs (69%) when compared with the NR2B-containing ones (34%), whereas there was no significant difference in the diffusion of the respective mobile fraction (NR2A median = 0.04 $\mu m^2/s$, IQR = 0.01–0.16 $\mu m^2/s$, $n = 28$; NR2B median = 0.08 $\mu m^2/s$, IQR = 0.02–0.18 $\mu m^2/s$, $n = 82$; $P > 0.05$, Mann–Whitney *U* test). Thus, within the plasma membrane, extrasynaptic NR2A-containing NMDARs diffuse less than extrasynaptic NR2B-containing NMDARs because of a higher proportion of immobile receptors. Within the synaptic area (synapse plus 300-nm annulus), the same difference was observed: the NR2A-containing NMDARs diffused significantly less than NR2B-containing ones (NR2A median = 2×10^{-4} $\mu m^2/s$, IQR = 0–0.01 $\mu m^2/s$, $n = 28$; NR2B median = 500×10^{-4} $\mu m^2/s$, IQR = 43×10^{-4}-0.125 $\mu m^2/s$, $n = 665$; $P < 0.001$) (Fig. 2*c Right*) and the proportion of immobile NR2A-containing NMDARs was 2.5-fold higher than that of NR2B-containing NMDARs (75% versus 29%). We further compared subunit surface diffusion in the synapse by using the single-molecule approach. The instantaneous diffusion coefficient of NR2A-containing NMDAR diffusion was lower than that of NR2B-containing NMDARs. The percentage of immobile NR2A- and NR2B-containing NMDARs was 82% and 56%, respectively (Fig. 2 *e* and *f*). Thus, consistent with the QD-based data, the synaptic diffusions of surface NR2A- and NR2B-containing NMDARs are different.

Although our approach does not permit to target specifically NMDAR triheteromers (e.g., NR1/NR2A/NR2B), the current data indicate that NR2A-containing NMDAR membrane diffusion overlap the one of NR2B-containing NMDARs only for low-diffusion coefficients (Fig. 2*d*), implying that such triheteromers would diffuse within the plasma membrane with instantaneous coefficient <0.025 $\mu m^2/s$. To investigate whether NMDAR triheteromers have distinct properties, i.e., whether NR2A subunit expression affect the behavior of NR2B-containing NMDARs, we performed experiments in which the surface diffusion of NR2B-containing NMDARs were measured in neurons overexpressing either NR2B (*t*-NR2B) or NR2A (*t*-NR2A) subunits (Fig. 3 *a* and *b*; *Supporting Methods*, which is published as supporting information on the PNAS web site). Interestingly, the overexpression of NR2A subunits significantly reduced the surface diffusion of NR2B-containing NMDARs (*t*-NR2B median = 9×10^{-5} $\mu m^2/s$, IQR = 3.10^{-6} to 8.10^{-2} $\mu m^2/s$, $n = 927$; *t*-NR2A median = 5×10^{-6} $\mu m^2/s$, IQR = 0–9 $\times 10^{-4}$ $\mu m^2/s$, $n = 1{,}157$; $P < 0.001$, Mann–Whitney *U* test) (Fig. 3 *b* and *c*), by decreasing both the number of mobile receptors (*t*-NR2B = 32%; *t*-NR2A = 14%) and the membrane diffusion of the mobile ones (Fig. 3*d*). These results indicate that the presence of surface NR2A subunit influence the surface diffusion of NR2B-containing NMDARs, suggesting that NR2A subunit is present in NMDAR triheteromers and that NR2A subunit presence has a major role in NMDAR surface diffusion properties.

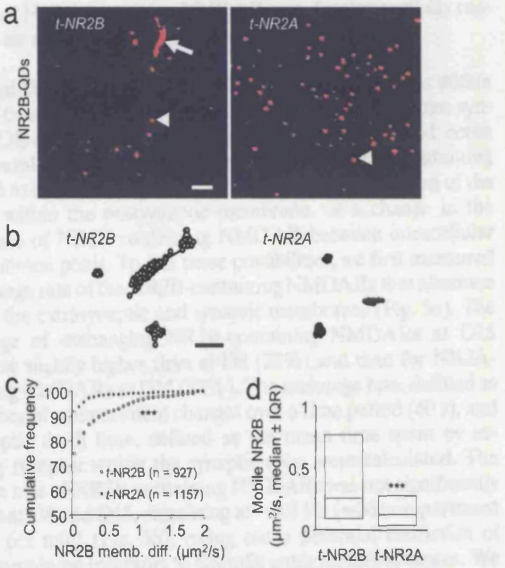

Fig. 3. Overexpression of NR2A subunit affect the surface diffusion of NR2B-containing NMDARs in days *in vitro* 10–15 hippocampal-cultured neurons. (*a*) Representative summed trajectories of QDs coupled to NR2B-containing NMDAR (red traces) recorded at the surface of transfected neurons by SEP-NR2B (*Left*) or SEP-NR2A (*Right*). QDs were only tracked at the somatic surface of SEP-NR-positive neurons to ensure that only NR2-overexpressing neurons were analyzed. Typical immobile trajectory of NR2B-containing NMDAR are indicated by arrowheads, whereas a diffusing NR2B-containing NMDAR is pointed out by an arrow line. (Scale bar: 1 μm.) (*b*) Examples of NR2B-containing NMDAR from SEP-NR2B-positive (*Left*, open circle) or SEP-NR2A-positive (Right, filled circle) neurons. (Scale bar: 175 nm.) (*c*) Cumulative distributions of the instantaneous diffusion coefficient of surface NR2B-containing NMDARs from neurons overexpressing either NR2B (NR2B *t*, open circle) or NR2A (NR2A *t*, filled circle) subunits (bin size = 0.075 $\mu m^2/s$). The NR2B-containing NMDAR surface diffusion was reduced significantly in neurons overexpressing NR2A subunits (***, $P < 0.001$, Mann–Whitney test). (*d*) The surface diffusion of mobile NR2B-containing NMDARs was significantly slower in NR2A-overexpressing neurons when compared with NR2B overexpressing ones (***, $P < 0.001$, Mann–Whitney test).

Native NR2A and NR2B Subunit Surface Diffusions and Distributions Overdevelopment. To investigate the developmental changes of NR2A and NR2B-containing NMDAR surface diffusion, we first performed live immunostainings of native NR2A- or NR2B-containing NMDARs at the surface of dendritic arbors (somatic staining was not considered) of live hippocampal cultured neurons at two different developmental stages: D7–9, referred as "D8" and D14–16, referred as "D15." In agreement with previous reports, surface NR2A and NR2B subunit immunostainings were different: (*i*) the dendritic surface NR2A subunit staining significantly increased during this period, whereas the surface density of NR2B subunit slightly, but not significantly, decreased during this period, and (*ii*) the percentage of NR2A subunit staining that colocalize with the presynaptic marker, synaptotagmin, significantly increased during this period, whereas the opposite trend was observed for NR2B subunit staining (Fig. 6, which is published as supporting information on the PNAS web site). Moreover, respective to function, we recorded NMDAR-mediated miniature excitatory postsynaptic currents (mEPSCs) at these two developmental stages (*Supporting Methods*). The NMDAR mEPSC decay time decreased from D8 to D15 neurons (D8 : two exponential fit: $\sigma_1 = 20 \pm 4$ ms and $\sigma_2 = 196 \pm 38$ ms, $n = 5$; D15 : $\sigma_1 = 9 \pm 4$ ms and $\sigma_2 = 91 \pm 17$ ms, $n = 5$), suggesting a functional switch in the NR2 subunit composition of synaptic NMDAR from NR2B-containing receptors to NR2A-containing ones, as previously reported by numerous studies with cultured neurons (5, 9, 12, 14, 25–27).

NEUROSCIENCE

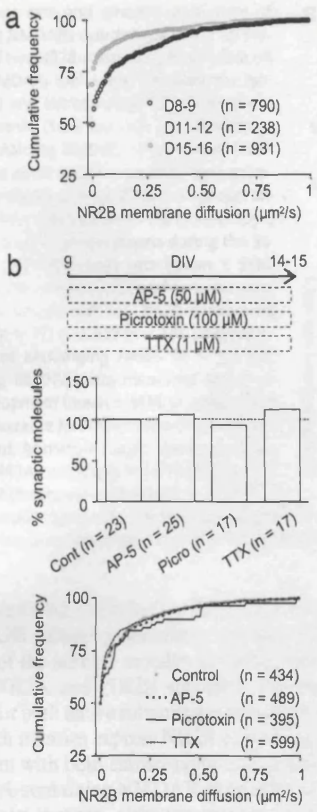

Fig. 4. The surface diffusion of NR2B-containing NMDARs decreases overdevelopment in an activity-independent manner. (*a*) Cumulative distributions of the instantaneous diffusion coefficient of extrasynaptic NR2B-containing NMDAR at three developmental stages: days *in vitro* (D)8–9 (open dots), D11–12 (gray dots), and D15–16 (dark gray dots) neurons. The first point of the distributions corresponds to the percentage of immobile receptors (bin size = 0.0075 $\mu m^2/s$). Note the significant diffusion decreases at D15–16 when compared with D8–9 ($P < 0.001$, Kolmogorov–Smirnov test). (*b*) Chronic treatments with AP5, tetrodotoxin (TTX), or picrotoxin were applied from D9 to D15 (*Top*) to block the global neuronal activity. None of these treatments affected the surface distribution of NR2B-containing NMDARs, as shown by the percent of synaptic molecules in all conditions ($P > 0.05$, n = number of dendritic fields examined) (*Middle*). The membrane diffusion distributions in all conditions were statistically not different (*Bottom*).

Based on these findings, we then asked whether such developmental change correlated with changes in surface diffusion of NR2B-containing NMDAR between D8 and D15. The diffusion of NR2B-containing NMDARs decreases significantly from D8 to D15, mostly because of a higher proportion of immobile receptors (first point in the cumulative curves) (Fig. 4*a*). We further tested whether surface diffusion and distribution of NR2B-containing NMDARs are modulated by changes in global neuronal activity. To determine the NR2B-containing NMDAR surface distribution, the relative content of synaptic, perisynaptic (300-nm annulus around the synapse), and extrasynaptic detected molecules was quantified. In control conditions, 21 ± 4% of molecules were synaptic, 15 ± 3% perisynaptic, and 64 ± 6% extrasynaptic (n = 23 dendritic fields). After a chronic incubation of neurons from D9 to D15 with an NMDAR antagonist (50 μM AP-5), a $GABA_A$ receptor channel blocker (100 μM picrotoxin), or a sodium channel blocker [1 μM tetrodotoxin (TTX)], NR2B-containing NMDAR surface distribution did not significantly change ($P > 0.05$ in all conditions) (Fig. 4*b Middle*). Moreover, the surface diffusion of NR2B-containing NMDARs remains unaffected by these treatments (Fig. 4*b*). All together, these results indicate that the surface distribution and diffusion of NR2B-containing NMDARs are developmentally regulated in an activity-independent manner.

Differential Stability of NR2A- and NR2B-Containing NMDARs Within Synapses Overdevelopment. The decreased content of surface synaptic NR2B-containing NMDAR overdevelopment could come from several processes, i.e., a restriction of NR2B-containing NMDAR to enter laterally the synapse, a lack of stabilization of the receptor within the postsynaptic membrane, or a change in the cycling rate of NR2B-containing NMDAR between intracellular and membrane pools. To test these possibilities, we first measured the exchange rate of the NR2B-containing NMDARs that alternate between the extrasynaptic and synaptic membranes (Fig. 5*a*). The percentage of exchanging NR2B-containing NMDARs at D15 (29%) was slightly higher than at D8 (22%) and than for NR2A-containing NMDARs at D15 (22%). The exchange rate, defined as the number of compartment changes over a time period (60 s), and the synaptic dwell time, defined as the mean time spent by exchanging receptor within the synaptic area, were calculated. The exchange rate of NR2B-containing NMDARs was not significantly different at D8 and D15, remaining at ≈0.6 Hz (≈36 compartment changes per min) (Fig. 5*b*), ruling out a potential restriction of NR2B-containing receptors to laterally enter mature synapses. We then measured the residency time of exchanging NR2B-containing NMDARs within synapses to estimate receptor stabilization within the postsynaptic membrane. Interestingly, the residency time was significantly decreased by a factor of three from D8 to D15 (Fig. 5*c*), indicating a higher surface stabilization of NR2B-containing NMDAR in early synapses when compared with more mature ones. It can be noted that at D15 the residency time of NR2A-containing NMDAR was significantly higher than that of NR2B-containing NMDAR, indicating a better stabilization of NR2A-containing NMDAR within mature synapse. We thus propose that the relative decreased content of NR2B-containing NMDAR within mature synapse is due to instability of the surface receptor within the postsynaptic membrane. Finally, the observed decreased content of surface synaptic NR2B-containing NMDAR overdevelopment that would come from an increased internalization of the receptor is unlikely because NR2B-containing NMDAR internalization remains constant overdevelopment (from D5 to D12) (17). Along this line, we measured the internalization rate of all NMDARs by using an anti-NR1 antibody directed against an extracellular epitope (19) (*Supporting Methods*) and found that the internalization of NMDARs during development is significantly decreased (D8: 32 ± 3% of internalized NR1-containing NMDARs, n = 5; D15: 10.5 ± 5%, n = 5; $P < 0.05$). Thus, the decreased contribution of synaptic NR2B-containing NMDARs is not due to an increased internalization of NMDAR overdevelopment.

Discussion

In the present study, we show that part of the surface mobility of NMDARs depends on the NR2A-2B subunit subtype, NR2A-containing NMDARs being more stable than NR2B-containing ones. The synaptic composition of NMDARs changed over maturation with an increase in the NR2A/NR2B subunit ratio. Interestingly, the developmental switch in the synaptic NR2A- and NR2B-containing NMDAR surface distribution correlates with developmental changes in the time spent by subunits within synapses without any change in the lateral exchange of the receptors (Fig. 5*f*). These data shed light on how surface NR2A- and NR2B-containing NMDARs can be differentially trafficked and they propose a developmental model in which the regulation of synaptic NMDAR subtypes depends on the synaptic surface stabilization of the receptors.

Our current knowledge of the differential distribution of NR2A and NR2B-containing NMDARs at the neuronal surface has come from either electrophysiological approaches or detection of genet-

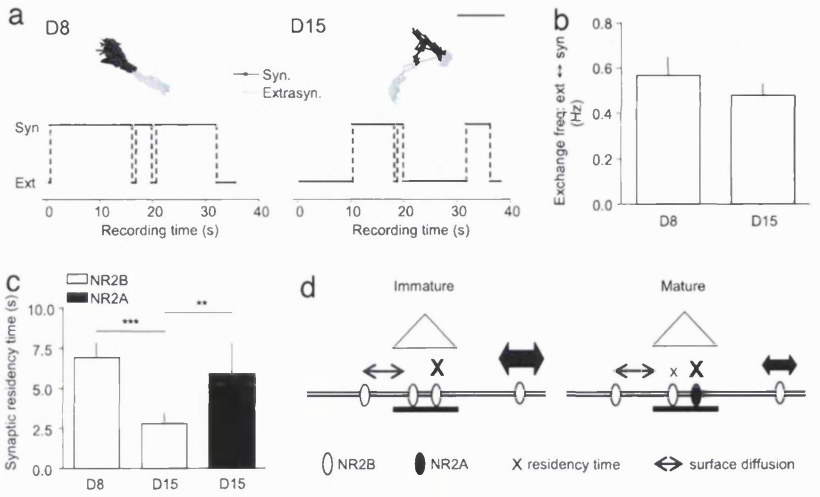

Fig. 5. Exchange rate and synaptic dwell-time of NR2B-containing NMDARs overdevelopment. (*a*) Surface trajectory of two NR2B-containing NMDARs at D8 and D15. The NMDARs exchanged between the synaptic (*black line*) and extrasynaptic (*gray line*) membrane compartments. (Scale bar: 300 nm.) Recordings of the NR2B-containing NMDAR compartment localization over time at D8 and D15. In these two examples, the NR2B-containing NMDARs exchange approximately three to four times between the synaptic (Syn) and extrasynaptic (Ext) compartments during the 35- to 40-s recording. (*b*) Exchange rate (mean ± SEM, Hertz) between the extrasynaptic and synaptic compartments was calculated for NR2B-containing NMDARs at D8 (n = 17) and D15 (n = 18). (*c*) Synaptic residency time of exchanging NR2A- (n = 18) and NR2B-containing NMDARs was measured and compared overdevelopment (mean ± SEM, seconds). Note the significant decrease for NR2B-containing NMDARs overdevelopment. At mature stages, the synaptic residency time of NR2A-containing NMDARs was similar as the one of NR2B-containing NMDARs at immature stages. (*d*) Schematic representation of the regulation of NR2A- and NR2B-containing NMDAR surface diffusion over neuronal maturation. The synapse is represented by the presynaptic element (open triangle) and the postsynaptic density (filled bar).

ically engineered NR2 subunits (2). The antibodies directed against NR2A or NR2B subunit extracellular epitopes allowed the direct investigation of the surface mobility of native, and not genetically engineered, NR2A and NR2B subunits. The observed surface distributions for both native subunits are consistent with the current model in which neurons express NR2B-containing NMDAR early in development with both extrasynaptic and synaptic localizations, whereas NR2A-containing NMDAR expression appears later and are restricted to synapse, although present in the extrasynaptic membrane (present study; refs. 5 and 9). The data show a colocalization of both NR2 subunits in mature synapses, indicating various possible combinations for NMDAR composition, including the well described triheteromeric one (1, 5, 9, 10, 12–14). The surface diffusion of NMDARs has been described by single-molecule tracking (19) and by electrophysiological means (18). In the present study, the use of individual nanometer-sized fluorescent objects, the QDs, uniquely allow the tracking of individual or small assemblies of surface NMDARs for long recording periods in various membrane compartments, including confined spaces (e.g., synaptic cleft) (19, 23, 28). It further provides a way to measure the time spent by NMDAR in a specific membrane compartment, i.e., extrasynaptic and synaptic membranes, and to quantify the lateral exchange rate between membrane compartments. It can be noted that surface extrasynaptic NR2A-containing NMDARs were not observed by immunocytochemical means, whereas they were detected and tracked by single-molecule/particle approaches, indicating a lower detection threshold for the latter (29) and the presence of NR2A-containing NMDARs outside synapse (9). Although NR2B-containing NMDARs outnumbered NR2A-containing NMDARs in the extrasynaptic membrane, we found a similar proportion of exchanging NR2B- and NR2A-containing NMDARs between the extrasynaptic membrane and synapse, in which they were only temporary stabilized. Such a result suggests that the surface distribution of NR2A- and NR2B-containing NMDARs also likely result from differences in cycling processes (outside synapse) between intracellular and membranes receptor pools (17, 30, 31).

Differences in surface diffusion of NR2A- and NR2B-containing NMDARs are likely the result of multiple cellular processes, including binding affinity to scaffold proteins, phosphorylation state of the NR subunits, and/or extracellular factors. Two membrane-associated guanylate kinases (MAGUKs), synapse associated protein 102 (SAP-102) and postsynaptic density 95 (PSD-95), which both contribute to form a scaffold for ionotropic glutamate receptors at the postsynaptic density, indeed have been proposed to play a role in the NMDAR subunit switch during development (4). Schematically, a preference of certain MAGUKs for different NMDAR subtypes suggest that different NMDAR scaffolding proteins could affect the trafficking and synaptic localization of NR2A- and NR2B-containing NMDARs during synaptic development (11, 32, 33). In this model, NR2A-containing NMDARs are synaptically incorporated, PSD95 is inserted into the center of the postsynaptic density and displaces the NR2B subunit–SAP102 complexes, which were initially located at the postsynaptic density, to the perisynaptic and extrasynaptic membranes (32, 34, 35). Our current data on the surface mobility of NR2A/B subunits support this hypothesis and further indicate that the lateral shift of the subunits observed by electrophysiological means likely results from differences in lateral mobility and stabilization of the subunits. Indeed, surface NR2A-containing NMDARs are more stable than NR2B-containing ones within mature synapses, possibly due to a high proportion of PSD-95 over SAP-102 in the postsynaptic density. Interestingly, the domains on the C-terminal tail are critical to retain NR2A- (36) and NR2B-containing NMDARs (30) within synapses and the binding of NMDARs to PDZ proteins is a regulated process, depending on kinase activation (37), suggesting that NR2A/B surface mobility is indeed dynamically regulated by intracellular interactions. To The synaptic retention of NMDARs also depends on extracellular factors such as the EphB receptor, which interacts with NMDARs through N-terminal extracellular domains (38), cell-adhesion molecules (e.g., integrins) (39), and proteins of the extracellular matrix (e.g., reelin) (40). Interestingly, the type of presynaptic neuron is a critical determinant of the subunit composition of NMDARs expressed at synapses (41), suggesting that appropriate expression of molecules in both pre- and postsynaptic compartments is necessary for NMDAR maturation.

In conclusion, the surface mobility of NMDARs depends, in part, on the NR2A versus 2B subunit composition. The presence of triheteromeric structure (NR2A and NR2B subunits) or other NR subunits such as NR3A early in development (42) is also likely to play a role in determining surface mobility of NMDARs. Our results unravel a way to differentially traffic NR2A- and NR2B-containing NMDARs at the neuronal surface and indicate that the maturation of excitatory glutamate synapses is accompanied by changes in the stability of specific NMDAR subtypes.

Methods

Cell Culture, Synaptic Live Staining, and Protein Expression in Neurons. Preparation of the cultured neurons for single molecule/particule staining has been done as described in refs. 19 and 24.

Schematically, hippocampal neurons from 18-day-old rat embryos were cultured on glass coverslips by following the Banker technique. To label synapses, neurons were incubated for 1–2 min at 20°C with 1 nM Mitotracker (Deep Red-Fluorescent Mitotracker; Molecular Probes, Leiden, The Netherlands). For protein expression, days *in vitro* 10–15 hippocampal-cultured neurons were transducted 24–36 h before experiment by using Lipofectamine 2000 reagent (Invitrogen, Carlsbad, CA). SEP-NR2A and SEP-NR2B cDNAs were constructed by fusing the superecliptic pHluorin (enhanced mutant of pH-sensitive GFP) to the N terminus of rat NR2A and NR2B subunits, respectively. For transfection, culture coverslips were incubated with ≈1 μg cDNA for 40 min at 37°C. The superecliptic pHluorin allow the specific visualization of surface SEP-NR subunits (43, 44), which ensure that the overexpressed proteins were well targeted to the plasma membrane.

Immunocytochemistry. Surface NR2A or NR2B subunits were stained specifically by using the newly developed rabbit polyclonal antibodies. Briefly, neurons were fixed with 4% paraformaldehyde and incubated with 6 μg of affinity-purified antibodies directed against NR2A or NR2B subunits for 30 min. The primary antibodies were revealed by using anti-rabbit Alexa 568 antibodies (8 μg for 2–3 h). To label synaptic sites, neurons then were permeabilized by using 0.3% Triton X-100, incubated with a rabbit polyclonal anti-synaptotagmin antibody (6 μg for 1 h), followed by secondary incubation with a anti-rabbit Alexa 488 antibodies (5 μg for 30 min). For the surface fluorescence quantification, the average total intensity and the pixel area were measured within only dendritic field (soma excluded from analysis). For the colocalization measurement, the pixel area of synaptotagmin and NR2 subunit staining were compared, and the percentage of overlap between the two was calculated. The fluorescence analysis was realized by using Metamorph software (Universal Imaging, Downingtown, PA).

Single-Molecule and -Particle (QD) Tracking. Cyanine 3 was coupled to the affinity-purified rabbit polyclonal anti-NR2A or anti-NR2B antibodies that are both directed against extracellular epitopes of NR2 subunits. All neurons, which are mainly excitatory ones, were incubated for 10 min at 37°C with the respective cyanine–antibody complexes. As described in ref. 19, all recording sessions were acquired within 30 min after primary antibody incubation to minimize receptor endocytosis. Single-molecule detection was realized as described in refs. 19 and 24. Briefly, a custom wide-field single-molecule fluorescence inverted microscope equipped with a ×100 oil-immersion objective was used. The samples were illuminated for 30 msec at a wavelength of λ = 532 nm by a frequency doubled YAG laser (Coherent, Les Ulis, France) at a rate of 15 Hz. Appropriate filter combination (DCLP550, HQ600/75; Chroma Technology, Brattleboro, VT) allowed the detection of individual fluorophore by a CCD camera system (Micromax; Princeton Instruments, Trenton, NJ). Using the same excitation path, Red Deep Mitotracker (Molecular Probes) was excited with the λ = 633 nm line of a He-Ne laser (JDS Uniphase, Manteca, CA) at an illuminating intensity of 7 ± 1 kW/cm^2. We imaged and resolved discrete fluorescence spots (45). Fluorescence spots exhibit one-step photobleaching and not gradual decay as for ensemble photobleaching. We calculated the instantaneous diffusion coefficient, D, for each trajectory, from linear fits of the first four points of the mean-square-displacement versus time function by using MSD(t) = $<r^2>$ (t) = 4Dt. The 2D trajectories of single molecules in the plane of focus were constructed by correlation analysis between consecutive images by using a Vogel algorithm. For QD tracking, QD 655 Goat F(ab')2 anti-Rabbit IgG (0.1 μM; Ozyme, Paris, France) first were incubated for 30 min with the polyclonal antibodies against NR2A (1 μg) and NR2B subunits (1 μg). Nonspecific binding was blocked by additional casein (Vector Laboratories, Paris, France) to the QD 15 min before use. Neurons were incubated for 10 min at 37°C in culture medium with precoated QD (final dilution 0.1 nM). QDs were detected by using a xenon lamp (excitation filter HQ500/20X (Chroma Technology; Mitotrack) 560RDF55 (Omega, QD) and appropriate emission filters [respectively, HQ560/80M (Chroma Technology), and 655WB20; Omega Filters]. Images were obtained with an integration time of 50 msec respectively with up to 1200 consecutive frames. Signals were detected by using a CCD camera (Cascade; Princeton Instruments). QD-labeled NR2 subunits were followed on randomly selected dendritic regions for up to 30 min. The trajectory reconstruction was carried out as for single-molecule tracking (see above).

We thank Martha Constantine-Paton and Cansu Tunca (Massachusetts Institute of Technology, Boston, MA) for the gift of wild-type and NR2A (−/−) mouse brains, Jacques Neyton (École Normale Supérieure, Paris, France) for cDNA constructs, Carlos Dotti (University of Leuven, Leuven, Belgium) for synaptotagmin antibodies, Kieran Brickley for animal immunizations, Pascale Chavis for critical reading of the manuscript, and Mike D. Ehlers for helpful discussions. This work was supported by grants from the Centre National de la Recherche Scientifique, The Conseil Régional d'Aquitaine, The Ministère de la Recherche, European Community Grant CT-2005-005320 (Glutamate Receptor Interacting Proteins as Novel Neuroprotective Targets), and the Biotechnology and Biological Sciences Research Council (U.K.).

1. Sheng M, Cummings J, Roldan LA, Jan YN, Jan LY (1994) *Nature* 368:144–147.
2. Wenthold RJ, Prybylowski K, Standley S, Sans N, Petralia RS (2003) *Annu Rev Pharmacol Toxicol* 43:335–358.
3. Nowak L, Bregestovski P, Ascher P, Herbet A, Prochiantz A (1984) *Nature* 307:462–465.
4. van Zundert B, Yoshii A, Constantine-Paton M (2004) *Trends Neurosci* 27:428–437.
5. Tovar KR, Westbrook GL (1999) *J Neurosci* 19:4180–4188.
6. Monyer H, Burnashev N, Laurie DJ, Sakmann B, Seeburg PH (1994) *Neuron* 12:529–540.
7. Carmignoto G, Vicini S (1992) *Science* 258:1007–1011.
8. Liu XB, Murray KD, Jones EG (2004) *J Neurosci* 24:8885–8895.
9. Thomas CG, Miller AJ, Westbrook GL (2006) *J Neurophysiol* 95:1727–1734.
10. Luo J, Wang Y, Yasuda RP, Dunah AW, Wolfe BB (1997) *Mol Pharmacol* 51:79–86.
11. Shi J, Aamodt SM, Constantine-Paton M (1997) *J Neurosci* 17:6264–6276.
12. Kew JN, Richards JG, Mutel V, Kemp JA (1998) *J Neurosci* 18:1935–1943.
13. Stocca G, Vicini S (1998) *J Physiol* 507:13–24.
14. Li JH, Wang YH, Wolfe BB, Krueger KE, Corsi L, Stocca G, Vicini S (1998) *Eur J Neurosci* 10:1704–1715.
15. Barria A, Malinow R (2002) *Neuron* 35:345–353.
16. Roche KW, Standley S, McCallum J, Dune Ly C, Ehlers MD, Wenthold RJ (2001) *Nat Neurosci* 4:794–802.
17. Lavezzari G, McCallum J, Dewey CM, Roche KW (2004) *J Neurosci* 24:6383–6391.
18. Tovar KR, Westbrook GL (2002) *Neuron* 34:255–264.
19. Groc L, Heine M, Cognet L, Brickley K, Stephenson FA, Lounis B, Choquet D (2004) *Nat Neurosci* 7:695–696.
20. Chazot PL, Cik M, Stephenson FA (1995) *Mol Membr Biol* 12:331–337.
21. Papadakis M, Hawkins LM, Stephenson FA (2004) *J Biol Chem* 279:14703–14712.
22. Thompson CL, Drewery DL, Atkins HD, Stephenson FA, Chazot PL (2000) *Neurosci Lett* 283:85–88.
23. Dahan M, Levi S, Luccardini C, Rostaing P, Riveau B, Triller A (2003) *Science* 302:442–445.
24. Tardin C, Cognet L, Bats C, Lounis B, Choquet D (2003) *EMBO J* 22:4656–4665.
25. Li B, Otsu Y, Murphy TH, Raymond LA (2003) *J Neurosci* 23:11244–11254.
26. Lindlbauer R, Mohrmann R, Hatt H, Gottmann K (1998) *J Physiol* 508:495–502.
27. Fu Z, Logan SM, Vicini S (2005) *J Physiol* 563:867–881.
28. Howarth M, Takao K, Hayashi Y, Ting AY (2005) *Proc Natl Acad Sci USA* 102:7583–7588.
29. Triller A, Choquet D (2005) *Trends Neurosci* 28:133–139.
30. Prybylowski K, Chang K, Sans N, Kan L, Vicini S, Wenthold RJ (2005) *Neuron* 47:845–857.
31. Li B, Chen N, Luo T, Otsu Y, Murphy TH, Raymond LA (2002) *Nat Neurosci* 5:833–834.
32. Yoshii A, Sheng MH, Constantine-Paton M (2003) *Proc Natl Acad Sci USA* 100:1334–1339.
33. Sans N, Petralia RS, Wang YX, Blahos J, II, Hell JW, Wenthold RJ (2000) *J Neurosci* 20:1260–1271.
34. Townsend M, Yoshii A, Mishina M, Constantine-Paton M (2003) *Proc Natl Acad Sci USA* 100:1340–1345.
35. Shi J, Townsend M, Constantine-Paton M (2000) *Neuron* 28:103–114.
36. Steigerwald F, Schulz TW, Schenker LT, Kennedy MB, Seeburg PH, Kohr G (2000) *J Neurosci* 20:4573–4581.
37. Chung HJ, Huang YH, Lau LF, Huganir RL (2004) *J Neurosci* 24:10248–10259.
38. Dalva MB, Takasu MA, Lin MZ, Shamah SM, Hu L, Gale NW, Greenberg ME (2000) *Cell* 103:945–956.
39. Chavis P, Westbrook G (2001) *Nature* 411:317–321.
40. Sinagra M, Verrier D, Frankova D, Korwek KM, Blahos J, Weeber EJ, Manzoni OJ, Chavis P (2005) *J Neurosci* 25:6127–6136.
41. Gottmann K, Mehrle A, Gisselmann G, Hatt H (1997) *J Neurosci* 17:2766–2774.
42. Perez-Otano I, Lujan R, Tavalin SJ, Plomann M, Modregger J, Liu XB, Jones EG, Heinemann SF, Lo DC, Ehlers MD (2006) *Nat Neurosci* 9:611–621.
43. Kopec CD, Li B, Wei W, Boehm J, Malinow R (2006) *J Neurosci* 26:2000–2009.
44. Ashby MC, Ibaraki K, Henley JM (2004) *Trends Neurosci* 27:257–261.
45. Schmidt T, Schutz GJ, Baumgartner W, Gruber HJ, Schindler H (1995) *J Phys Chem* 99:17662–17668.

DEMONSTRATION OF THE ASSOCIATION AND MODULATION OF NR1/NR2C AND NR1/NR2D NMDA RECEPTORS WITH PSD-95

Sarah Cousins Michalis Papadakis and F. Anne Stephenson

School of Pharmacy, University of London, 29/39 Brunswick Square, London, WC1N 1AX, UK.

INTRODUCTION

N-Methyl-D-aspartate (NMDA) receptors are a subclass of excitatory glutamate, ionotropic receptors. They are composed of obligatory NR1 subunits co-assembled with NR2 subunits of which there are four types yielding four major NMDA receptor subclasses NR1/NR2A – NR1/NR2D. NMDA receptors are clustered at synapses via their interaction with the scaffolding protein, post-synaptic density-95 (PSD-95). The association between NMDA receptors and PSD-95 is mediated via the motif, ES(D/E)V, that is common to all NR2 C-termini and in the C2' exon of NR1-3a,b and NR1-4a,b splice variants. The interaction with PSD-95 has multiple effects on NMDA receptor function and cell surface expression. For example, association of PSD-95 with NR1/NR2B regulates cell surface NMDA receptor expression via inhibition of internalization (1); with NR1/NR2B, it facilitates phosphorylation and dephosphorylation via src and fyn tyrosine kinases and PTPξ tyrosine phosphatase (2); it controls calpain-mediated cleavage of NR2B subunits (3); it inhibits protein kinase C-mediated potentiation of NR1/NR2A and NR1/NR2B receptors (4,5) and it contributes to the cell surface expression of NMDA receptors via controlling the export of NR1-3a subunits from the endoplasmic reticulum (6). In our laboratory, we have previously reported that association of PSD-95 with NR1/NR2A and NR1/NR2B receptors results in a selective enhanced expression of NR2A and NR2B subunits (7). Further, we found that in the presence of PSD-95, the molecular pharmacological properties of NR1/NR2A receptors were changed which led us to propose that association with PSD-95 results in a decreased gating of NMDA receptor channels (8). This was recently confirmed by Lin et al. (9).

Although NR2C and NR2D subunits possess the PSD-95 ESEV binding domain, only one study to date has shown evidence for an interaction between PSD-95 and NR1/NR2C and NR1/NR2D receptors where it was found in heterologous systems that association eliminated insulin potentiation of NR1/NR2C and NR1/NR2D channels (10). Indeed, it has been proposed that NR1/NR2D receptors may be extra-synaptic suggesting that they do not associate with PSD-95 (11). A more recent study however showed that NR2D-containing NMDA receptors do associate with PSD-95 in spinal neurons albeit with a reduced affinity compared to NR2A-containing receptors (12).

In this study, we have investigated the interaction between NR1/NR2C and NR1/NR2D NMDA receptors and PSD-95 in a heterologous expression system.

METHODS

Transfection of mammalian cells: Human embryonic kidney (HEK) 293 cells were transfected with pCISNR1-1a/pCISNR2A, pCISNR1-1a/pCISNR2C or pCISNR1-1a/pcDNANR2D ± pGW1PSD-95$_{c\text{-}Myc}$ by the calcium phosphate method. Cell homogenates were collected 24 h post-transfection and analysed as below.

Quantitative immunoblotting: Triplicate samples from control and test transfections were analyzed by immunoblotting using either anti-NR1 C2, anti-NR2A (1381-1394), anti-NR2C (1227-1237), anti-NR2D (1307-1323) or anti-c-Myc 4A6 antibodies as appropriate. Immune bands were quantified using the GeneGnome Chemiluminescence Capture and Analysis System and the associated Genome Tools program.

Immunoprecipitations: Triton X 100 (1% v/v) extracts were prepared from transfected cells and immunoprecipitations were carried out using anti-NR1 C2 antibodies (5 µg) or non-immune IgG antibodies (5 µg) as a control. Immune pellets were precipitated by the addition of protein A Sepharose and then analyzed by immunoblotting using anti-NR1 C2, anti-NR2A (1381-1394), anti-NR2C, (1227-1237), anti-NR2D (1307-1323) or anti-c-Myc 4A6 antibodies as appropriate.

RESULTS

Figure 1 : Effect of PSD-95α$_{c\text{-}Myc}$ on levels of NMDA receptor subunits following co-expression with NR1-1a/NR2A, NR1-1a/NR2C or NR1-1a/NR2D combinations in HEK 293 cells

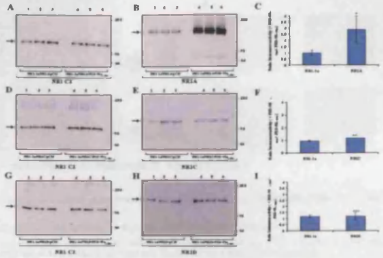

A, B, C = NR1-1a/NR2A ± PSD-95α$_{c\text{-}Myc}$

D, E, F = NR1-1a/NR2C ± PSD-95α$_{c\text{-}Myc}$

G, H, I = NR1-1a/NR2D ± PSD-95α$_{c\text{-}Myc}$

A, D and G = immunoblotting with anti-NR1 C2 antibodies where NR1-1a M_r = 117 ± 7 kDa (n = 34), an NR1-NR1 dimer is seen at M_r = 209 ± 5 kDa (n = 16)

B = immunoblotting with anti-NR2A antibodies where NR2A M_r = 177 ± 6 kDa (n = 36)

E = immunoblotting with anti-NR2C antibodies where NR2C M_r = 146 ± 4 kDa (n = 36); an additional band is sometimes seen at M_r = 252 ± 7 kDa (n = 21)

H = immunoblotting with anti-NR2D antibodies where NR2D M_r = 155 ± 5 kDa (n = 36). An additional band is sometimes observed M_r = 286 ± 8 kDa (n = 18)

The gel lay-out is identical for all samples where lanes 1- 3 are triplicate samples - PSD-95α$_{c\text{-}Myc}$ and lanes 4 – 6 are triplicate samples + PSD-95α$_{c\text{-}Myc}$

The histograms show the ratio of the respective NMDA receptor subunits ± PSD-95α$_{c\text{-}Myc}$. They are the means ± SD for n = 3 independent transfections. * $p < 0.001$; ** $p < 0.025$; *** $p < 0.05$. The molecular weight standards, in kDa, are shown on the right.

Figure 2 : Demonstration of the association of NR1-1a/NR2C NMDA receptors with PSD-95α$_{c\text{-}Myc}$ by immunoprecipitation following expression in HEK 293 cells

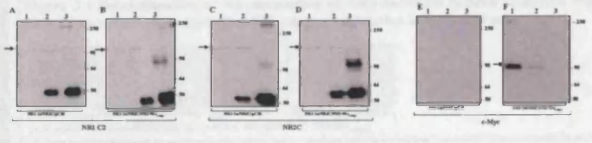

A, C and E = NR1-1a/NR2C/pCIS

B, D and E = NR1-1a/NR2C/ PSD-95α$_{c\text{-}Myc}$

A and B = Immunoblotting with anti - NR1 C2 antibodies

C and D = Immunoblotting with anti - NR2C antibodies

E and F = Immunoblotting with anti - c-Myc 4A6 antibodies

The same gel lay-out is used for each immunoblot where lane 1 = detergent soluble extract, lane 2, anti-NR1 C2 immune pellet and lane 3, control non-immune IgG pellet. The results are representative of n = 2 immunoprecipitations from n = 2 independent transfections. The molecular weight standards, in kDa, are shown on the right.

Figure 3 : Demonstration of the association of NR1-1a/NR2D NMDA receptors with PSD-95α$_{c\text{-}Myc}$ by immunoprecipitation following expression in HEK 293 cells

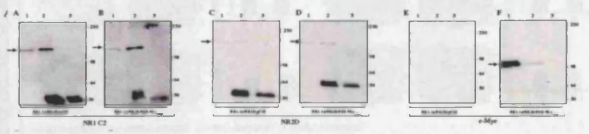

A, C and E = NR1-1a/NR2D/pCIS

B, D and E = NR1-1a/NR2D/ PSD-95α$_{c\text{-}Myc}$

A and B = Immunoblotting with anti - NR1 C2 antibodies

C and D = Immunoblotting with anti - NR2D antibodies

E and F = Immunoblotting with anti - c-Myc 4A6 antibodies

The same gel lay-out is used for each immunoblot where lane 1 = detergent soluble extract, lane 2, anti-NR1 C2 immune pellet, lanes 3, control non-immune IgG pellet. The results are representative of n = 2 immunoprecipitations from n = 2 independent transfections. The molecular weight standards, in kDa, are shown on the right.

Figure 4 : PSD-95α$_{c\text{-}Myc}$ associates with NR1/NR2A^{TRUNC} NMDA receptors lacking the NR2A C-terminal ESDV PSD-95 binding domain

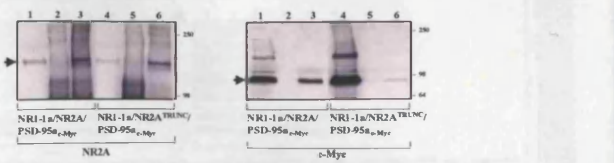

The NR2A cDNA was mutated by site-directed mutagenesis such that the codon for E in the ESDV domain was changed to a stop codon thereby deleting the C-terminal PSD-95 ESDV binding motif and generating NR2A^{TRUNC}.

A = Immunoblotting with anti-NR2Aantibodies

B= Immunoblotting with anti-c-Myc 4A6 antibodies

The gel lay-out is the same for both immunoblots, where lanes 1, 2, and 3 are NR1-1a/NR2A/ PSD-95α$_{c\text{-}Myc}$ and lanes 4,5, and 6 are NR1-1a/NR2A^{TRUNC}/ PSD-95α$_{c\text{-}Myc}$. Lanes 1 and 4, detergent soluble extract, lanes 2 and 5, the control non-immune pellet IgG; lanes 3 and 6, anti-NR2A immune pellet. The immunoblots are representative of n = 2 independent immunoprecipitations. The molecular weight standards, in kDa, are shown on the right.

Figure 5: Amino acid sequence alignment of the C-terminal domains of NMDA receptor NR2A, NR2B, NR2C and NR2D subunits

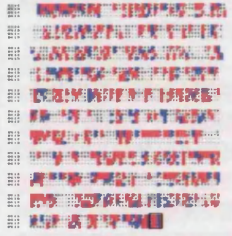

The C-terminal domains of NR2A (838 - 1464), NR2B (839 – 1482) , NR2C (836 -1239) and NR2D (862 – 1323) subunits were predicted using the SMART analysis tools program (http://smart.embl-heidelberg.de/) and they were aligned using the ClustalW program

amino acid identity, amino acid similarities, the PSD-95 binding domain

CONCLUSIONS

- PSD-95α$_{c\text{-}Myc}$ was found to have no significant effect on the expression level of NR1-1a in NR1-1a/NR2C and NR1-1a/NR2D combinations.
- PSD-95α$_{c\text{-}Myc}$ was found to have no significant effect on the expression level of NR2C or NR2D in NR1-1a/NR2C and NR1-1a/NR2D combinations respectively.
- PSD-95α$_{c\text{-}Myc}$ was shown to associate with NR1-1a/NR2C and NR1-1a/NR2D receptors by immunoprecipitation following their respective co-expression in HEK 293 cells.
- Thus NR1-1a/NR2C and NR1-1a/NR2D receptors like NR1-1a/NR2A and NR1-1a/NR2B do associate with PSD-95 in heterologous expression systems however they differ in that PSD-95 does not result in enhanced expression of NR2C and NR2D subunits.
- NR2A^{TRUNC} was shown to associate with PSD-95α$_{c\text{-}Myc}$ despite the ESDV motif being deleted suggesting that other PSD-95 binding determinants may be present within the C-terminal domain may present.
- These results concur with (12) in that NR2D subunits can associate with PSD-95 albeit with a reduced affinity compared to NR1/NR2A receptors.

Supported by the BBSRC (UK).

References:

1. Roche, K.W., Standley, S., McCallum, J., Dune Ly, C., Ehlers, M.D. and Wenthold, R.J. (2001) Nat. Neuroscience 4, 794-802.
2. Nakazawa, T., Komai, S., Tezuka, T., Hisatsune, C., Umemori, H., Semba, K., Mishina, M., Manabe, T. and Yamamoto, T. (2001) J. Biol. Chem 276, 693-699.
3. Dong, Y.N., Waxman, E., A. and Lynch, D., R. J. Neuroscience 24, 11035-11045.
4. Yamada, Y., Iwamoto, T., Watanabe, Y., Sobue, K. and Inui, M. (2002) J. Neurochemistry 81, 758-764.
5. Yamada, Y., Chochi, Y., Takamiya, K., Sobue, K.,and Inui, M. (1999) J. Biol. Chem. 274, 6647-6652.
6. Standley, S., Roche, K. R., McCallum, J., Sans, N. and Wenthold, J.W. (2000) Neuron 28, 887-898.
7. Rutter, R. A. and Stephenson, F. A. (2000) J. Neurochemistry 75, 2501-2510.
8. Rutter, R. A., Freeman, F. M. and Stephenson, F. A (2002) J. Neurochemistry 81, 1298-1307.
9. Lin, Y., Skeberdis, A., Francesconi, A., Bennett, M. V. L. and Zukin, R.S. (2004) J. Neuroscience 24, 10138-10148.
10. Yamada, Y., Iwamoto, T. and Inui, M. (2002) Japanese J. Pharmacology 88, 338.
11. Brickley, S. G., Misra, C., Mok, M. H., Mishina, M. and Cull-Candy, S. G. (2003) J. Neuroscience 33, 4958-66.
12. Mi, R., Sia, G-K., Rosen, K., Tang, X., Moghekar, A., Black, J. L., McEnery, M., Huganir, R. L. and O'Brien, R. J. (2004) Neuron 44, 335-349.

DIFFERENTIAL INTERACTION OF PSD-95 AND CHAPSYN-110 WITH NR1/NR2A, NR1/NR2B AND NR1/NR2C, NR1/NR2D NMDA RECEPTORS

Sarah Cousins Michalis Papadakis and F. Anne Stephenson

School of Pharmacy, University of London, 29/39 Brunswick Square, London, WC1N 1AX, UK

INTRODUCTION

N-Methyl-D-aspartate (NMDA) receptors are a subclass of excitatory glutamate, ionotropic receptors. They are composed of obligatory NR1 subunits co-assembled with NR2 subunits of which there are four types yielding four major NMDA receptor subclasses NR1/NR2A – NR1/NR2D. NMDA receptors are clustered at synapses via their interaction with the scaffolding protein, post-synaptic density-95 (PSD-95) and/or chapsyn-110. The association between NMDA receptors and PSD-95 is mediated via the motif, ES(D/E)V, that is common to all NR2 C-termini and in the C2' exon of NR1-3a,b and NR1-4a,b splice variants. The interaction with PSD-95 has multiple effects on NMDA receptor function and cell surface expression. For example, association of PSD-95 with NR1/NR2B regulates cell surface NMDA receptor expression via inhibition of internalization (1); with NR1/NR2B, it facilitates phosphorylation and dephosphorylation via src and fyn tyrosine kinases and PTPξ tyrosine phosphatase (2), it controls calpain-mediated cleavage of NR2B subunits (3); it inhibits protein kinase C-mediated potentiation of NR1/NR2A and NR1/NR2B receptors (4,5) and it contributes to the cell surface expression of NMDA receptors via controlling the export of NR1-3a subunits from the endoplasmic reticulum (6).

In our laboratory, we have previously reported that association of PSD-95 with NR1/NR2A and NR1/NR2B receptors results in a selective, enhanced expression of NR2A and NR2B subunits (7). Further, we found that in the presence of PSD-95, the molecular pharmacological properties of NR1/NR2A receptors were changed which led us to propose that association with PSD-95 results in a decreased gating of NMDA receptor channels (8). This was recently confirmed by Lin et al. (9).

Although NR2C and NR2D subunits possess the PSD-95 ESEV binding domain, only one study to date has shown evidence for an interaction between PSD-95 and NR1/NR2C and NR1/NR2D receptors where it was found in heterologous systems that association eliminated insulin potentiation of NR1/NR2C and NR1/NR2D channels (10). Indeed, it has been proposed that NR1/NR2D receptors may be extra-synaptic suggesting that they do not associate with PSD-95 (11). A more recent study however showed that NR2D-containing NMDA receptors do associate with PSD-95 in spinal neurons albeit with a reduced affinity compared to NR2A-containing receptors (12).

In this study, we have investigated the interaction between NR1/NR2A, NR1/NR2B, NR1/NR2C and NR1/NR2D NMDA receptors and PSD-95α or chapsyn - 110 in a heterologous expression system.

METHODS

Transfection of mammalian cells: Human embryonic kidney (HEK) 293 cells were transiently transfected with pCISNR1-1a/pCISNR2A, pCISNR1-1a/pCISNR2B, pCISNR1-1a/pCISNR2C or pCISNR1-1a/pcDNANR2D ± pGW1PSD-95$\alpha_{c\text{-}Myc}$ or ± pGW1chapsyn - 110$_{c\text{-}Myc}$ by the calcium phosphate method. Cell homogenates were collected 24 h post-transfection and analysed as below.

Quantitative immunoblotting: Individual triplicate samples from control and test transfections were analyzed by immunoblotting using either anti-NR1 C2, anti-NR2A (1381-1394), anti-NR2A/B (NR2A sequence, 1454-1464), anti-NR2C (1,227-1,237), or anti-NR2D (1,307-1,323) antibodies as appropriate. Immune bands were quantified using the GeneGnome and the associated Genome Tools program.

Immunoprecipitations: Triton X 100 (1% v/v) extracts were prepared from transfected HEK 293 cells and immunoprecipitations were carried out using either anti-NR1 C2 (5 µg), anti-NR2A (5 µg) or non-immune IgG antibodies (5 µg) as a control. Immune pellets were precipitated by the addition of protein A Sepharose and then analyzed by immunoblotting using anti-NR1 C2, anti-NR2A, anti-NR2C, anti-NR2D or anti-c-Myc 4A6 antibodies as appropriate.

RESULTS

Figure 1 : Effect of PSD-95α on expression levels of NMDA receptor subunits, NR1-1a/NR2A, NR1-1a/NR2B, NR1-1a/NR2C and NR1-1a/NR2D following their co-transfection in HEK 293 cells

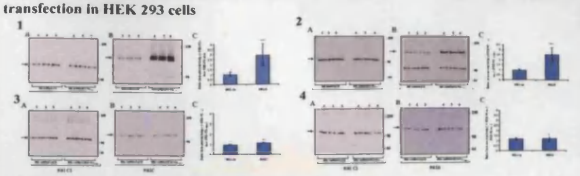

1 = NR1-1a/NR2A; 2 = NR1-1a/NR2B; 3 = NR1-1a/NR2C; 4 = NR1-1a/NR2D

For each:

The gel lay-out is identical for all samples where lanes 1- 3 are triplicate samples - PSD-95α and lanes 4 – 6 are triplicate samples + PSD-95α

A= immunoblotting with anti-NR1 C2 antibodies where NR1-1a M_r = 117 ± 7 kDa (n = 34)

B = immunoblotting with the appropriate anti-NR2 antibody where- 1B, NR2A M_r = 177 ± 6 kDa (n = 36); 2B, NR2B M_r = 181 ± 11 kDa (n = 36); 3B = NR2C M_r = 146 ± 4 kDa (n = 36) and 4B, NR2D M_r = 155 ± 5 kDa (n = 36).

C= Histograms showing the ratio of the respective NMDA receptor subunits ± PSD-95α. Values are the means ± SD fro n = 3 independent transfections. **** p < 0.001; *** p < 0.01 ; ** p < 0.025; * p < 0.05.

Figure 2 : Demonstration of the association of NR1-1a/NR2C NMDA receptors with PSD-95α by immunoprecipitation following co-expression in HEK 293 cells

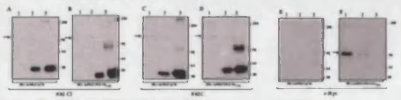

A, C and E = NR1-1a/NR2C/pCIS: B, D and E = NR1-1a/NR2C/ PSD-95α

The same gel lay-out is used for each immunoblot where lane 1 = detergent soluble extract, lane 2, anti-NR1 C2 immune pellet and lane 3, control non-immune IgG pellet.

A and B = Immunoblotting with anti - NR1 C2 antibodies; C and D = with anti - NR2C antibodies; E and F = with anti - c-Myc 4A6 antibodies. The results are representative of n = 2 immunoprecipitations from n = 2 independent transfections.

Figure 3 : Demonstration of the association of NR1-1a/NR2D NMDA receptors with PSD-95α by immunoprecipitation following co-expression in HEK 293 cells

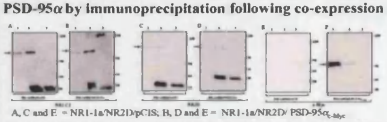

A, C and E = NR1-1a/NR2D/pCIS; B, D and E = NR1-1a/NR2D/ PSD-95$\alpha_{c\text{-}Myc}$

The same gel lay-out is used for each immunoblot where lane 1 = detergent soluble extract; lane 2, anti-NR1 C2 immune pellet; lanes 3, control non-immune IgG pellet.

A and B = Immunoblotting with anti - NR1 C2 antibodies, C and D = Immunoblotting with anti - NR2D antibodies, E and F = Immunoblotting with anti - c-Myc 4A6 antibodies. The results are representative of n = 2 immunoprecipitations from n = 2 independent transfections.

Figure 4 : Effect of Chapsyn-110 on expression levels of NMDA receptor subunits, NR1-1a/NR2A, NR1-1a/NR2B, NR1-1a/NR2C and NR1-1a/NR2D following their co-transfection in HEK 293 cells

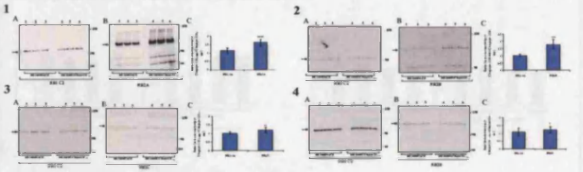

1 - NR1-1a/NR2A; 2 = NR1-1a/NR2B; 3 = NR1-1a/NR2C; 4 = NR1-1a/NR2D

For each:

The gel lay-out is identical for all samples where lanes 1- 3 are triplicate samples – chapsyn-110 and lanes 4 – 6 are triplicate samples + chapsyn -110.

A= immunoblotting with anti-NR1 C2 antibodies

B = immunoblotting with the appropriate anti-NR2 antibody where1B, NR2A; 2B, NR2B; 3B, and 4B, NR2D.

C= Histograms showing the ratio of the respective NMDA receptor subunits ± chapsyn -110. Values are the means ± SD for n = 3 independent transfections. **** p < 0.01 ; *** p < 0.005; ** p < 0.025; * p < 0.1.

Figure 5 : Determination of the association of PSD-95α with NR1-1a/NR2A and NR1-1a/NR2A^{TRUNC} receptors

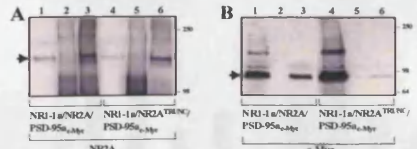

HEK 293 cells were transfected with NR1-1a/NR2A/PSD-95α or NR1-1a/NR2A^{TRUNC}/ PSD-95α, where NR2A^{TRUNC} has a stop codon introduced to remove the NR2A C-terminal PSD-95 binding motif. Cell homogenates were collected 24 h post-transfection, detergent solubilised extracts were then immunoprecipitated using anti NR2A (1,381-1,394)antibodies and analysed by immunoblotting with A, anti-NR2A (1,381-1,394), and B, anti-c-Myc 4A6 antibodies. Lanes 1,4, solubilised transfected cells; lanes 3,6 anti-NR2A immune pellet and lanes 2, 5 non-immune Ig pellet. The arrows show NR2A M_r = 180 kDa and PSD-95α M_r = 95 kDa. The immunoblots are representative of n = 2 immunoprecipitations from n = 2 independent transfections.

Figure 6: Amino acid sequence alignment for the predicted C-terminal domains of NR2A, NR2B, NR2C and NR2D subunits

The C-terminal domains of NR2A (838 – 1464), NR2B (839 – 1482), NR2C (836 -1259) and NR2D (862 – 1323) subunits were predicted using the SMART analysis tools program (http://smart.embl-heidelberg.de/). They were aligned using the ClustalW program

( ) = amino acid identity; [ ] = amino acid similarity

A summary of the NR2 C-terminal amino acid sequence identities and similarities

	NR2A C-terminal	NR2B C-terminal	NR2C C-terminal	NR2D C-terminal
NR2A C-terminal		51% (65%*)	40% (56%*)	49% (65%*)
NR2B C-terminal	51% (65%*)		39% (56%*)	51% (66%*)
NR2C C-terminal	40% (56%*)	39% (56%*)		47% (65%*)
NR2D C-terminal	49% (65%*)	51% (66%*)	47% (65%*)	

* = Percentage amino acid sequence identity

^ = Percentage amino acid sequence similarity

CONCLUSIONS

- PSD-95α and chapsyn-110 were found to have no significant effect on the expression level of NR1-1a in NR1-1a/NR2A, NR1-1a/NR2B, NR1-1a/NR2C and NR1-1a/NR2D combinations.
- As previously shown (7), there is a selective enhancement of expression of NR2A and NR2B in the presence of PSD-95α, in NR1-1a/NR2A or NR1-1a/NR2B combinations. A selective enhancement of expression of NR2A and NR2B is also observed with chapsyn – 110.
- PSD-95α and chapsyn-110 were found to have no significant effect on the expression level of NR2C or NR2D in NR1-1a/NR2C and NR1-1a/NR2D combinations respectively.
- PSD-95α was shown to associate with NR1-1a/NR2C and NR1-1a/NR2D receptors by immunoprecipitation following their respective co-expression in HEK 293 cells.
- Thus NR1-1a/NR2C and NR1-1a/NR2D receptors like NR1-1a/NR2A and NR1-1a/NR2B do associate with PSD-95 in heterologous expression systems however they differ in that PSD-95 does not result in enhanced expression of NR2C and NR2D subunits.
- These results concur with (12) in that NR2D subunits can associate with PSD-95 albeit with a reduced affinity compared to NR1/NR2A receptors.
- NR2A^{TRUNC} was shown to associate with PSD-95α despite the ESDV motif being deleted suggesting that other PSD-95 binding determinants may be present within the C-terminal domain may present.
- Different members of the MAGUK family do associate with NMDA receptors but differences were found with regard to enhancement of NR2 subunit expression. This suggests differential interactions of NMDA receptor subtypes with scaffolding proteins and thereby possible differences in downstream signalling mechanisms or differences in the regulation of NMDA receptor activity and cell surface expression at synapses.

Supported by the BBSRC (UK)

Differential interaction of NMDA receptor subtypes with the PSD-95 family of MAGUK proteins

Sarah Cousins Michalis Papadakis and F. Anne Stephenson

School of Pharmacy, University of London, 29/39 Brunswick Square, London, WC1N 1AX, UK

INTRODUCTION

N-Methyl-D-aspartate (NMDA) receptors are a subclass of excitatory glutamate, ionotropic receptors. They are composed of obligatory NR1 subunits co-assembled with NR2 subunits of which there are four types yielding four major NMDA receptor subclasses NR1/NR2A – NR1/NR2D. NMDA receptors are clustered at synapses via their interaction with the scaffolding protein, post-synaptic density-95 (PSD-95) and/or chapsyn-110. The association between NMDA receptors and the PSD-95 family of proteins is mediated via the motif, ES(D/E)V, that is common to all NR2 C-termini and also found in the C2' exon of NR1-3a,b and NR1-4a,b splice variants. The interaction with PSD-95 has multiple effects on NMDA receptor function and cell surface expression. For example, association of PSD-95 with NR1/NR2B regulates cell surface NMDA receptor expression via inhibition of internalization (1); with NR1/NR2B, it facilitates phosphorylation and dephosphorylation via src and fyn tyrosine kinases and PTPξ tyrosine phosphatase (2); it controls calpain-mediated cleavage of NR2B subunits (3); it inhibits protein kinase C-mediated potentiation of NR1/NR2A and NR1/NR2B receptors (4,5); it contributes to the cell surface expression of NMDA receptors via controlling the export of NR1-3a subunits from the endoplasmic reticulum (6) and it forms a link of synaptic NMDA receptors to the CREB pathway (7).

In our laboratory, we have previously reported that association of PSD-95 with NR1/NR2A and NR1/NR2B receptors results in a selective, enhanced expression of NR2A and NR2B subunits (8). Further, we found that in the presence of PSD-95, the molecular pharmacological properties of NR1/NR2A receptors were changed which led us to propose that association with PSD-95 results in a decreased gating of NMDA receptor channels (9). This was recently confirmed by Lin *et al.* (10).

Although NR2C and NR2D subunits possess the PSD-95 ESEV binding domain, only two studies to date have shown evidence for an interaction between PSD-95 and NR1/NR2C and NR1/NR2D receptors (11,12). The NR2C C-terminal domain has been shown to associate with PSD-95 using the yeast two-hybrid system (12). It has been proposed that NR1/NR2D receptors may be extra-synaptic suggesting that they do not associate with PSD-95 (13). A more recent study however showed that NR2D-containing NMDA receptors do associate with PSD-95 in spinal neurons albeit with a reduced affinity compared to NR2A-containing receptors (14).

In this study, we have investigated the interaction between NR1/NR2A, NR1/NR2B, NR1/NR2C and NR1/NR2D NMDA receptors and PSD-95α, chapsyn-110, SAP-97 or SAP-102 in a heterologous expression system.

A schematic diagram showing the known interactions between NMDA receptors and the MAGUK family of scaffolding proteins at glutamatergic excitatory synapses

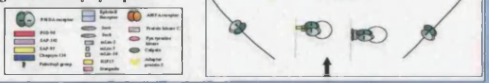

METHODS

Transfection of mammalian cells: Human embryonic kidney (HEK) 293 cells were transiently transfected with pCISNR1-1a/pCISNR2A, pCISNR1-1a/pCISNR2B, pCISNR1-1a/pCISNR2C or pCISNR1-1a/pcDNANR2D ± pGW1PSD-95α$_{c\text{-}Myc}$ ± pGW1chapsyn -110, ± pCMVneoSAP-102$_{c\text{-}Myc}$, or ± pGW1SAP-97 by the calcium phosphate method. Cell homogenates were collected 24 h post-transfection and analysed as below.

Quantitative immunoblotting: Individual triplicate samples from control and test transfections were analyzed by immunoblotting using either anti-NR1 C2, anti-NR2A (1381-1394), anti-NR2A/B (NR2A sequence, 1454-1464), anti-NR2C (1,227-1,237), or anti-NR2D (1,307-1,323) antibodies as appropriate. Immune bands were quantified using the GeneGnome and the associated Genome Tools program.

Immunoprecipitations: Triton X 100 (1% v/v) extracts were prepared from transfected HEK 293 cells and immunoprecipitations were carried out using either anti-NR1 C2 (5 µg), anti-NR2A (5 µg) or non-immune IgG antibodies (5 µg) as a control. Immune pellets were precipitated by the addition of protein A Sepharose and then analyzed by immunoblotting using anti-NR1 C2, anti-NR2A, anti-NR2C, anti-NR2D or anti-c-Myc 4A6 antibodies as appropriate.

RESULTS

Figure 1 : Effect of PSD-95α on expression levels of NMDA receptor subunits, NR1-1a/NR2A, NR1-1a/NR2B, NR1-1a/NR2C and NR1-1a/NR2D following their co-transfection in HEK 293 cells

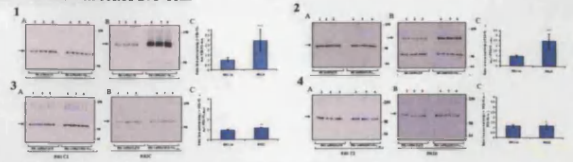

1 = NR1-1a/NR2A: 2 = NR1-1a/NR2B: 3 = NR1-1a/NR2C: 4 = NR1-1a/NR2D

For each: The gel lay-out is identical for all samples where lanes 1- 3 are triplicate samples - PSD-95α and lanes 4 – 6 are triplicate samples + PSD-95α.

A= immunoblotting with anti-NR1 C2 antibodies where NR1-1a M_r = 117 ± 7 kDa (n = 34)

B = immunoblotting with the appropriate anti-NR2 antibody where= 1B, NR2A M_r = 177 ± 6 kDa (n = 36); 2B, NR2B M_r = 181 ± 11 kDa (n = 36); 3B = NR2C M_r = 146 ± 4 kDa (n = 36) and 4B, NR2D M_r = 155 ± 5 kDa (n = 36).

C= Histograms showing the ratio of the respective NMDA receptor subunits ± PSD-95α. Values are the means ± SD from n = 3 independent transfections; **** p < 0.001; *** p < 0.01 ; ** p < 0.025; * p < 0.05.

Figure 2 : Demonstration of the association of NR1-1a/NR2C NMDA receptors with PSD-95α by immunoprecipitation following co-expression in HEK 293 cells

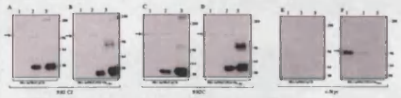

A, C and E = NR1-1a/NR2C/pCIS: B, D and E = NR1-1a/NR2C/ PSD-95α

The same gel lay-out is used for each immunoblot where lane 1 = detergent soluble extract, lane 2, anti-NR1 C2 immune pellet and lane 3, control non-immune IgG pellet.

A and B = Immunoblotting with anti - NR1 C2 antibodies; C and D = with anti - NR2C antibodies; E and F = with anti - c-Myc 4A6 antibodies. The results are representative of n = 2 immunoprecipitations from n = 2 independent transfections.

Figure 3 : Demonstration of the association of NR1-1a/NR2D NMDA receptors with PSD-95α by immunoprecipitation following co-expression in HEK 293 cells

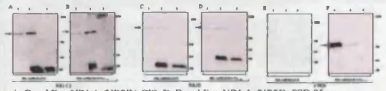

A, C and E = NR1-1a/NR2D/pCIS; B, D and E = NR1-1a/NR2D/ PSD-95α$_{c\text{-}Myc}$

The same gel lay-out is used for each immunoblot where lane 1 = detergent soluble extract, lane 2, anti-NR1 C2 immune pellet, lanes 3, control non-immune IgG pellet.

A and B = Immunoblotting with anti - NR1 C2 antibodies, C and D = Immunoblotting with anti - NR2D antibodies, E and F = Immunoblotting with anti - c-Myc 4A6 antibodies. The results are representative of n = 2 immunoprecipitations from n = 2 independent transfections.

Figure 4 : Effect of chapsyn-110, SAP-97 or SAP-102 on expression levels of NMDA receptor subunits, NR1-1a/NR2A, NR1-1a/NR2B, NR1-1a/NR2C and NR1-1a/NR2D following their co-transfection in HEK 293 cells

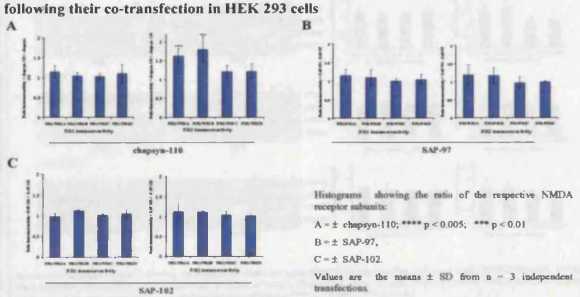

Histograms showing the ratio of the respective NMDA receptor subunits:

A = ± chapsyn-110; **** p < 0.005; *** p < 0.01

B = ± SAP-97,

C = ± SAP-102.

Values are the means ± SD from n = 3 independent transfections.

Figure 5 : PSD-95α, chapsyn 110 but not SAP-97 nor SAP-102 enhance cell surface NMDA receptor expression following co-transfection in HEK 293 cells

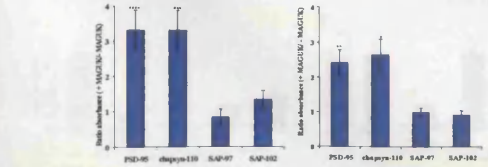

Cell surface ELISA assays were performed with NR1/NR2A or NR1/NR2B NMDA receptors ± PSD-95α, ± chapsyn-110, ± SAP-97 or ± SAP-102, see Rutter *et al* (9) for method. Histograms show the ratio absorbance of NR1/NR2A (A) or NR1/NR2B (B) containing NMDA receptors either ± each PSD-95 MAGUK family member. Values are the means ± SEM from n = 5 independent transfections; **** p < 0.005; ***p < 0.01 ; ** p < 0.005; * p < 0.025.

Figure 6: Amino acid sequence alignment for the predicted C-terminal domains of NR2A, NR2B, NR2C and NR2D subunits highlight similarities between the subunit pairs NR2A and NR2B versus NR2C and NR2D

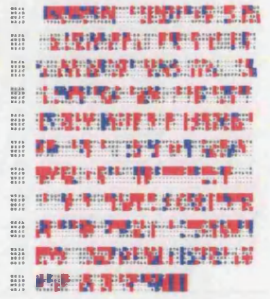

A summary of the NR2 C-terminal amino acid sequence identities and similarities

	NR2A C-terminal	NR2B C-terminal	NR2C C-terminal	NR2D C-terminal
NR2A C-terminal		53% identity	45% identity	45% identity
NR2B C-terminal	67% identity		45% identity	No significant match
NR2C C-terminal	59% identity	59% identity		57% identity
NR2D C-terminal	59% identity	No significant match	67% identity	

* = Percentage amino acid sequence identity

Δ = Percentage amino acid sequence similarity

CONCLUSIONS

- Each NR2 subunit (NR2A, NR2B, NR2C and NR2D) was shown to interact with PSD-95α, chapsyn-110, SAP-102 and SAP-97 by immunoprecipitation.
- Co-expression of PSD-95α, chapsyn-110, SAP-97 and SAP-102 had no significant effect on the expression level of NR1-1a in NR1-1a/NR2A, NR1-1a/NR2B, NR1-1a/NR2C and NR1-1a/NR2D combinations.
- As previously shown (7), a selective enhancement of NR2A and NR2B expression in the presence of PSD-95α, in NR1-1a/NR2A or NR1-1a/NR2B combinations was found. Similar findings were made for chapsyn-110.
- In contrast to PSD-95α and chapsyn-110, SAP-97 and SAP-102 did not enhance NR2A or NR2B subunit expression.
- Cell surface expression of NR1/NR2A or NR1/NR2B NMDA receptors was enhanced in the presence of PSD-95 or chapsyn-110. However, no enhancement of expression was seen in the presence of SAP-97 or SAP-102.
- PSD-95α, chapsyn-110, SAP-97 and SAP-102 had no significant effect on the expression level of NR2C or NR2D in NR1-1a/NR2C and NR1-1a/NR2D combinations.
- PSD-95α was shown to associate with NR1-1a/NR2C and NR1-1a/NR2D receptors by immunoprecipitation following their respective co-expression in HEK 293 cells.
- Thus although NR1-1a/NR2C and NR1-1a/NR2D receptors like NR1-1a/NR2A and NR1-1a/NR2B do associate with PSD-95 and chapsyn-110 in heterologous expression systems they differ in that no enhanced expression levels are found.
- Overall, different members of the PSD-95 MAGUK family do associate with NMDA receptors but differences were found with regard to enhancement of NR2 subunit expression. This may have implications for the stabilisation, turnover and compartmentalisation of NMDA receptor subtypes in neurones.

pCISNR1-1a/pCISNR2A, pCISNR1-1a/pCISNR2B, pCISNR1-1a/pCISNR2C, pCISNR1-1a/pcDNANR2D, pGW1PSD-95α$_{c\text{-}Myc}$, pGW1chapsyn -110$_{c\text{-}Myc}$, pCMVneoSAP-102$_{c\text{-}Myc}$ and pGW1SAP-97 constructs were a gift from Dr M. Sheng (Massachusetts Institute of Technology, USA)

Differential interaction of NMDA receptor subtypes with the PSD-95 family of MAGUK proteins

Sarah Cousins, Michalis Papadakis and F. Anne Stephenson

School of Pharmacy, University of London, 29/39 Brunswick Square, London, WC1N 1AX, UK

INTRODUCTION

N-Methyl-D-aspartate (NMDA) receptors are a subclass of excitatory glutamate, ionotropic receptors. They are composed of obligatory NR1 subunits co-assembled with NR2 subunits of which there are four types yielding four major NMDA receptor subclasses NR1/NR2A – NR1/NR2D. NMDA receptors are trafficked to the cell surface via mechanisms that involve association with the PSD-95 MAGUK family of scaffolding proteins that includes PSD-95, Chapsyn-110, SAP-102 and SAP-97. PSD-95 and SAP-102 are known to traffic NR1/NR2B NMDA receptors to the cell surface by association with either KIF17 via the mLin family (PSD-95, 1) or with the exocyst complex via sec8 and sec6 (SAP-102, 2). Also, SAP-102 forms a complex with mPins to traffic NR1/NR2B independently of the exocyst complex (3). In addition to trafficking to the cell surface, in neurones NMDA receptors also need to be appropriately targeted to synaptic or extra-synaptic sites. Thus differential association with the PSD-95 MAGUK family members may be important for the regulation of cell surface receptor number, the stabilisation, clustering, turnover and compartmentalisation of NMDA receptor subtypes in neurones during development and in the mature brain (4 – 10).

In our laboratory, we have previously reported that association of PSD-95 with NR1/NR2A and NR1/NR2B receptors results in a selective, enhanced expression of NR2A and NR2B subunits (11). Further, we found that in the presence of PSD-95, the molecular pharmacological properties of NR1/NR2A receptors were changed which led us to propose that association with PSD-95 results in a decreased gating of NMDA receptor channels (12). This was recently confirmed by Lin *et al.* (13).

Although NR2C and NR2D subunits possess the PSD-95 ESEV binding domain, only two studies to date have shown evidence for an interaction between PSD-95 and NR1/NR2C and NR1/NR2D receptors (14,15). The NR2C C-terminal domain has been shown to associate with PSD-95 using the yeast two-hybrid system (15). It has been proposed that NR1/NR2D receptors may be extra-synaptic suggesting that they do not associate with PSD-95 (16). A more recent study however showed that NR2D-containing NMDA receptors do associate with PSD-95 in spinal neurons albeit with a reduced affinity compared to NR2A-containing receptors (17).

In this study, we have investigated the interaction between NR1/NR2A, NR1/NR2B, NR1/NR2C and NR1/NR2D NMDA receptors and PSD-95α, chapsyn-110, SAP-97 or SAP-102 in a heterologous expression system.

A schematic diagram showing the known interactions between NMDA receptors and the MAGUK family of scaffolding proteins at glutamatergic excitatory synapses

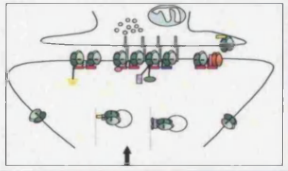

METHODS

Transfection of mammalian cells: Human embryonic kidney (HEK) 293 cells were transiently transfected with pCISNR1-1a/pCISNR2A, pCISNR1-1a/pCISNR2B, pCISNR1-1a/pCISNR2C or pCISNR1-1a/pcDNANR2D ± pGW1PSD-95α$_{c\text{-}Myc}$ ± pGW1chapsyn -110, ± pCMVneoSAP-102$_{c\text{-}Myc}$ or ± pGW1SAP-97 by the calcium phosphate method. Cell homogenates were collected 24 h post-transfection and analysed as below.

Quantitative immunoblotting: Individual triplicate samples from control and test transfections were analyzed by immunoblotting using either anti-NR1 C2, anti-NR2A (1381-1394), anti-NR2A/B (NR2A sequence, 1454-1464), anti-NR2C (1227-1237), or anti-NR2D (1307-1323) antibodies as appropriate. Immune bands were quantified using the GeneGnome and the associated Genome Tools program.

Immunoprecipitations: Triton X 100 (1% v/v) extracts were prepared from transfected HEK 293 cells and immunoprecipitations were carried out using either anti-NR1 C2 (5 µg), anti-NR2A (5 µg) or non-immune IgG antibodies (5 µg) as a control. Immune pellets were precipitated by the addition of protein A Sepharose and then analyzed by immunoblotting using anti-NR1 C2, anti-NR2A, anti-NR2A/B, anti-NR2C, anti-NR2D, anti-SAP-97(115- 133) or anti-c-Myc 4A6 antibodies as appropriate.

Cell suface ELISA assays: ELISA assays were conducted as written in Rutter *et al.*, 2002 (12), using anti-NR2A (44-58) or anti-NR2B (48-60) antibodies as appropriate.

RESULTS

Figure 1 : Effect of PSD-95α on expression levels of NMDA receptor subunits, NR1-1a/NR2A, NR1-1a/NR2B, NR1-1a/NR2C and NR1-1a/NR2D following their co-transfection in HEK 293 cells

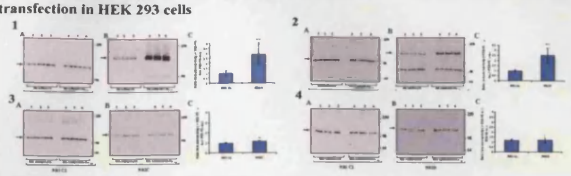

1 = NR1-1a/NR2A; 2 = NR1-1a/NR2B; 3 = NR1-1a/NR2C; 4 = NR1-1a/NR2D

For each: The gel lay-out is identical for all samples where lanes 1- 3 are triplicate samples - PSD-95α and lanes 4 – 6 are triplicate samples + PSD-95α.

A= immunoblotting with anti-NR1 C2 antibodies where NR1-1a M_r = 117 ± 7 kDa (n = 34)

B = immunoblotting with the appropriate anti-NR2 antibody where:- 1B, NR2A M_r = 177 ± 6 kDa (n = 36); 2B, NR2B M_r = 181 ± 11 kDa (n = 36); 3B = NR2C M_r = 146 ± 4 kDa (n = 36) and 4B, NR2D M_r = 155 ± 5 kDa (n = 36).

C= Histograms showing the ratio of the respective NMDA receptor subunits ± PSD-95α. Values are the means ± SD from n = 3 independent transfections; **** p < 0.001; *** p < 0.01 ; ** p < 0.025; * p < 0.05.

Figure 2 : Demonstration of the association of NR1-1a/NR2A; NR1-1a/NR2B; NR1-1a/NR2C and NR1-1a/NR2D NMDA receptors with PSD-95°, chapsyn-110, SAP-97 and SAP-102 by co-immunoprecipitation following their co-expression in HEK 293 cells

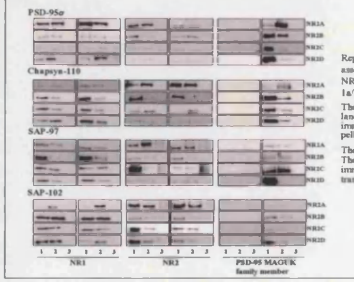

Representative immunoblots demonstrating the association of each PSD-95 family member with NR1-1a/NR2A, NR1-1a/NR2B, NR1-1a/NR2C or NR1-1a/NR2D NMDA receptors.

The same gel lay-out is used for each immunoblot where lane 1 = detergent soluble extract, lane 2, anti-NR1 C2 immune pellet, and lane 3, control non-immune IgG pellet.

The respective antibodies used are indicated on the figure. The results are representative of at least n = 2 immunoprecipitations from n = 2 independent transfections.

Figure 4 : Effect of chapsyn-110, SAP-97 or SAP-102 on expression levels of NMDA receptor subunits, NR1-1a/NR2A, NR1-1a/NR2B, NR1-1a/NR2C and NR1-1a/NR2D following their co-transfection in HEK 293 cells

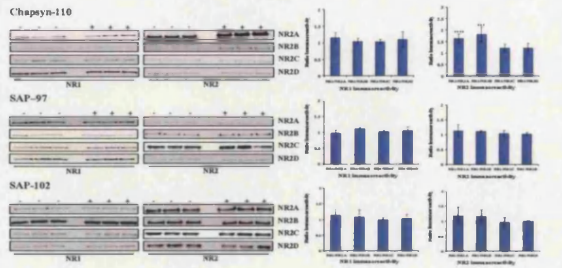

Representative immunoblots following co-expression studies of each PSD-95 family member with each major NMDA receptor subtype, NR1-1a/NR2A, NR1-1a/NR2B, NR1-1a/NR2C or NR1-1a/NR2D. Histograms show the ratio of the respective NMDA receptor subunits. Values are the means ± SD from n = 3 independent transfections. **** p < 0.005, *** p < 0.01

Figure 5 : PSD-95α, chapsyn-110 but not SAP-97 nor SAP-102 enhance cell surface NMDA NR1/NR2A and NR1/NR2B receptor expression following co-transfection in HEK 293 cells

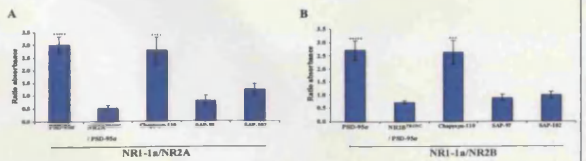

Cell surface ELISA assays were performed with NR1/NR2A or NR1/NR2B NMDA receptors ± PSD-95α, ± chapsyn-110, ± SAP-97 or ± SAP-102. Histograms show the ratio of absorbance of NR1/NR2A (A) or NR1/NR2B (B) +PSD-95 MAGUK family member: NR1/NR2A (A) or NR1/NR2B (B) - PSD-95 MAGUK family member. Values are the means ± SEM from n = 5 independent transfections; ***** = p < 0.0005; **** = p < 0.005; *** = p < 0.01

Figure 6: Amino acid sequence alignment for the predicted C-terminal domains of NR2A, NR2B, NR2C and NR2D subunits highlight similarities between the subunit pairs NR2A and NR2B versus NR2C and NR2D

The C-terminal domains of NR2A (836 - 1464), NR2B (839 - 1482), NR2C (836 - 1239) and NR2D (862 – 1323) subunits were predicted using the SMART analysis tools program (http://smart.embl-heidelberg.de/). They were aligned using the ClustalW program (www.ch.embnet.org/software/ClustalW.html)

: amino acid identity; : amino acid similarity

A summary of the NR2 C-terminal amino acid sequence identities and similarities

	NR2A C-terminal	NR2B C-terminal	NR2C C-terminal	NR2D C-terminal
NR2A C-terminal		53% 68% *	40% 56% *	40% 56% *
NR2B C-terminal	53% 68% *		39% 56% *	41% 56% *
NR2C C-terminal	40% 56% *	39% 56% *		47% 62% *
NR2D C-terminal	40% 56% *	41% 56% *	47% 62% *	

* = Percentage amino acid sequence identity

Δ = Percentage amino acid sequence similarity

CONCLUSIONS

- NR2A, NR2B, NR2C and NR2D subunits were all shown to interact in a heterologous expression system with each PSD-95 MAGUK member by immunoprecipitation.
- Co-expression of PSD-95α, chapsyn-110, SAP-97 and SAP-102 had no significant effect on the expression level of NR1-1a in NR1-1a/NR2A, NR1-1a/NR2B, NR1-1a/NR2C and NR1-1a/NR2D combinations.
- As previously shown (11), a selective enhancement of NR2A and NR2B expression in the presence of PSD-95α, in NR1-1a/NR2A or NR1-1a/NR2B combinations was found. Similar findings were made for chapsyn-110.
- In contrast to PSD-95α and chapsyn-110, SAP-97 and SAP-102 did not enhance NR2A or NR2B subunit expression.
- Cell surface expression of NR1/NR2A or NR1/NR2B NMDA receptors was enhanced in the presence of PSD-95 or chapsyn-110. However, no significant enhancement of expression was seen in the presence of SAP-97 or SAP-102.
- PSD-95α, chapsyn-110, SAP-97 and SAP-102 had no significant effect on the expression level of NR2C or NR2D in NR1-1a/NR2C and NR1-1a/NR2D combinations.
- Thus although NR1-1a/NR2C and NR1-1a/NR2D receptors like NR1-1a/NR2A and NR1-1a/NR2B do associate with PSD-95 and chapsyn-110 at least in heterologous expression systems they differ in that no enhanced expression levels are found.
- Overall, different members of the PSD-95 MAGUK family do associate with NMDA receptors but differences were found with regard to the regulation of NR2 subunit expression. This may have implications for the stabilisation, turnover and compartmentalisation of NMDA receptor subtypes in neurones.

Acknowledgements: pCISNR1-1a, pCISNR2A, pCISNR2B, pCISNR2C, pCISNR2D and pCISNR1-1a/pcDNANR2D constructs were a kind gift from Dr S. Nakanishi (Kyoto University, Japan). pGW1PSD-95α, pGW1chapsyn -110, pCMVneoSAP-102, and pGW1SAP-97 constructs were a kind gift from Dr M. Sheng (Massachusetts Institute of Technology, USA).

Yeast cell growth on -Leu/-Trp selective dropout plates indicated successful co-transformation of both the DNA-binding domain containing and activation domain containing plasmids. The determination of protein interactions required yeast cell growth present on the -Leu/-Trp/-His/-Ade selective dropout plates. Yeast cell growth on the -Leu/-Trp/-His/-Ade selective dropout plates demonstrates the activation of reporter genes, summarised in Section 6.1.2.

2.2.1.3.5 Yeast-two hybrid library screening to identify positive interactors for the NR2D subunit C-terminal domain

An overview of the screening methods carried out are shown in Figure 2.3.

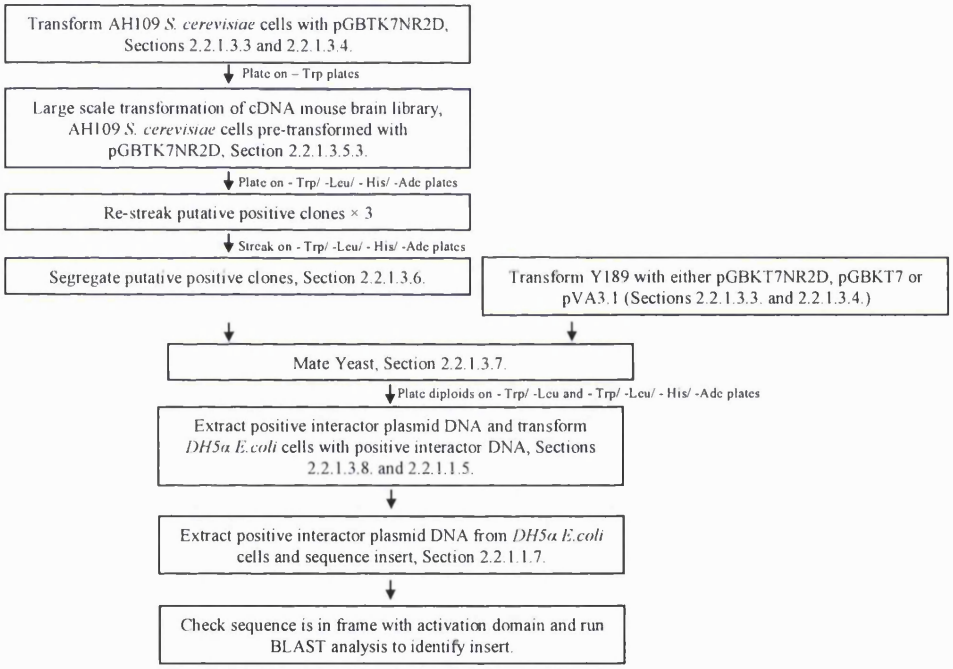

Figure 2.3 Identification of positive interactions of the NR2D C-terminal domain by mouse brain cDNA library screening using the yeast two-hybrid system

The above flow diagram shows the methods used to identify positive interactions in the yeast two-hybrid following cDNA mouse brain library screening using pGBKT7NR2D clones as bait..

2.2.1.3.5.1 Amplification of mouse brain cDNA library cloned into pACT2

The mouse brain cDNA library was sourced from 200 BALB/c males, aged 9 – 12 weeks, normal whole brains. The number of independent clones present was 3.5×10^6 which had an average insert size of 2.0 kb and a range of 0.4 – 4.0 kb. The library was amplified as